The Dissertation Committee for Mingjuan Shi certifies that this is the approved version of the following dissertation:

Characterizing Heterogeneity in Low-permeability Strata and Its Control on Fluid Flow and Solute Transport by Thermalhaline Free Convection

Committee:

John M. Sharp, Supervisor

William E. Galloway

Alan R. Dutton

Craig T. Simmons

Zong-liang Yang

Characterizing Heterogeneity in Low-permeability Strata and Its Control on Fluid Flow and Solute Transport by Thermalhaline Free Convection

by

Mingjuan Shi, B.E.; M.S.

Dissertation

Presented to the Faculty of the Graduate School of

The University of Texas at Austin

in Partial Fulfillment

of the Requirements

for the Degree of

Doctor of Philosophy

The University of Texas at Austin

May, 2005

To My Parents and Haixiang

Acknowledgments

I wish to thank my adviser Jack Sharp for his guidance, great support, and kind understanding during the process of my PhD study at UT Austin. His intelligence and knowledge of the latest development in the area has benefited this study and influenced me a lot. I also would like to thank my committee members: Dr. Bill Galloway, Dr. Alan Dutton, Dr. Craig Simmons and Dr. Liang Yang for discussions and insightful suggestions.

I would like to thank the following persons with whom I have had deep discussions: Tom Fenstemaker for his help with starting 2D SUTRA and some of the codes in this study are based on his previous work; Juliette Woods for discussing variable-density flow models and each model's numerical errors; Paul Knox for talking about shale sealing and referring me to many useful references on shale studies; Kitty Milliken for referring mudstone study by Katsube et al.; Craig Simmons (Australia) for discussion on the boundary layer study and aspect ratio; Awadesh Prasad (Australia) for his example of heterogeneous permeability study; Thomas Graf (Canada) for his help with frac3dvs/hydrosphere software; Paul Marschall of Swiss NAGRA for discussions on the radioactive waste disposal projects. Funding for this research was provided through Dr. Sharp's DOE project and ACS Petroleum Research Fund, a graduate research fund received by the author from Geological Society of America Hydrogeology Division, and Geology Foundation at UT Austin.

I want to thank many colleagues and friends in the Department of Geological Sciences and the Institute of Geophysics for their helpful discussions and great friendship: Tom Fenstemaker, Todd Halihan, Kitty Milliken, Thandar and Thet Phyu, Terence Garner, Patty Curry, Xinxia Wu, Clark Thompson, Ricardo Comballot, Joel Stevens, Trevor Budge, Suzanne Pierce, Dan Lin, Beatriz Garcia-Fresca, Wei Gao, Guoyue Niu, Sylvia Nordfjord, Alejandro Escalona, Tim Whiteaker, Ray S., Faming Wang, Lloyd Hemphill, Marcus Gary, Brad Wholaver, Kristin White, Nico Hauwert, Seay Nance, Paul Knox, Sasha Carter, and Hongbo Lu,

I thank my family and my husband's family for their love and support. Many times I seek advices from my husband and I couldn't finish this work without his love and encouragement. There are many people I should thank too, these include all the teachers that have been in my life and especially Mr. Chengbo Ge, Dr. Dave Evans, Dr. Jack Sharp and Dr. Bill Galloway who have helped me in many ways and showed me an excellent example of how to be a good teacher.

Characterizing Heterogeneity in Low-permeability Strata and Its Control on Fluid Flow and Solute Transport by Thermalhaline Free Convection

Publication No. _____

Mingjuan Shi, Ph.D.

The University of Texas at Austin, 2005

Supervisor: John M. Sharp, Jr.

Studies of salinity-driven free convection across low-permeability strata indicate that permeability heterogeneity is an important factor in controlling solute transport in the system. Heterogeneity exists at different scales in natural geological materials and presents a significant challenge to many aspects of geological science and petroleum studies. The traditional Rayleigh number criterion is overly conservative in predicting thermohaline convection in a heterogeneous system. Heterogeneity effects are investigated with numerical models to study salinity-driven groundwater flow and solute transport through

heterogeneous low-permeability units. Monte Carlo stochastic simulations of the permeability fields are applied to model saturated variable-density flow and to examine how the internal structure of the permeability field controls fluid flow and contaminant transport in low-permeability strata. Simulations show that dense plumes take preferential pathways to sink through low-permeability strata; patch analysis using percolation theory shows the threshold permeability for the onset of free convection can be as low as 10^{-16} m^2 when the mean permeability of the distribution is 10^{-18} m^2. The threshold permeability for a percolation cluster decreases with increasing concentration gradient, vertical correlation length, mean permeability, and standard deviation. The connectedness of the relative high permeability zones is important in initiating and controlling plume fingers of free convection. Numerical modeling results also show that free convection occurs more easily and often when there is a sand or sandstone layer on top of the low-permeability shale layer or below with different boundary conditions.

For a fractured low-permeability shale layer, free convection can easily occur along the fracture plane which suggests the inadequacy of two-dimensional fracture model for simulating free convection in parallel-plate discrete fractures. Free convection through hydraulically active tiny fractures can be an important mechanism for flow and solute transport even though these tiny fractures in the shale unit can not be detected by vertical boreholes and flow in most part of the unit is diffusion-dominated.

Table of Contents

List of Tables

List of Figures

Chapter 1 INTRODUCTION

Studies of hydrodynamic processes in the sediments of Gulf of Mexico Basin indicate that large volumes of high-temperature, geopressured buoyant fluids (Bethke, 1986a) are released by compaction and hydrocarbon maturation reactions in the deepest portion of the basin (Bredehoeft and Hanshaw, 1968; Anderson et al. 1991b; Land, 1991; Sharp et al., 2001; Simmons et al., 2000). When geopressures build up to cause repeated hydraulic fracturing of the geopressured chambers (Mello and Karner, 1992), large volumes of water with oil and gas are released along growth faults and into overlying high permeability sand intervals within the sand-shale sequence (Bodner, 1985; Land,; Anderson et al., 1994; Mello and Karner, 1996; 1991Losh et al., 1999). The form and magnitude of fluid flow are controlled by both the buoyant forces of the fluids (temperature, pressure, chemical gradients and fluid densities) and the permeability pathways available to the fluids (Bodner et al., 1988; Anderson et al., 1991a; Anderson, 1995). Morton and Land (1987), Sharp et al.(1988), Land (1991), and McKenna and Sharp (1997) document salinity inversions in the Gulf of Mexico Basin. The inversions are located near the transition zone between hydrostatic pressures and overpressures which contains most of the hydrocarbon accumulations in the gulf (Anderson et al., 1991; Mello et al., 1994, 1995). The positioning of more saline waters over less saline formation fluids provides a

significant buoyancy force, which in turn may cause the system to be unstable and free convection occurs (Blanchard and Sharp, 1985; Sharp et al., 2001; Simmons et al., 2001). Free convection has been studied as the major mechanism for driving fluid flow and solute transport in many geothermal systems and around salt domes (Hassanizadeh, 1988; Ranganathan and Hanor, 1988, 1989; Evans et al., 1989, 1991; Oldenburg and Pruess, 1995).

Study of the plausibility of salinity-driven free convection in sediments of the South Texas portion of the Gulf of Mexico Basin by analysis of salinity data, Rayleigh Number calculations and numerical models shows that free convection at depth in sedimentary basins may be more common than hitherto expected because heterogeneities in shale permeabilities enhance convective solute transport and make traditional Rayleigh Number calculations overly conservative in predicting thermohaline convection (Blanchard, 1987; Sharp et al., 2001; Simmons et al., 2001). Traditional Rayleigh Number (Rayleigh, 1916; Nield, 1968) is a dimensionless number used to predict situations in which free convection will occur. It is a ratio of the buoyant forces promoting free convection to the viscous resistance to flow and diffusive processes inhibiting free convection:

$$\mathrm{Ra} = \frac{\alpha \rho_0 g k \Delta C H}{\mu D} + \frac{\beta \rho_0 g k \Delta T H}{\mu \kappa} \geq \mathrm{Ra}_{cr} \qquad (1.1)$$

where g is gravitational acceleration (L/T^2), H is the thickness of a laterally extensive homogeneous permeable layer, k is intrinsic permeability, ρ_0 is base fluid density, μ is dynamic viscosity, κ is thermal diffusivity (the ratio of thermal conductivity to specific heat), D is effective diffusivity, which is porosity times molecular diffusion coefficient, ΔC and ΔT are concentration difference and temperature difference for the layer, α is the linear expansion coefficient of fluid density change with respect to concentration (as salinity changes from the reference or base state (ρ_0 (0) at C(0)), and β is the linear expansion coefficient of fluid density change with respect to temperature.

Shales are usually good seals for hydrocarbons and barriers to fluid flow in sedimentary basins (Brace, 1980; Weaver et al., 1991; Aplin et al., 1999). However, under geopressured conditions and where fractures exist, shales can conduct flow comparable to that in the sandstone (Neuzil, 1986; Anderson et al., 1991a) and geopressure is a common phenomena in other sedimentary basins (Berlitz and Bredehoeft, 1988; Corbet and Bethke, 1992). In many other parts of the world, such as the Niger Delta and North Sea Tertiary basin, migration of petroleum through thick sequences of mudstones is a common and critical, but poorly understood phenomenon (Aplin et al., 1999). Previous studies have shown free convection can occur at low permeabilities (10^{-16}–10^{-18} m^2) that may approximate the permeabilities of shales in the zone of extreme overpressures over geologic time (Fenstemaker, 2000). Wooding et al.(1997) also studied the

possibility of density-driven free convection occurring across homogeneous low-permeability strata beneath playa lakes.

Shales are often treated as homogeneous very low-permeability media in analyzing subsurface flow and reservoir modeling. However, permeability variations exist because of mircrostructural differences (Olsen, 1962; Mitchell et al., 1965; Best and Katsube, 1993). Study by Neuzil (1994) showed how heterogeneous shales can be in terms of permeability. By synthesizing the best available laboratory and field permeability data, the log-linear relation between permeability versus porosity shows a wide range of about eight orders of magnitude for the natural argillaceous media (Neuzil, 1994). The study also indicated the scale dependence of permeability in argillaceous rocks could be small, which means the heterogeneity of permeability was created by inter-layering more permeable coarse-grained sediments.

The case of homogeneous shale layers containing vertical zones of higher permeability (one order of magnitude greater) shows earlier breakthrough of solute plumes compared to the homogeneous case without fractures (Fenstemaker, 2000). Heterogeneities in shale permeability enhance the potential for free convection at lower permeabilities. Schincariol et al. (1990, 1994, 1997) conducted numerical simulations incorporating heterogeneity in the permeability field and found that the mean, variance, and correlation length scales of the permeability were critical in the onset and subsequent growth or decay of

instabilities. Simmons et al. (1999b) used both stochastic and ordered permeability fields to study the instability of plume in the Murray-Darling saline water disposal basin of Australia. Recent study of unstable density-driven flow in heterogeneous porous media within a stochastic framework by Prasad and Simmons (2003) used a set of quantitative descriptors of instability to show that , as the degree of heterogeneity increases, the degree of free convection, as measured by the mean values of indicator variables, increases initially but decreases over longer time scales. These findings are due to the specific boundary conditions of the Elder problem when the bottom boundary is a no-flow boundary and solute accumulates at later time steps.

In studies of density-driven convection across low-permeability strata in the Gulf of Mexico Basin (Sharp et al., 1988, 2001; Fenstemaker, 2000), instabilities occur as downward plume fingers in the shale layer. Whether these plumes will pass through the layer or be killed inside the shale by heterogeneity is a question unsolved and important to understanding the basinal diagenesis (Bjorlykke and Palm, 1988; Land et al., 1997; Lynch, 1994, 1997) and fluid flow and solute transport in the context of both hydrogeology and petroleum maturation and migration.

Research objectives

Where a denser fluid overlies less dense fluid in heterogeneous media, instability may propagate downward along the highest permeability pathways. This study uses geostatistical models, numerical models, and patch analyses to 1) generate stochastic heterogeneous permeability realizations; 2) analyze the internal structure of each heterogeneous permeability field; and 3) examine heterogeneity controls on the onset and further development of free convection.

The hypotheses for my research are outlined as follows:

a. For density-driven flow through a single heterogeneous shale unit, the plume will find the highest permeability path, and the internal structure of the permeability field determines fluid flow and solute transport across low-permeability strata.
b. Vertical connectivity of the relatively high permeability zones controls and enhances free convection, while horizontal connectivity impedes or dissipates high-density plumes.
c. Connected high permeability patches are important in initiating the instability. The closer to the top boundary of the unit, the easier and sooner instability starts.
d. Boundary conditons are also important for the onset of free convection.
e. When shales are fractured, fractures are the preferential paths for convective flow, and free convection can occur inside the fractures.

f. Fracture aperture is the most critical factor for the onset of free convection. Permeability of the fracture and thickness of the layer are also factors affecting the initiation and development of free convection in fractured shale.

This study is important because convection could be an important mechanism for groundwater flow and solute transport through heterogeneous sediments in the basin. In addition to previous studies on free convection through homogeneous shales by Fenstemaker (2000), Sharp et al. (2001), and Simmons et al. (2003), this research examines free convection in heterogeneous geologic media that bridge the gap between totally random fields to regular or ordered heterogeneous media.

This dissertation uses numerical models to study salinity-driven free convection and to test the above hypotheses on heterogeneous shales at the macroscopic and microscopic scales. Shales are heterogeneous in that their permeability distribution and structure are strongly related to facies architecture and composition, bedding type, and grain size because of the different depositional environments and history. Shales are also heterogeneous when they are fractured by geologic processes, including hydrofracturing, and have fracture permeability several orders of magnitude higher than the matrix permeability.

The contents of the dissertation consist of two parts: the following two chapters (Chapter 2 and Chapter 3) are studies on heterogeneous unfractured

shale. Fractured shale is covered in Chapter 4. Chapter 5 summaries the results and evaluates the hypotheses.

The methodology is explained in Chapter 2, which describes geostatistical models to generate random distributions (realizations) of permeability using the Monte-Carlo technique for unfractured shales, numerical modeling of saturated flow and solute transport through heterogeneous shales, and patch analysis using percolation theory to analyze the internal structures of the permeability fields. First, sequential Gaussian simulation is explained to generate needed synthesized permeability fields that are log-normally distributed. These permeability distributions are not totally random, but have the same statistical characteristics, such as mean or standard deviation. The permeability realizations are the inputs for the numerical models for saturated flow and solute transport. Numerical modeling software SUTRA from the USGS is used for the two dimensional convection simulations. Analyzing the structure of the permeability distribution is carried out by patch analysis, which is based on a percolation search algorithm.

Chapter 3 describes the conceptual modeling scenarios for unfractured shale and illustrates modeling results from 2D SUTRA simulation of transient flow and solute transport. Different boundary conditions are incorporated into model scenarios and statistical and sensitivity studies are performed to examine the onset and further development of convective instabilities in heterogeneous layers. Defining and determining the threshold permeability and critical

permeability enable us to examine the general trends of convection occurring and development in heterogeneous low-permeability geologic units.

Chapter 4 studies the onset condition of free convection in smooth parallel-plate fractures. Due to the large aspect ratio of fracture aperture to height for a microfracture, the onset condition for free convection is different than that for the horizontally infinite layer. This part of the study finds that the two-dimensional fracture flow model is inappropriate for modeling free convection in dual porosity low-permeability media when the interaction between the fracture and matrix is not important or negligible. Also the study finds the critical Rayleigh Number can be approximated by a function depending only on the dimensionless aperture. Convection transport is occurring along the fracture plane and the pattern of convective cells observed from numerical modeling results on a cross-section perpendicular to the fracture plane is different than that on the fracture plane. Numerical modeling results from 3D SUTRA demonstrate the development of free convection along the fracture plane with contour axes parallel to the fracture aperture.

Finally, Chapter 5 summarizes the findings with respect to salinity-driven free convection through heterogeneous shales.

Chapter 2 METHODOLOGY

This research studies the onset and further development of free convection in heterogeneous low-permeability units. Heterogeneity describes how permeability values change with space in two or three dimensions in shales or mudstones. Study by Koltermann and Gorelick (1996) reviewed different methods used to simulate heterogeneity in sedimentary deposits because paucity of data of shale permeability (Aplin, et al., 1999; Neuzil, 1994; Dewhurst et al., 1999), flow systems, heterogeneity, and petrology/geochemistry unfortunately preclude most mapping or direct observational studies. Instead, stochastic simulations of heterogeneous permeability distribution and numerical modeling of fluid flow and solute transport are designed to achieve the goals of this study (Freeze, 1975; Chiles, 1999).

2.1 Stochastic modeling of shale permeability

Stochastic simulations of heterogeneous shale permeability are based on assumptions of log-normal distribution of permeability and Gaussian variograms (Webb et al., 1998; Yin et al., 1993; Clennell et al., 1999). There are two types of heterogeneous shale: unfractured and fractured shale.

2.1.1 Unfractured shale

Shale is a fissile mudstone composed of clay and silt, and has a predominant grain size less than 1/16 mm (62.5 μm) (Blatt et al., 1980; Katsube et al., 1991). Mudstones are sedimentary rocks comprising predominantly silt-sized (<62.5 μm) and clay-sized (<2 μm) particles lack fissility. Shales contain clay minerals, and also, in most cases, clay- and silt-sized quartz, feldspar and mica.

Shale permeabilities (Freeze and Cherry, 1979; Leroueil et al., 1990; Revil et al., 1999) can vary by as much as thirteen orders of magnitude. Neuzil (1994) collated the few permeability data for clays and mudstones that satisfy a range of criteria related to the quality of data (see Figure 2.1 and Figure 2.2). Background information for laboratory permeability data plotted in Figure 2.1 and inverse permeability estimates plotted in Figure 2.2 are included in Tables 2.1 and 2.2 respectively. Numbers 1 to 4 on Figure 2.1 represents permeability data of bottom mud deposits from the North Pacific region (Silva et al., 1981, 1984; Morin and Silva, 1984). Number 5 is from lacustrine clay of Sweden (Tavenas et al., 1983a, b). Shales in the Gulf of Mexico Basin are shown in Figure 2.1 as number 6 data (Bryant et al., 1975). Pierre Shale is number 8 (Neuzil, 1987, 1993). Number 7 is Sutherland Group data from Saskatchewan (Keller et al., 1989). Number 9 is for lower Cretaceous clayey siltstone from Western Canada (Young et al., 1964). Number 10 is for argillite from the Eleana Formation in Nevada (Lin, 1978). Number 12 is from Upper Triassic and Mid-Miocene clay and shale of Italy

(Neglia, 1979). Mudstone permeability in basin simulators is often expressed as a function of porosity. Figure 2.3 shows a compilation of permeability and porosity data for mudstone and shales(Dewhurst et al, 1995, 1998; Schlomer and Krooss, 1997; Katsube and Williamson, 1994, 1995). Examples from the Venture gas field (offshore Nova Scotia) give shale permeability as low as 10^{-22} m^2 at depth of 4-6 km (Best and Katsube, 1995). Shale permeability is controlled by pore-size distribution. In reality, mudstone pores have a wide distribution of diameters (e.g. Olsen 1962; Heling 1970; Borst 1982; Griffiths & Joshi 1989, 1990; Katsube & Williamson 1994a,b,c, 1995; Dewhurst et al. 1998). Mudstones exhibit a much wider grain-size distribution than sandstones, with grain diameters typically ranging over five orders of magnitude (Aplin et al., 1995; Dewhurst et al., 1998). Data from both geotechnical and geological literatures show that the mean pore throat diameter of muds declines with increasing depth or effective stress, typically reaching values of <10 nm at depths of 3-5 km (Dewhurst et al., 1999).

The transient pulse technique and consolidation test are most commonly used for the extremely low permeability measurements (Brace et al., 1968; Walls et al., 1982). Permeability k [L^2] is the ease with which a fluid can flow through a porous medium under a hydraulic gradient. It relates to hydraulic conductivity K [$L\ T^{-1}$], which is a coefficient defined in Darcy's Law as the rate of fluid flow q [L^3T^{-1}] per unit cross-sectional area A [L^2] and per hydraulic gradient $\boldsymbol{i}$ [L/L]:

$$K = \frac{Q}{A\nabla h} \qquad (2.1)$$

and

$$K = \frac{\rho g k}{\mu} \tag{2.2}$$

where ρ is fluid density [ML^{-3}]; k is the intrinsic permeability; and μ is dynamic viscosity [$MT^{-1}L^{-1}$] of the fluid; $\boldsymbol{g}$ is the acceleration of gravity [LT^{-2}].

Because of the limited permeability data for heterogeneous shales, the only way to generate enough data for subsurface flow study is by stochastic modeling. Stochastic model produces multiple outcomes based on the statistics of the data set. The reason to use stochastic model is that it faces the problem of data uncertainty and does not require a unique input variable because the values of subsurface parameters (such as permeability or porosity) can never be known perfectly.

Two-dimensional permeability realizations are generated by Monte Carlo simulations for shale in both the single layer model and the layer-cake model (Galloway and Sharp, 1998a,b; Davis et al., 1997) that are described below. The variogram is a statistical tool used to estimate the spatial variability of permeability (Goovaerts, 1997). It provides an estimate of the distance over which permeabilities are correlated, or alternatively, an indication of the absence of correlation in the data. Standard equation for the exponential variogram in one dimension is (Kitanidas, 1997):

$$\gamma(h) = 1 - \exp\left(-\frac{h}{\tau}\right) \tag{2.3}$$

where $\gamma(h)$ is the variogram defined as half the average squared difference between the paired permeability (k) values and is commonly used to describe the spatial continuity of a variable:

$$\gamma(h) = \frac{1}{2N(h)} \sum (k_i - k_j)^2 \tag{2.4}$$

where h is the lag and τ is the length parameter. It has an effective range 3τ defined as the distance at which the variogram value is 95% of its sill (the upper bound that a variogram can reach). A range (also called correlation range) is a finite lag distance at which a variogram reaches its sill and after which the autocorrelation becomes zero.

If a distribution is described as:

$$X \to N[\mu, \sigma] \tag{2.5}$$

where $X = \log(k)$, k is intrinsic permeability, μ is the mean, and σ is standard deviation. Using a transformation of $X = \frac{Z - \mu}{\sigma}$, the log permeability distribution is obtained based on a standard normal distribution of $Z \to N[0,1]$.

The anisotropy factor ($= \tau_x / \tau_y$) in the GSLIB software (Deutsch et al., 1997) takes into account of the fact that clay particles are mainly deposited and compacted in the horizontal direction (x axis) as most sediments are.

To study heterogeneity effects on the onset of free convection and its further development, multiple realizations of heterogeneous permeability fields

are generated for a given set of statistical parameters. An example of the synthesized permeability fields is illustrated in Figure 2.4 in which the mean and standard deviation are kept constant, but the internal structures of permeability distribution with respect to high permeability and low permeability locations are different. After stochastic permeability distributions are generated, they are taken as inputs to the variable-density flow model to examine how heterogeneity controls the onset of free convection and plume development in the low-permeability shale layer.

2.1.2 Fractured shale

Field-scale shale permeabilities are commonly greater than those measured on core plugs in the laboratory. For example, Bredehoeft et al. (1980) calculated a regional absolute permeability of 10^{-16} m^2 (about 0.1 millidarcy (md) or 10^{-4} m/day hydraulic conductivity) in the Pierre Shale, although Neuzil (1993) showed the matrix permeability of 10^{-20} m^2 at the laboratory scale. This implies that shales have a heterogeneous permeability structure influenced by fractures, faults, or the interlayering of more permeable coarser-grained sediments. Neuzil (1994) found that permeability was scale dependent in argillaceous media at only the largest regional scales, which he inferred was caused by the existence of widely spaced transmissive fractures. Walraevens and Cardenal (1999) inferred that preferential groundwater flow pathways through shallow buried, Tertiary

Bartonian Clay in Belgium exist based on the inconsistency between laboratory permeability tests and the distribution of hydraulic heads in the region. In many cases, the incipient pathways of fluid flow are present as faults, transecting the low permeability formations, or as interconnecting networks of smaller fractures or fissures (Horseman & Harrington, 1996)

Microfractures can form in shales when fluid pressures exceed the minimum principal stress and the tensile strength of the rock *in situ*. Wang & Xie (1998) carried out systematic numerical experiments to study the compaction-induced hydrofracturing commonly occurred in shale-rich basins and in sand-shale sequences. They showed that at vertical permeability of 10^{-18} m^2 and sedimentation rate greater than 50 mm/yr, compaction-induced hydrofracturing maybe a common process in shale-rich basins even at relatively shallow depths.

Capuano (1993) showed images of deeply buried fractured shale from the Oligocene Frio Formation of Texas with fracture fills of calcium sulfate and organic material. The samples were taken from cores at depths of 3-5 km. The Frio Formation consists of interfingered marine and nonmarine sandstones and shales, with the shales comprising about 80% of the section (Galloway et al., 1982). Two fracture patterns are observed in these shales, one is a series of anastomosing horizontal fractures; the other type is "blocky" with nearly horizontal and nearly vertical fractures that intersect at approximately 90°, but the horizontal fractures are approximately three times more frequent than the vertical

fractures. The calculated fracture permeability of the shales in this case is on the order of 10^{-13} m^2, which is the same as that of Frio sandstones. At a macroscopic scale, Cartwright (1994) documented extensive (>10^5 km^2) intra-formational polygonal fault systems which were first discovered in smectite-rich, Tertiary mudstones in the North Sea and have now been documented in mudstones from many sedimentary basins (Cartwright & Dewhurst, 1998; Dewhurst et al., 1999a). The faults system consists of densely packed, layer-bound, minor normal faults with throws from 5-100 m, average spacing of 200-500 m and fault traces are arranged in polygonal patterns in plan view. Vertically, the system is organized in tiers of stratigraphically bound layers of faults and separate tiers usually have distinct fault spacings, orientations and fault trace shapes (Lonergan et al., 1999).

Therefore, fractures (fractures, faults, fissures, etc.) in shales needed be considered in heterogeneous shale because their presence can greatly affect permeability and onset of free convection and dominate solute transport. Heterogeneity in fractured shales is modeled by having discrete parallel-plate fractures with large aspect ratios of aperture to height embedded in low-permeability matrix block. The permeability of an open fracture is quite high compared to the permeability for the surrounding rock. Detailed theoretical analysis and numerical modeling of convective transport through fractured shales are described in Chapter 4.

2.2 Analysis of heterogeneous permeability distribution

The weighted arithmetic mean is one measure used to analyze the structure of a permeability field generated from above for non-fractured shale (Hohn, 1988). The weighted arithmetic mean (M_j) of each column of the permeability field is defined as (Shi & Sharp, 2001):

$$M_j = \frac{1}{nz}\sum_{i}^{nz} W_i\left(-\log k_{ij} - \log k_{\min}\right) \tag{2.6}$$

Where *nz* is the total number of nodes in *z* direction; W_i is the weighting factor for the i^{th} row; *j* is the column number; k_{ij} is the permeability of each cell and k_{min} is the minimum *k* value of the permeability field.

Series of Monte Carlo simulations of different statistically equivalent permeability fields allow for statistical analysis of heterogeneity controls on salinity-driven free convection in shale.

2.3 Numerical modeling of density-driven flow and solute transport

In the past few decades, there have been abundant studies of variable-density flow and transport in porous media. Diersch and Kolditz (2002), Simmons et al. (2001), and Simmons and Sharp (2000) review the state of art in modeling

density-driven flow problems and illustrate future challenges of research on heterogeneity and large scale problems. Various studies employed different numerical models to model fluid flow and solute transport (Kolditz et al., 1998) and study benchmark problems for variable-density flow modeling (Elder, 1967; Henry, 1964; Simpson and Clement, 2003; Graf and Thierren, 2004), among which SUTRA (Voss, 1984) has been a popular tool for modeling saturated or unsaturated variable-density flow and solute transport (Voss and Souza, 1987; Simmons et al., 1997, 1999; Smith, 2004). It is a robust code that can model both free and forced convection in porous media by solving simultaneously coupled fluid flow and density caused by concentration variations. The equations solved by SUTRA are the fluid mass balance equation and the solute mass balance equation (see Appendix A). The code has been examined by Woods et al. (2003) with other numerical methods, such as the Crank-Nicolson FDM and the higher-order FDM. It has been found that the code is indeed numerically stable for all grid levels used in the study. Although the code has its limitations, i.e., a numerical dispersion error suggested by Woods et al. (2003), it's been widely used in groundwater modeling for salinity-driven flow systems (Voss and Souza, 1987; Simmons, et al., 1997, 2001; Sharp, et al., 2001). The purpose of using SUTRA is to model both transient fluid flow and solute transport processes through the low permeability shale layer and examine how the fingering of dense plumes develops in shale. Model sensitivity studies of spatial and temporal

discretizations have been conducted and grid convergence test helps to determine the suitable grid size to observe convective solute transport processes.

Model setup and modeling scenarios

Conceptual models for both unfractured heterogeneous shale and fractured low-permeability shale are set up accordingly based on different geometries.

2.3.1 Unfractured shale

Unfractured heterogeneous shale models include single-layer model and layer-cake model of interbedded sandstone and shales.

2.3.1.1 Single layer model

The first conceptual model is a single layer of shale with a heterogeneous distribution of permeability (Figure 2.5). The thickness of a shale unit in the sediment deposit sequences is based upon the study of Galloway et al. (1982) for the Frio Formation in the Texas Gulf Coast (Figure 2.6). Data from well logs show that the median shale thickness in coastal and alluvial assemblages is in the range of 10 meters to 30 meters (Figure 2.7). The average thickness of shale for the five facies assemblages (except shelf facies) is around 20 meters. A model domain of 300m long by 20m thick is set up with the left, right and bottom boundaries being no-flow boundaries. The top boundary has a constant

concentration of NaCl of 300,000 ppm (parts per million) which is equivalent to a *0.3* kg/kg when the base density of fluid is 1000 kg/m^3. This value is corresponding to the highest salinity data documented by McKenna and Sharp (1996) and McKenna (1997). Initial pressures within the model domain are hydrostatic, which is $p = \rho_0 gh$, and initial concentration of the fluid in the domain is set to zero everywhere except the upper boundary. The specified pressures at the bottom two end corners are hydrostatic and they are the only points that allow flow in or out. Key parameters used for this study are shown in Table 2.1 (after Fenstemaker, 2000). The spatial discretization takes into account of the concepts of boundary layer thickness (Wooding et al., 1997) and aspect ratio in order to use the Rayleigh number criteria to predict free convection in each grid cell (Weatherill et al., 2004). The vertical step is chosen to be greater than the boundary layer thickness (δ) of 0.315 m and aspect ratio (A = X/Y) greater than or equal to 1 for which the critical Rayleigh number is $4\pi^2$ for a single homogeneous cell. Therefore, the model with dimensions of 300 m by 20 m is discretized with horizontal step of $\Delta x = 1.0\ m$ and vertical step of $\Delta y = 1.0\ m$ respectively, which gives a total number of elements of 6000. Total simulation time for flow and solute transport is set for 20 years because of model size and computation time. But for some cases, a longer time period of 3000 years has also been used to examine if the fingers developed during the 20 year period continue to percolate and reach the bottom of the layer.

For spatial discretization scheme used in this model, a grid resolution test was performed to see if better results would be obtained with finer grids. The grid for most of the modeling work shown in this study has a total of 6000 elements (300 horizontal and 20 vertical). Finer grids with twice amount of the elements showed no significant improvement in the number of instabilities and penetration depth of the plumes (see Figures 2.8 to Figure 2.11). Therefore, the current mesh with 6000 elements is acceptable for our modeling purposes and for patch analysis. To overcome the problem of non-convergence for some realizations at higher standard deviation of permeability, both the longitudinal and transverse dispersivities are tested and increased from 0 to values on the order of the element size of 1 meter (as suggested by Prasad and Simmons, 2003, based on their numerical modeling test).

Stochastic modeling and statistic analysis requires sets of simulations for each set of parameters, so that a batch processing of the model runs and plotting of modeling results was required. DOS batch programming is applied to run preprocessing, post-processing and SUTRA processes under WINDOWS. Plotting of the modeling results of solute concentrations, velocity, and pressure changing with time, permeability fields, and patch analysis results are carried out using SURFER 8^{TM} automation scripts.

2.3.1.2 Layer-cake model

Sediments in Texas Gulf Coast Basin consist of inter-fingered marine and non-marine sands and shales. Sands or sandstones are usually more permeable than shale. Sandstone permeability is on the order of 10^{-12} m^2 (Fetter, 2001). Free convection would occur more readily in sands because of the high permeability and large Rayleigh number. For a sand-shale layer-cake model assembling the inter-bedded sequences of sand and shale, sands can be treated as homogeneous considering the frequency of free convection happening so that we can focus on studying free convection through heterogeneous shale.

Model setup (Figure 2.12) is the same as the single layer models in terms of geometry and source location, but the boundary conditions differ. The bottom of the shale layer is a high permeability sand layer. Flow is attracted into sand across the boundary and the bottom of sand layer now is the no-flow boundary. There are two conceptual models for a sand-shale sequence system in which: 1) shale overlies the sand layer; and 2) sand lies both on top of and beneath the shale layer.

2.3.2 3D fractured shale model

Free convection occurring in single discrete fractures embedded in a 3D shale system is discussed in detail in Chapter 4. Model scenarios inlcude macro-

scale fracture and micro-scale fracture with shale matrix permeability on the order of 10^{-18} m^2.

2.4 Percolation and patch analysis

The standard theory of percolation (Broadbent and Hammersley, 1957; Frisch and Hammersley, 1963; Stauffer, 1985) originated from statistical physics and has been shown to have applications to a broad variety of problems in hydrogeology (Berkowitz and Balberg, 1992, 1993; Berkowitz, 1994, 1995) and petroleum engineering (Zhou and Stenby, 1993; Larson et al., 1981). If a fluid flows through a medium, which is itself in some sense disordered (or random), the flow through the system may be described by a percolation process. Most real systems possess a much less "ordered" network, and a distribution of k permeability values. For example, groundwater flow in real porous media, fractured rocks, and other geological and hydrological systems.

Percolation theory describes the relation of connectivity of the elements (microscopic) of the system to the physical properties (macroscopic, such as hydraulic conductivity and porosity) of the entire system. A porous medium can be considered or idealized to be a network of sites and bonds arranged as shown in Figure 2.13. The bonds represent the pore throats and the sites, pore bodies of the medium. Any two sites/nodes are considered "connected" only if there is continuous path of bound sites (open to flow) between them. Obviously, a

connected path allows the flow from one end of the system to another. The connectivity of the pores in a medium is defined as the node number, which indicates how many pores directly connect to each other. Percolation theory shows that there is a threshold value, p_c, of fraction of pores necessary to form a continuous path from one side of the medium to the other. This threshold value depends on the node number and the dimensions of the medium. The dimensions of the model used to study flow across shale zones in sedimentary basins are large enough to be considered as almost infinite compared with the pore scale. Therefore, the threshold value is only a function of node number. A basic assumption of percolation theory is that the site occupation process is random, which means the occupation of one site is independent of occupation of its neighbors or of any other site. This assumption is not applicable to solute transport process in porous media, but the invasion percolation theory is appropriate for the study of solute transport in heterogeneous media. The invasion percolation automatically finds the critical points of the system because it explicitly takes into account the transport process taking place and it may be applied to any kind of invasion process that proceeds along a path of least resistance. The percolation threshold values are the same as in ordinary percolation theory (Wilkinson & Barsony, 1984). In the case of density-driven flow problems, invasion percolation theory (Wilkinson and Willemsen, 1983)

provides a way to characterize plume development along the most permeable (least resistance) pathways in shales.

Let p represents the probability that a node is occupied (open to flow), statistic study shows that with increasing p, the probability of finding larger clusters increases and there will be a p value that is sufficiently large to ensure that at least one cluster connects the bottom and top ends of the system, this cluster (group of connected sites) is called the percolation cluster, so p_c is the critical value of p.

$$p = \frac{N}{N_0} \tag{2.7}$$

where N is the number of nodes open to flow and N_0 is the number of total nodes) above which fluid will reach the outlet of the system. Values of p_c for different systems can be obtained by Monte Carlo simulations (Stauffer, 1985; Djordjevic et al., 1982; Wilkinson & Barsony, 1984).

The internal structure of any heterogeneous permeability field is critical in predicting fluid flow and solute transport through the medium (Gueguen et al., 1991, Casting et al., 2002). Statistically equivalent permeability fields have different behavior depending upon available permeability pathways open to flow. The spatial locations of connected high permeability pores or conduits/fractures relative to the top boundary in the model are critical in initiating instability, and connectivity of these high permeability zones is crucial to the sinking of dense

saline water through shales. Only zones consisting of high permeability elements can act as fluid pathways and enhance plume development downward. Finding these elements and studying how well they are connected is the first step in analyzing the internal structure of a permeability field.

Invasion percolation theory is applied in this study by defining the connectivity of the system, which is an important factor in controlling fluid flow through and across the shale layer. By finding the connectivity of each permeability field generated stochastically, a prediction is made as to whether convection occurs and how the plumes develop afterwards within the layer. The heterogeneous permeability field is generated on a discretized grid system and each permeability value is recorded at the center of each grid cell. The equally discretized model becomes a square lattice system and the percolation threshold can be found for such a system. It is convenient to transfer the whole grids in the system to a numerical model modeling flow and solute transport to evaluate the predictions made from percolation theory.

Patch analysis borrows the concepts from percolation theory and analyzes the spatial statistics of delineated high-permeability patches from SUTRA modeling results. This is a new way to characterize the heterogeneity effects on dense "fingering" plumes penetrating the heterogeneous layer.

When applying percolation theory, the first step is to determine the site occupation probability p and search for percolation clusters. Each permeability

field is analyzed to find the maximum and minimum values of permeability (Shi and Sharp, 2003). An automatic search algorithm is developed to find sites open to flow and find connected pathways. The site occupation function $\Gamma(k)$ is then defined as a step function:

$$\Gamma(k) = \begin{cases} 1 & (open\ \ to\ \ flow) \qquad if \quad k > k_t \\ 0 & (close\ \ to\ \ flow) \qquad if \quad k < k_t \end{cases} \tag{2.8}$$

where k_t is called threshold permeability, above which the instabilities are seen as connected patches. We define k_c as the critical permeability above which at least one percolation cluster connects one boundary to the opposite side. Critical permeability is the permeability value that forms a continuous flow pathway so that fluid and solute can convect to the bottom layer.

After occupation analysis, the system becomes a "binary" system with cells being 1 or 0. The occupation probability p of the system can be calculated as a ratio of the number of grid cells open to flow to the total number of mesh elements. Patch analysis searches the whole mesh to find high permeability cells and group the connected cells into different single patches. The searching algorithm is a directional search, basically looking in 4 directions adjacent to the current cell (Figure 2.13).

Percolation clusters are analyzed to obtain horizontal (C_x) and vertical (C_y) connectivity indices, which are defined as follows for each high permeability patch within the field:

$$Cx(j) = \frac{\max(Lx(1), Lx(2), \cdots Lx(M(j))}{NX} \times \frac{\sum_{i=1}^{M(j)} Lx(i)}{M(j) \times NX} \qquad \in [0,1] \qquad (2.9)$$

and

$$Cy(j) = \frac{\max(Ly(1), Ly(2), \cdots Ly(N(j))}{NY} \times \frac{\sum_{i=1}^{N(j)} Ly(i)}{N(j) \times NY} \qquad \in [0,1] \qquad (2.10)$$

where *M(j)* is the total rows in the j^{th} patch, *Lx(i)* is the length of the i^{th} row, *N(j)* is the total columns for the j^{th} patch, *Ly(i)* is the length of the i^{th} column, *NX* is the number of elements in the ***x*** direction, *NY* is the number of elements in the ***y*** direction. The first term in both equations calculates the maximum penetration length and the second term calculates the spreading effect perpendicular to the direction of finger penetration.

Table 2.1 Background information for laboratory permeability data plotted in Figure 2.1 (adapted from Neuzil, 1994)

Number	Formation	Lithology	Type of Test	Number of measurements	Source
1	bottom deposit (North Pacific)	bottom mud (illite, smectite)	mechanical transient, steady flow, and quasi-steady flow (seawater)	48	Silva et al. (1981)
2	bottom deposit (North Pacific)	bottom mud (illite, smectite)	steady flow (seawater)	19	Morin and Silva (1984)
3	bottom deposit (North Pacific)	bottom mud (illite, chlorite)	mechanical transient, steady flow, and quasi-steady flow (seawater)	26	Silva et al. (1981)
4	bottom deposit (North Pacific)	bottom mud (illite, chlorite)	steady flow (seawater)	22	Morin and Silva (1984)
5	Pleistocene to Recent (Quebec, Mississippi Delta, Sweden)	marine and lacustrine clay	steady flow and quasi-steady flow (natural pore water and distilled water)	600	Tavenas et al. (1983)
6	Gulf of Mexico	unconsolidated sediment, varing proportions of clay, silt, and sand	mechanical transient (seawater)	250	Bryant et al. (1975)
7	Sutherland Group (Saskatchewan)	glacial till (montmorillonite, illite, kaolinite)	mechanical transient and quasi-steady flow (natural pore water and distilled water)	27	Keller et al. (1989)
8	Pierre Shale (central South Dakota)	claystone (mixed layer, montmorillonite, illite)	mechanical transient, hydraulic transient, steady flow (pore water duplicate and distilled water)	85	Neuzil (unpublished data, 1987)
9	Lower Cretaceous (Western Canada)	clayey siltstone, clayey sandstone	steady flow (3.5 and 5.8% sodum chloride)	25	Young et al. (1964)
10	Eleana Formation (Nevada)	argillite (quartz, illite, chlorite, kaolinite)	hydrualic transient	23	Lin (1978)
11	(Japan and Alberta, Canada)	mudstone, sandy mudstone, siltstone, shale		33	Magara (1978)
12	Upper Triassic, Mid-Miocene, Lower Pliocene (Italy)	clay, shale		8	Neglia (1979)

Table 2.2 Background information for inverse permeability estimates plotted in Figure 2.2 (adapted from Neuzil, 1994)

Number	Formation	Lithology	Type of Analysis	Vertical and Horizontal Dimensions	Source
1	(Barbados Accretionary Ridge complex)	clay, calcareous mudstone	transient flow	1 and 15 km	Screaton et al. (1990)
2	Sutherland Group (Saskatchewan)	glacial till (montmorillonite, kaolinite)	transient flow	<50 and ~10m	Keller et al. (1989)
3	Pierre Shale (central South Dakota)	claystone (mixed layer, montmorillonite illite)	transient flow	0.3 and >1 km	Neuzil (1993)
4	Colorado Group and Upper Manville Shales (Alberta)	claystone, shale	transient flow	0.5 and >100 km	Corbet and Bethke (1992)
5	Gulf of Mexico	clay, shale	transient flow	10 and > 300 km	Bethke (1986)
6	Pierre, Carlile, Graneros Shales (Denver Basin)	claystone and shale	steady state flow	3 and 800 km	Belitz and Bredehoeft (1988)
7	(Siberia)	argillaceous rock	transient flow		Nesterov and Ushatinskii as reported by Brace (1980)

Table 2.3 Parameter values used for the single layer model.

	meaning	value
D	molecular diffusivity (m^2/s)	1.0×10^{-9}
ε	porosity	0.15
ν	kinematic viscosity (m^2/s)	1.0×10^{-3}
$\rho_0^{-1}(\partial\rho/\partial C)$	coefficient of density variation	0.7
α	fluid compressibility ($kg\ s^2/m$)	4.5×10^{-10}
β	matrix compressibility ($kg\ s^2/m$)	1.0×10^{-8}
α_L	longitudinal dispersivity (m)	1.0
α_T	transverse dispersivity (m)	1.0

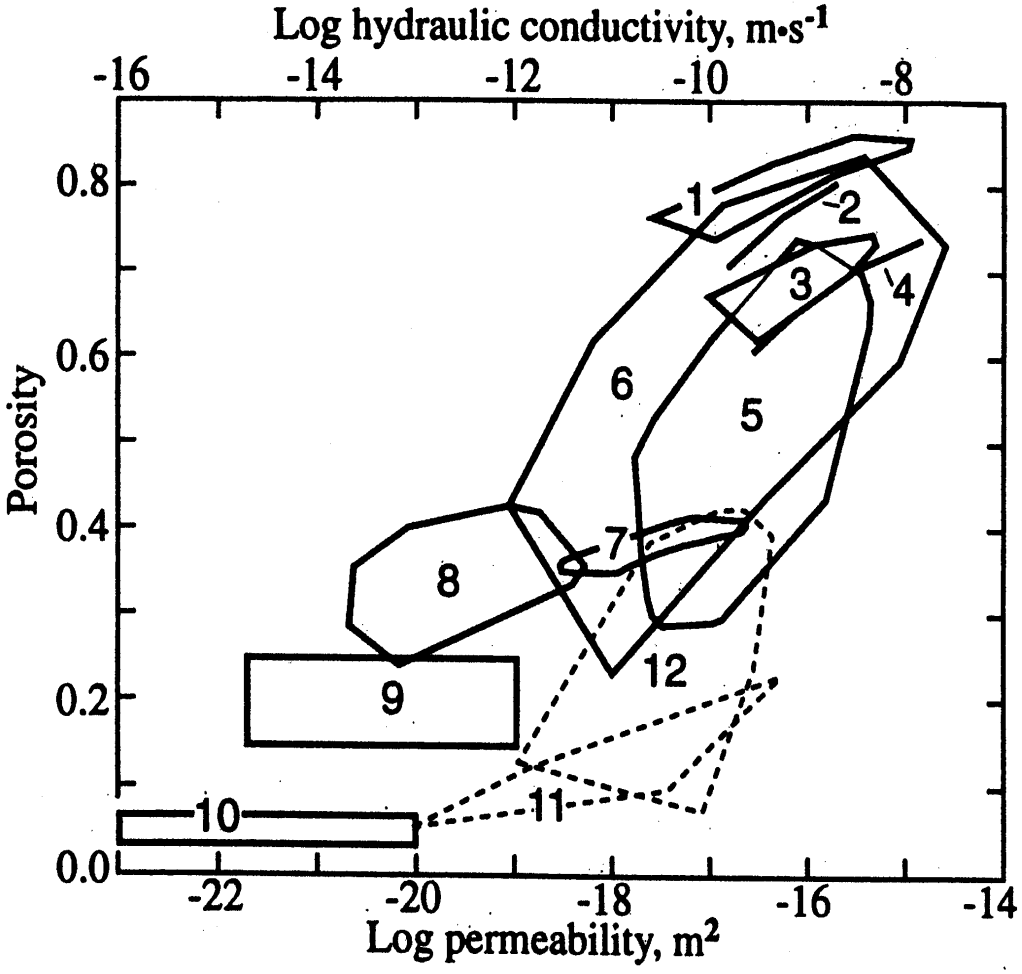

Figure 2.1 Permeability data versus porosity for a variety of shales from laboratory measurements (Neuzil, 1994). Numbers represent source of data. Top axis shows corresponding hydraulic conductivity.

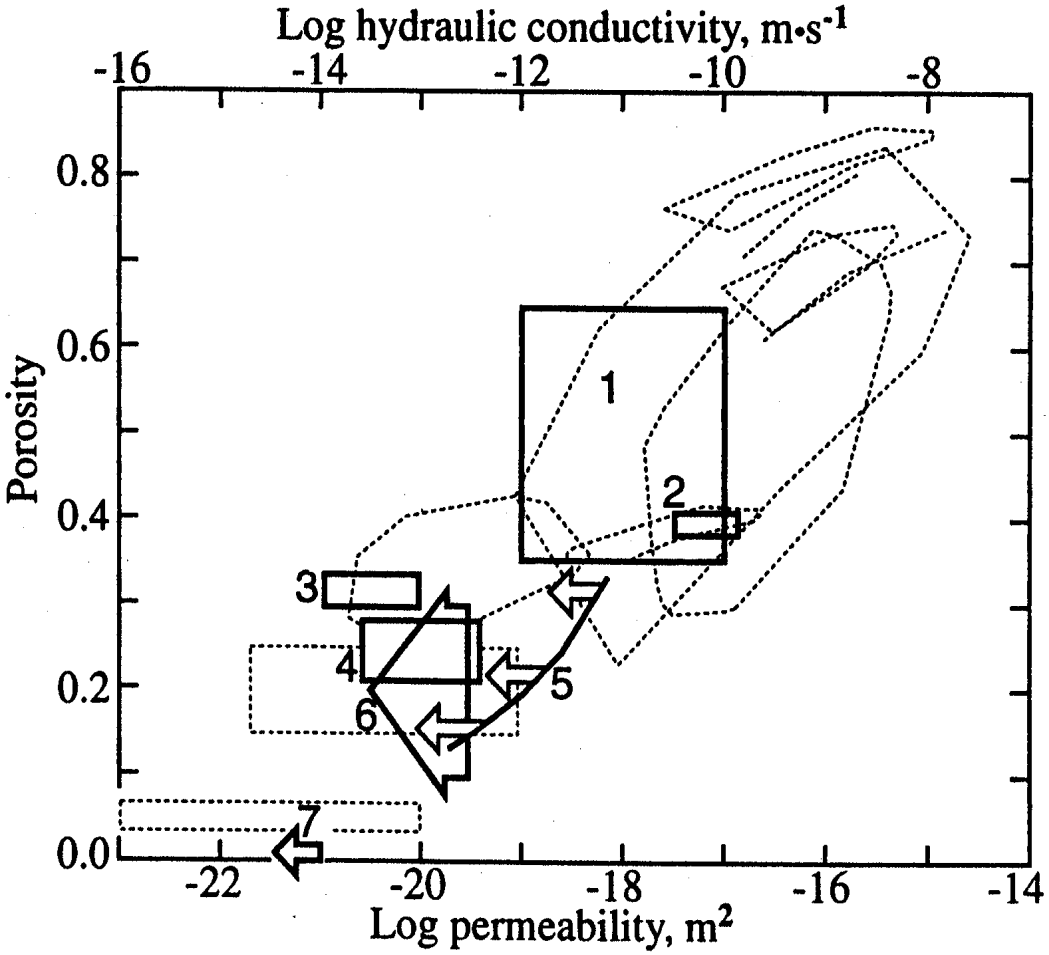

Figure 2.2 Shale permeability data versus porosity from inverse analyses of flow systems on large scale (Neuzil, 1994). Numbers indicate sources of data and the top axis shows corresponding hydraulic conductivity. Dotted lines correspond to regions/numbers plotted on Figure 2.1.

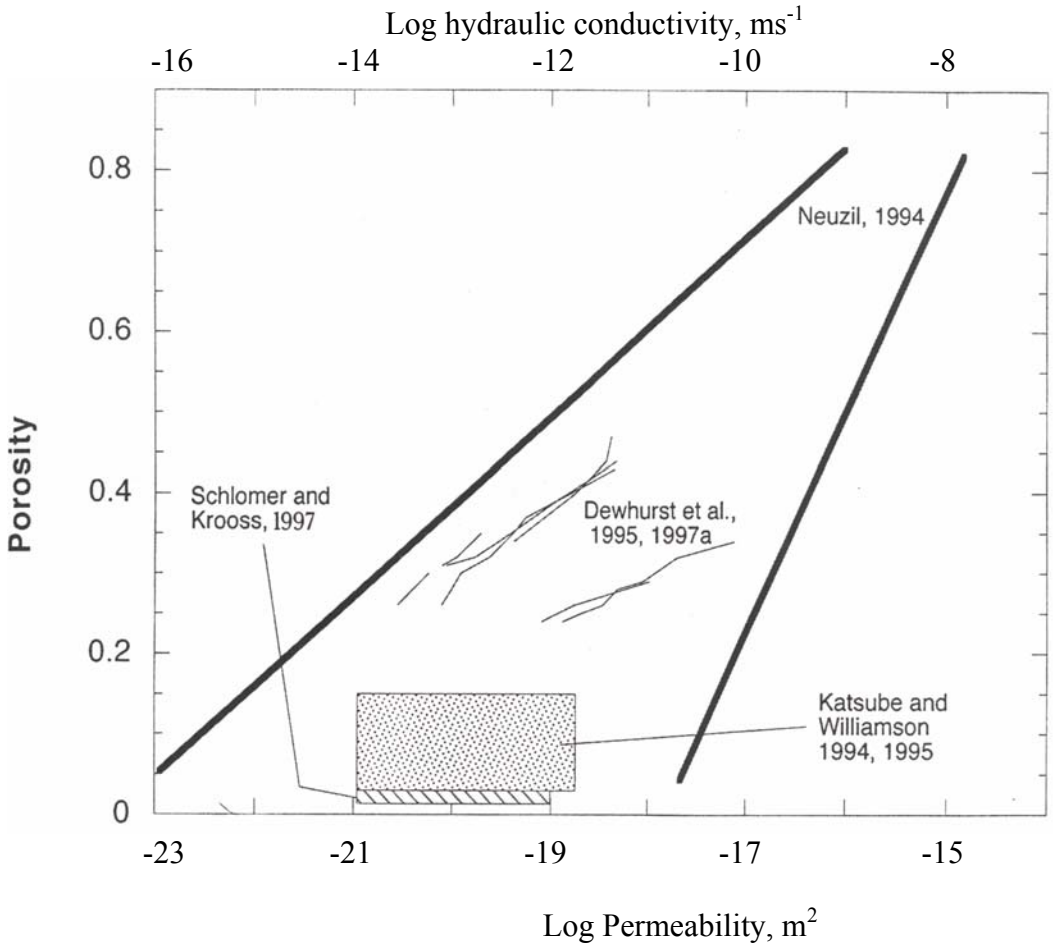

Figure 2.3 Range of published porosity-permeability data for shales and mudstones (Dewhurst et al., 1999). The two bold lines define the range of values published by Neuzil (1994).

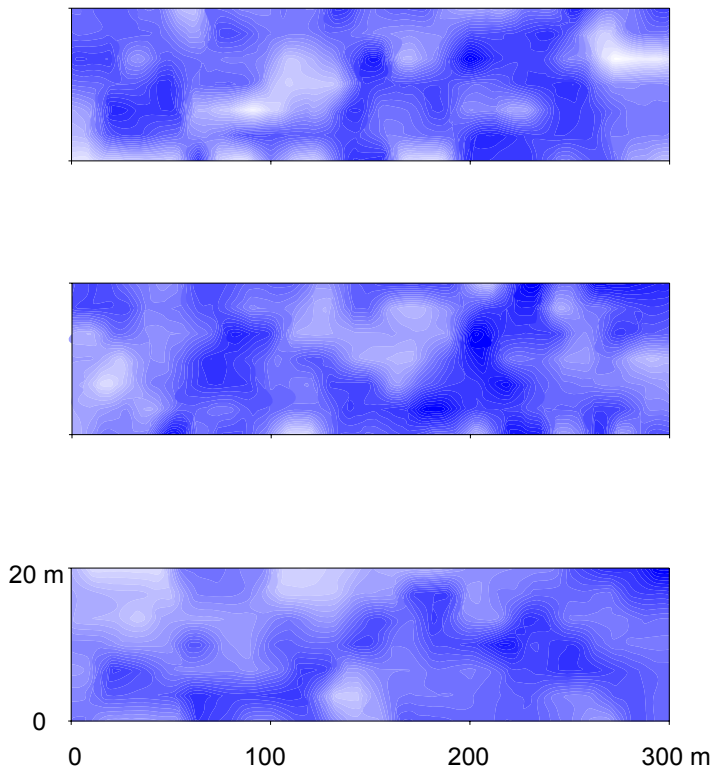

Figure 2.4 Simulated permeability distributions of shales for the same set of statistical parameters: mean $\mu = 10^{-16}$ m^2, standard deviation $\sigma = 2.0$, and horizontal correlation length $\tau_x = 300$ m and vertical correlation length $\tau_y = 1.5$ m. Vertical exaggeration is about 3. Light color represents high permeability and dark blue color stands for low permeability.

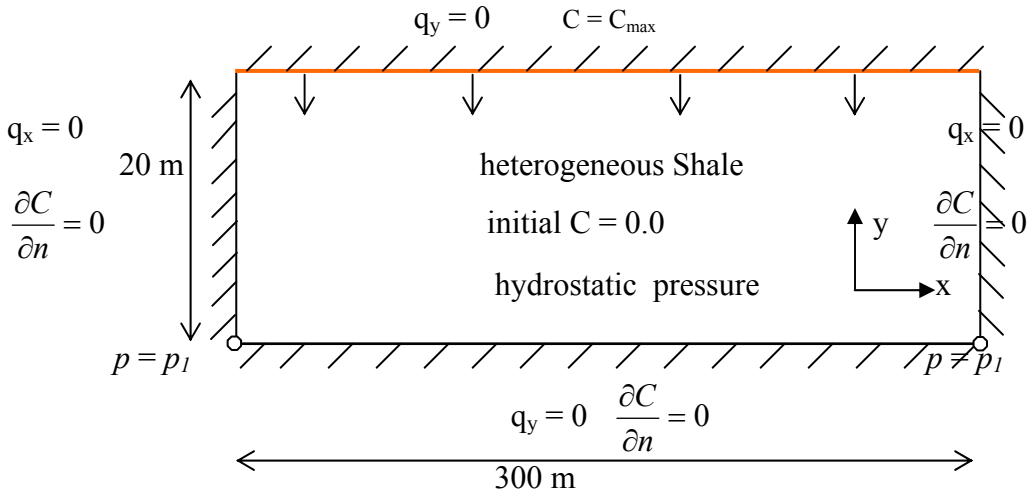

Figure 2.5 Single heterogeneous layer model of shale.

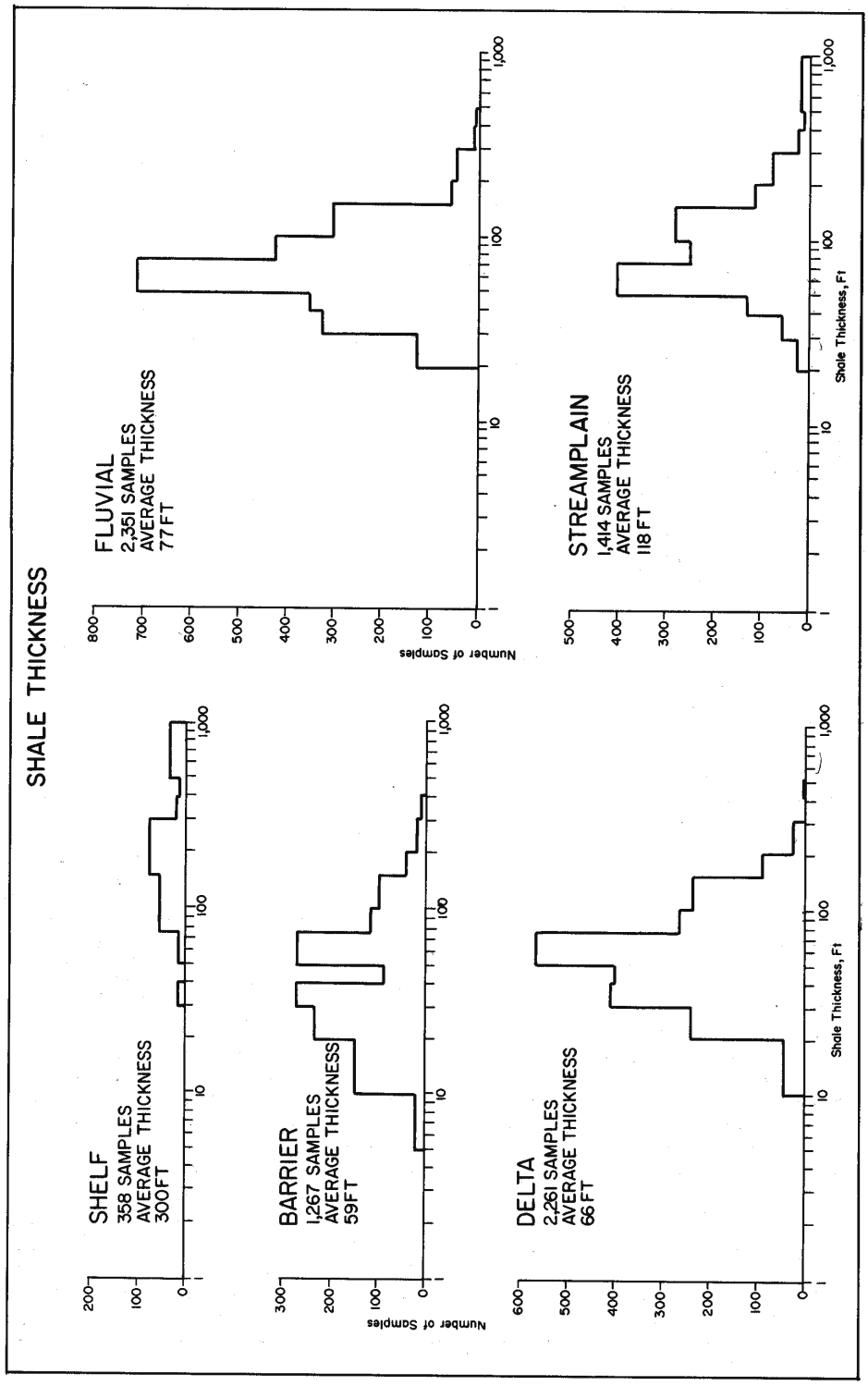

Figure 2.6 Distribution of shale thickness data for the five facies assemblages of the Frio Formation (Galloway et al., 1982).

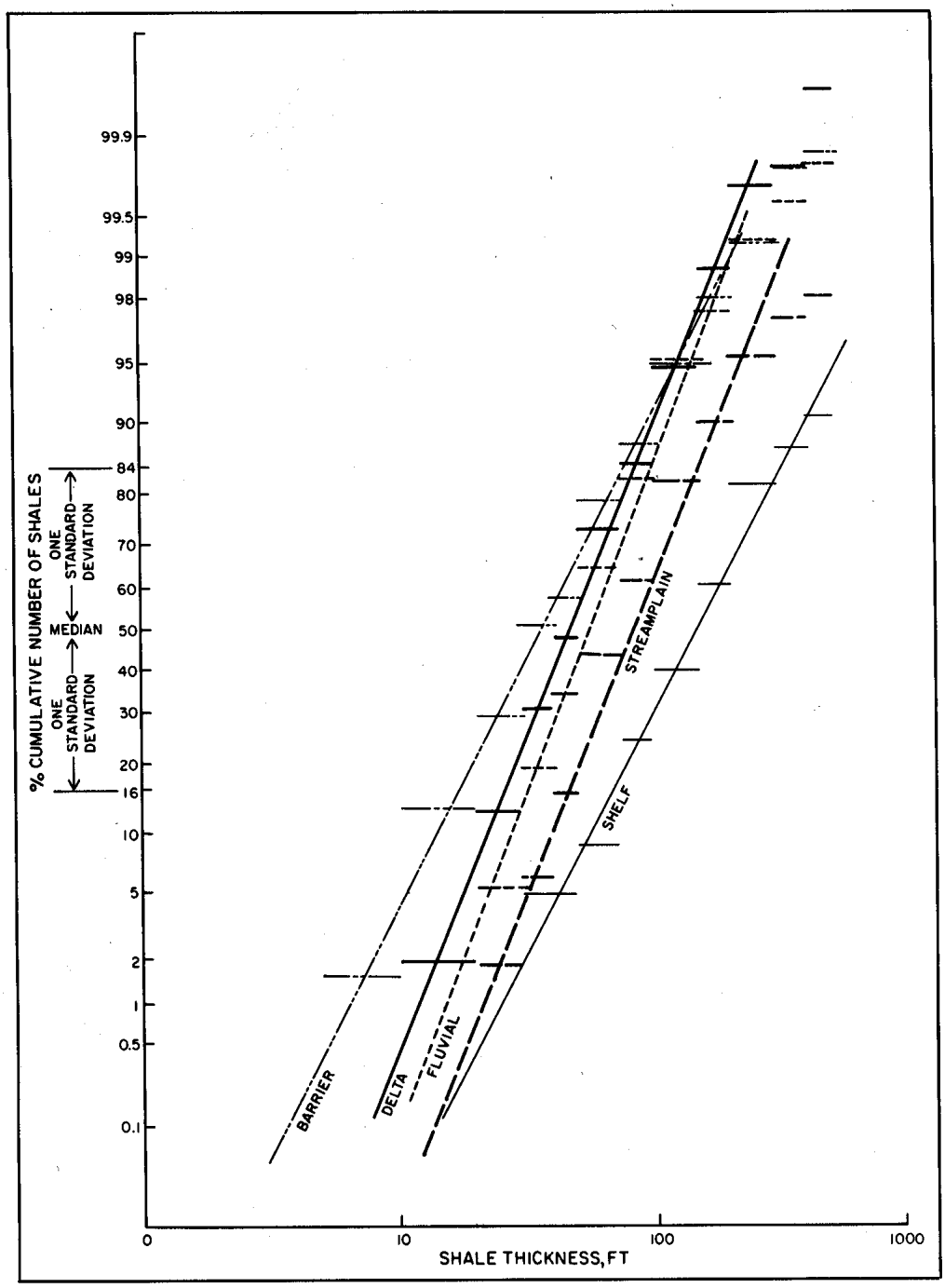

Figure 2.7 Statistics of shale thickness for the five facies assemblages shown in Figure 2.6 (Galloway et al., 1982).

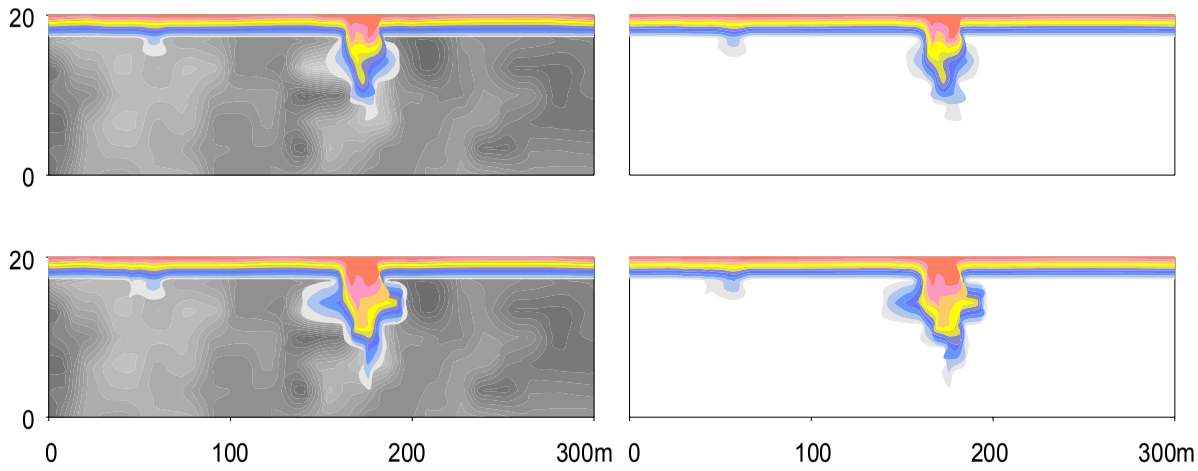

Figure 2.8 Grid resolution study of different discretization on plume development. Left model used 12000 elements, while right model used 6000 elements. Simulation times are 2 months (top) and 1 year (bottom). C_{max} = 1.0 on the top boundary (red color). Vertical exaggeration is about 4.5.

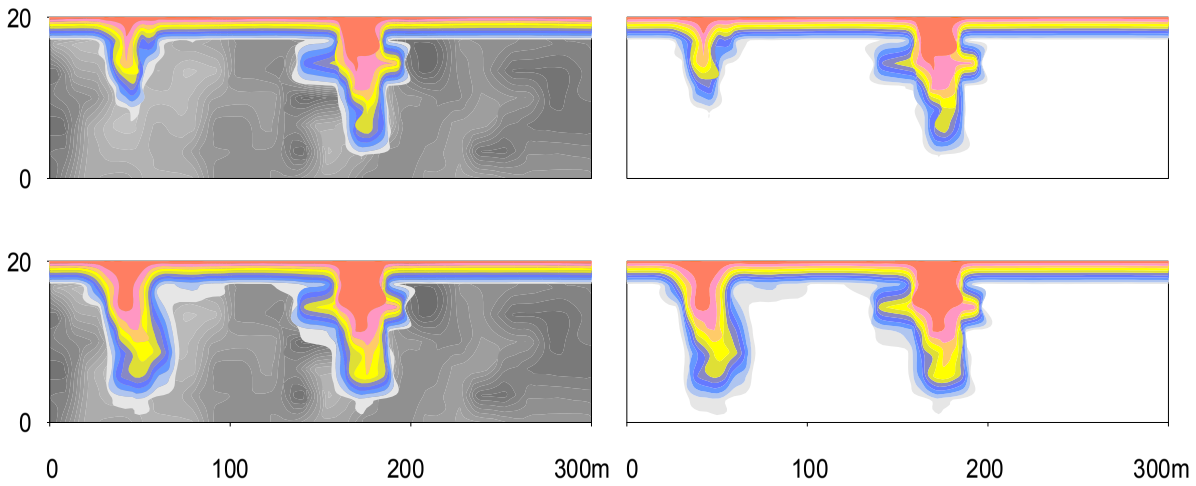

Figure 2.9 Grid resolution study of different discretization on plume development. Left model used 12000 elements, while right model used 6000 elements. Simulation times are 5 years (top) and 14 years (bottom).

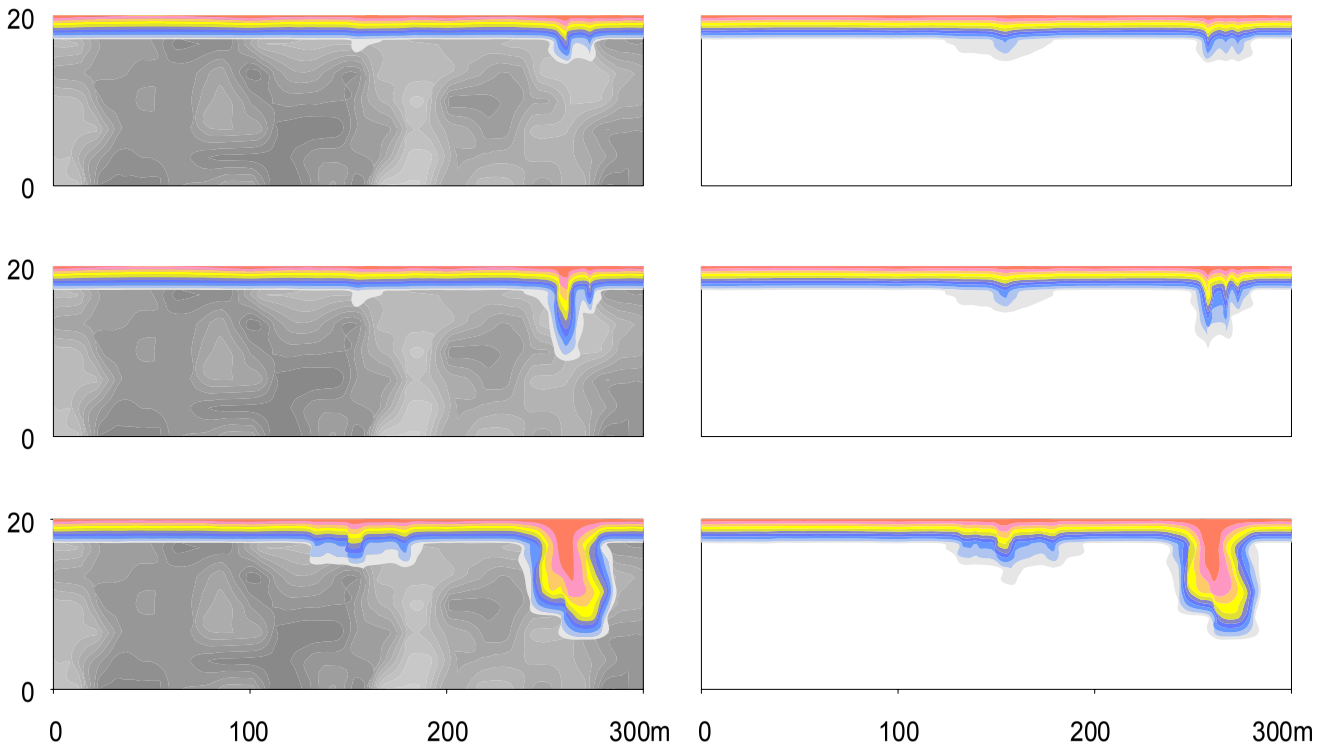

Figure 2.10 Grid resolution study of different discretization on plume development. Left model used 12000 elements, while right model used 6000 elements. Simulation times are 2 months (top), 4 months (middle), and 2 years (bottom).

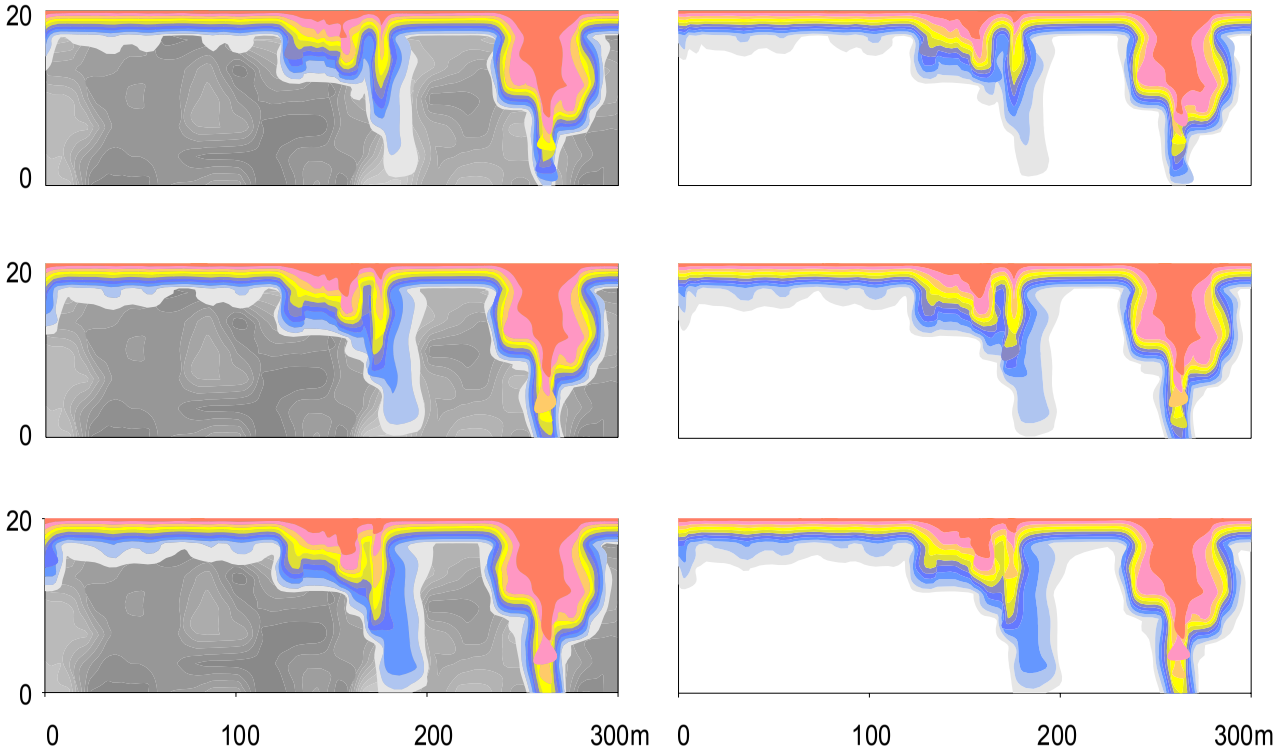

Figure 2.11 Grid resolution study of different discretization on plume development. Left model used 12000 elements, while right model used 6000 elements. Simulation times are 12 years (top), 16 years (middle), and 20 years (bottom).

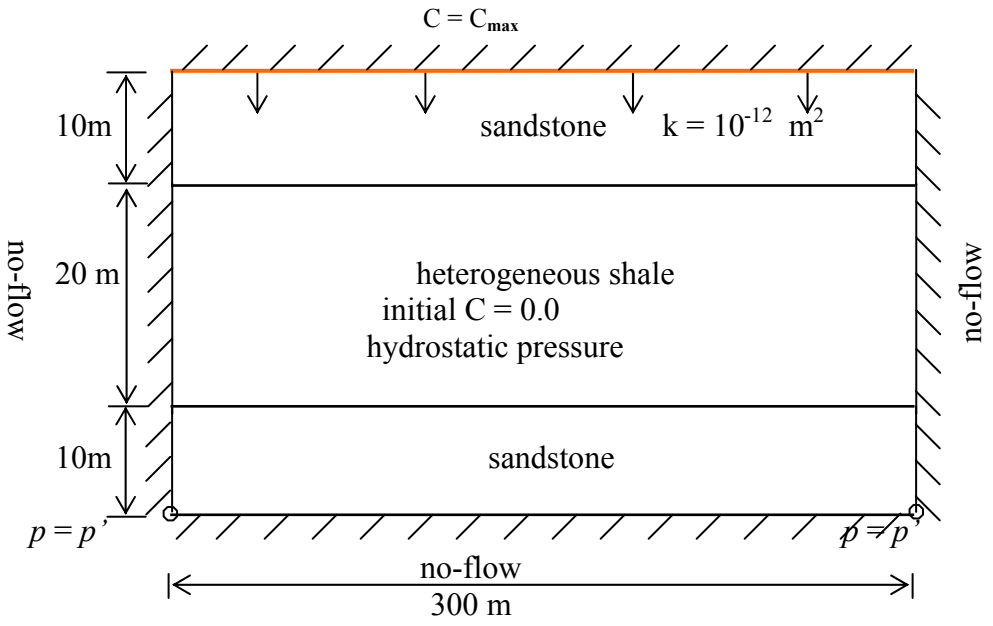

Figure 2.12 Geometry, initial and boundary condition for sand-shale model.

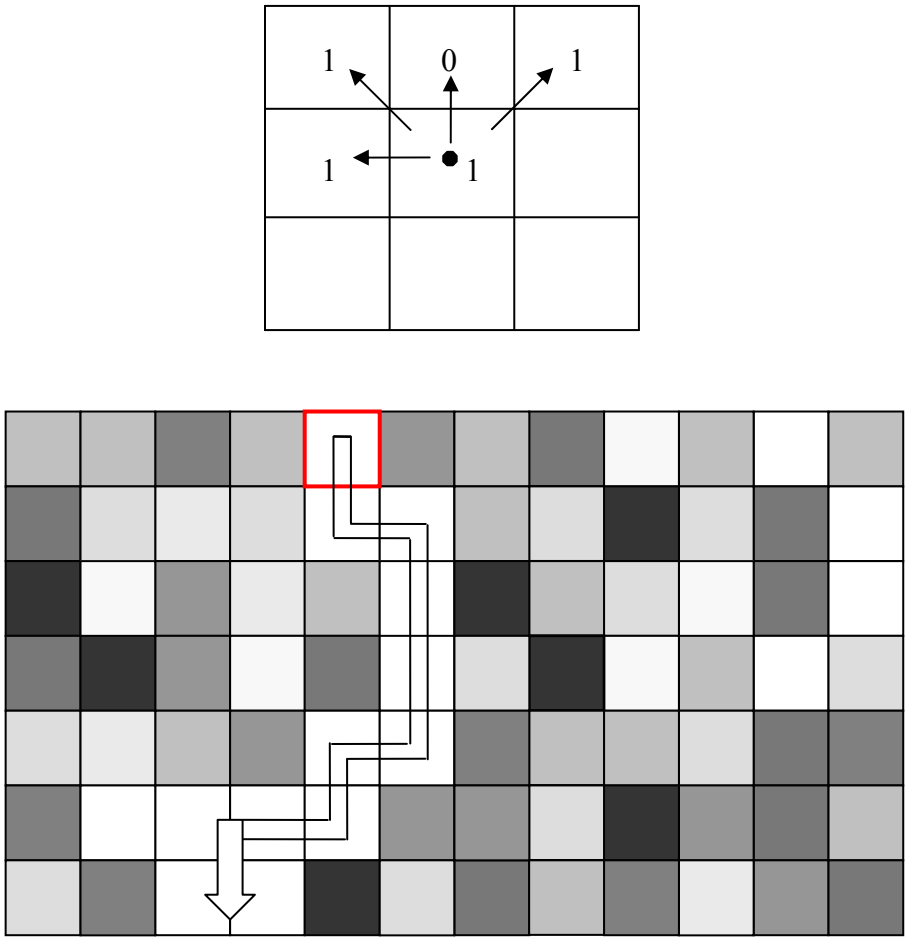

Figure 2.13 Directional searching for connected patches (upper) and a percolation cluster (lower) showing a connected pathway from top to bottom with the threshold permeability being highlighted. Darken grids denote lower permeability.

CHAPTER 3 DENSITY-DRIVEN FREE CONVECTION IN HETEROGENEOUS UNFRACTURED SHALE

Analytical solutions for the onset conditions of density-driven free convection in heterogeneous media are mathematically obtainable only for simple geometry and boundary conditions (Nield and Bejan, 1999; McKibbin and O'Sullivan, 1980; Malkovski and Pek, 1999). Numerical modeling for convective flow and solute transport through shales with quite heterogeneous permeability distributions are described in this Chapter. The purpose is to test whether or not free convection could occur in extremely low-permeability shales, such as in the Gulf of Mexico Basin, and whether permeability heterogeneity stops free convection or promotes it. The modeling scenarios focus on low permeability shales (10^{-17} m^2) which are different from those described in previous work by Prasad and Simmons (2003) (on the order of 10^{-13} m^2) and Schincariol et al. (1997, 1998) (on the order of 10^{-11} m^2). In addition, models with different geometry and boundary conditions include sands above and below a heterogeneous shale layer and are thus different from the Elder problem. These models are more appropriate for applications to the sediments in sand-shale sequences, such as in the Gulf of Mexico Basin. This study extends previous study by Sharp et al. (2001), Simmons et al. (1999), and Prasad and Simmons (2003) with regard to how permeability heterogeneity controls the onset and

development of free convection and instabilities. In addition, patch analysis examines the internal structure and connectivity of the permeability field by delineating connected high-permeability patches based on threshold and critical permeabilities.

3.1 Heterogeneous layer model

The Rayleigh number for a homogeneous layer is directly proportional to the concentration difference between the source and the ambient fluid in the layer. Therefore, testing concentration change effects on the onset of free convection is equally important for heterogeneous medium. Usually concentration of chloride in groundwater is measured in parts per million (ppm) which needs to be converted to a ratio of the mass of solute to the mass of fluid in kg/kg. For a solute concentration of 200,000 ppm found in the salinity inversion profile (Sharp, 1988; McKenna and Sharp, 1996), the equivalent concentration is about 0.2 kg/kg at a temperature of 25°C.

Results of concentration distribution from SUTRA show that concentration differences between the dense fluid and less dense fluid can affect the onset of free convection and the plume development, but that the basic patterns of the dense plumes are the same if the permeability structures are the same (Figure 3.1). Modeling results of solute transport in Figure 3.1-3.2 demonstrate the same plume pattern for different concentration distributions in two model setups. One model

in Figure 3.1(top) with a maximum concentration of 0.2 kg/kg at the top boundary has fingering penetration to a depth of 4 meters below the surface at about 5 years, while it takes the other model (bottom) with a maximum concentration of 1.0 kg/kg about 7 months to reach the same depth. Fingers developed within these two models are almost the same and therefore the shape, location and propagation of the fingers are mainly controlled by the structure of the permeability field. Figure 3.2 shows two major fingering plumes developed; one reaches the bottom of the layer about 5 years after the simulation starts. It takes about 20 years for the model with C_{max} = 0.2 to reach the bottom. Therefore, to save computation time and effort, "blow up" the dense plumes, and speed simulation scenarios, a unit concentration is chosen for modeling purposes. This affects primarily the time for finger breakthrough but not the conclusions drawn later in this chapter. Choosing a unit concentration is also consistent with the studies of the Elder problem by Prasad et al. (2003), Simmons et al. (2001), and Woods et al. (2003).

3.2 Sensitivity analysis

Statistical studies using different means, standard deviations, and correlation lengths in the permeability distribution demonstrate the "general" effects of permeability heterogeneity on the onset of free convection and finger plume development in low-permeability layers. Each set of model scenario consists of 30 or 60 realizations of the permeability field. Sensitivity analysis results are

generally consistent with what others have found with respect to the onset of free convection under different permeability fields (e.g., Schincariol et al, 1997; Sharp et al, 2001; Simmons et al, 2001; Prasad and Simmons, 2003). However, the system geometry and boundary conditions used in our study are different from previous studies and our models are for low-permeability fields with permeability values of 10^{-14} to 10^{-23} m^2. These analyses show new findings with respect to the onset and percolation of free convection in heterogeneous medium because of different boundary conditions and using different indicators, such as threshold permeability and critical permeability.

3.2.1 Mean permeability

Mean permeability or hydraulic conductivity is often the most important parameter to use in numerical modeling and in Rayleigh Number calculation to study free convection when heterogeneous aquifers are treated homogeneous. For heterogeneous layer study, three sets of models, each with 30 realizations of permeability fields having mean permeabilities (statistically) of 10^{-15} m^2, 10^{-16} m^2 and 10^{-18} m^2, are generated and compared with respect to the total number of fingers and maximum penetration depth of the plumes.

Figures 3.3 to 3.9 show the plume development in permeability fields with different log mean. All have the same standard deviation of 2.0, horizontal correlation of 300 meters, and vertical correlation length of 3 meters. The

boundary conditions for the model are shown in Figure 2.5. Figures 3.3-3.5 show modeling results of solute transport in a permeability field with the lowest log mean of -18.0. Diffusion dominates the flow system until about 85 years, when the major fingering plume appears. At simulation time of 725 years the plume reaches the bottom, and at about 1124 years the diffusion dominated flow reaches the bottom. Increasing the log mean of the permeability field to -16.0 promotes free convection with increased number of fingers as shown in Figures 3.6 to 3.7. The first finger appears as early as 7 months and the second finger appears at about 3 years. Both fingers grow with time and reach the bottom at about 20 years. Figures 3.8 to 3.9 show faster growth and more solute flux of the instable fingers with the highest log mean of -15.0 for the permeability distribution. The first finger reaches the bottom at about 1 year, and the large red area shows more solute flux going through the layer. Increasing the mean value of a permeability field leads to a larger Rayleigh number for each single element (or grid cell) as well as for the whole layer. High mean permeability guarantees finger initiation with easy and rapid penetration. Reducing the mean permeability of a field stabilizes the flow because all elements of the k field now are less conductive. Figure 3.10 shows the three model scenarios with different log mean and the corresponding convective velocity for each of the fields. The general Rayleigh number calculation still applies to free convection prediction for a heterogeneous

medium in this sense. The more permeable the medium is, the more amenable it is for free convection.

3.2.2 Standard deviation

Standard deviation describes the spread of permeabilities about the mean value in a heterogeneous permeability field. Increasing standard deviation allows wider spread and larger range of permeability in distribution. For a log-normally distributed permeability field, a small increase of standard deviation will generate a larger range of permeability because of the logrithmatic scale. Therefore, distribution of permeability with larger standard deviation includes more high permeabilities to make the medium more conducive for free convection. Modeling results of concentration contours in Figures 3.11-3.17 show that extensive vertical high permeability zones will occur with high standard deviation resulting in more fingers develop and penetrate through the layer. This finding differs from that of Simmons et al. (2001), who inferred that σ produces local zones of lower permeability stabilizes the flow by providing a barrier to the necessary vertical flows associated with convective instabilities. This difference is due to the different boundary condition assigned in Figure 2.5. It is inferred that increasing standard deviation extends the continuation of the high permeability zones and the convective flux generated can circulate more solute to form more convection cells and propagate farther down the preferential pathways. In the

permeability models for these simulations (e.g., Figures 3.11 to 3.17), a small value change in standard deviation doesn't change the structure of the permeability field. Therefore, as long as the high permeability zones are connected to provide a pathway for initial fingers to start, increasing the standard deviation (while keeping all the other parameters the same) promotes free convection through the high permeability pathways. In Figure 3.18, the top simulation with the low standard deviation has few, if any, fingers as invading plumes. The other simulations with higher standard deviations (Figure 3.18 middle and lower) show more fingers initiated and a higher percentage of them penetrate the layer.

3.2.3 Correlation length

Correlation length of a permeability field relates to the continuity of the permeability data. Although it doesn't show the connectivity of the permeability pathway, study of the changes of both vertical and horizontal correlation lengths demonstrates how instability develops within different permeability fields.

With increasing vertical correlation length τ_y (horizontal correlation length τ_x unchanged), both the high and low permeability zones along the vertical direction are extended to form banded potential pathways or barriers to the solute plumes. Increasing vertical correlation length changes the structure of the permeability field by extending the continuous conduits of high permeability

zones. As a result, the number of instabilities and connected high permeability zones increase with increasing τ_y (see Figures 3.19 and 3.20) because free convection is strongly affected by vertical correlation length. Figure 3.21 displays two models (top 21A and bottom 21B) generated from same mean, standard deviation and horizontal correlation length, but with differing vertical correlation lengths that show different free convection in terms of number of instabilities and penetration depth. Concentration distribution in Figure 3.21A shows the extended low permeability zone impeding or dampening free convection in between the two extended high-permeability zones, which on the contrary, promote instability. Also extended vertical high-permeability zones reduce or inhibit horizontal dispersive mixing to allow more penetration depth of the fingers.

Results for increasing horizontal correlation length τ_x are contrary to those for the vertical correlation length τ_y. Increasing horizontal correlation length results in extensive horizontal barriers to the vertical solute plumes (as well as extensive horizontal pathways). Therefore, instabilities dissipate horizontally (see Figures 3.22 and 3.23). Additional model simulations (Figure 3.24) show that the penetration depth of the vertical fingers decreases with increasing horizontal correlation length as they are impeded by extensive horizontal low permeability zones shown as dark areas. Figure 3.24 shows two models with different horizontal correlation length. For smaller horizontal correlation length, the

penetration depth is much greater and some of the fingers penetrate through the layer.

Figure 3.25 shows that the total number of percolating instabilities increases with increasing vertical correlation length (top graph), based on the 30 realizations. Increasing horizontal correlation length decreases the number of instabilities and therefore stabilizes flow (Figure 3.25 bottom graph).

3.3 Patch analysis of the internal structure of the permeability field

Statistic analysis of heterogeneous permeability fields shows the onset and continued development of free convection are strongly associated with zones of high permeability or continuous conduits. The internal structure and the connectedness of each single k value in the permeability field are important in generating instability. Although the weighted arithmetic mean profile can indicate the relative locations of high permeability along the major dimension (Shi and Sharp, 2001), this indicator does not explain how the internal structure affects free convection and solute transport. Therefore, patch analysis based on percolation theory is used to show how details of the permeability structure affect instability and finger development (Shi and Sharp, 2003). Our modeling results and findings are consistent with studies of Schincariol et al. (1994, 1997), Simmons et al. (1999a and b; 2001) and Prasad et al. (2003) relating free convection to the

characteristics of the heterogeneous media. The internal structure of the permeability field and the heterogeneity effect are characterized by patch analysis using percolation theory in terms of threshold permeability and critical permeability.

We perform percolation analysis by searching the continuous conduits for free convection and find a threshold permeability, k_t, which is the least permeability required for the dense brine water to start convecting and form initial fingering plumes. Figure 3.26 shows the delineated flow pathways after patch analysis and the corresponding permeability field. The 0.2 and 0.6 concentration contours from modeling results are overlying the connected high permeability patches to illustrate they are well matched by and contained within the delineated pathways. Once the permeability field has enough high permeability cells to form a continuous percolating flow pathway and the vertical connectivity index becomes 1.0, a critical permeability is identified for this field. Another example (Figure 3.27) shows the percolated flow pathways with the 0.2 and 0.6 concentration contours on top and the corresponding permeability field. The delineated pathway is the least resistant pathway in the sense that the permeability is sufficiently high to allow solute plumes to reach the bottom boundary.

3.3.1 Threshold permeability k_t

Threshold permeability is defined as the lowest possible k value (within the flow pathway) in a heterogeneous permeability field for the onset of free convection. Patch analysis identifies the threshold permeability and delineates connected high permeability zones, which are tested against SUTRA modeling results to see whether these pathways are the true convective flow routes in the heterogeneous media. Patch analysis is performed on each of the 30 realizations of the permeability distribution, each with its unique structure, to find the threshold permeability and critical permeability.

For heterogeneous permeability distributions with same standard deviation and same correlation lengths, but with different mean, results from patch analysis show that threshold permeability (Figure 3.28a) decreases with increasing mean values. For fields with low mean permeability of 10^{-18} m^2, free convection can initiate at a threshold permeability on the order of 10^{-16} m^2. When the permeability is below this threshold value, a stabilized saline layer can develop in which the downward free convection is inhibited by diffusion and/or horizontal dispersive mixing. Wooding et al. (1997) gave threshold permeability on the order of 10^{-14} m^2 for a typical salt lake free convection problem (homogeneous media). It is inferred that under certain conditions, free convection can happen at even lower permeability in heterogeneous system.

Threshold permeability increases with increasing standard deviation as shown in Figure 3.29(a). Wide spread of permeability distribution for high standard deviation includes more high permeability values to form longer and wider flow pathways. Therefore, free convection can initiate more often and easily when these long and wide connected pathways are present. Among the three sets of a total of 90 realizations, it is found the lowest threshold permeability that free convection can initiate is on the order of 10^{-16} m^2 when the mean permeability is 10^{-17} m^2, a value for which free convection would not occur at all if the medium is homogeneous.

Threshold permeability for the onset of downward free convection increases with increasing horizontal correlation length (Figure 3.30(a)). Increasing the horizontal correlation length τ_x changes the structure of the permeability field and extends both horizontal barriers to the vertical down flow and pathways for horizontal flow. The combination of horizontal barriers and pathways inhibit and impede the initiation of vertical free convection. Patch analysis results show that the threshold permeability is on the order of 10^{-16} m^2 when the correlation length is 90 meters ($\tau_x/X=0.3$ in Figure 3.29), but increases to 10^{-15} m^2 when the correlation length is 300m ($\tau_x/X=1.0$). However, threshold permeability decreases with increasing vertical correlation length as shown in Figure 3.31(a) because it is more helpful for free convection to initiate from the top boundary where there exist extended vertical high permeability zones resulting from increased vertical

correlation length. Results from both horizontal and vertical correlation length show that the lowest permeability for free convection to happen is on the order of 10^{-15} m^2 when the mean permeability of the field is 10^{-17} m^2.

3.3.2 Critical permeability k_c

Critical permeability in patch analysis is a permeability that is sufficiently large to ensure at least one cluster connects the top boundary to the bottom side of the layer so that freely convective fingers can propagate through the layer. This critical permeability is always greater or equal to the threshold permeability whenever there is a percolation cluster connecting the source (top boundary) to the exit (bottom boundary) of the system. The vertical connectivity (C_y), which is the ratio of the maximum vertically connected depth of the patches to the thickness of the model domain, is 1.0 for a continuously connected pathway from the top to the bottom. With increased mean of the permeability distribution, critical permeability increases because the field is more permeable and the preferential flow pathways become more prominent and effective (Figure 3.28b). The increasing of critical permeability is more dramatic towards the high mean permeability end in Figure 3.24, which means the dense plume fingers can penetrate the heterogeneous layer more easily. Compare (a) and (b) in Figure 3.28, it is easy to see that with higher mean permeability distribution, the number

of cases of percolated dense plumes increases from 1 (for mean k of 10^{-18} m^2) to 25 (for mean k of 10^{-15} m^2) for each scenario of 30 realizations.

The critical permeability value also increases with increasing standard deviation as shown in Figure 3.29(b) because a permeability field with high standard deviation includes more high permeabilities and thus increases the potential to form a well-connected percolation cluster. Although more low permeabilities are also included with high standard deviation, the preferential pathways are not affected as long as the structure of the field does not change by low permeability zones. Therefore, the solute plumes will grow larger as a result of increased size of percolation clusters.

With increasing horizontal correlation length, the critical permeability decreases (Figure 3.30b), which means there are fewer continuous penetrated vertical pathways because the high and low permeability zones are extended horizontally with large τ_x. As explained before, the horizontal continuities of both high-permeability pathways and low-permeability barriers are greater for large τ_x, which in turn impedes the vertical free convection. To the contrary, the critical permeability increases with increasing vertical correlation length (Figure 3.31b). Greater vertical correlation length τ_y has shown to form longer vertical pathways and therefore helps promote downward solute transport.

3.3.3 Critical probability p_c

In percolation theory, there is a critical probability which is the ratio of the number of nodes open to flow to the number of total nodes (p_c=N/N_0). After successfully delineating the percolate clusters for each model scenario consisting of 30 realizations, the critical probability values can be calculated with known number of cells in the percolation clusters that are open to flow. Results of critical probability versus correlation lengths (τ_x and τ_y) are shown in Table 3.2, which shows that the critical probability increases with increasing horizontal correlation length and decreases with increasing vertical correlation length. Critical probability values are available in percolation theory only for some simple systems, such as 0.5923 for a simple square lattice system. The maximum critical probability for the simulations is around 0.261 which is much less than the value for a square system, which means free convection propagates into larger area in the system.

3.4 Dual heterogeneity

Sediments in Texas Gulf Coast Basin consist of inter-fingering marine and non-marine sands and shales. Sands or sandstones are more permeable than shale unless the sandstones are well cemented and the shales are fractured. Sand permeability is generally on the order of 10^{-12} m^2 (10^3 md or 10^{-19} m/s). Free convection can occur more easily in sands because of high permeability. For a n

inter-bedded sand-shale model, sands can be treated as homogeneous, considering the frequency of free convection happening so that we can focus on studying free convection through heterogeneous shale.

Model setup (see Figure 2.12) is the same as previous models in terms of geometries and source location except boundary conditions. The bottom of shale layer is not a no-flow boundary because with the high-permeability sand layer flow occurs in sand across the boundary. The bottom of sand layer is treated as a no-flow boundary. We implemented two conceptual models: 1) shale overlying a sand layer; and 2) sands above and below the shale.

Having a sand layer at the bottom of shale promotes and enhances free convection and solute transport through shale only when free convection already started in shale along the connected high permeability pathways (Figure 3.32a). Free convection could not propagate to sand layer if there is a low permeability barrier to the flow near the bottom of the layer. Therefore, the onset and development of free convection are controlled by the structure of the shale permeability field. Calculated solute flux shown in Figure 3.32 illustrates the accumulated flux first crosses the shale-sand boundary at about 1 year and increases in magnitude and spreading out along the boundary. Vertical convective flux demonstrates on the figure as downward flow (down-welling) (positive flux) and upward flow (up-welling) (negative flux). Since the bottom boundary is a no-flow boundary for the single layer model, there exists no flux across the bottom

boundary. Our model with sand on the bottom shows increasing convective flux with time, and at simulation time of 20.17 years there exists a great amount of convective flux down across the boundary between shale and sand and there are a few areas along the boundary that have upward flow shown as negative flux (Figure 3.32b). The comparison of convective flux across the top source boundary (actually at the center of the first row of elements) shows that at early time solute flux of the initial free convection flow are the same for both models with sand and without sand at the bottom (see Figure 3.33a). As time increases, the difference in convective flux for free convection for the two models increases (Figure 3.33) which demonstrates that having a sand bottom layer actually promotes convective flux generating from the top boundary.

Because solute transport processes are sensitive to the locations of high and low permeability zones relative to the source, especially near the top boundary in our model, adding the sand layer on top of a low-permeable shale promotes free convection (see Figure 3.34). The reasons for enhanced free convection are threefold. First, the flux of downward free convection initiated in the sand layer can transport large amount of solute down to shale and continue to generate instabilities. It is inferred that the inertial effects help to generate perturbation or interfacial disturbances. Second, the high permeability sand can connect to high permeability zones near the top boundary of shale to form a continuous preferential pathway for free convection to percolate through, and

once free convection propagates into the shale, it will either grow (if the pathway exists) or dissipate (if low-permeability zones intercept the pathway) depending on the internal structure of the shale permeability. Third, re-examination of the study by Lapwood (1948) finds that the critical Rayleigh number for the onset of free convection in a horizontally infinite layer bounded on top by a permeable boundary decreases from $4\pi^2$ (about 39.45 for impermeable top boundary) to 27.1. Therefore, a permeable sand layer on top of the shale promotes free convection occurring in the shale layer.

Examples of free convection percolated through the shale layer are illustrated in Figure 3.34. Free convection quickly started in the top sand layer because the sand has a much greater permeability (5 orders of magnitude) than the shale. This allows dense solute to start convection at locations along the top boundary and then quickly spread out as the up-welling and down-welling cells within the whole layer. As these cells grow deeper to reach the top of shale, free convection propagates along the most permeable pathways in shale and the flows are faster reaching the bottom of the shale layer. Once the dense plumes reach the bottom boundary between shale and sand, the front diffuses and disperses into the sand layer well before the center of the plume arrives. There is one plume on the right edge of Figure 3.34(e) that does not percolate through shale because near the bottom there is a low-permeability barrier, while the one to the left which started

later than this one but catches up quickly because a high-permeability pathway is present in the shale.

Figure 3.35 shows vertical convective flux distribution along the top boundary between sand and shale changing with time. In general, the magnitude of convective flux decreases with time because the decrease in concentration difference and down movement of high concentration plumes. Figure 3.35(a) shows zero flux at simulation time of 4.16 months because the convective plumes have not yet reached the bottom boundary. After the convective flow reaches the boundary, it starts to generate instabilities (Figure 3.35(b)) and the inertial force initiates free convective flow in areas of low permeability (Figure 3.35(c)).

3.5 Discussion and conclusions

The overlying of saline formation fluids on top of less dense formation fluids creates a potential for free convection to occur even through low-permeability shales. Density-driven free convection can occur within and even across the low-permeability heterogeneous shale under certain conditions. Stochastic modeling of variable-density flow in a single heterogeneous shale layer shows the fingers of solute may occur and penetrate through the layer.

In density-driven flow across a heterogeneous low-permeability layer, instabilities occur where high-permeability zones exist and their finger development depends on the connectedness of these high permeability zone(s).

Percolation analysis defines threshold permeability for the onset of free convection and a critical percolation permeability to form percolation clusters that provide flow pathways through low-permeability layers that would otherwise prevent fingering. Statistical analyses of the heterogeneous permeability fields and numerical modeling show that high concentration gradients, vertical connectivity of high permeability zones, large vertical correlation length-to-dimension ratio, high mean permeability for the k field and large standard deviation of permeability all promote free convection where buoyancy gradients are present. This general finding is consistent with Simmons et al. (2001), Sharp et al. (2001), Schinariol et al. (1997), and Prasad and Simmons (2003), although we use different system geometry, boundary conditions, and permeabilities. It further proves the general cause and effect conclusions from previous work on heterogeneity effects on free convection.

The structure of the permeability is critical in initiating the instabilities and the further development of the fingers depends on the connected high permeability zones in the stochastic heterogeneous permeability fields. Zones or patches consisting of high-permeability elements can act as fluid pathways and enhance plume development downward. Finding these elements and studying how well they are connected is important in analyzing the internal structure of a permeability field. High permeability zones in shale can exist due to particle arrangement during deposition and diagenesis. Even though they may occupy a

small portion of the total volume, they are very important for free convection and can have a dominant effect on fluid flow and contaminant transport. The closer the high-permeability zones to the source (top boundary), the more likely instability is going to happen. Among the three parameters for statistical analyses, correlation length is the most important and controlling parameter with respect to changing the structure of a permeability field. Correlation length variations bridge the gap between totally random fields to regular or ordered heterogeneous media.

For these multiple realizations of permeability distribution, numerical modeling results of flow and solute transport have shown some of them are diffusion-dominated for the whole simulation time period. For those convection-dominated simulations, there are regions that are still diffusion-dominated and therefore it is difficult to test or prove free convection occurring unless sampling is directly undertaken in the convection-dominated regions.

The onset of free convection is especially sensitive to the boundary conditions. The layer cake model of sand and shale illustrates free convection is promoted by the sand layers above and below the low-permeability strata. This has the implication of free convection happening more often than expected in the sediments, such as in Gulf of Mexico Basin.

In conclusion, stochastic simulation and modeling indicates that:

1) Free convection can occur through heterogeneous low permeability media;

2) Increases in the mean, standard deviation, and vertical correlation length of the permeability field promote free convection in models with different system geometries and boundary conditions.

3) The internal structure of the heterogeneous field is critical in controlling the onset and development of the instabilities.

4) There is a threshold permeability for free convection to occur.

5) Critical permeability from patch analysis of the permeability structure further proves that free convection is enhanced with increasing mean, standardard deviation, and vertical correlation length. Whether or not initial instabilities grow or decay depends on on the distribution of permeability.

6) A threshold permeability must be exceeded in order to have instabilities to start to grow;

7) A critical permeability value must be exceeded in order to have a well-connected flow path for convection to penetrate through.

Thus, free convection in heterogeneous media is amenable to prediction by mapping the permeability field and analyzing the high conductive zones that form potential percolation pathways.

Table 3.1 critical probability values

Model scenario	τ_x (m)	τ_y (m)	k_c (m^2)	p_c
C1	300	1.5	1.58×10^{-16} - 1.05×10^{-14}	0.061 - 0.261
C2	300	10	3.16×10^{-16} - 9.77×10^{-15}	0.028 - 0.171
C3	300	20	1.17×10^{-15} - 1.26×10^{-13}	0.033 - 0.230
C4	300	30	1.58×10^{-16} - 2×10^{-13}	0.037 - 0.185
C5	150	20	1.02×10^{-16} - 3.16×10^{-13}	0.057 - 0.208
C6	90	20	3.55×10^{-16} - 5.01×10^{-12}	0.020 - 0.133

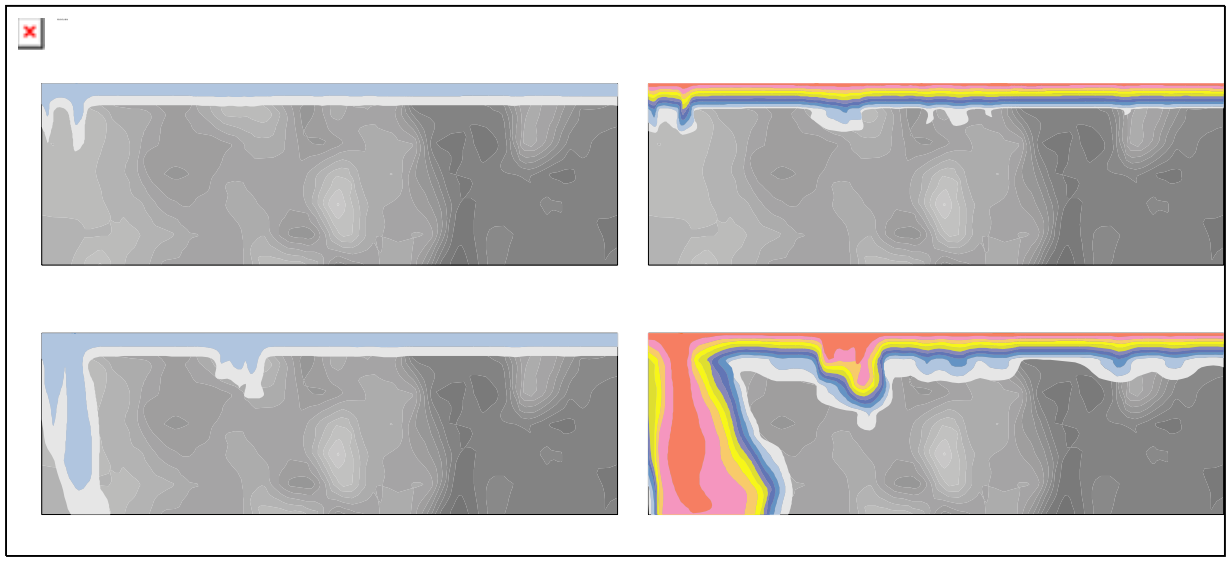

Figure 3.1 Effect of concentration difference between upper and lower boundary on plume development. Left model used C_{max} = 0.2 kg/kg and the right model used C_{max} = 1.0 kg/kg.

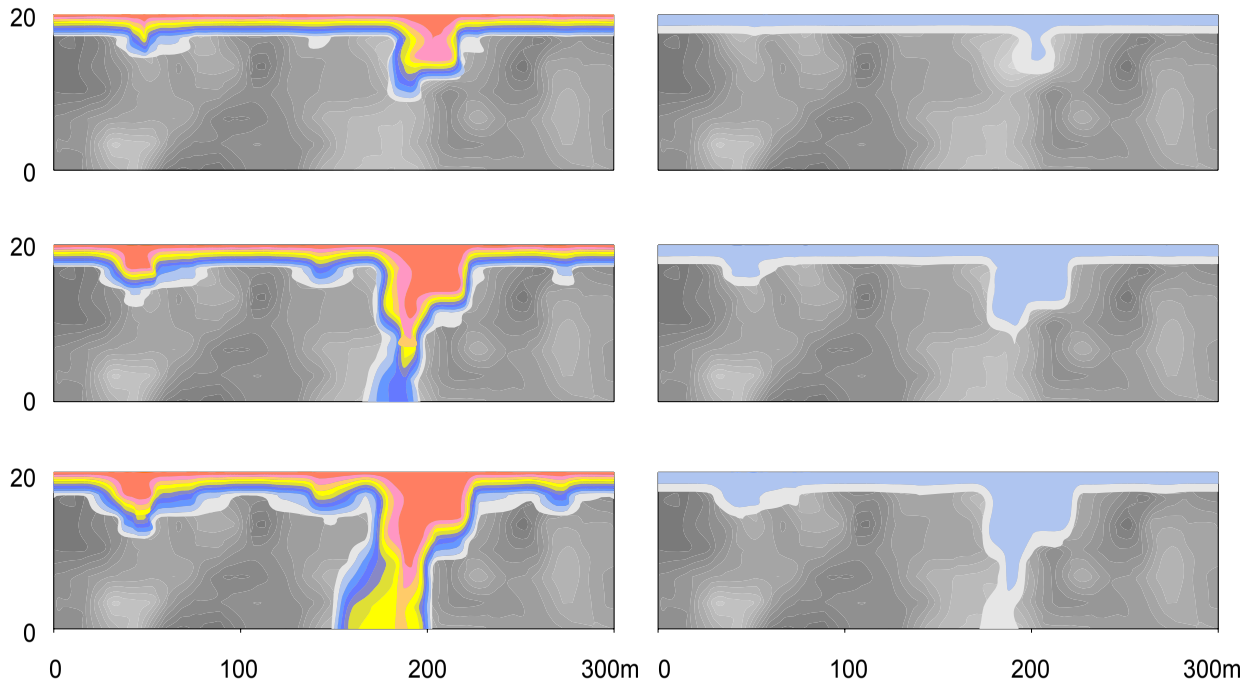

Figure 3.2 Effect of concentration difference between upper and lower boundary on plume development. Model on the right used C_{max} = 0.2 kg/kg and the left model used C_{max} = 1.0 kg/kg. Simulation time is about 2 months (top), 5 years (middle),and 20 years (bottom).

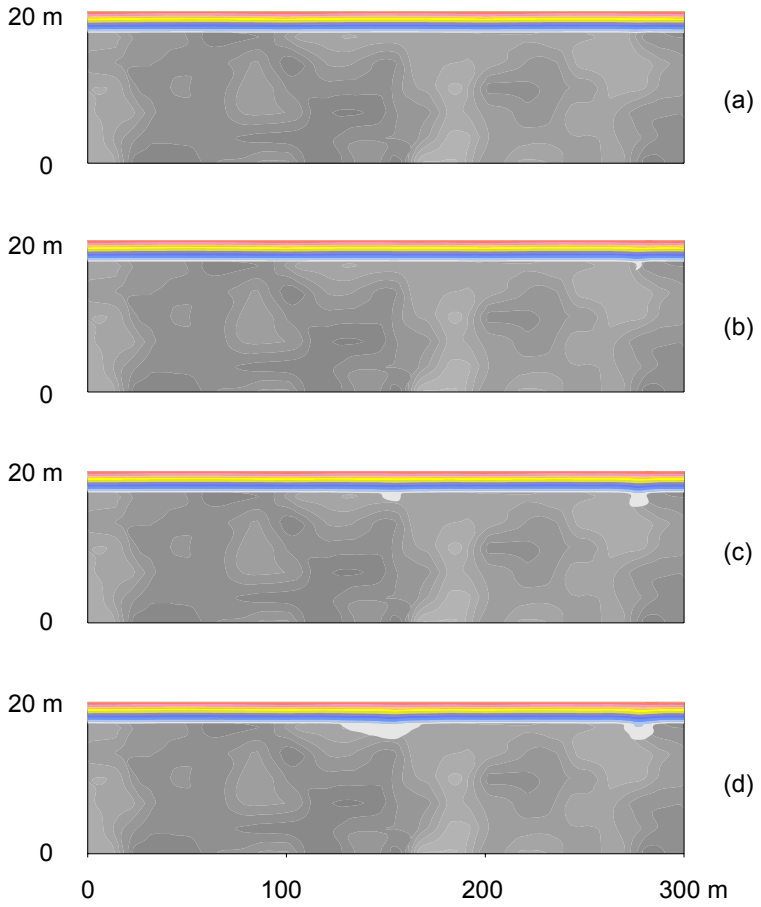

Figure 3.3 Solute transport in a heterogeneous layer with statistical log mean = 10^{-18} m^2, standard deviation = 2.0 , horizontal correlation length τ_x = 300 m, vertical correlation length τ_y = 3 m. Simulation time is about (a) 2 months, (b) 4 years, (c) 6 years, and (d) 10 years.

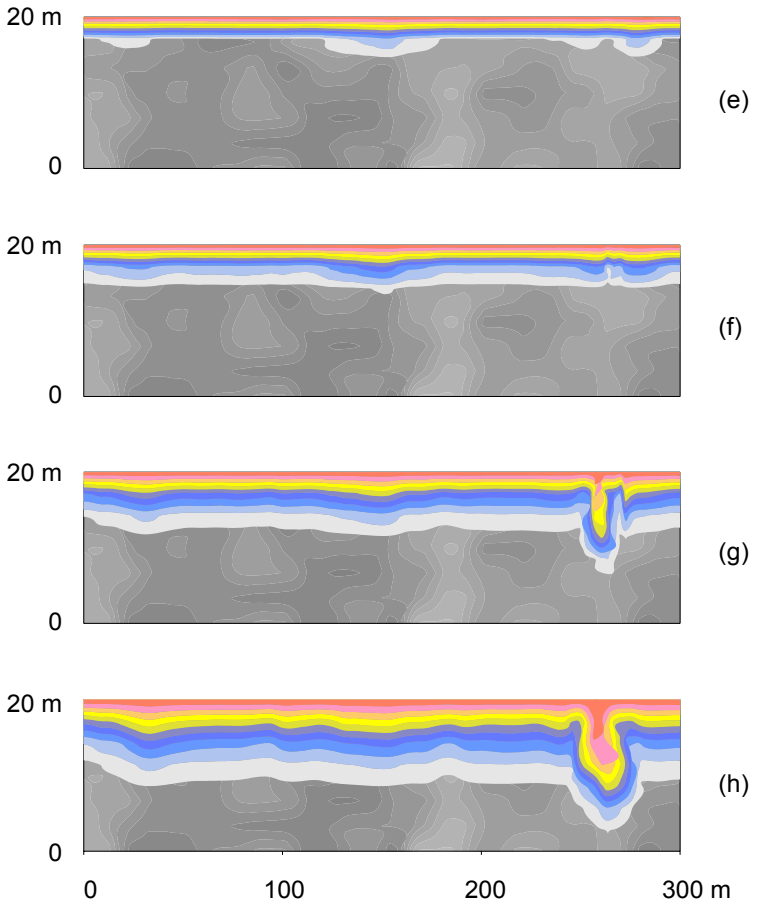

Figure 3.4 Solute transport in a heterogeneous layer with statistical log mean 10^{-18} m^2, standard deviation = 2.0 , horizontal correlation length τ_x = 300 m, vertical correlation length τ_y = 3 m. Simulation time is at (e) 18 years, (f) 52 years, (g) 85 years, and
(h) 324 years.

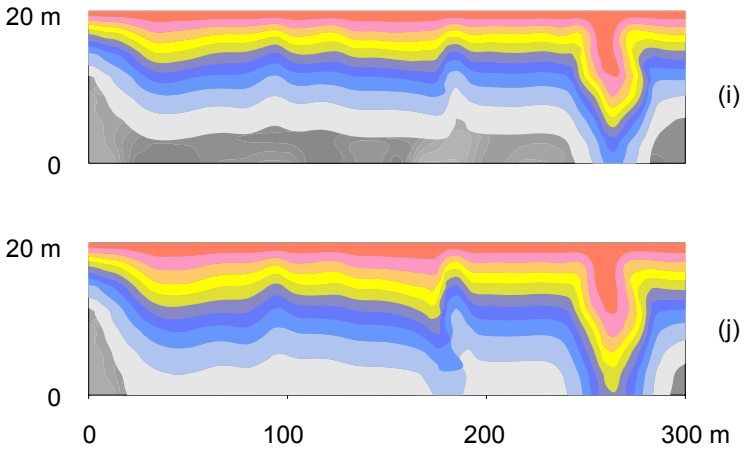

Figure 3.5 Solute transport in a heterogeneous layer with statistical log mean = 10^{-18} m^2, standard deviation = 2.0 , horizontal correlation length τ_x = 300 m, vertical correlation length τ_y = 3 m. Simulation time is at (i) 724 years and (j) 1124 years.

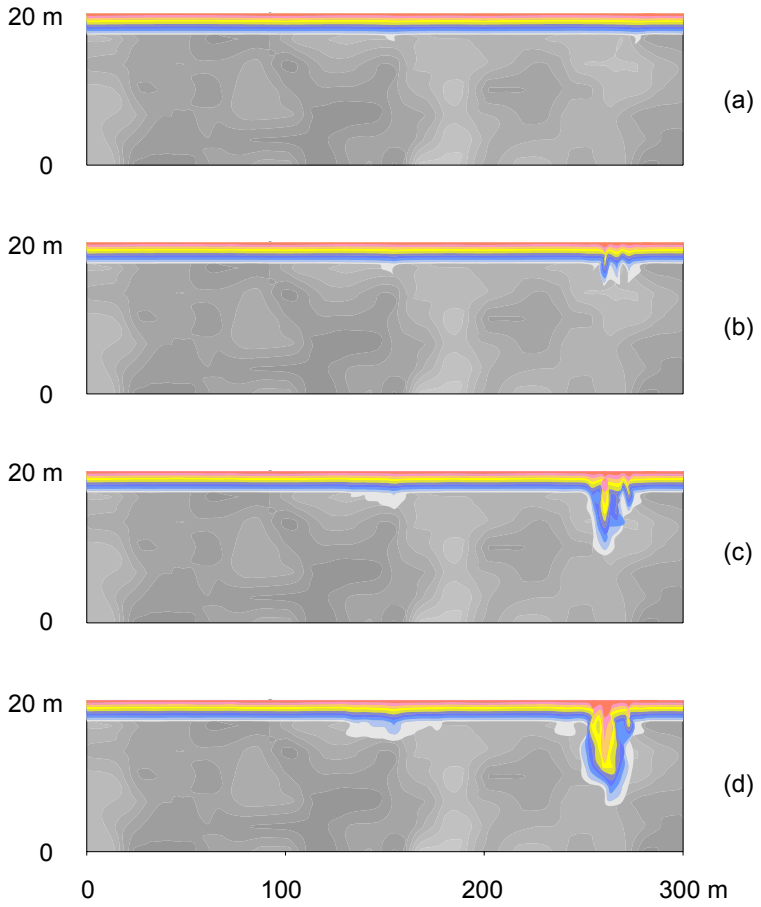

Figure 3.6 Solute transport in a heterogeneous layer with statistical log mean = 10^{-16} m^2, standard deviation = 2.0 , horizontal correlation length τ_x = 300 m, vertical correlation length τ_y = 3 m. Simulation time is at (a) 2 months, (b) 7 months, (c) 1 year, (d) 2 years.

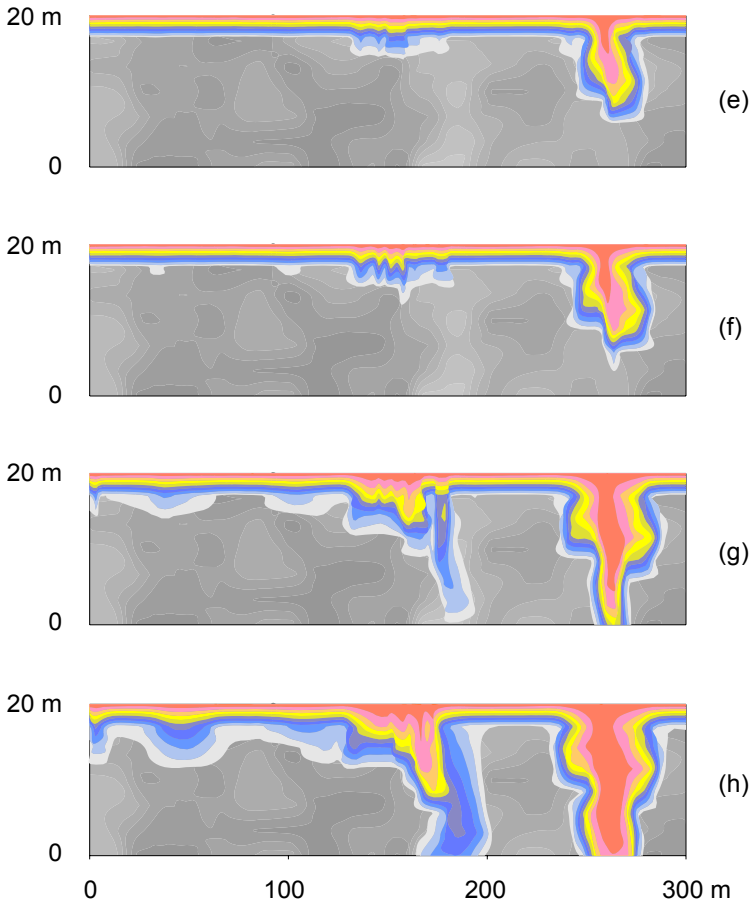

Figure 3.7 Solute transport in a heterogeneous layer with statistical log mean = 10^{-16} m^2, standard deviation = 2.0 , horizontal correlation length τ_x = 300 m, vertical correlation length τ_y = 3 m. Simulation time is at about (e) 3 years, (f) 4 years, (g) 10 years, and (h) 20 years.

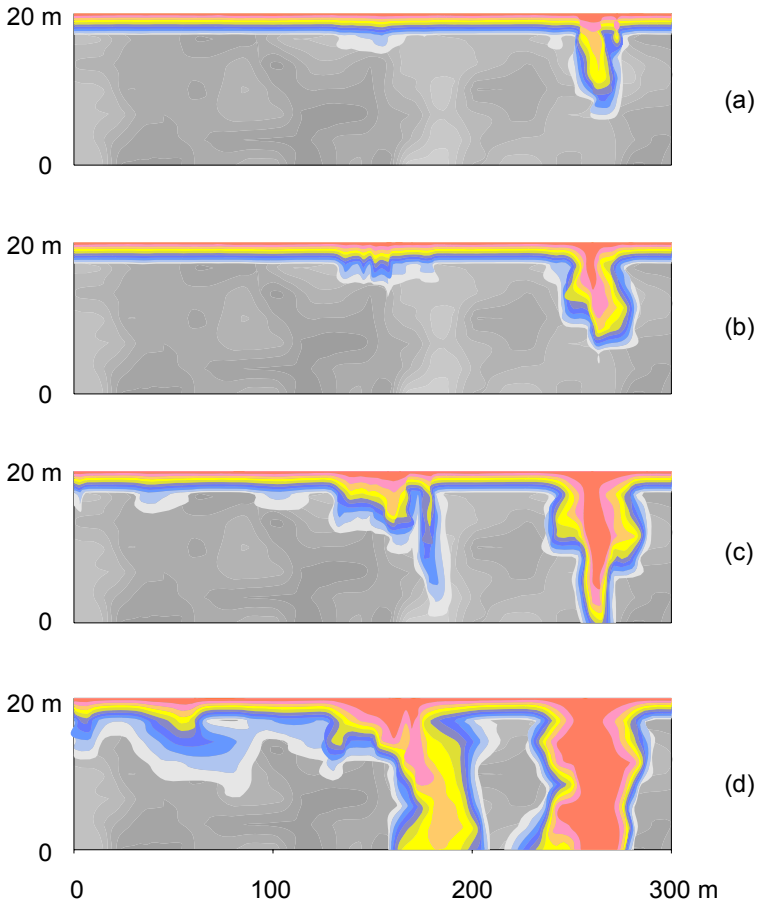

Figure 3.8 Solute transport in a heterogeneous layer with statistical log mean = 10^{-15} m^2, standard deviation = 2.0 , horizontal correlation length τ_x = 300 m, vertical correlation length τ_y = 3 m. Simulation time is at (a) 2 months, (b) 4 months, (c) 1 year, (d) 5 years.

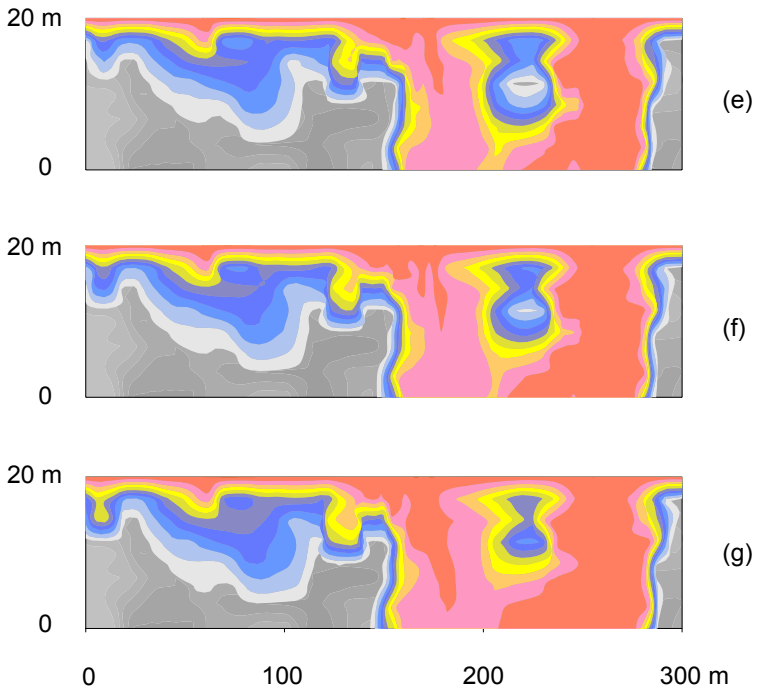

Figure 3.9 Solute transport in a heterogeneous layer with statistical log mean = 10^{-15} m^2, standard deviation = 2.0 , horizontal correlation length τ_x = 300 m, vertical correlation length τ_y = 3 m. Simulation time is at (e) 12 years, (f) 15 years, and (g) 20 years.

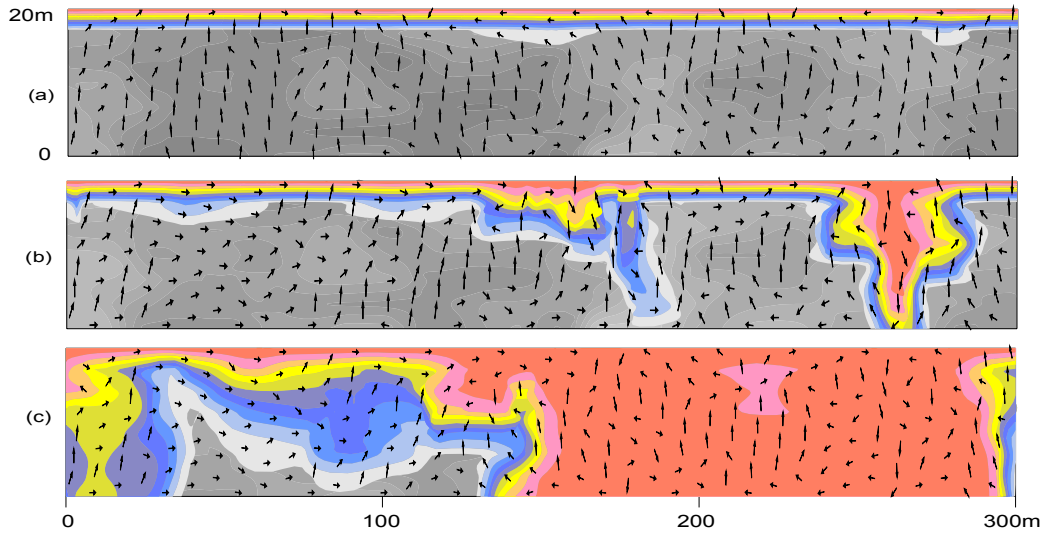

Figure 3.10 Convective flow and solute transport in a heterogeneous k field with different mean. The length of the arrows represent the magnitude of the convective flow velocity. All three permeability distributions have same τ_x = 300m, τ_y = 3m, σ = 2.0, and simulation time is 10 years. Mean permeability for a) = 10^{-18} m^2, b) = 10^{-16} m^2, and c) = 10^{-15} m^2.

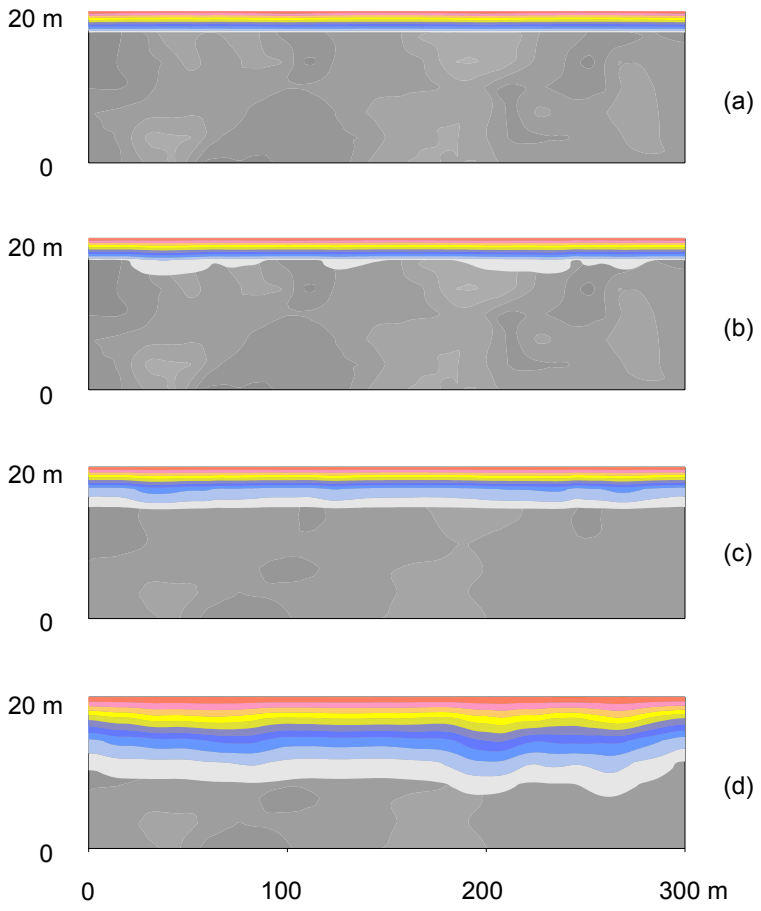

Figure 3.11 Solute transport in a heterogeneous layer with statistical log mean = 10^{-17} m^2, horizontal correlation length τ_x = 300 m, and vertical correlation length τ_y = 3 m. Standard deviation σ = 1.0. Simulation time is at (a) 2 months, (b) 15 years, (c) 52 years, (d) 324 years.

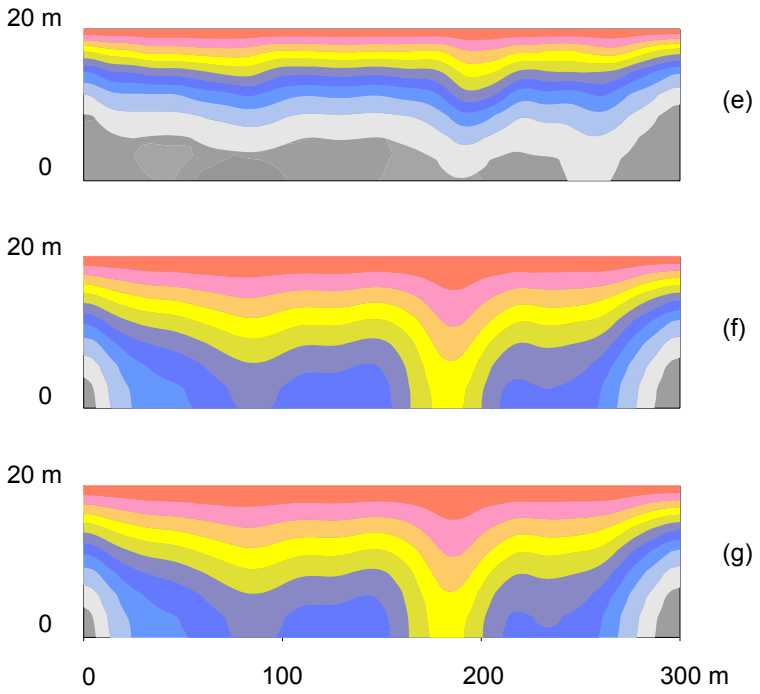

Figure 3.12 Solute transport in a heterogeneous layer with statistical log mean = 10^{-17} m^2, horizontal correlation length τ_x = 300 m, and vertical correlation length τ_y = 3 m. Standard deviation σ = 1.0. Simulation time is at (e) 624 years, (f) 1724 years, and (g) 2724 years.

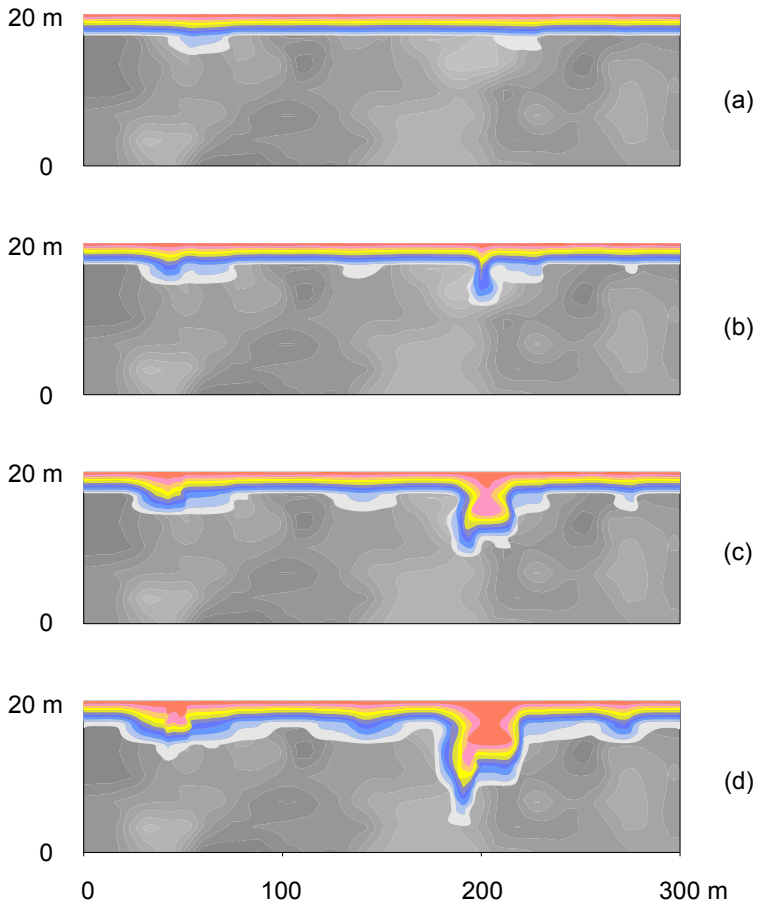

Figure 3.13 Solute transport in a heterogeneous layer with statistical log mean = 10^{-17} m^2, horizontal correlation length τ_x = 300 m, and vertical correlation length τ_y = 3 m. Standard deviation σ = 2.0. Simulation time is at (a) 2 months, (b) 1 year, (c) 5 years, (d) 20 years.

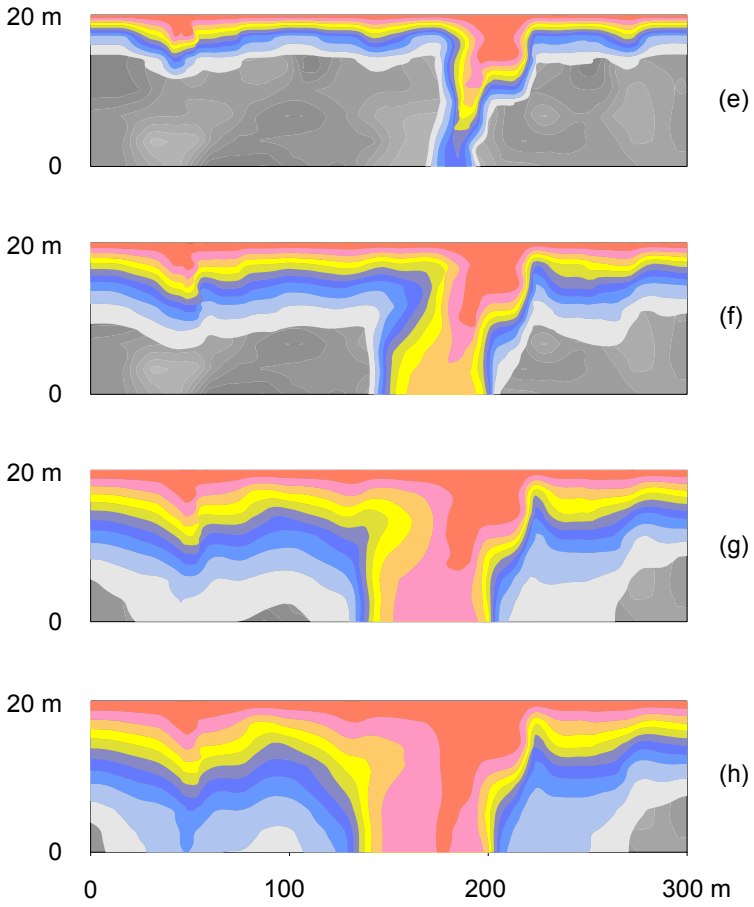

Figure 3.14 Solute transport in a heterogeneous layer with statistical log mean = 10^{-17} m^2, horizontal correlation length τ_x = 300 m, and vertical correlation length τ_y = 3 m. Standard deviation σ = 2.0. Simulation time is at (e) 52 years, (f) 324 years, (g) 824 years, (h) 1124 years.

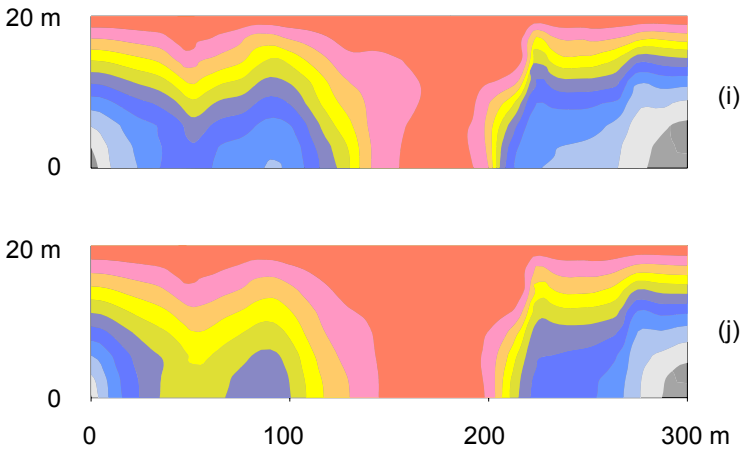

Figure 3.15 Solute transport in a heterogeneous layer with statistical log mean = 10^{-17} m^2, horizontal correlation length τ_x = 300 m, and vertical correlation length τ_y = 3 m. Standard deviation σ = 2.0. Simulation time is at (i) 1924 years, (j) 2224 years.

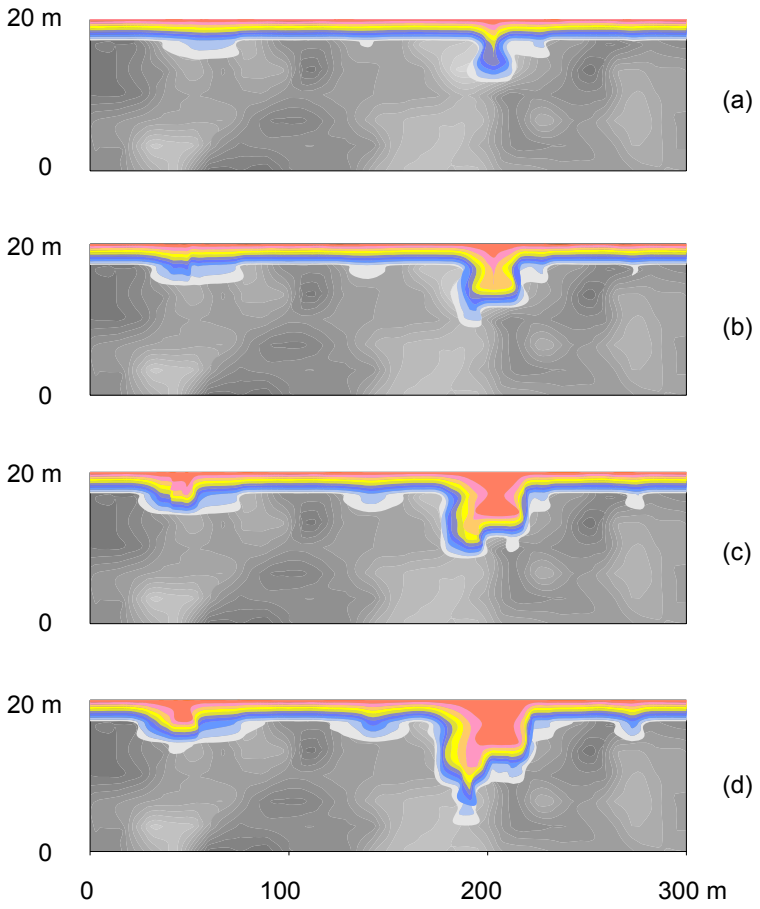

Figure 3.16 Solute transport in a heterogeneous layer with statistical log mean = 10^{-17} m^2, horizontal correlation length τ_x = 300 m, and vertical correlation length τ_y = 3 m. Standard deviation σ = 3.0. Simulation time is at (a) 2 months, (b) 7 months, (c) 3 years, (d) 8 years.

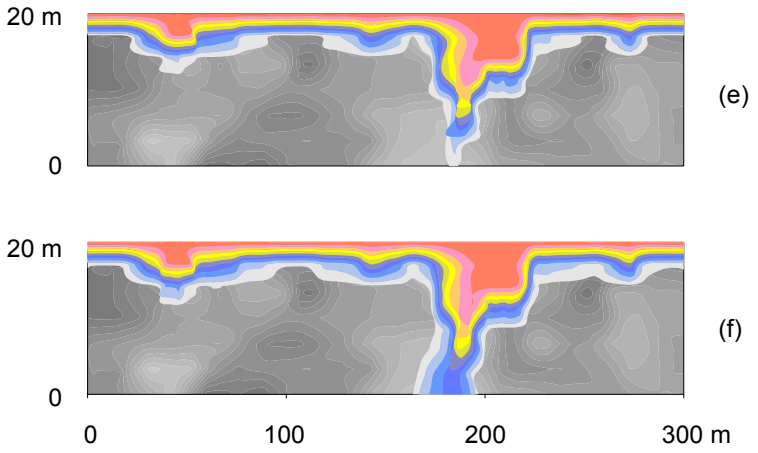

Figure 3.17 Solute transport in a heterogeneous layer with statistical log mean = 10^{-17} m^2, horizontal correlation length τ_x = 300 m, and vertical correlation length τ_y = 3 m. Standard deviation σ = 3.0. Simulation time is at (e) 12 years and (f) 20 years.

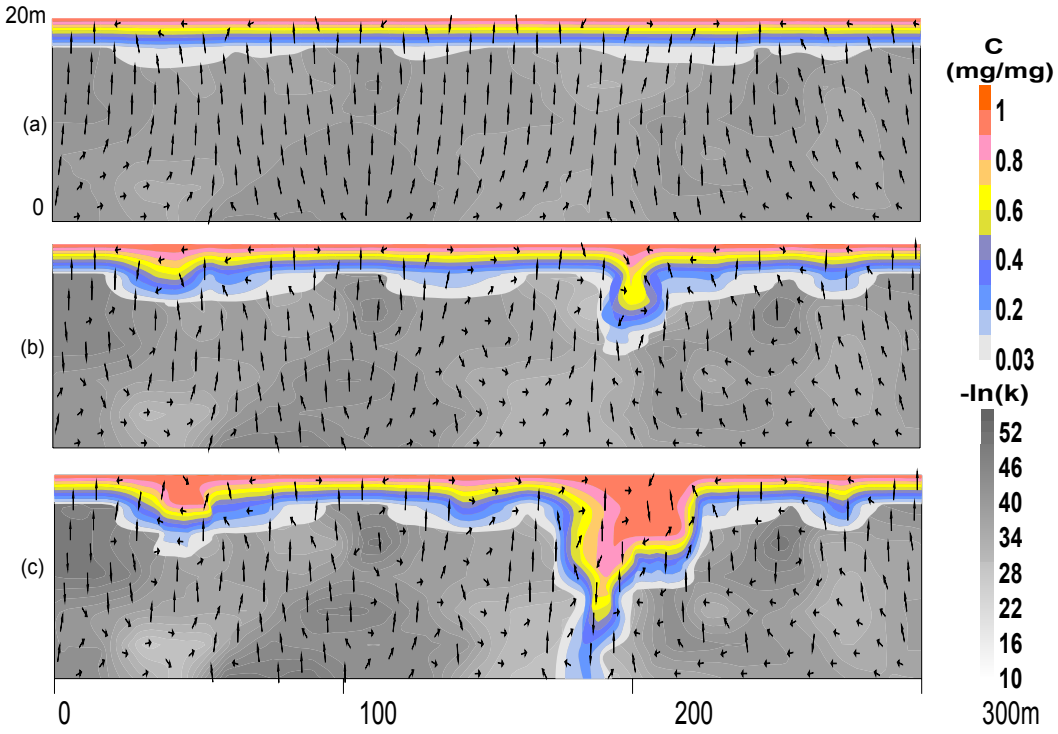

Figure 3.18 Free convection in a heterogeneous k field with different standard deviation. All three permeability distribution models have same $\mu = 10^{-17}$ m^2, τ_x = 300m, τ_y = 3m and simulation time is at 15 years. Standard deviation σ for a) = 1.0, b) = 2.0, and c) = 3.0.

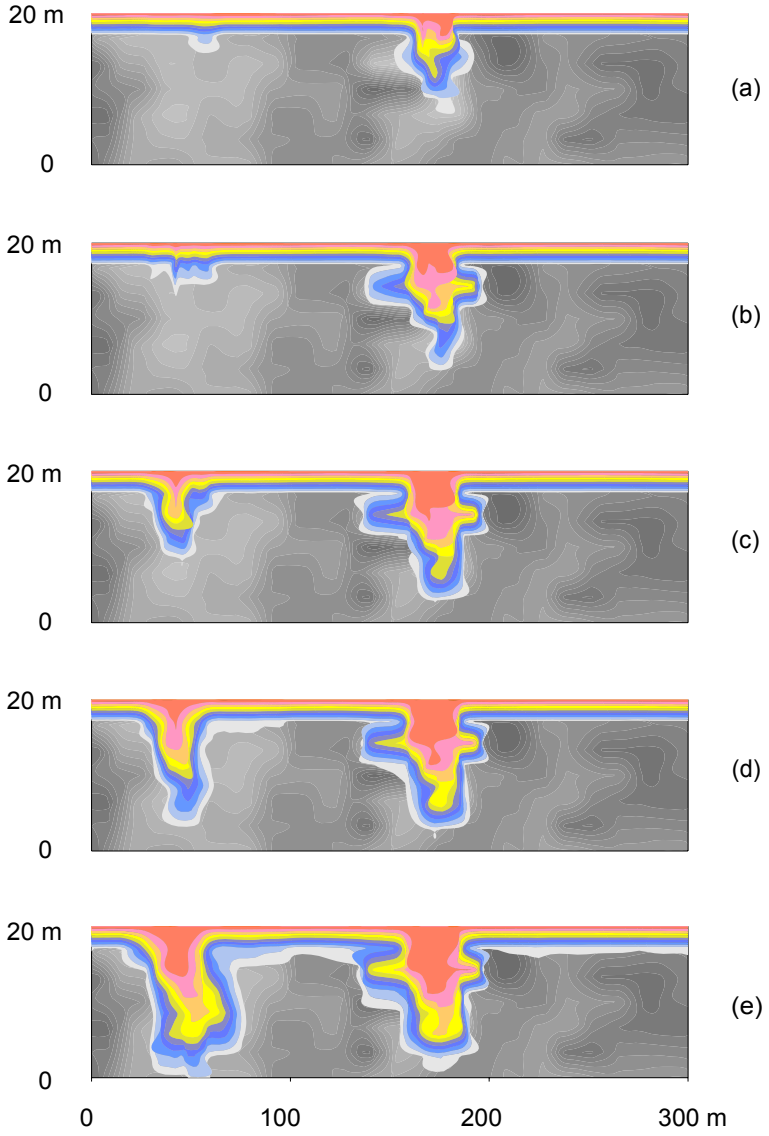

Figure 3.19 Solute transport in a heterogeneous layer with statistical log mean = 10^{-17} m^2, horizontal correlation length τ_x = 300 m, and vertical correlation length τ_y = 1.5 m. Standard deviation σ = 3.0. Simulation time is at (a) 2 months, (b) 2 years, (c) 5 years, (d) 8 years, (e) 20 years.

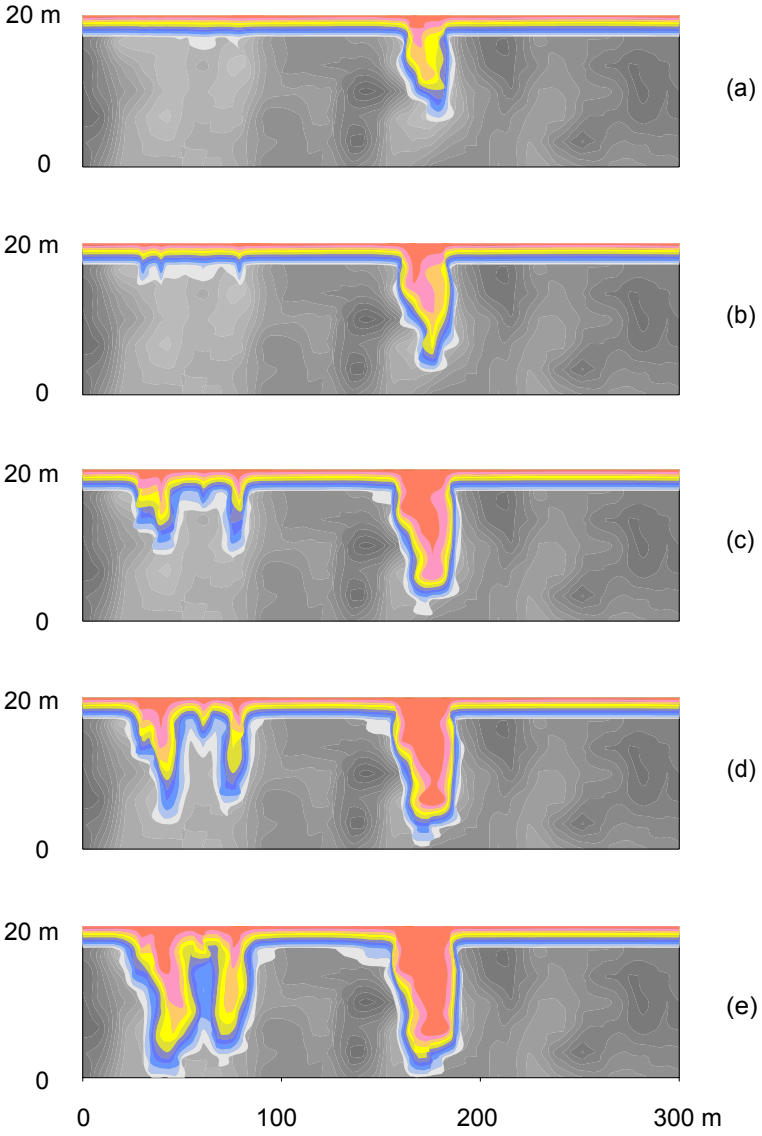

Figure 3.20 Solute transport in a heterogeneous layer with statistical log mean = 10^{-17} m^2, horizontal correlation length τ_x = 300 m, and vertical correlation length τ_y = 30 m. Standard deviation σ = 3.0. Simulation time is at (a) 2 months, (b) 7 months, (c) 3 years, (d) 5 years, (e) 12 years.

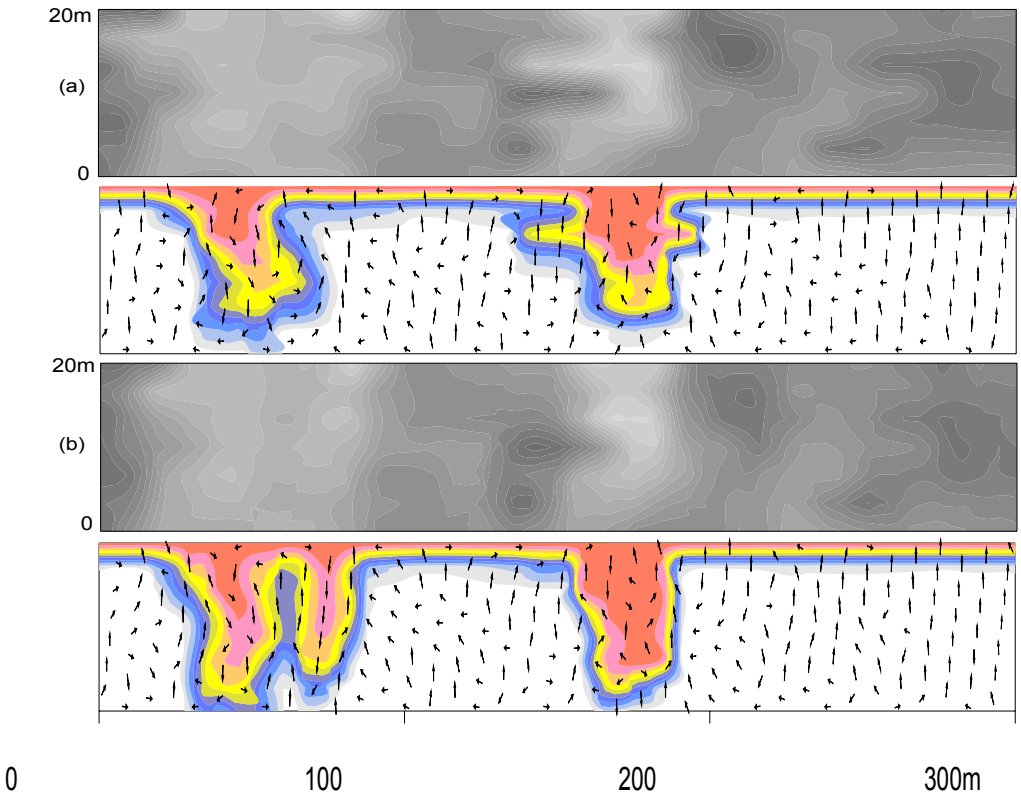

Figure 3.21 Two models ((a) and (b)) generated from same $\mu = 10^{-17}$ m^2, $\sigma = 3.0$ and $\tau_x = 300$m with different vertical correlation lengths (top $\tau_y = 1.5$m, bottom $\tau_y = 30$m). Simulation time is at 20 years.

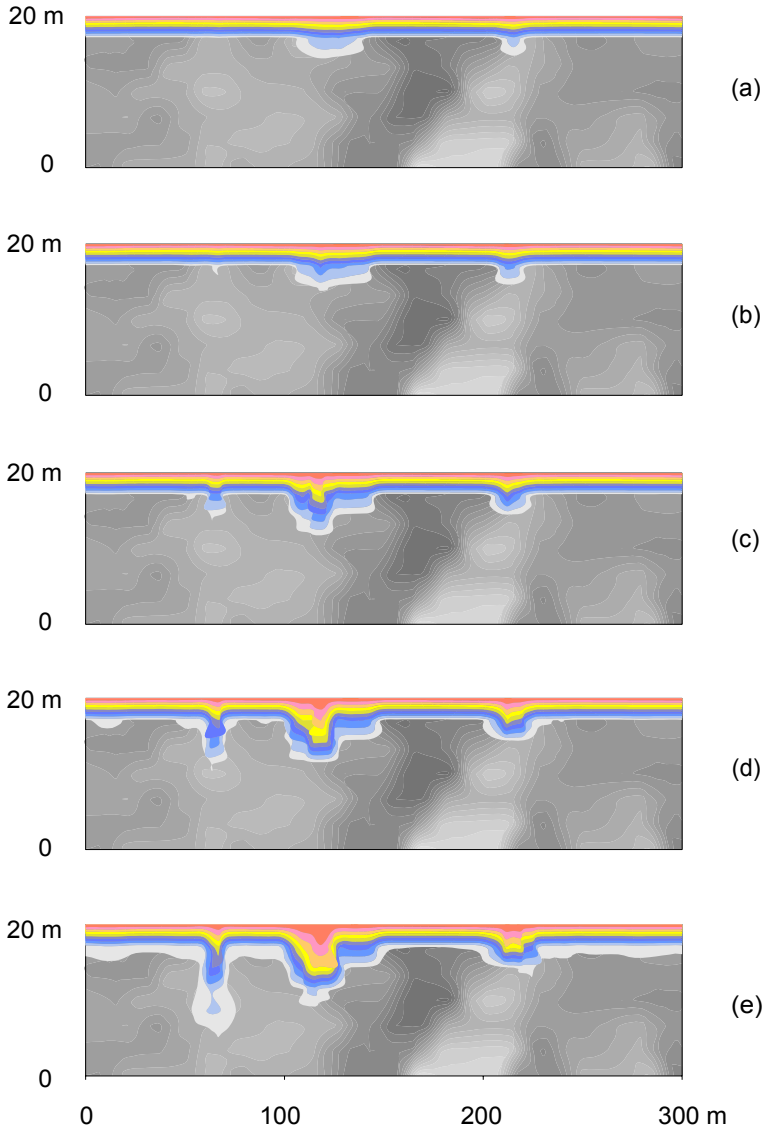

Figure 3.22 Solute transport in a heterogeneous layer with statistical log mean = 10^{-18} m^2, horizontal correlation length τ_x = 300 m, and vertical correlation length τ_y = 20 m. Standard deviation σ = 3.0. Simulation time is at (a) 2 months, (b) 2 years, (c) 6 years, (d) 12 years, (e) 20 years.

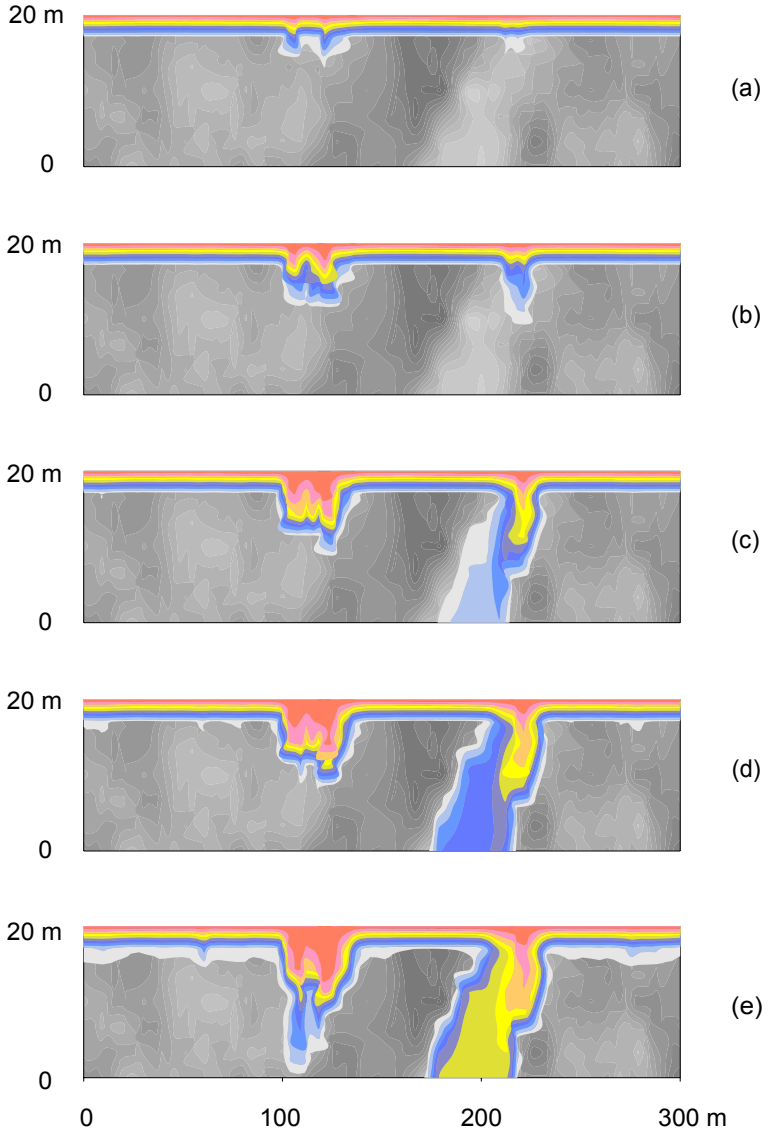

Figure 3.23 Solute transport in a heterogeneous layer with statistical log mean = 10^{-18} m^2, horizontal correlation length τ_x = 90 m, and vertical correlation length τ_y = 20 m. Standard deviation σ = 3.0. Simulation time is at (a) 2 months, (b) 1 year, (c) 5 years, (d) 10 years, (e) 20 years.

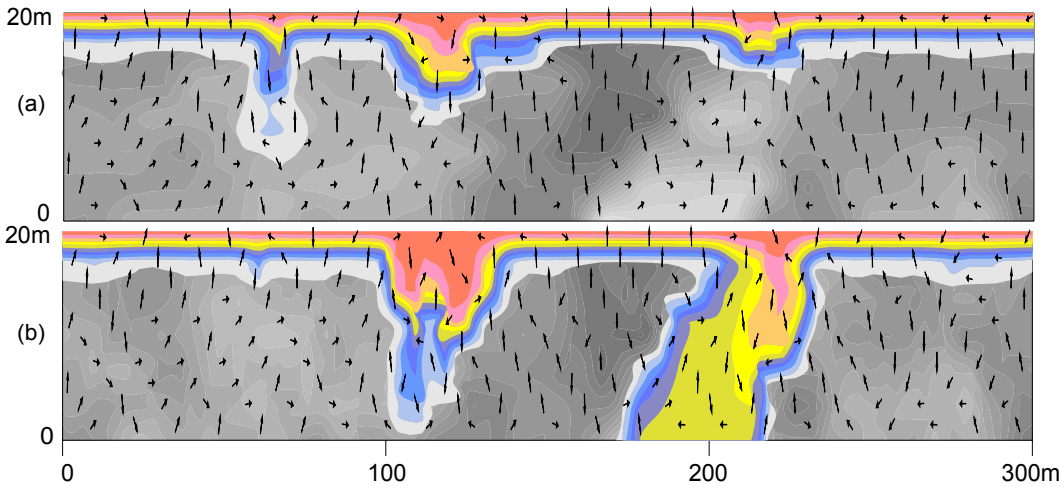

Figure 3.24 Free convection in a heterogeneous layer with different horizontal correlation length. a) τ_x =300m, b) τ_x = 90m. Both permeability distribution models have same $\mu = 10^{-18}$ m^2, $\sigma = 3.0$, $\tau_y = 20$m. Simulation time is at 20 years.

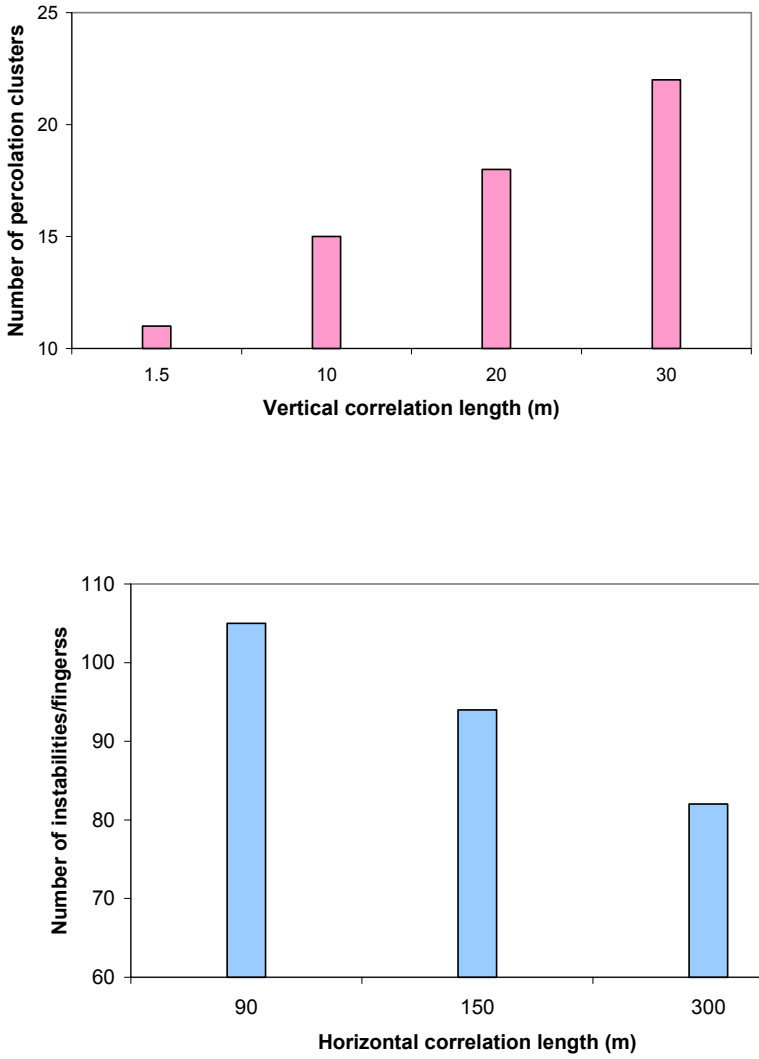

Figure 3.25 Number of instabilities increases with increasing vertical correlation length (top), but decreases with increasing horizontal correlation length (bottom).

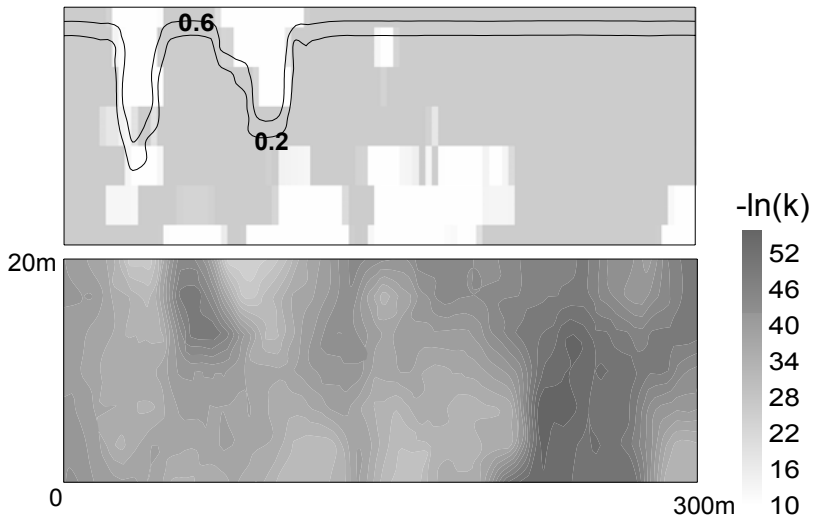

Figure 3.26 Delineated flow pathways are shown in upper graph as white area with overlying concentration contours of C=0.2 and C=0.6 at simulation time of 18 years. Threshold permeability identified for the lower permeability distribution field is $10^{-15.0}$ m^2. Permeability field has a mean $\mu = 10^{-17}$ m^2, standard deviation $\sigma = 3.0$, and vertical correlation length $\tau_y = 30$m.

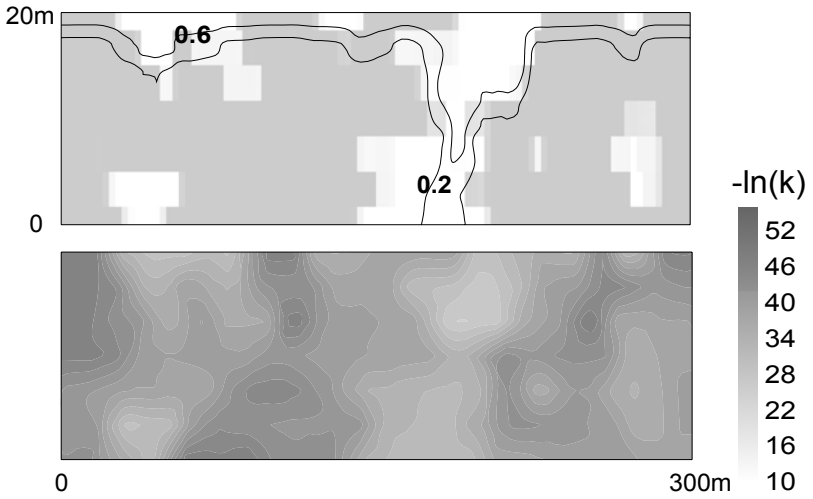

Figure 3.27 Delineated flow pathways are shown in upper graph as white, with 0.2 and 0.6 concentration contours at simulation time of 17 years overlying the patch results. The critical permeability for the connected percolated pathway is $10^{-15.2}$ m^2 for the lower permeability field. Statistic data for permeability distribution is: mean $\mu = 10^{-17}$ m^2, standard deviation $\sigma = 3.0$, and vertical correlation length $\tau_y = 3m$.

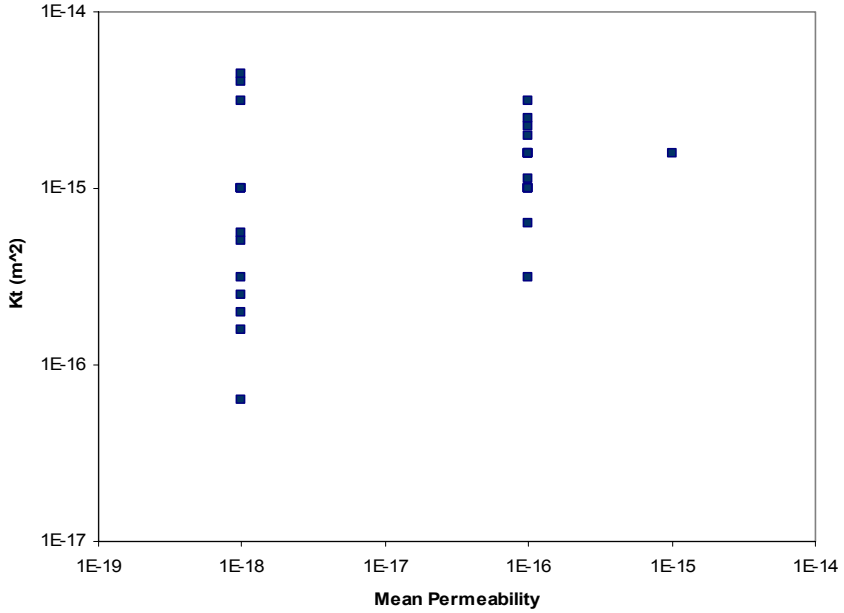

(a)

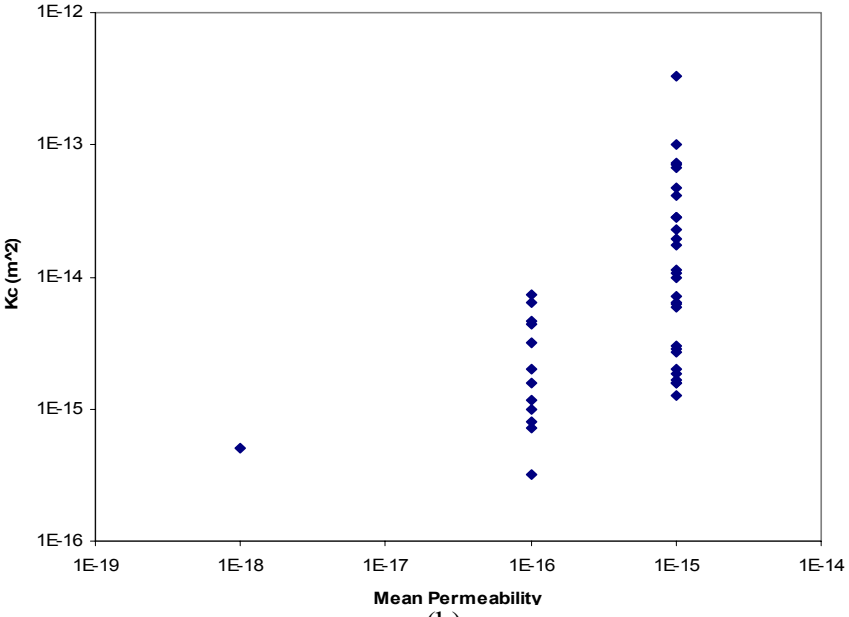

(b)

Figure 3.28 Patch analysis results for three sets of models (along x direction) with different mean permeability of 10^{-18} m^2, 10^{-16} m^2 and10^{-14} m^2. Each set consists of 30 different permeability distributions. Threshold permeability identified from patch analysis is shown as squares and critical permeability is shown as diamonds. Standard deviation for the permeability distribution is σ = 3.0, and vertical correlation length τ_y = 20m.

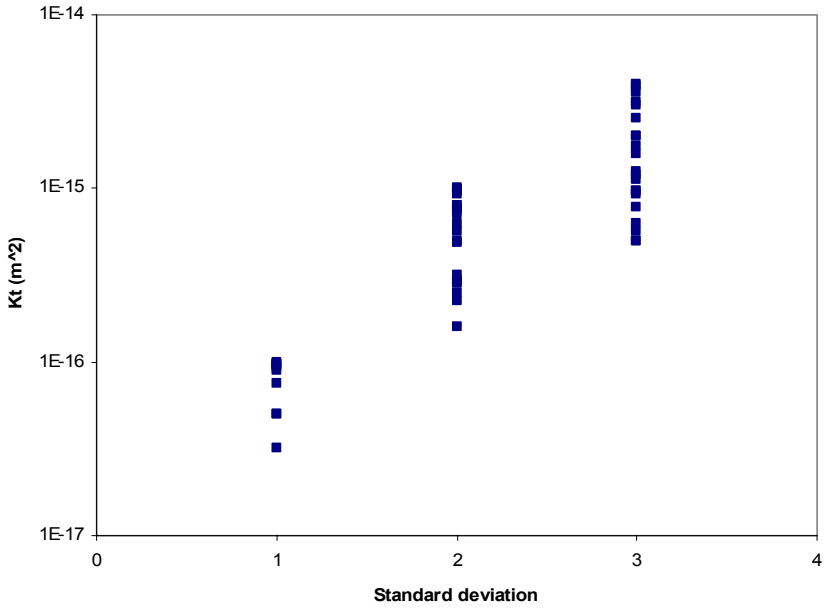

(a)

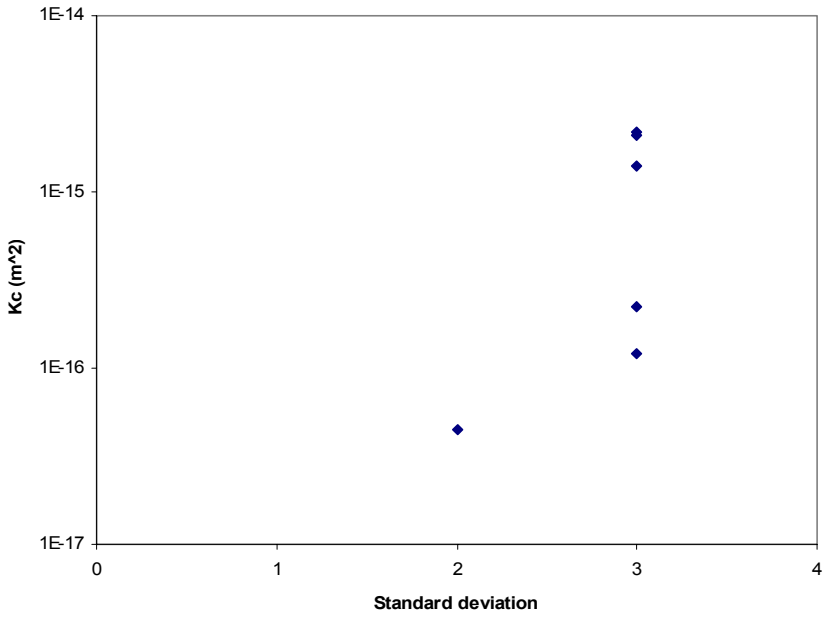

(b)

Figure 3.29 Patch analysis results of threshold permeability and critical permeability versus different standard deviations (σ =1, 2, 3). All three sets of models have the same mean permeability of 10^{-17} m^2 and correlation length τ_x = 300m, τ_y = 3m.

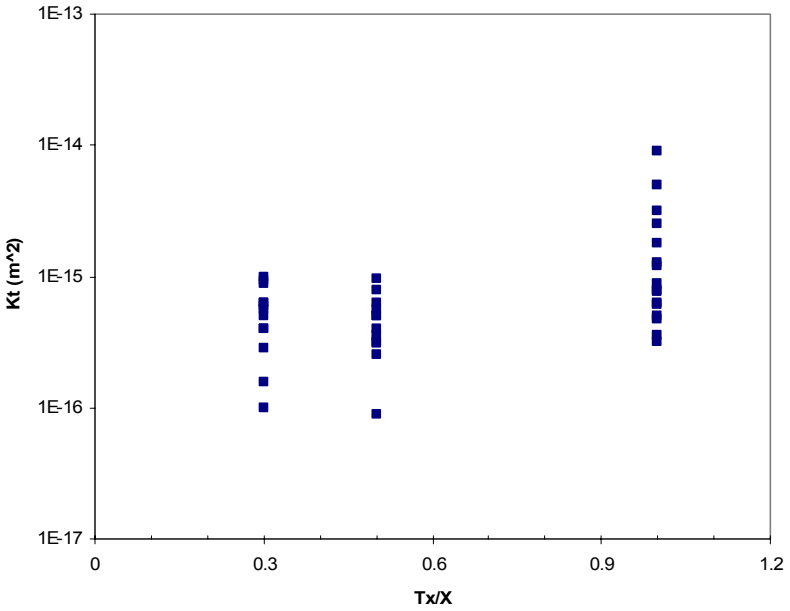

(a)

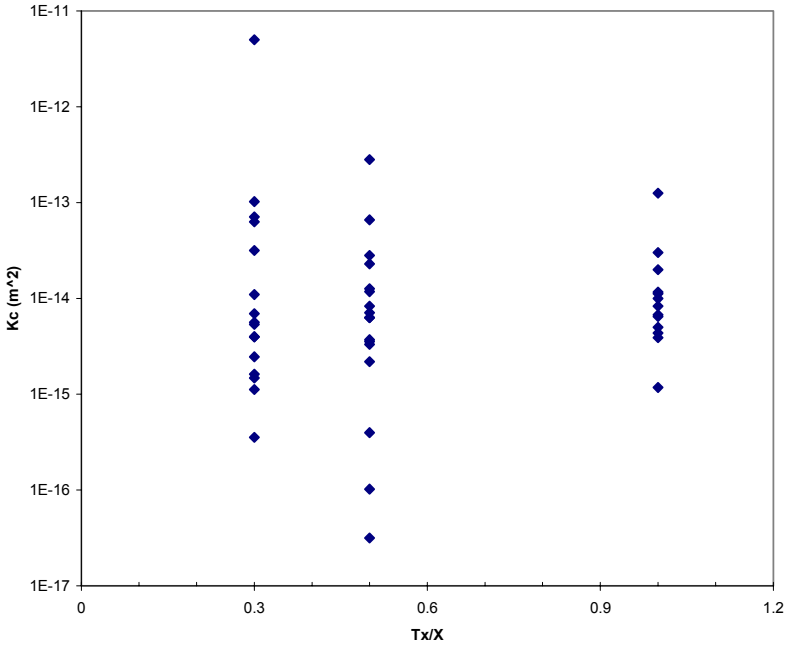

(b)

Figure 3.30 Patch analysis results versus the ratio of horizontal correlation length to the length of model domain. τ_x/X = 0.3, 0.5 and 1.0 correspond to horizontal correlation length of τ_x = 90m, 150m and 300m. Permeability distribution has a mean $\mu = 10^{-18}$ m^2, σ = 3.0, and τ_y = 20m.

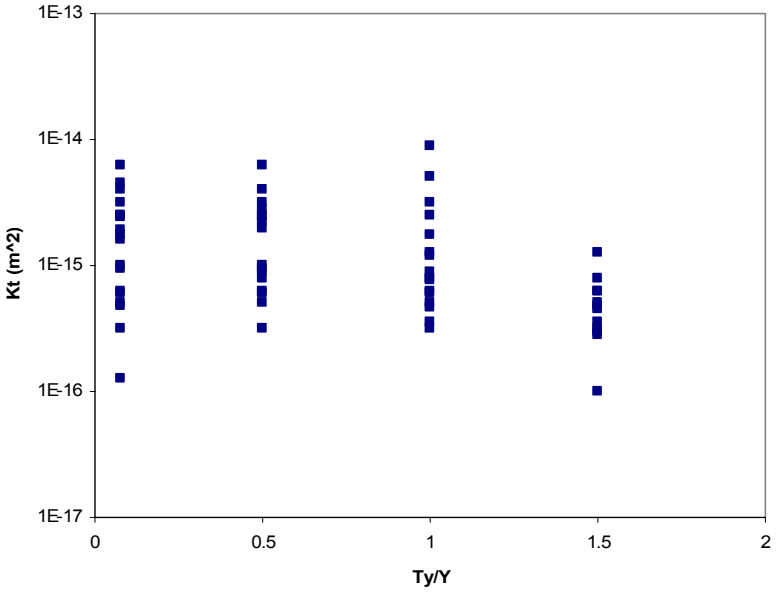

(a)

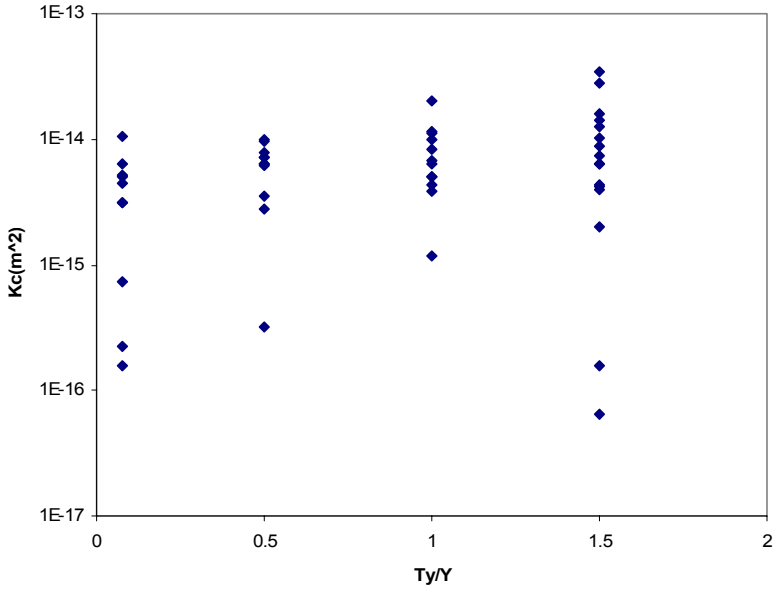

(b)

Figure 3.31 Patch analysis results for four sets of permeability distributions (each has 30 realizations) with different ratios of vertical correlation length to the vertical dimension of the model. τ_y/Y = 0.05, 0.3, 0.67 and 1.0 correspond to the vertical correlation length of 1.5m, 10m, 20m and 30m. Permeability distribution has a mean $\mu = 10^{-18}$ m^2, σ = 3.0, and τ_y = 20m.

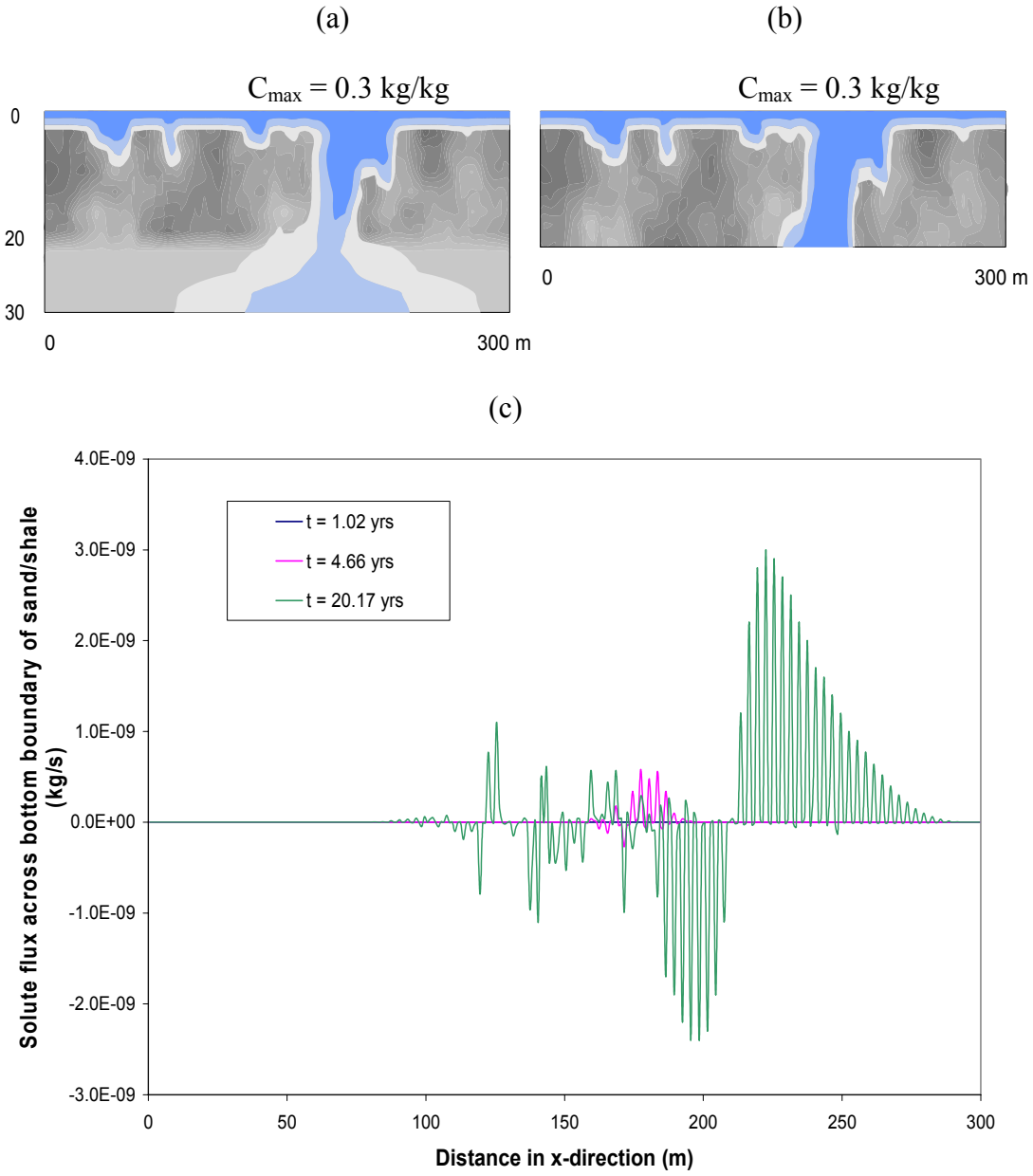

Figure 3.32 (a) Free convection in a shale-sand model (boundary condition is different than (b)). Bottom sand layer has a thickness of 10m and a permeability of 10^{-12} m^2. The permeability distribution for shale has a mean k = 10^{-17} m^2, σ = 3.0, τ_y = 20m and τ_x = 90m. (b) Free convection in a single shale layer. (c) Calculated vertical flux distribution along bottom boundary between shale and sand at different simulation times. The model with a single layer has zero flux across the bottom.

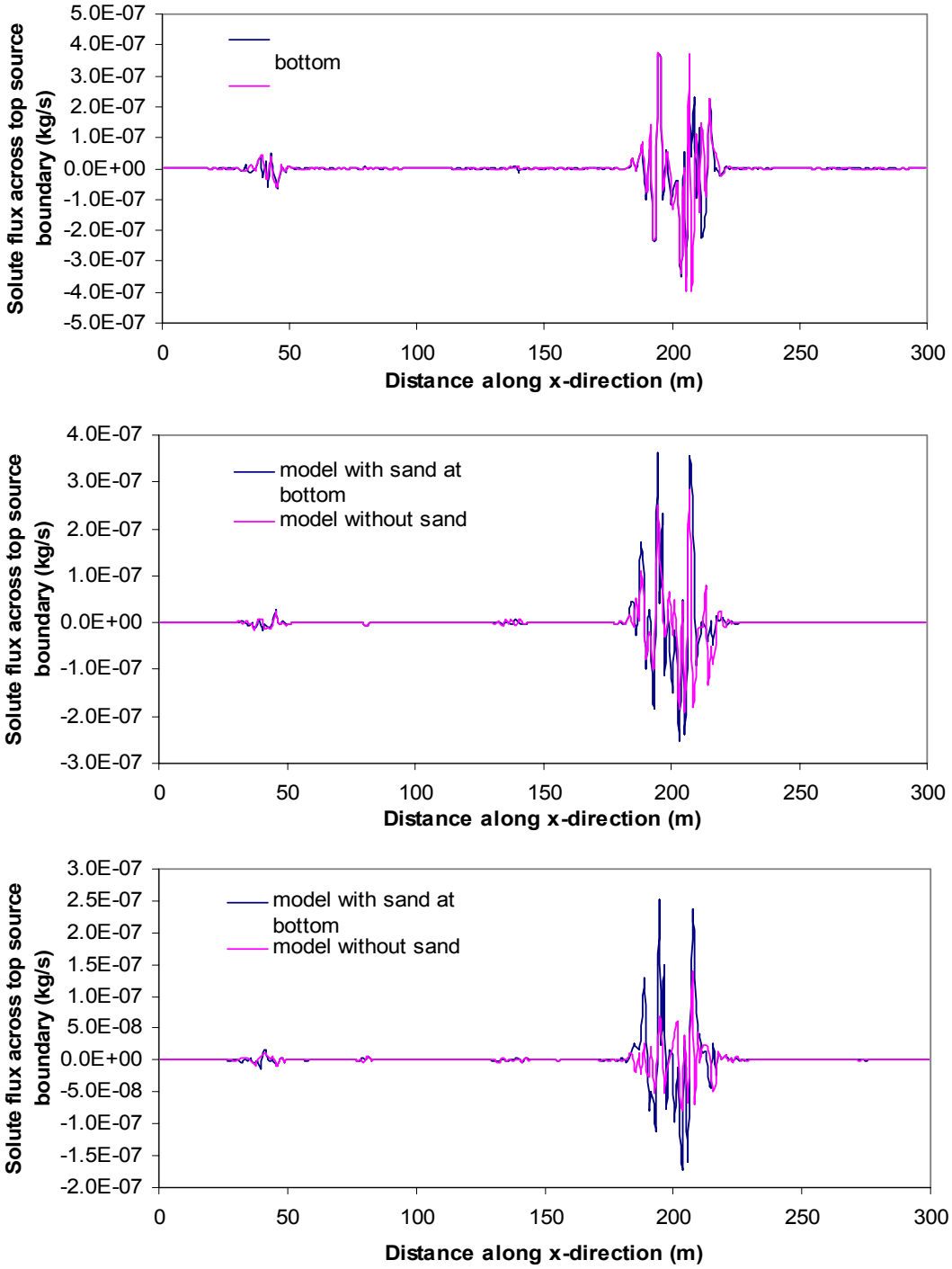

Figure 3.33 Vertical solute flux distribution along top boundary for model shown in Figure 3.32(a) at simulation times of 1.02 yrs (top), 4.66 yrs (middle), and 20.17 yrs (bottom).

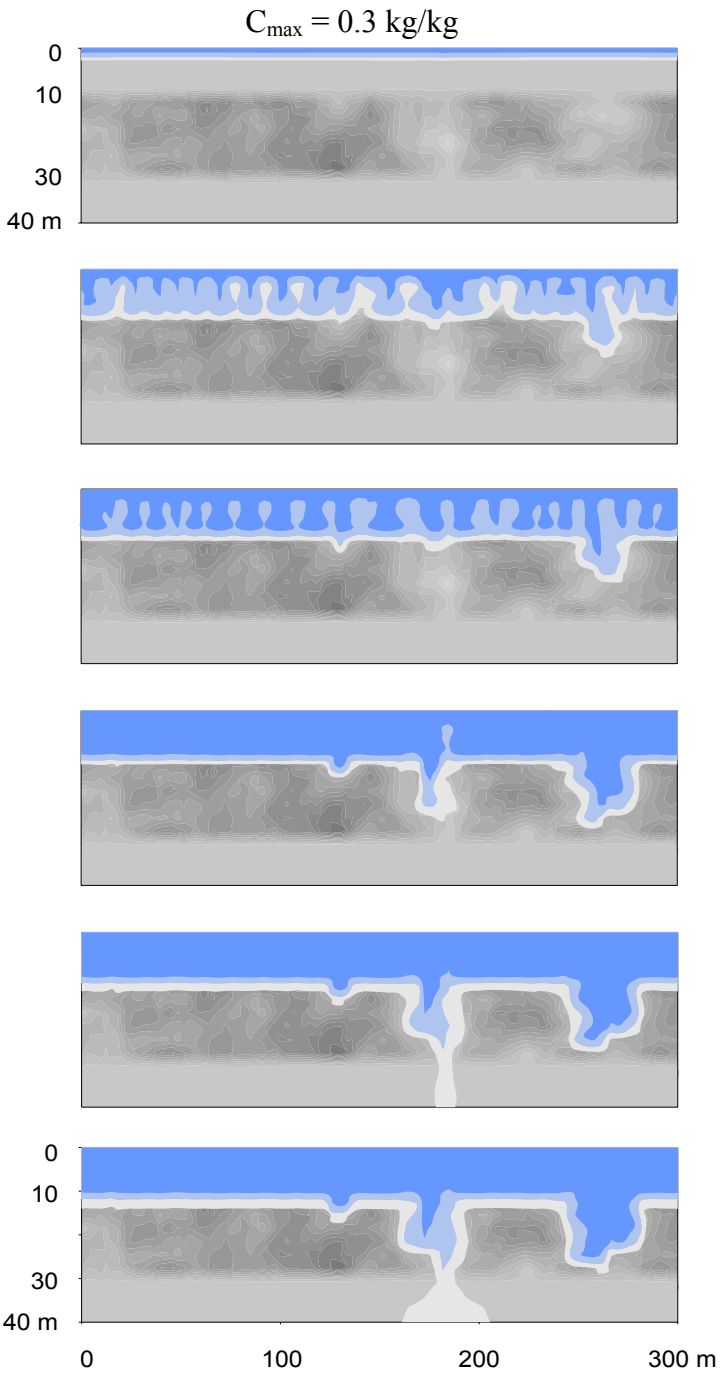

Figure 3.34 Modeling results of flow and solute transport in a sand-shale-sand layer model (see Figure 2.12). The 10-m thick sand layer has a permeability of 10^{-12} m^2. Simulation times are about (a) 4 month; (b) 3 years; (c) 4 years; (d) 10 years, (e) 15 years, and (f) 20 years.

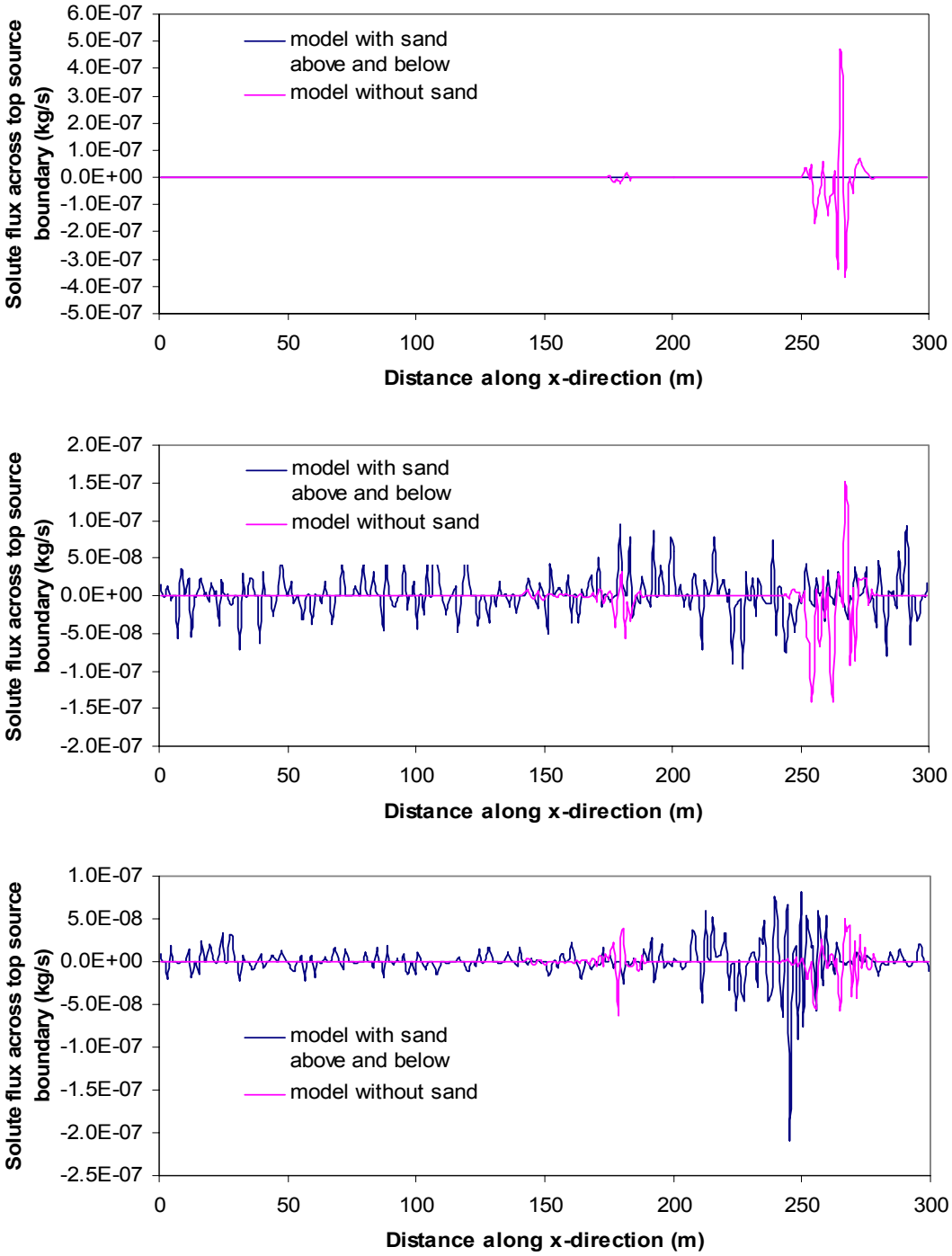

Figure 3.35 Vertical solute flux distribution along top boundary between sand and shale at different simulation times of 6.0 months(top), 3.65 yrs (middle), and 15.73 yrs (bottom).

Chapter 4 FREE CONVECTION IN FRACTURED SHALE

Fractures in the subsurface play a primary role in water, solute, and colloidal transport because fractures are, even with tiny apertures/openings, the main circulation paths and can sustain flow velocities significantly greater than those in the surrounding lower-permeability rocks (e.g., crystalline, granite, shale, glacial till, etc.). Because fractures can rapidly distribute pollutants over large distances and within short time periods, they are perceived as controlling water quality of the aquitard. Previous studies on flow through fractured aquifers generally ignore density-induced convective flow and consider only flow through fractures under hydraulic gradients (Bear et al., 1993; Sudicky et al., 1982, 1992; Tang et al., 1981).

Numerical modeling in the cases where fractures are present as preferential flow paths shows the deep and hot fluid nearby the disposed contaminant can circulate by thermal free convection to the biosphere and thus produce a potential impact on the environment (Yang et al., 2000). When there is dense fluid on top of a fractured shale and no vertical hydraulic gradient, solute is transported down in the fracture plane by free convection if the Rayleigh number (Ra) is greater than the critical Rayleigh number (Ra_{cr}). So far there are very few results available on haline free convection in fractures, although it has been shown that the advection (including convection) is a major mechanism for mass

and solute transport through fractures or fracture networks in low-permeability rocks (Sharp et al., 2001; Shikaze et al., 1994, 1998; Simmons et al., 1999b). Convective instabilities in vertical fractures and faults have been studied for the past few decades, most of which are focused on the effects of large faults on the regional scale thermal convections (Beck, 1972; Zebib and Kassoy, 1977; Lowell, 1977; Lowell and Shyu, 1978; Murphy, 1979; Tournier et al., 2000; Malkovsky and Pek, 1997, 2004) because free thermal convection is a basic mechanism of fluid movement in the crust (Fyfe et al., 1978; Turcotte and Schubert, 1982; Cathles, 1990). Density-induced isothermal mixed and free convections have been recognized as an important solute transport mechanism in porous and fractured aquifers (Mendoza and Frind, 1990; Shikaze et al., 1994, 1998; Schincariol et al., 1994). Investigations in fractured shale saprolite on the Oak Ridge Reservation show that fractures in shale allow for rapid flow in what would otherwise be a low hydraulic conductivity material (Shevenell et al. 1994). Density variation is now being solved simultaneously with groundwater flow in modeling flow and solute transport for the fully-integrated subsurface and surface aquifer systems (personal communication, Dr. Rene Therrien and Thomas Graf, 2004)

Simmons and Sharp (1999) show there are two conditions that permit solute convection in a fractured shale layer, but they do not discuss the condition for the onset of free convection. These two conditions for the minimum shale

layer thickness and minimum wavelength of fracture spacing to allow free convection are:

$$H_{\min} = \frac{12\Delta C \varepsilon \nu D}{\Delta C g b^2 \beta - 12\gamma C_U \varepsilon \nu D} = \frac{\frac{12\varepsilon \nu D}{g b^2 \beta}}{\left(1 - 12\gamma \frac{C_U}{\Delta C} \frac{\varepsilon \nu D}{g b^2 \beta}\right)} \tag{4.1}$$

$$\lambda_{\min} = \sqrt{\frac{48\varepsilon \nu D H_{\min}}{g b^2 \beta}} = \frac{\frac{24\varepsilon \nu D}{g b^2 \beta}}{\sqrt{1 - 12\gamma \frac{C_U}{\Delta C} \frac{\varepsilon \nu D}{g b^2 \beta}}} = \frac{2H_{\min}}{\sqrt{1 + \gamma \frac{C_U}{\Delta C} H}} \tag{4.2}$$

And whenever the denominator in Eq.(4.1) approaches 0, $H_{\min}$ will be infinitely large. To determine conditions necessary for the onset of free convection in a fault, Wang (1994) assumed convection can develop solely in the cross-section perpendicular to the fracture plane. Results from his study show that convection can occur only if the thickness of the fault zone is of the same order of magnitude as the height of the layer (i.e., the aspect ratio of aperture to height is ~ 1).

Studies of Murphy (1979) and Malkovsky and Pek (1997) using analytical stability analysis have shown that the critical Rayleigh number for the onset of thermal free convection in a fracture (perpendicular view) can greatly exceed the value $4\pi^2$, which is the value for an infinite porous medium determined by Lapwood (1948). Study of density-dependent solute transport in fractured media

by Shikaze et al. (1998) looked at solute transport in a two-dimensional plane perpendicular to the fractures. The fractures are represented by one-dimensional line segments superimposed on the rectangular mesh that represents the porous matrix. Solute transport pattern was found to be rather complex when considering the fracture-matrix interactions (shale permeability is 10^{-15} m^2) and the development of a dense plume in fractured media may not be amenable to prediction.

Free convection in fractures (fractures, faults, fissures et al.) in low-permeability shales must be considered in modeling groundwater flow and solute transport. The purpose of this chapter is to study the onset condition of free convection in fractures and to examine numerically free convection in fractures separated by two smooth parallel walls in the low-permeability host rock of shale.

4.1 Permeability of fractures in low-permeability rocks

Unfractured shale usually has a permeability in the range of 10^{-14} to 10^{-23} m^2 (Neuzil, 1993; Dewhurst et al., 1999). When shales are fractured, highly permeable fractures and faults can form the preferential flow pathways and, thus, dominate flow field. Field-scale shale permeabilities appear in some cases to be greater than those measured on core plugs in the laboratory because of fractures. For example, Bredehoeft et al. (1980) calculated a regional absolute permeability of 10^{-16} m^2 in the Pierre Shale, although Neuzil (1993) showed the matrix

permeability of 10^{-20} m^2 at the laboratory scale. This implies that shales have a heterogeneous permeability structure influenced by fractures, faults, or the interlayering of more permeable coarser-grained sediments. Neuzil (1994) found that permeability was scale dependent in argillaceous media at only the largest regional scales, perhaps suggesting the existence of widely spaced transmissive fractures. Walraevens and Cardenal (1999) inferred that preferential groundwater flow pathways through shallow buried, Tertiary Bartonian Clay in Belgium exist based on the inconsistency between laboratory permeability tests and the distribution of hydraulic heads in the region. In many cases, the incipient pathways of fluid flow are present as faults, transecting the low permeability formations, or as interconnecting networks of smaller fractures or fissures (Horseman & Harrington, 1996). Therefore, at the macroscopic level, very large-spacing fractures or fault zones are the preferential flow pathways. Many studies of large scale utilize a permeability value of 10^{-14} m^2 (Brace, 1980; Trimmer et al., 1980; Bredehoeft and Norton, 1990), which is the critical permeability value required to initiate free convection for a homogeneous boundary layer (Wooding, 1997). For largely spaced fractures or faults, the onset of free convection obeys the same critical Rayleigh Number criterion.

Microfractures, on the other end, can form in shales when fluid pressures exceed the minimum principal stress and the tensile strength of the rock *in situ*. Wang & Xie (1998) carried out systematic numerical experiments to study the

compaction-induced hydrofracturing commonly occurred in shale-rich basins and in sand-shale sequences. They showed that at vertical permeability of 10^{-18} m^2 and sedimentation rate greater than 50 mm/yr, compaction-induced hydrofracturing maybe a common process in shale-rich basins even at relatively shallow depths. Capuano (1993) showed images of deeply buried fractured shale from the Oligocene Frio Formation of Texas with fracture fills of calcium sulfate and organic material. The samples were taken from cores at depths of 3-5 km. The Frio formation consists of interfingered marine and nonmarine sandstones and shales, with the shales comprising about 80% of the section (Galloway et al., 1982). The calculated fracture permeability of the shales in this case is on the order of 10^{-13} m^2, which is the same as that of the Frio sandstone.

Usually, permeability of a smooth, uniform aperture is determined from the cubic law (Lamb, 1932; Snow, 1965):

$$k = \frac{b^2}{12} \tag{4.3}$$

where b is the fracture aperture (L).

When a fracture has an open aperture of 1mm, the permeability calculated based on (4.3) is about 8.3×10^{-8} m^2, which is the high end value for sands or gravels. Therefore, a 1-mm aperture fracture can transport large amounts of water under hydraulic gradient.

Large aperture fractures are commonly filled with materials either transported by groundwater flow or precipitated by chemical dissolution and precipitation. Permeability of the fracture is therefore affected by properties of the filling materials. Many regional studies (Brace, 1980; Bredehoeft and Norton, 1990) have adopted the value of $10^{-12} \sim 10^{-14}$ m^2 as the permeability for the faults or large fractures in shale. In this study, 10^{-12} m^2 is used in model scenarios for macrofractures.

4.2 **Onset condition of free convection in a single fracture**

The most important dimensionless number in isothermal haline convection study is the Rayleigh number:

$$Ra = \frac{\rho_0 g \beta k \Delta C H}{\varepsilon \mu D} \geq Ra_{cr} \tag{4.4}$$

where $\boldsymbol{\varepsilon}$ is porosity; $\boldsymbol{\mu}$ is dynamic viscosity (kg/m/s); D is diffusion coefficient (m); ρ_0 is fluid density at base concentration (kg/m^3); g is gravity acceleration (m/s^2); $\boldsymbol{\beta}$ is the expansion coefficient of concentration; $\boldsymbol{k}$ is the permeability of the layer (m^2); $\boldsymbol{\Delta} C$ is the concentration difference between the upper and bottom boundaries (kg/m^3); H is the height of the layer (m). Ra_{cr} is the critical Rayleigh number for the onset of free convection.

For a porous layer bounded laterally by walls that are adiabatic and impermeable, the critical Rayleigh number depends on the aspect ratios A and B in the two horizontal directions (Beck, 1972; Caltagirone, 1975).

$$Ra_{cr} = \min_{A,B} \frac{\pi^2 \left[\frac{i^2}{A^2} + \frac{j^2}{B^2} + k^2 \right] (A^2 i^2 k^2 + B^2 j^2 k^2 + (i^2 + j^2)^2)}{(i^2 + j^2)^2} \tag{4.5}$$

where $A = \frac{X}{H}$, X is the horizontal length of the layer along the x direction, H is the thickness of the layer; $B = \frac{Y}{H}$, Y is the horizontal length of the layer along the y direction; $\boldsymbol{i, j, k}$ = 1, 2, 3,….., n, and $\boldsymbol{i+j+k \neq 0}$.

For a two-dimensional porous medium, the critical Rayleigh number reaches the minimum value of $4\pi^2$ whenever A is an integer (1, 2, …., n, and $k = 1$) as shown in Figure 4.1. A three-dimensional fracture or fault can be represented by an elongated open space bounded by two smooth parallel plates with definite length and height. But for a *2D* cross-section perpendicular to the fracture plane, the aspect ratio for the fracture is $A = b / H$, where b and H are the fracture aperture and height perpendicular to the strike. Usually the fracture height H is much larger than the aperture b, the aspect ratio $A \to 0$ (in this 2D case, $\boldsymbol{j}$ = 0). Therefore the critical Rayleigh number is several orders of magnitude greater than the critical value $4\pi^2$.

Based on the analytical Rayleigh number given by Caltagirone (1975) (Equation 4.4), the critical Rayleigh number for the onset of free convection in a single fracture with impermeable upper and bottom boundaries is given in this study as a function of the fracture aspect ratio:

$$Ra_{cr}(\hbar) = \left[16 * \left(\frac{0.95}{\hbar} \right)^{2.52} + \left(4\pi^2 \right)^{1.25} \right]^{0.8} \tag{4.6}$$

where $\hbar = \frac{b}{H}$ is the dimensionless aperture of the fracture.

Figure 4.2 shows the theoretical critical Rayleigh number and critical Rayleigh number calculated from Eq.(4.6). For aspect ratio less than 0.5, the critical Rayleigh number function (Eq.(4.6)) is in good agreement with analytical critical Rayleigh number with errors less than 1%. Figure 4.3 shows the exponential relationship between critical Rayleigh number and the required fracture height to initiate free convection.

The threshold permeability for the onset of free convection in a fracture with known height H and a fixed concentration difference between the upper and bottom boundary ΔC can be derived from condition (Eq.4.4):

$$k_t = \frac{\mu D}{\rho_0 g \beta \Delta C H} Ra_{cr} \tag{4.7}$$

For a typical fracture with 1 millimeter aperture, 1 meter vertical height, and concentration difference of 300 kg/m^3, the threshold permeability is about 4.8×10^{-9} m^2. The flow regime I, as shown in Figure 4.2, demonstrates convection

dominated flow and flow regime II shows diffusion dominated. The transition between these two flow regimes is the critical Rayleigh number line.

Applying transport parameters in Table 4.1, the concentration difference between the dense fluid on the top boundary and the ambient groundwater in the fracture for the onset of free convection is calculated and shown in Figure 4.4. The concentration difference decreases exponentially with increasing fracture aperture, but reaches a constant value at a certain aperture. It also decreases with increasing fracture height. When the concentration difference is about 300 kg/m^3, which is approximately the maximum concentration difference observed in the salinity inversion profile in the Gulf of Mexico Basin (McKenna and Sharp, 1996), the minimum height of the layer for the onset of free convection in the layer is on the order of 10^{-5} m.

4.3 Numerical modeling of free convection in fractures

Modeling effort has been focused on macrofractures on the meter-scale and microfractures on the millimeter scale. Fractures in 2D and 3D matrices are represented by two parallel walls with a uniform aperture. Because the shale matrix has a very low permeability compared to that of the fracture and diffusion from the fracture to matrix is expected to be small and negligible, the purpose of the study is to examine the onset of free convection inside the fracture either on

the 2D cross-section perpendicular to the fracture plane or along the fracture plane.

The onset and development of free convection in fractures is studied with the USGS 3D SUTRA models (Voss and Provost, 2003) together with SUTRAGUI (Winston, 2004) as an extended module to commercial software ArgusOne (Argus Open Numerical Simulation v4.0) for the preprocessing and USGS Model Viewer 1.0 (Hsieh and Winston, 2003) for the post-processing and visualization. The properties of the matrix and fracture and solute transport used in the modeling are summarized in Table 4.1.

4.3.1 Macrofracture or fault in shale

The three-dimensional SUTRA model of a fractured shale is setup as 40m long by 40m wide with a 1-m fracture imbedded in the matrix (Figure 4.5). The fracture geometry is shown in Figure 4.6. First-type (type 1) concentration boundary conditions are applied at the top and bottom of the domain. The upper boundary has a specified and initial concentration of 300,000 ppm (parts per million) in chloride, the initial concentration is set to zero everywhere in the model domain. The upper and bottom boundaries are considered impermeable to flow and the diffusive flux of solute is zero (constant concentration boundary). The four vertical boundaries are assigned second-type zero flux for both flow and solute transport. The bottom boundary for transport is specified as a zero

dispersive flux boundary. Because there is no external pressure gradient applied on the model boundaries, any convection that occurs is driven by density gradient only.

The model domain is regularly discretized with spatial discretization of $\Delta x = \Delta y = \Delta z = 1$ m. The transient flow model has an initial time step of 43200 seconds (approximately 12 hours) and the maximum allowed simulation time is approximately 191.2 years. The aspect ratio (B=b/H) of fracture aperture to height is about 0.033 and the corresponding critical Rayleigh number is 10^4. Because the fracture is 1-meter wide, infill materials will determine the permeability of the fracture. We assume permeability of the fracture on the order of 10^{-12} m^2 which is equivalent to that of sandstone. The surrounding shale matrix has a permeability of 10^{-18} m^2. Because of such low permeability, flow and transport in the matrix is mainly controlled by diffusion. The onset condition for free convection initiation in the cross-section that is perpendicular to the fracture aperture (i.e., on the fracture plane) is the same as expressed in (1.1), i.e., $4\pi^2$ when the aspect ratio $A \geq 1$ (A = W/H, W is the width of the fracture along the strike). The calculated Rayleigh number for this model is about 4.1×10^7, which is greater than the required critical Rayleigh number and therefore, free convection is expected to occur.

Figure 4.7 shows modeling results at simulation times of approximately 4 months for solute plume developments along the fracture on the side view of the

3D block. The dual-porosity model takes into account of the fracture-matrix interaction and shows slower and minor diffusion into the matrix from the vertical fracture. But it is the fracture that provides the preferential flow path for plume penetration. In the beginning of the simulation, solutes slowly diffuse into the top boundary of the matrix and fracture and accumulate. After a certain period of time when there is enough solute concentration difference, instabilities start to grow into convective mode and free convection is shown to migrate down in the fracture. The bottom layer of sandstone has the same permeability as the fracture, therefore once the solute plume reaches the sandstone layer it spreads out into the bottom layer and later convection starts to generate in this bottom layer.

The modeling results of solute plume development inside the fracture are shown in Figure 4.8 by cropping the 3D model domain in the center. The convection cells are clearly shown on the cross-section of the fracture plane. The development of convective flow along the fracture plane is demonstrated in Figure 4.9 (a) to (f). Dense solute first filtrates through the top boundary and accumulates and instabilities started at the vertical boundaries and developed into lube shaped fingers at about 3.2 years (Figure 4.9 (c)). The solute front of 0.15 isoconcentration (green) reached the bottom sandstone layer at about 8.12 years (Figure 4.9 (e)). The maximum concentration reached the bottom boundary of the model at about 14.1 years (Figure 4.9 (f)).

4.3.2 Microfractures

The model setup for a parallel-plate microfracture embedded in the shale matrix is 40m long, 40m wide and 30m high. The model domain is almost the same as Figure 4.5 except that the fracture with a 1 mm aperture penetrates through the center of the matrix box without a bottom sandstone layer. Boundary and initial conditions are the same as these described for the macrofracture model. Spatial discretization is variable with very fine grid size around the tiny fracture. Initial time step is set at 60 sec. and maximum simulation time is about 10.6 days. The permeability of the open fracture is now calculated by cubic law.

For density-driven flow inside the parallel-plate fracture, the maximum velocity can be calculated :

$$V_c = \frac{\rho_0 g b^2 \beta \Delta C}{12\mu} \tag{4.8}$$

Figure 4.10 shows the solute transport through a microfracture at simulation time of 10 days. The plume already reached the bottom of the fracture because of fast convecting flow velocity. Figure 4.11 shows free convection occurring along the tiny fracture plane and the time series development of convection flow is shown in Figures 4. 12 (a) to (g). By cropping the model domain and look inside the single fracture, convection cells are shown to be affected less by the boundaries. The irregular pattern of convection cells is due to the large Rayleigh number. The flow regime for large Rayleigh number

(> 240~300) (Nield and Bejan, 1999) is referred as transient convection and the convection cells become highly unstable. The velocity field of free convection along the fracture plane shown in Figure 4.13 shows clearly the upwelling and downwelling flow regimes corresponding to the plumes in Figure 4.11.

For small aperture fractures, modeling results shown in Figures 4.14 illustrate that if convective instabilities occur convection cells manifest on the fracture plane and take the form of rolls with axes parallel to the aperture along y-axis (see Figure 4.5). This is consistent with theoretical study results by Davis (1967), Beck (1972) and Murphy (1979). Because for 3D discrete open fractures with parallel walls, the preferred cellular mode (***a, b***) for the convective circulation at Rayleigh number just above the critical value is always (2n, 0) when B or b is $\rightarrow 0$. Numerical modeling results show that the axes of the convective cells are perpendicular to the fracture plane and parallel to the x-z plane (Figure 4.5). Figure 4.15 shows a snapshot of the perfect symmetric convective cells.

4.4 Conclusions

Density-induced convection is an important mechanism for groundwater flow and transport through fractured media. This study examines the onset condition for free convection occurring within a single fracture with 3-D numerical models to examine free convection. Theoretical study and numerical modeling results on

the onset of free convection in fractures surrounded by low-permeability shale show that:

1) The critical Rayleigh number for the initiation of convective flow for a parallel-plate fracture is several orders in magnitude greater than that for horizontal infinite porous layer.
2) For large fractures with infills, the critical Rayleigh number is approximating $4\pi^2$ when the aperture is of the same order of magnitude as the height of the layer (i.e., the aspect ratio is ~1.0).
3) When the fracture aspect ratio (b/H) is smaller than 0.5, the critical Rayleigh number can be approximated by a function depending only on this dimensionless ratio. This critical Rayleigh number function (Eq.4.6) closely approximates the theoretical values at aspect ratio as small as 10^{-8}.
4) When free convection initiates, those convection cells show themselves on the fracture plane with axes parallel to the fracture aperture. Therefore, two-dimensional numerical models of fractures can never capture the convective motion of flow along the third dimension when the fractures have a non-unit thickness along the strike direction. Three-dimensional models can best describe the onset and development of free convection in low-permeability fractured media.

Numerical modeling results also show that transient convection occurs when the Rayleigh number is high. These transient convection cells generate

and disappear at different locations, and the pattern keeps changing through time (see Figures 4.12).

5) Therefore, free convection can easily occur in fractures and transport dense fluid through fractures under no hydraulic gradient.

Table 4.1 Parameters used for 3D fractured shale model

parameter	unit	value
D_0	molecular diffusivity (m^2/s)	1.0×10^{-9}
μ	dynamic viscosity (kg/m/s)	1.0×10^{-3}
ρ_0	density at base concentration (kg/m^3)	1.0×10^{-3}
β	coefficient of density variation	0.7
ΔC	maximum concentration difference (kg/m^3)	300
b	aperture (m)	1.0
W	fracture width (m)	40
L_x	length (m)	40
Ly	width (m)	40
H	layer height (m)	30
α	fluid compressibility ($kg\ s^2/m$)	4.5×10^{-10}
β	matrix compressibility ($kg\ s^2/m$)	1.0×10^{-8}
α_L	longitudinal dispersivity (m)	1.0
α_T	transverse dispersivity (m)	0.1

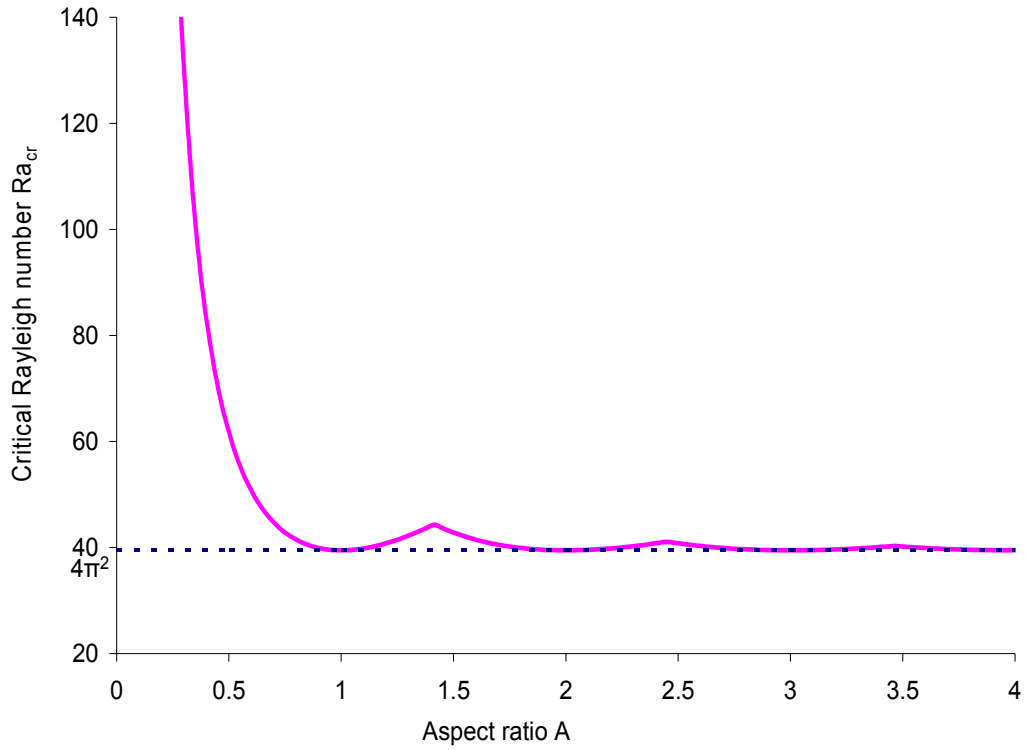

Figure 4.1 Critical Rayleigh number vs. aspect ratio A, which is the ratio of horizontal length to the vertical length in a 2D layer.

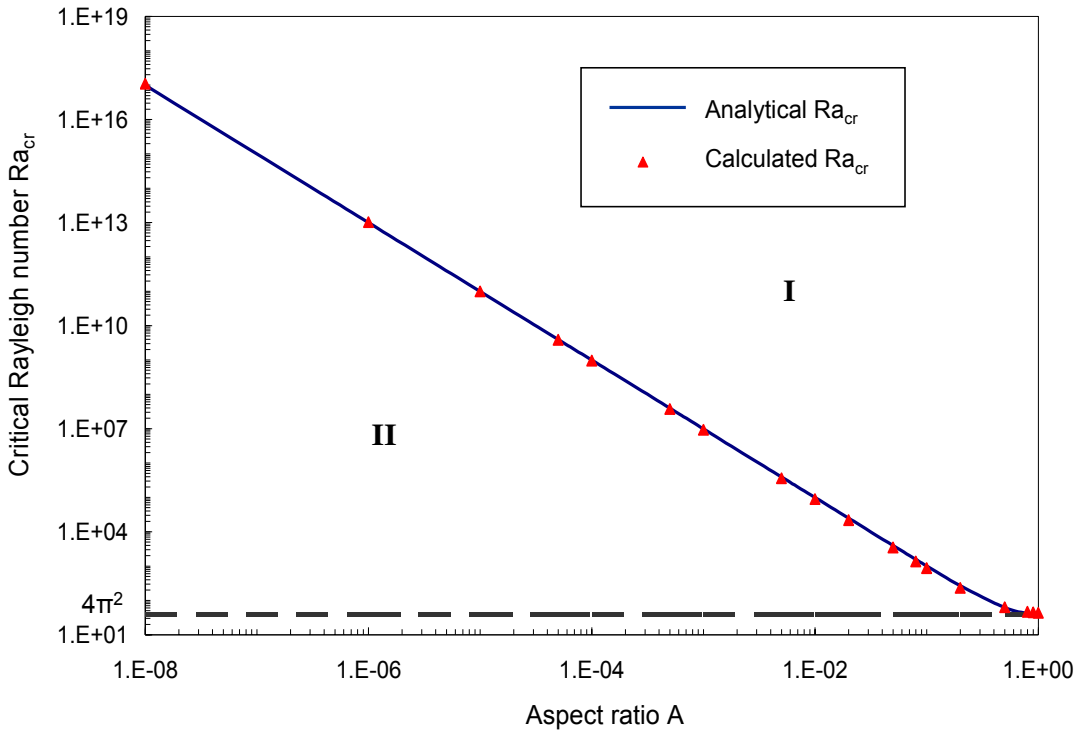

Figure 4.2 Calculated critical Rayleigh number as a function of aspect ratio. Region I stands for stable convection regime and region II is the diffusion dominated regime.

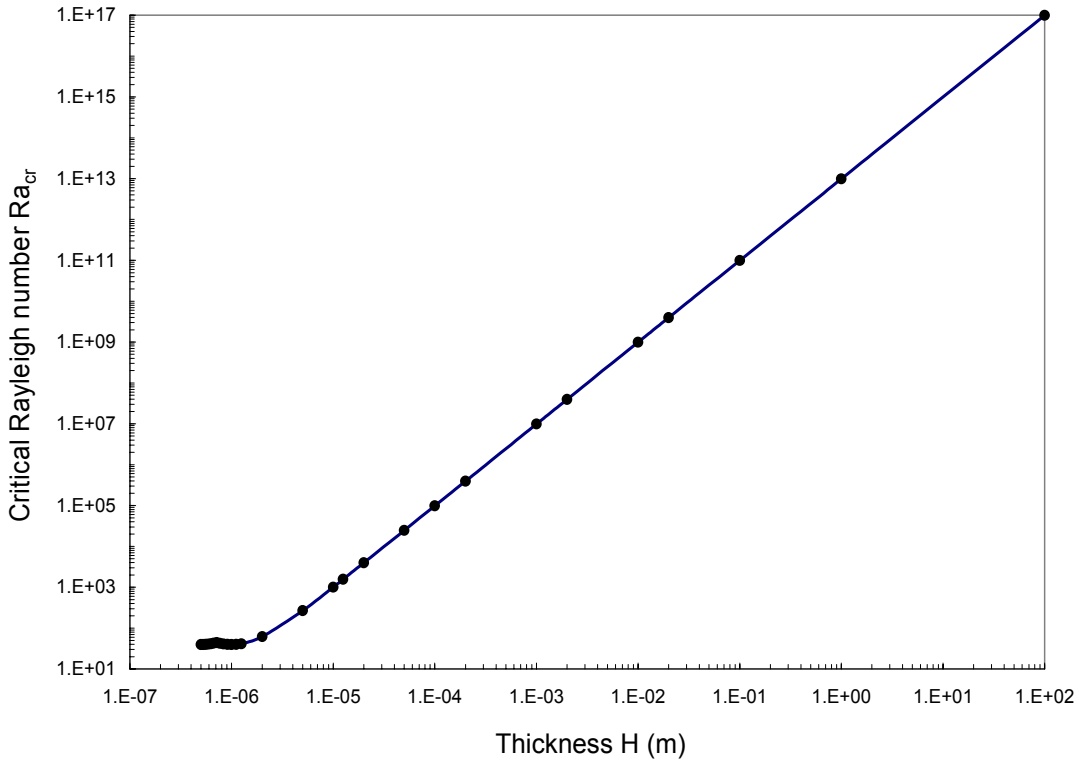

Figure 4.3 Relationship between critical Rayleigh number and thickness of the layer.

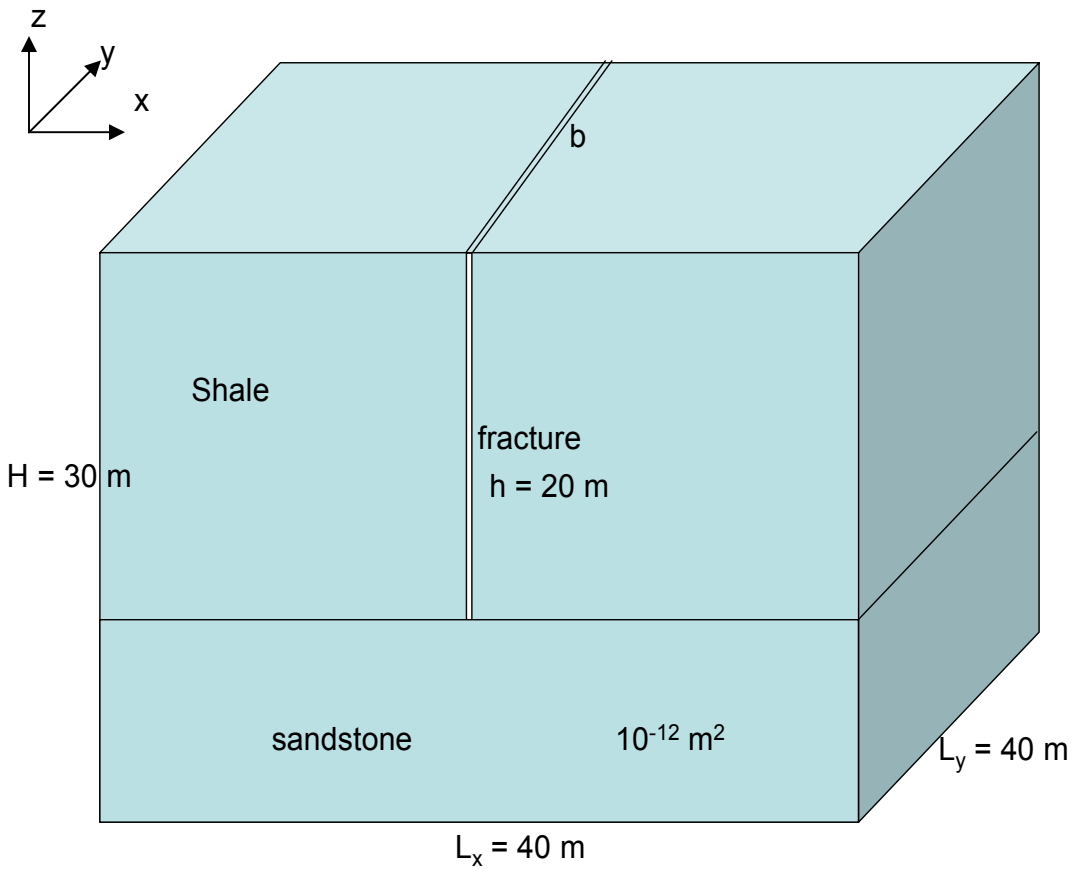

Figure 4.4 Fractured shale model setup. Shale permeability is 10^{-18} m^2.

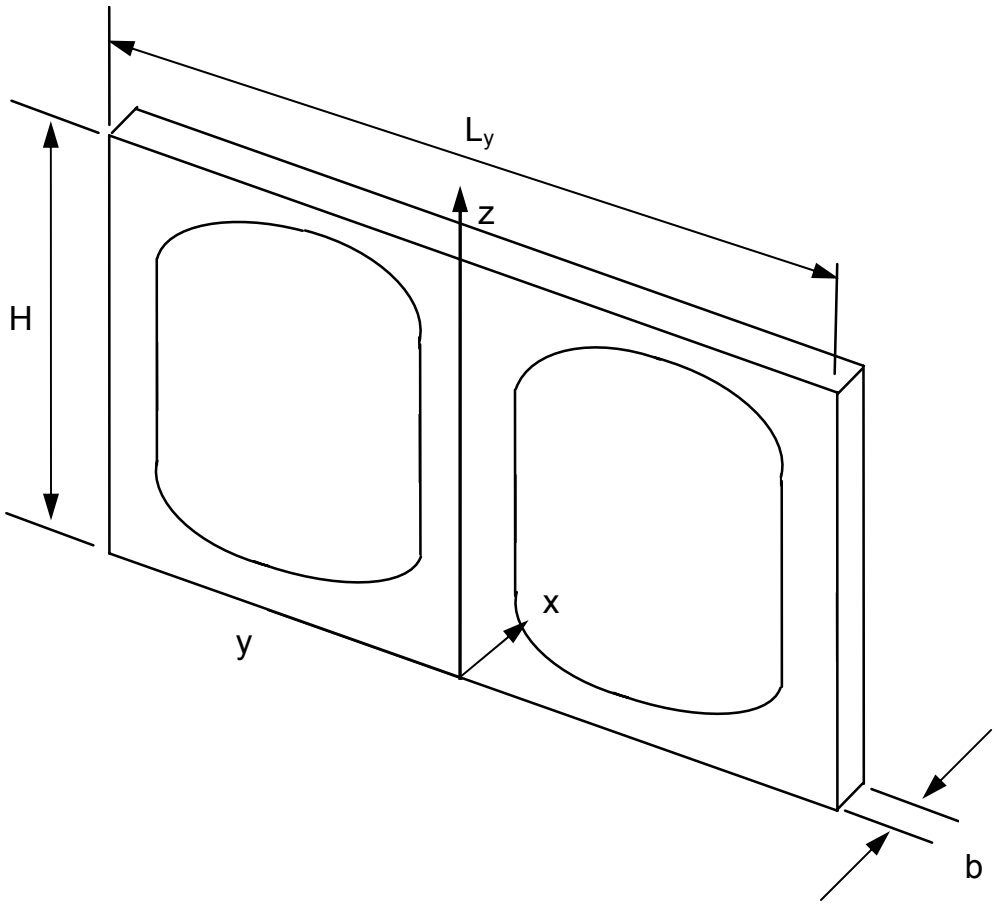

Figure 4.5 3D fracture geometry.

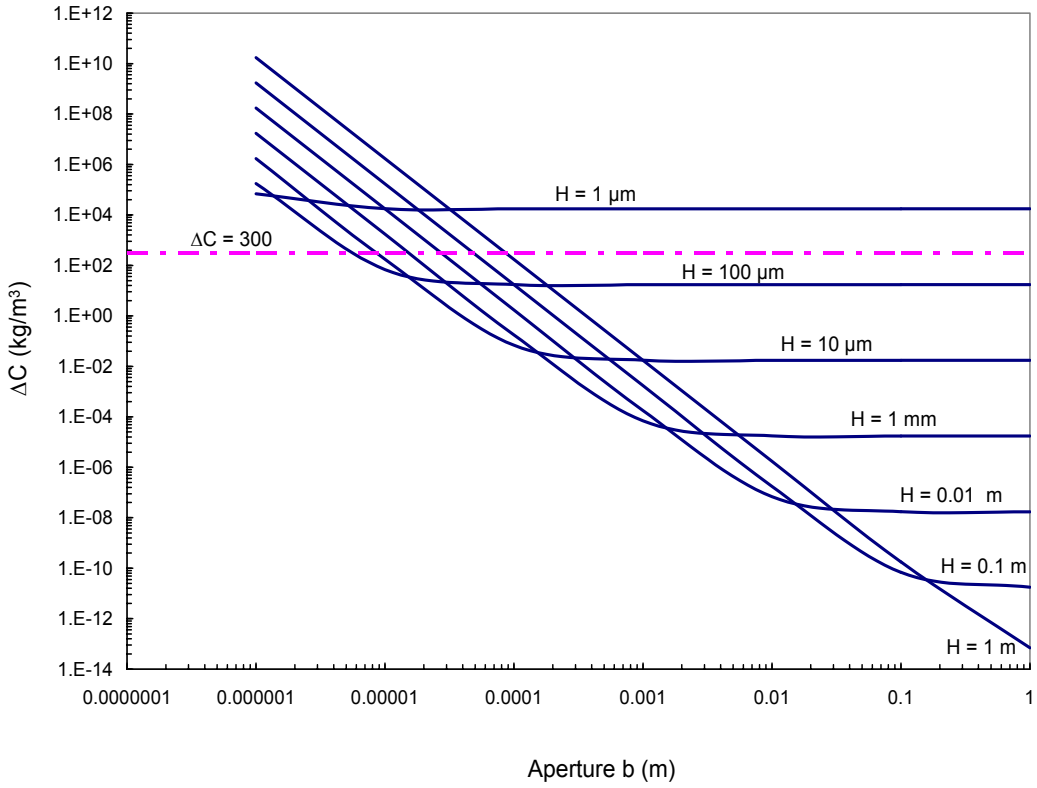

Figure 4.6 Maximum concentration difference changes with aperture for different layer thickness.

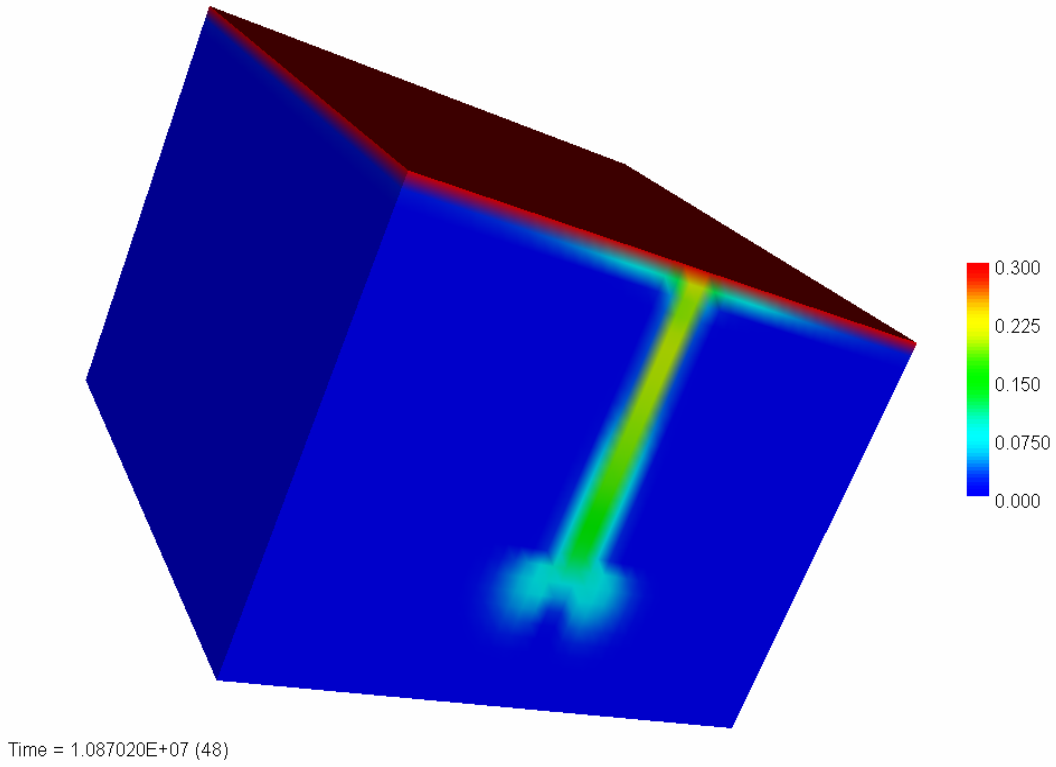

Figure 4.7 Solute transport through single fracture in low-permeability shale. Fracture permeability $k_f = 10^{-12}$ m^2, shale permeability $k_s = 10^{-18}$ m^2. Fracture aperture b = 1 meter. Concentration difference between dense fluid on the top and bottom is 300,000 ppm (about 0.3 kg/kg). Simulation time is about 4 months.

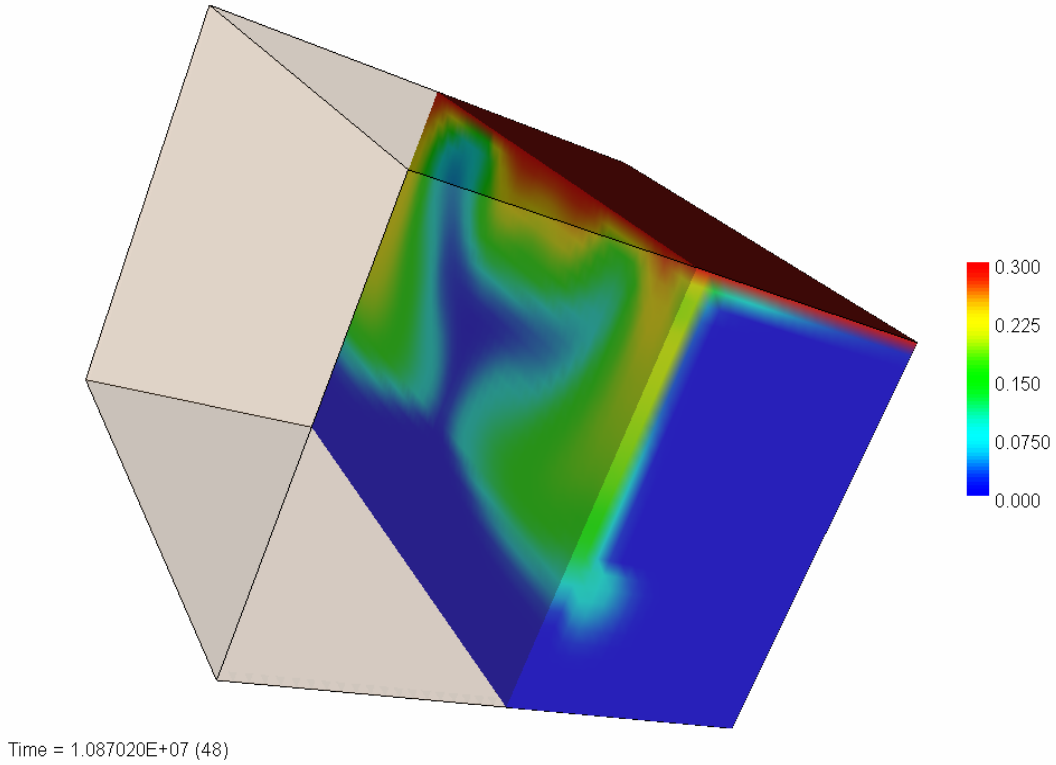

Figure 4.8 Solute transport inside the fracture (cropped from model shown in Figure 4.7).

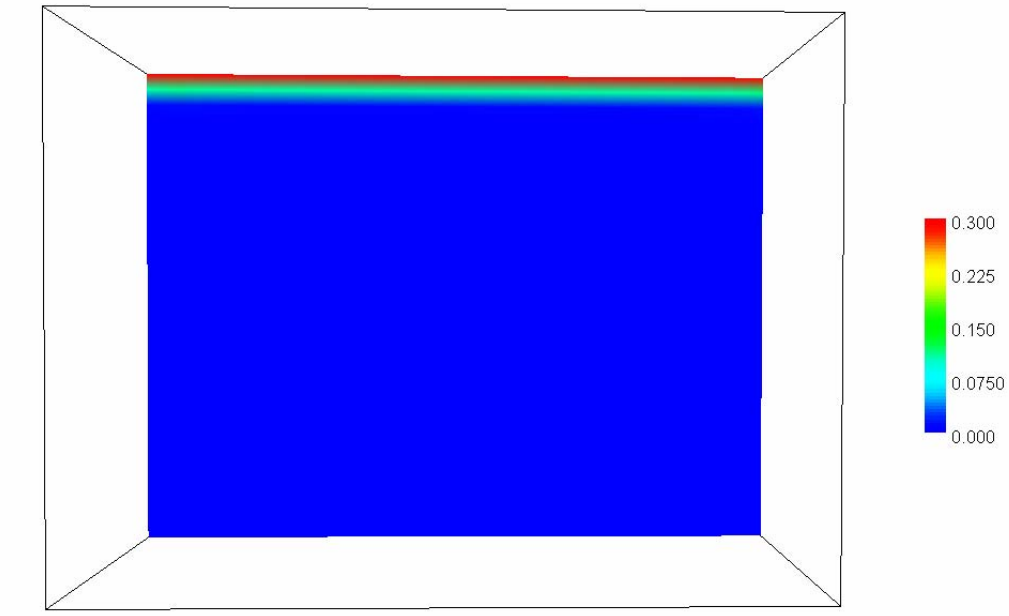

Time = 3.343362E+06 (25)

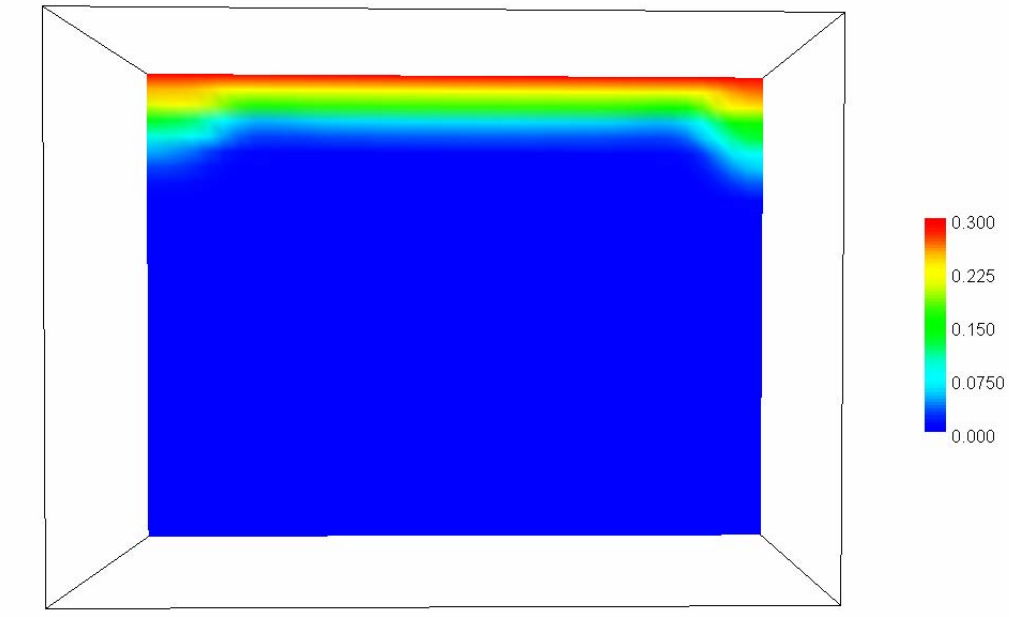

Time = 4.759248E+07 (85)

Figure 4.9 (a) Free convection occurring along the fracture plane.

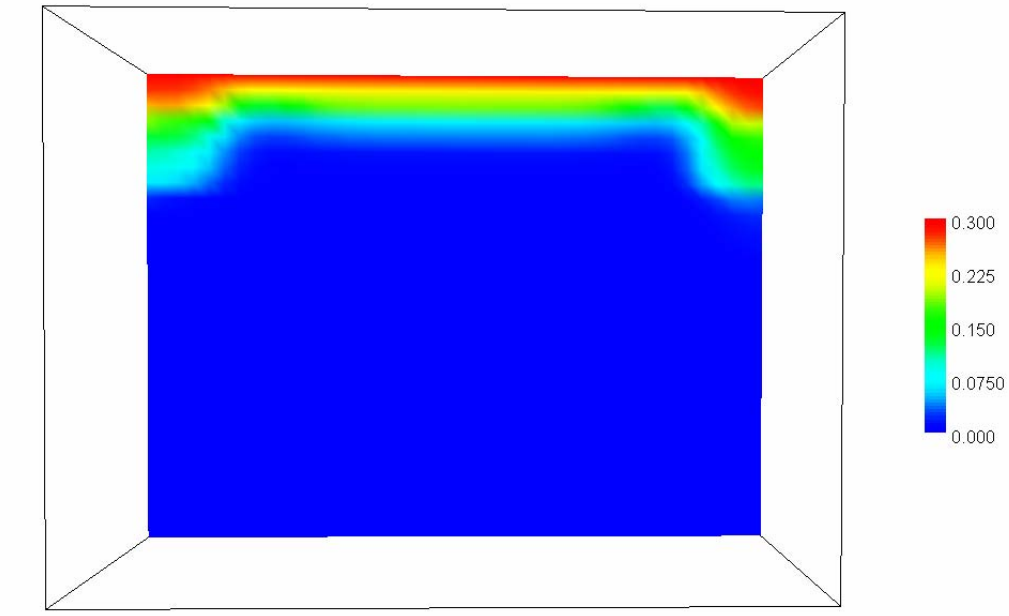

Time = 6.952159E+07 (95)

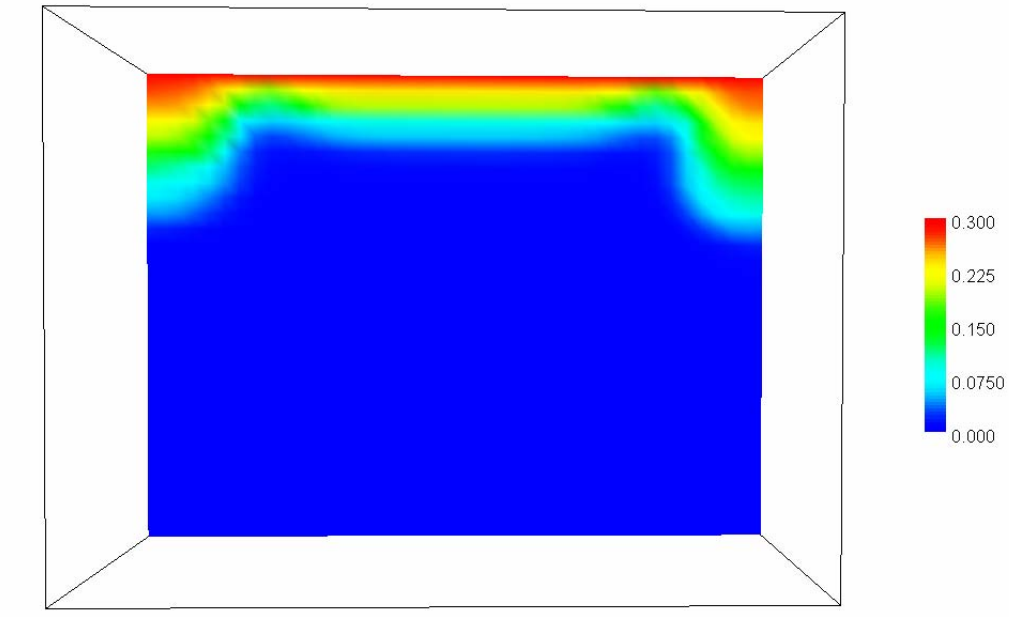

Time = 8.387518E+07 (100)

Figure 4.9 (b) - continued

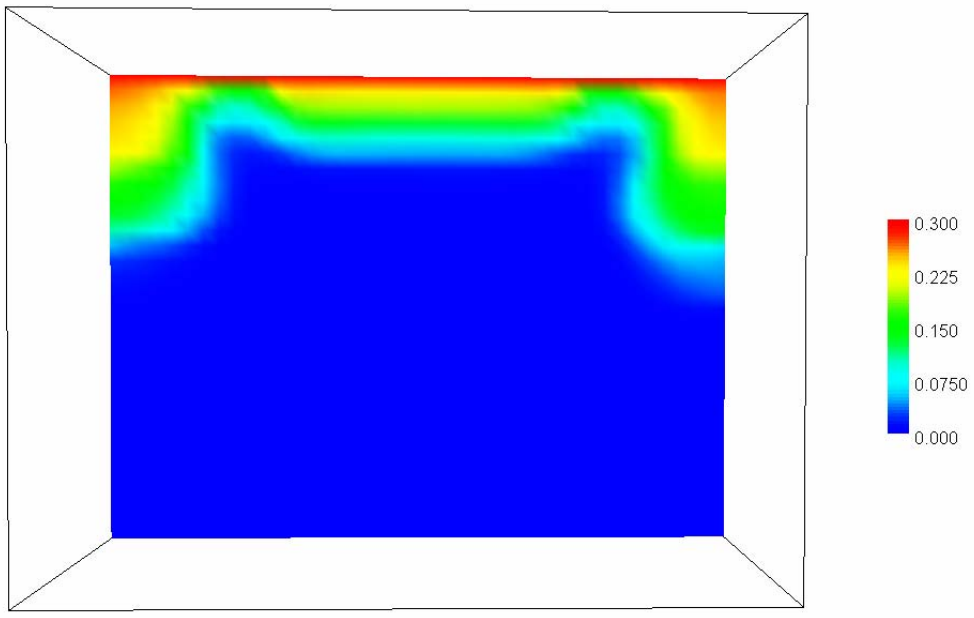

Time = 1.010995E+08 (105)

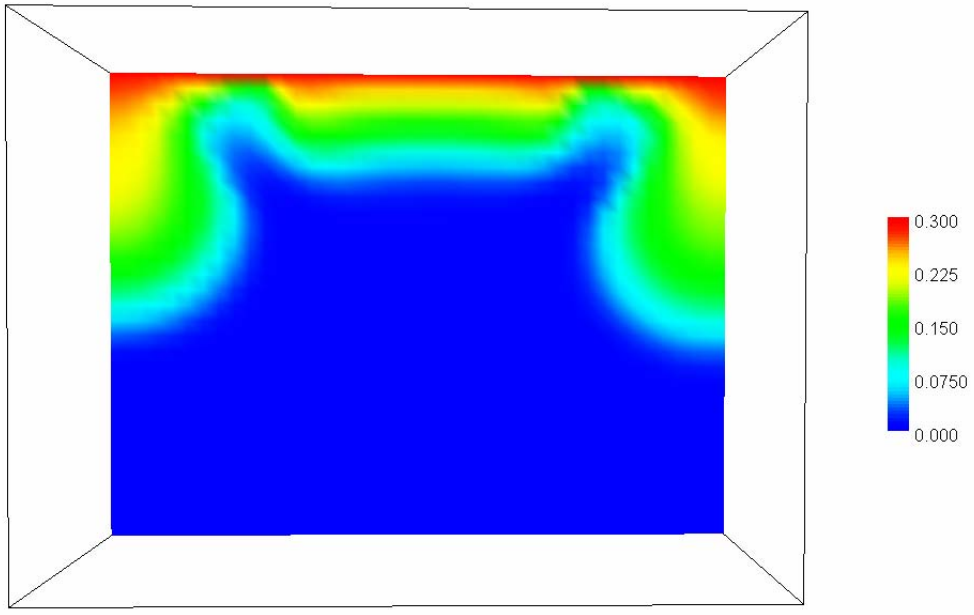

Time = 1.217687E+08 (110)

Figure 4.9 (c) - continued

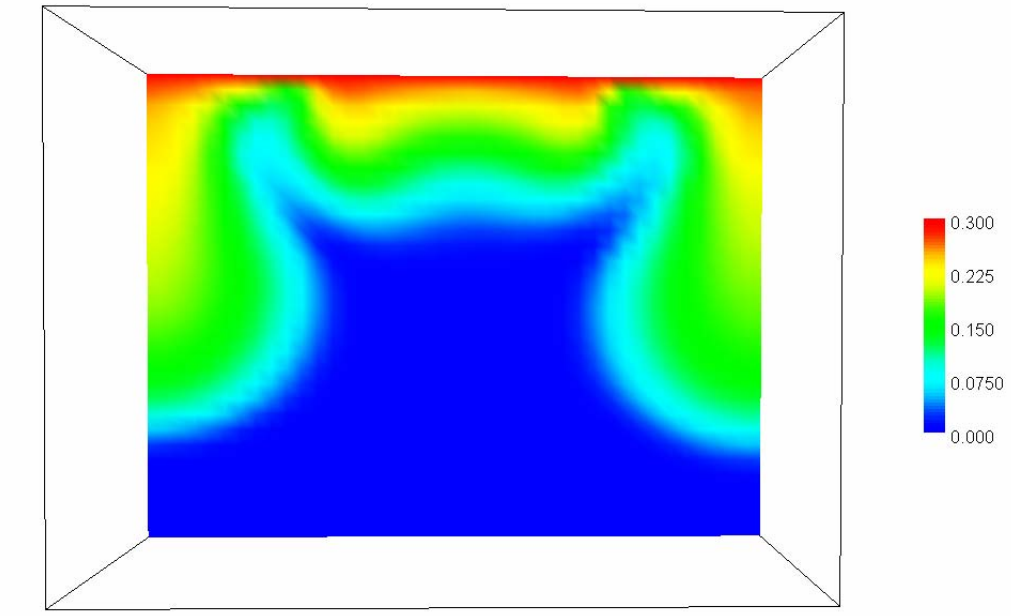

Time = 1.465717E+08 (115)

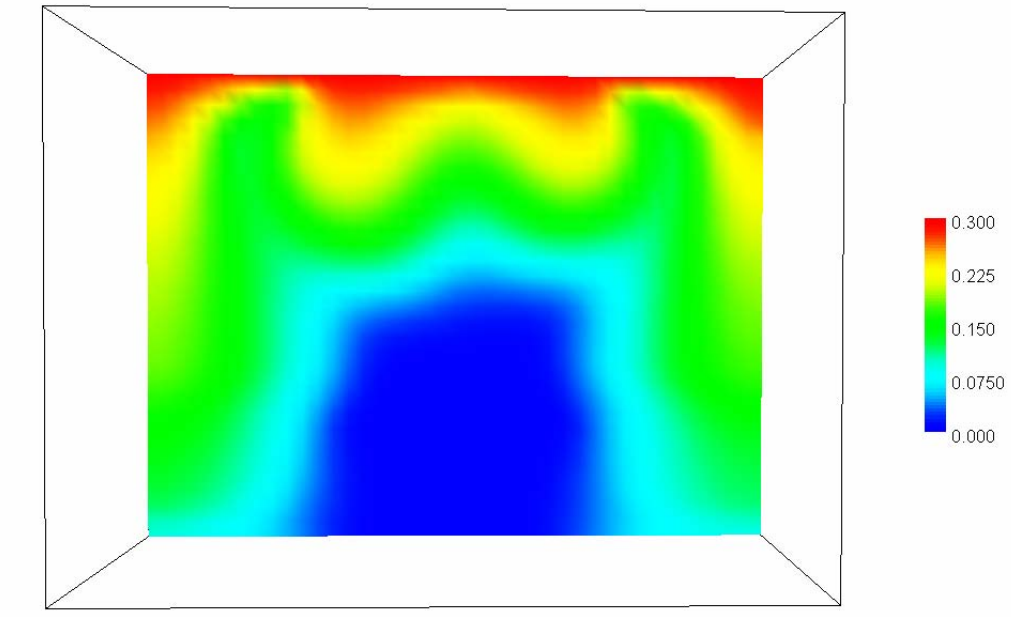

Time = 1.763353E+08 (120)

Figure 4.9 (d) -continued

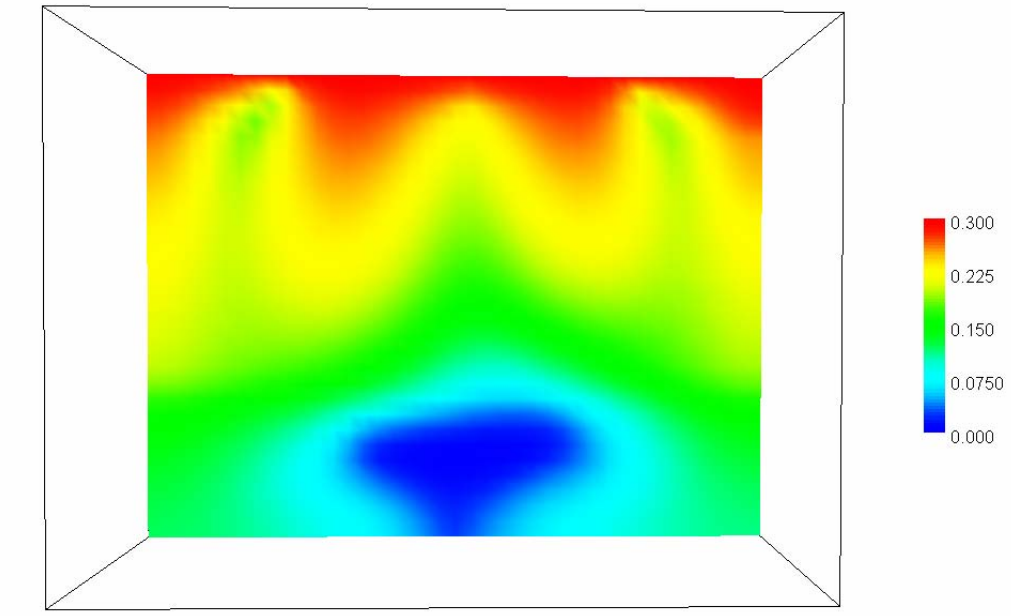

Time = 2.120517E+08 (125)

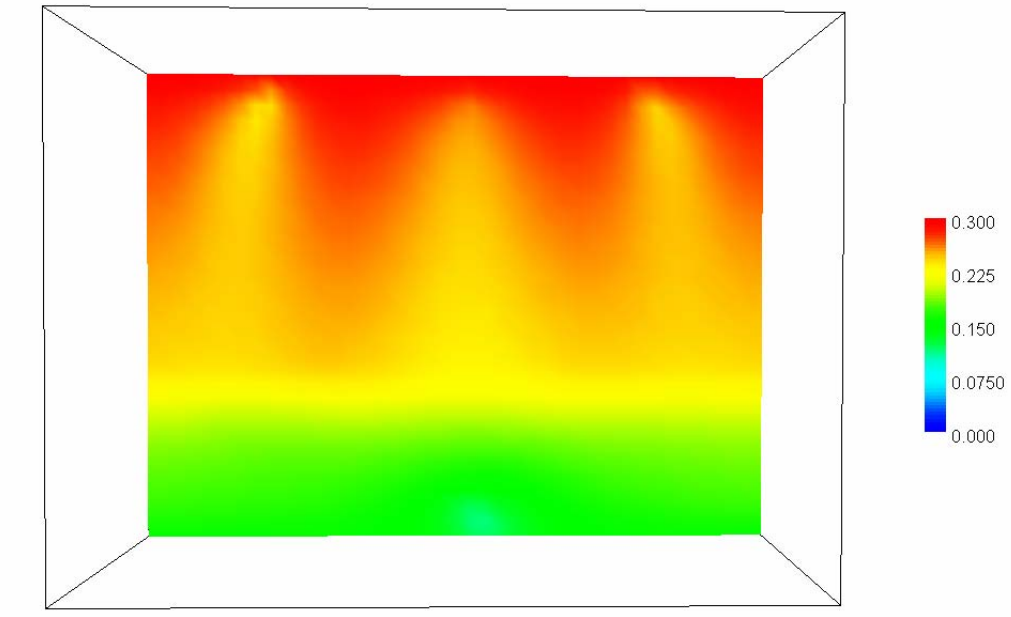

Time = 2.549113E+08 (130)

Figure 4.9 (e) - continued

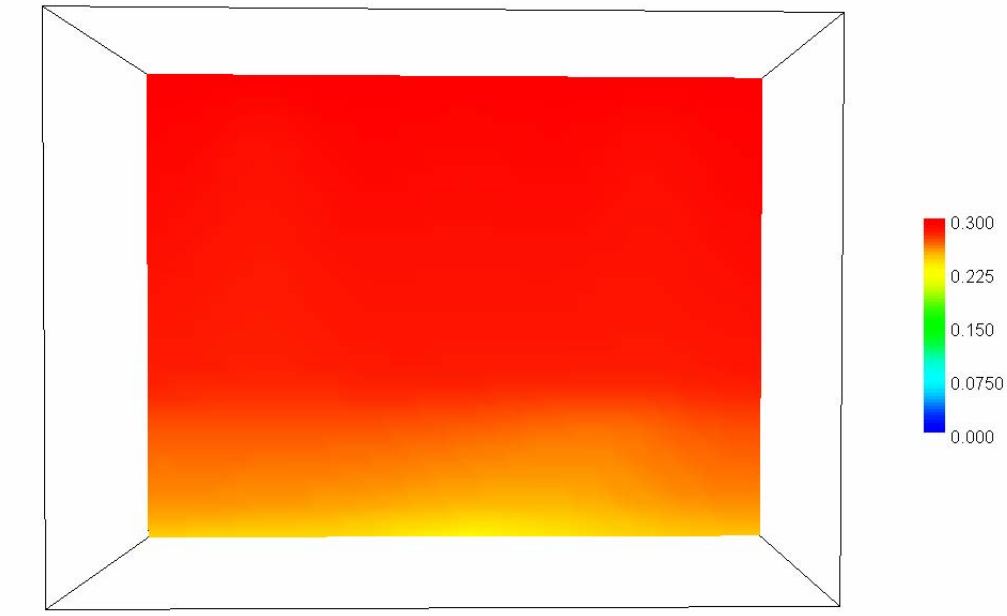

Time = 3.680606E+08 (140)

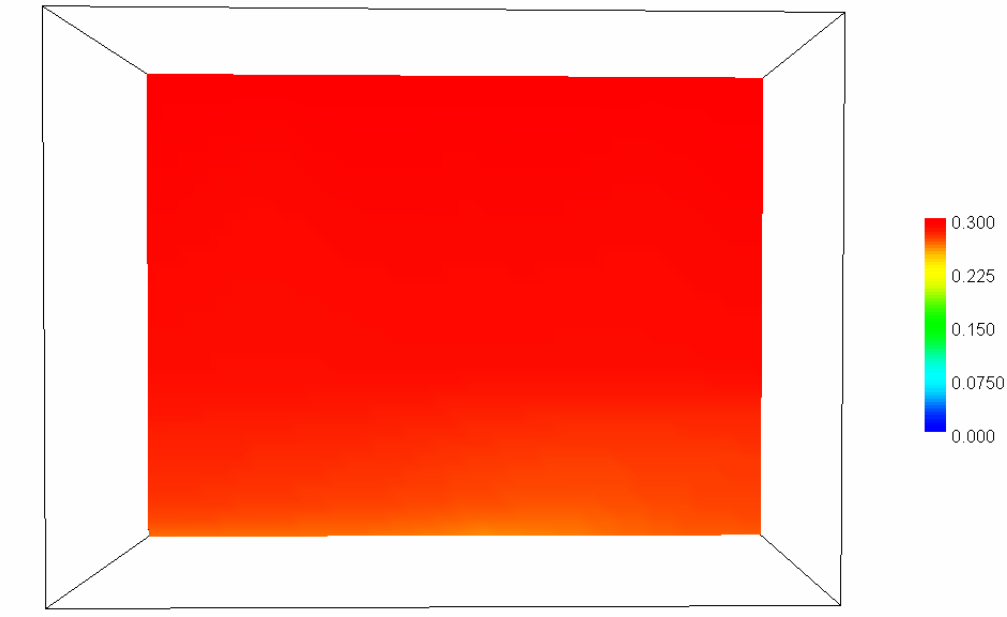

Time = 4.421221E+08 (145)

Figure 4.9 (f) - continued

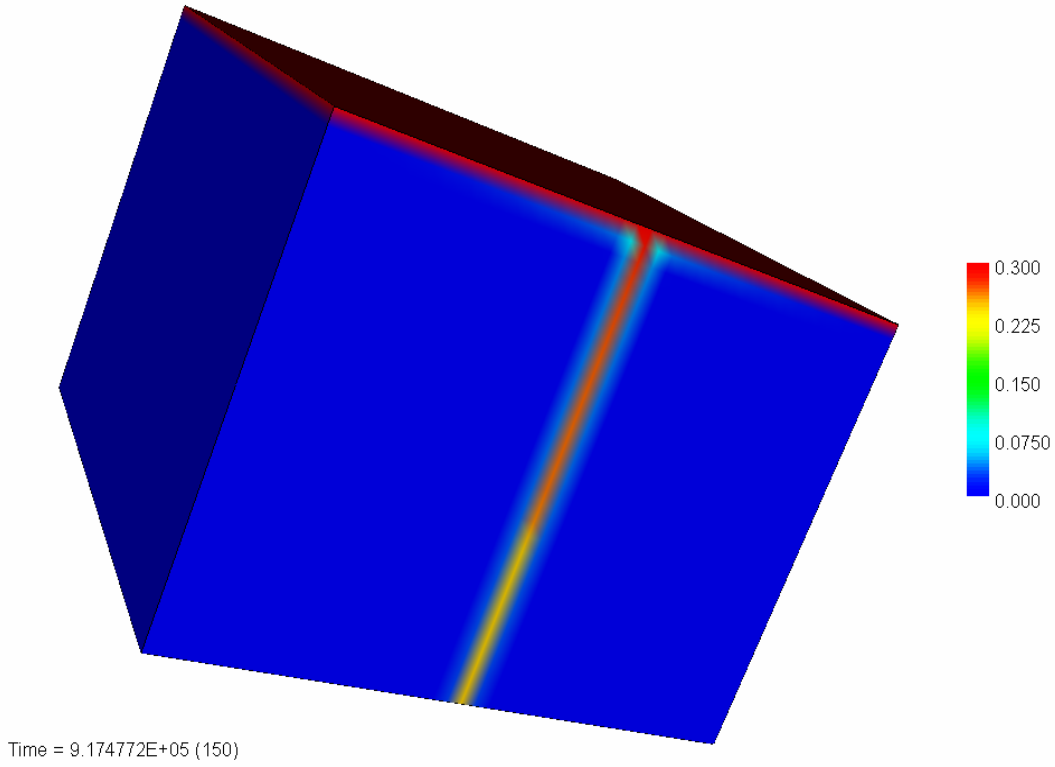

Figure 4.10 Solute transport through a microfracture. Fracture aperture b is 1 mm. Simulation time is about 10 days.

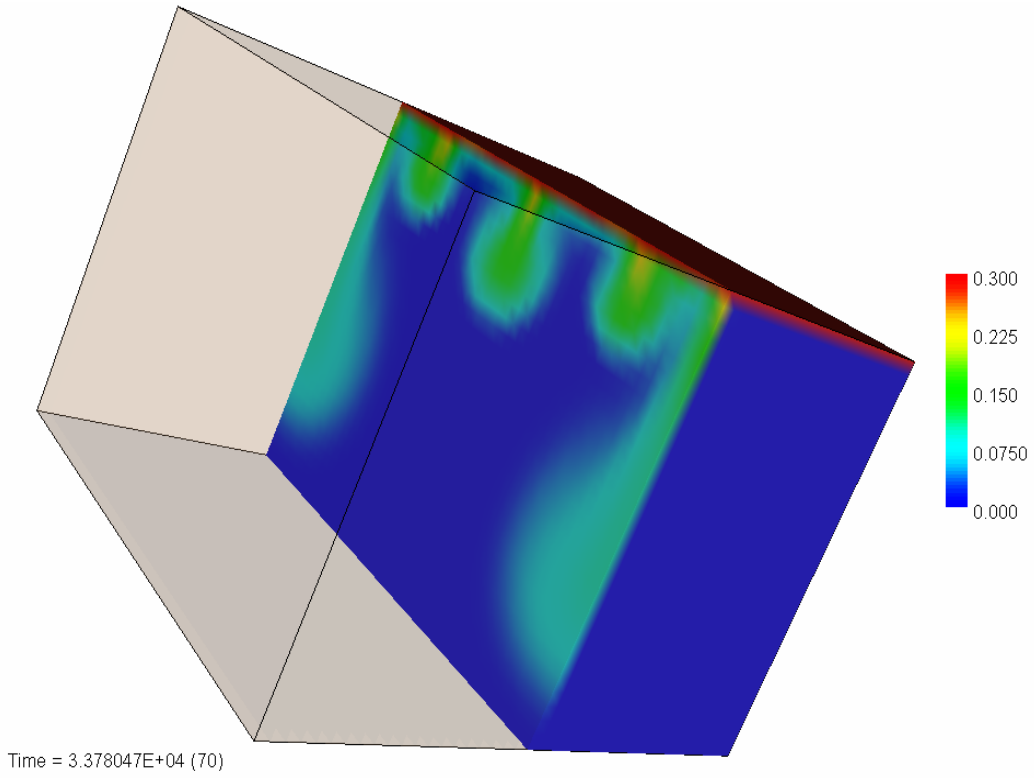

Figure 4.11 Plume development inside the microfracture (cropped from the model shown in Figure 4.10). Simulation time is about 9 hours.

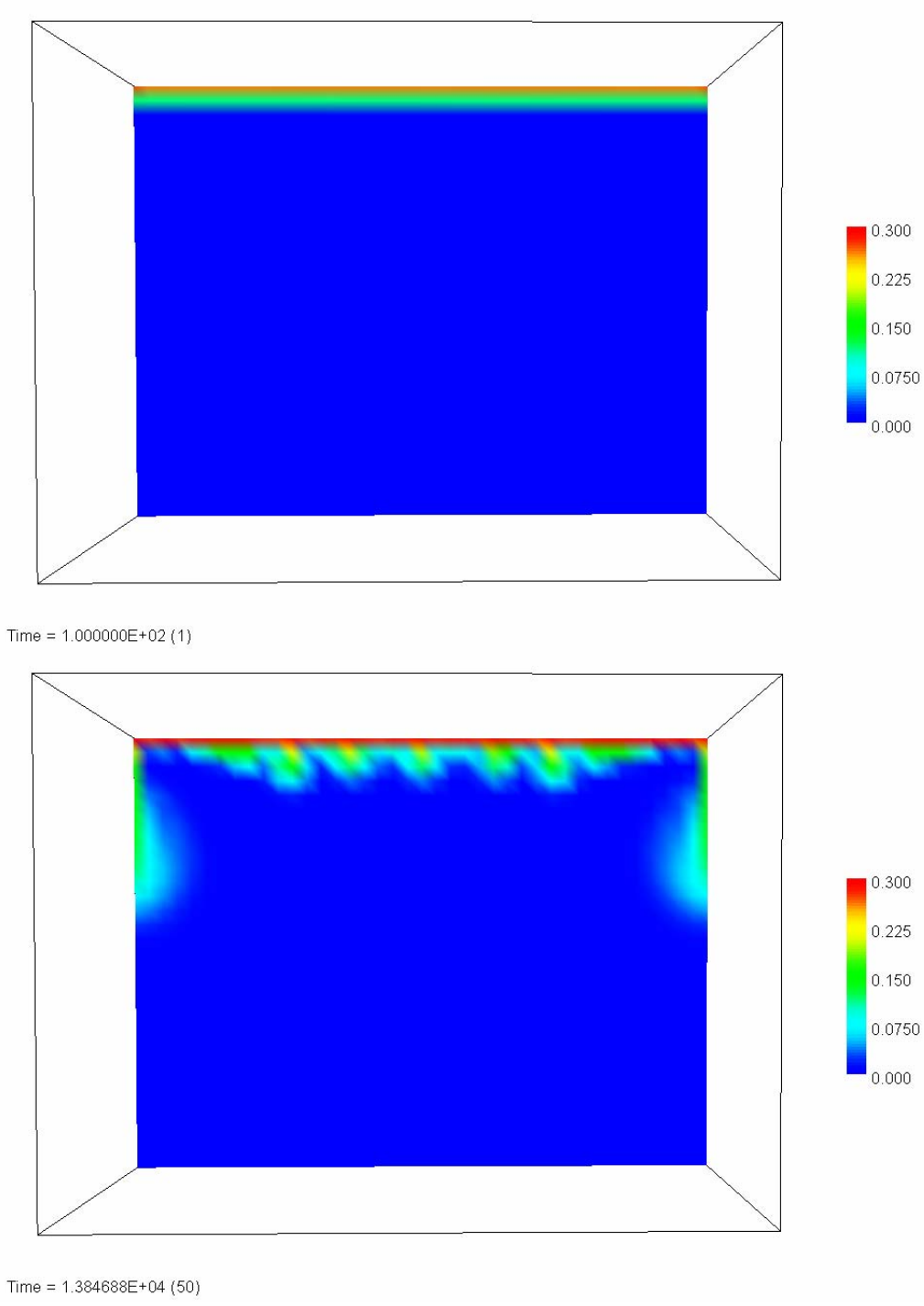

Figure 4.12 (a) Transient free convection occurring along the tiny fracture plane.

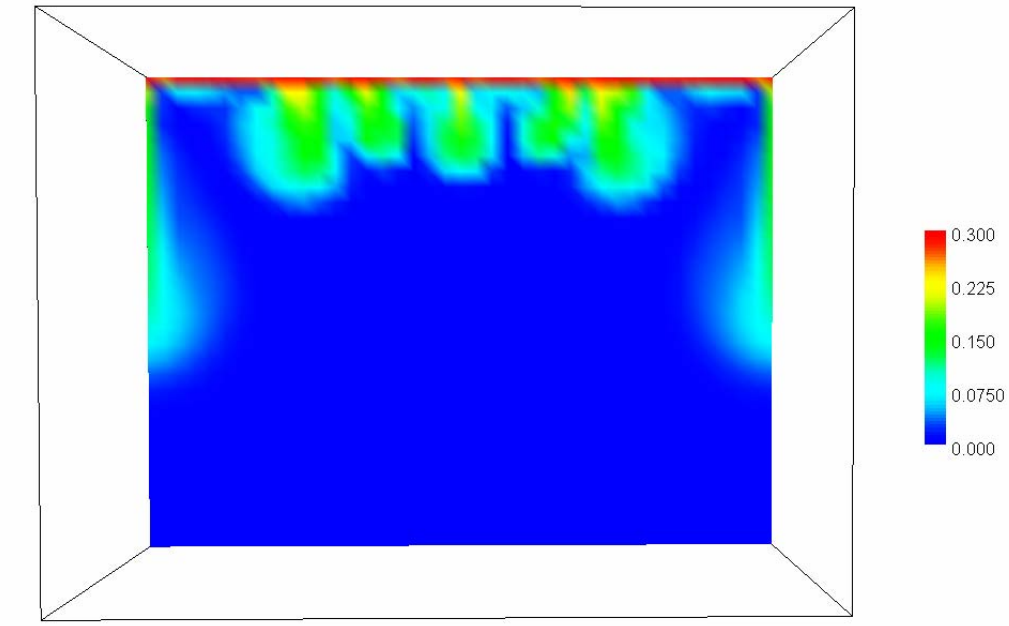

Time = 2.182031E+04 (60)

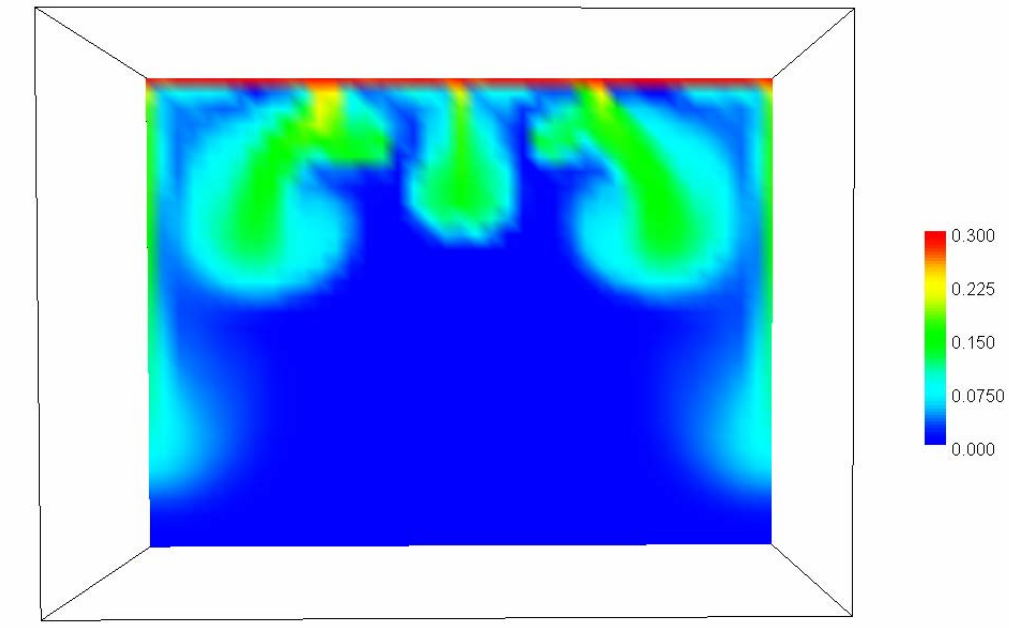

Time = 3.378047E+04 (70)

Figure 4.12 (b) – continued

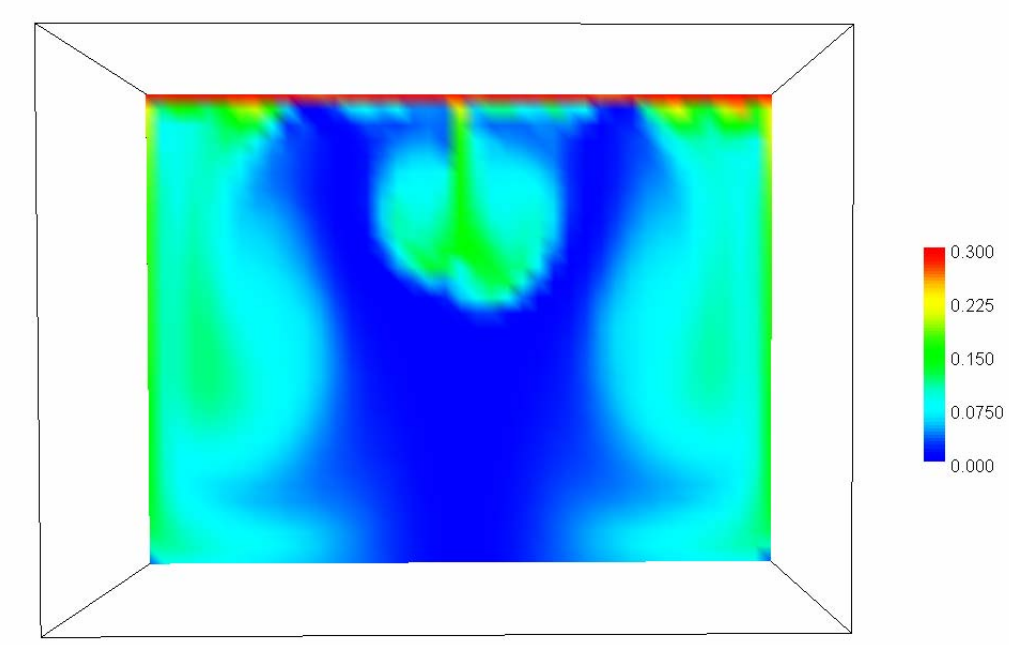

Time = 5.172070E+04 (80)

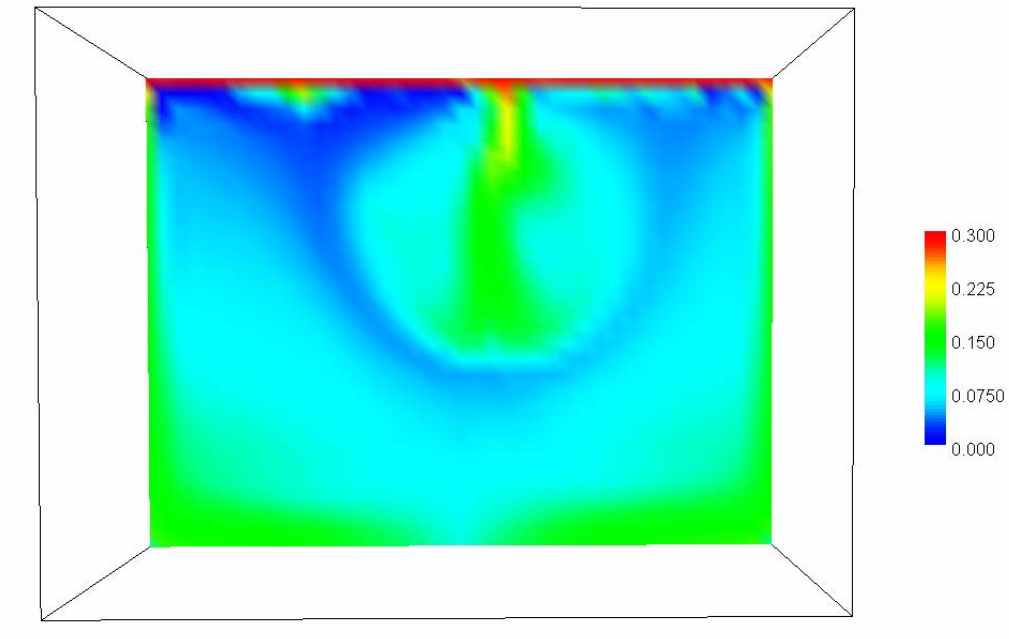

Time = 7.863105E+04 (90)

Figure 4.12 (c) – continued

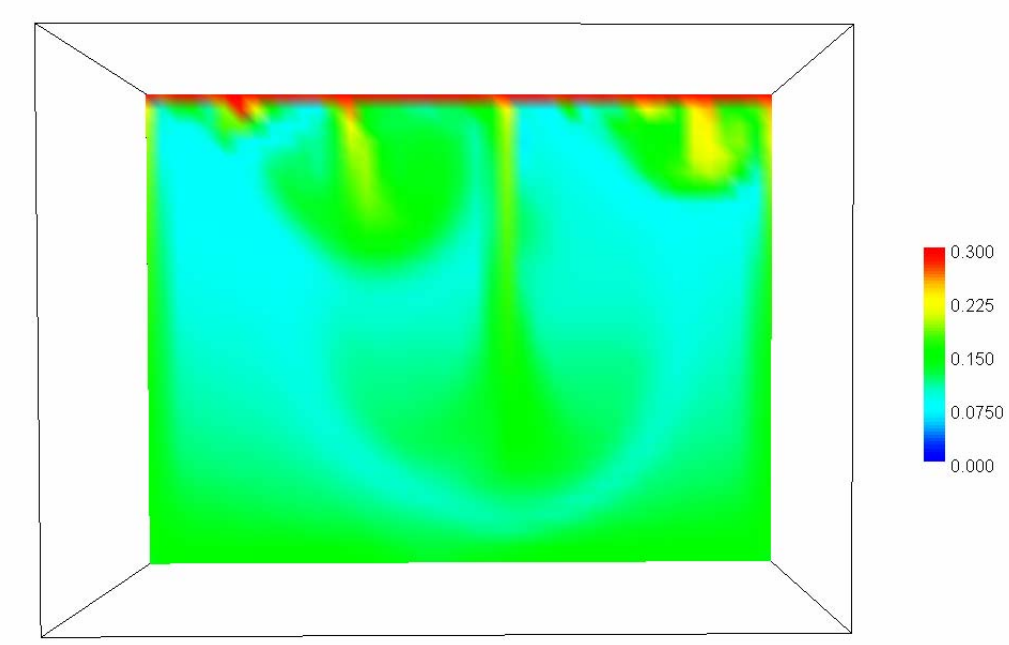

Time = 1.189966E+05 (100)

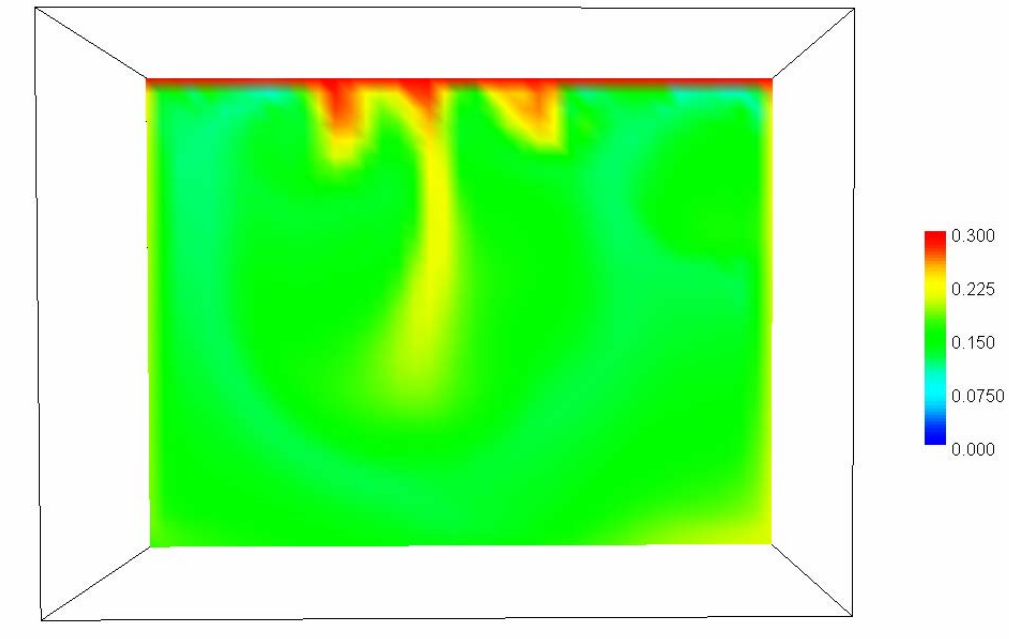

Time = 1.795449E+05 (110)

Figure 4.12 (d) - continued

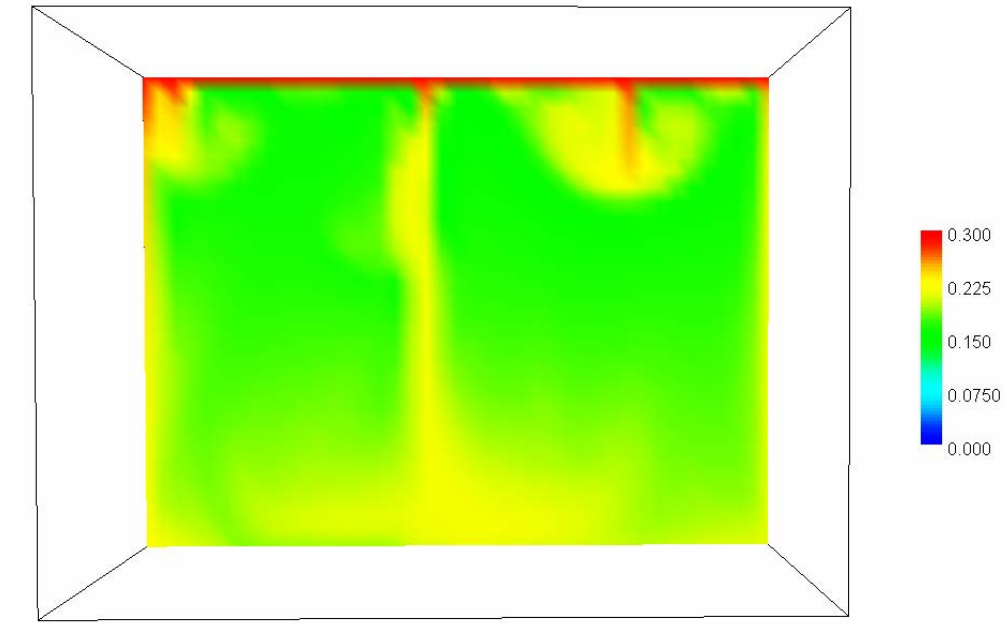

Time = 2.703673E+05 (120)

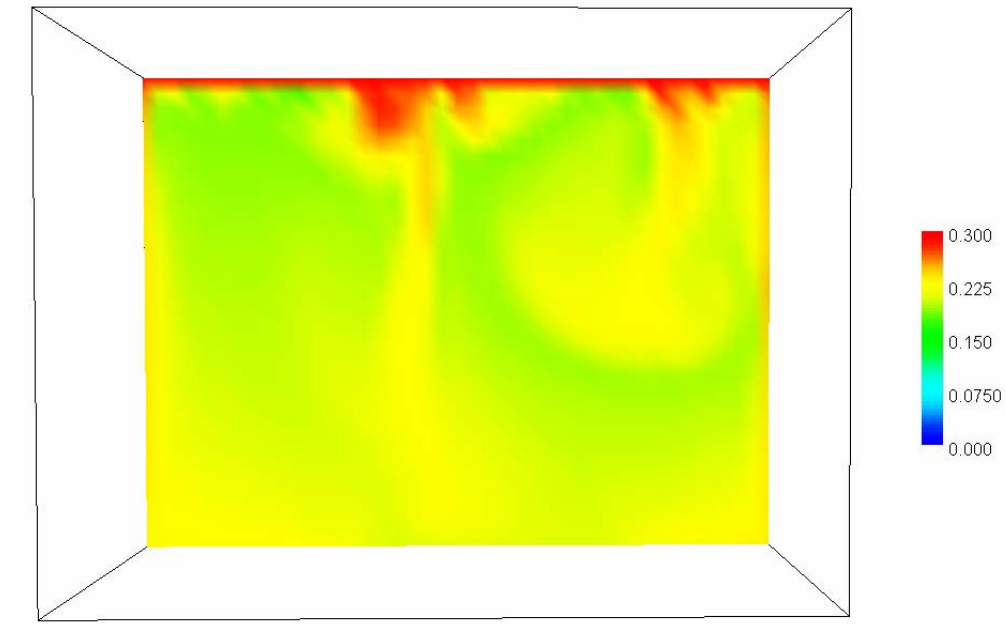

Time = 4.066010E+05 (130)

Figure 4.12 (e) - continued

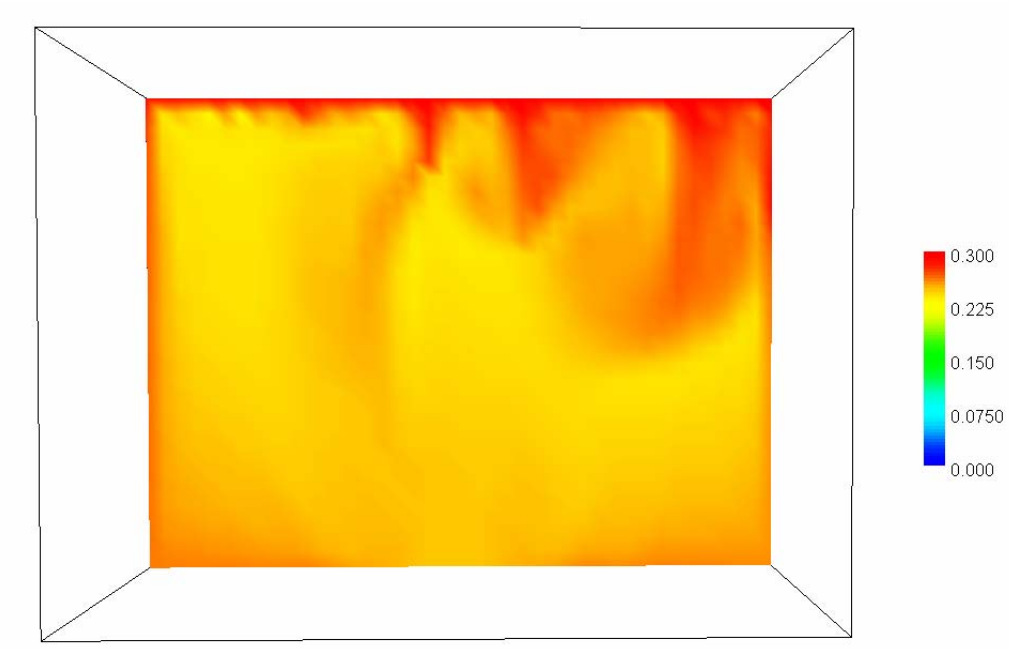

Time = 9.174772E+05 (150)

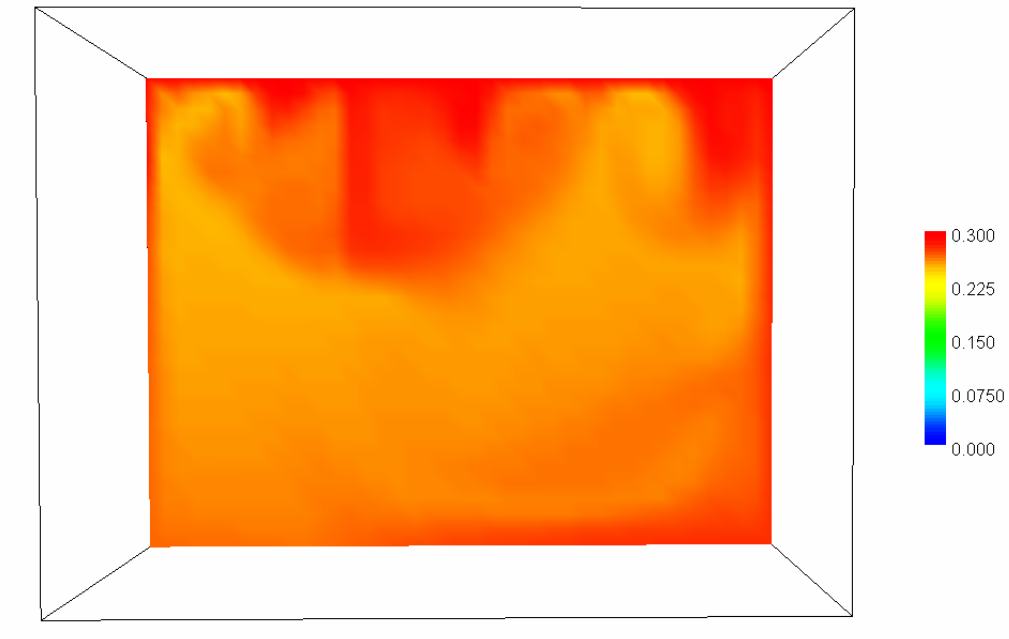

Time = 1.377266E+06 (160)

Figure 4.12 (f) - continued

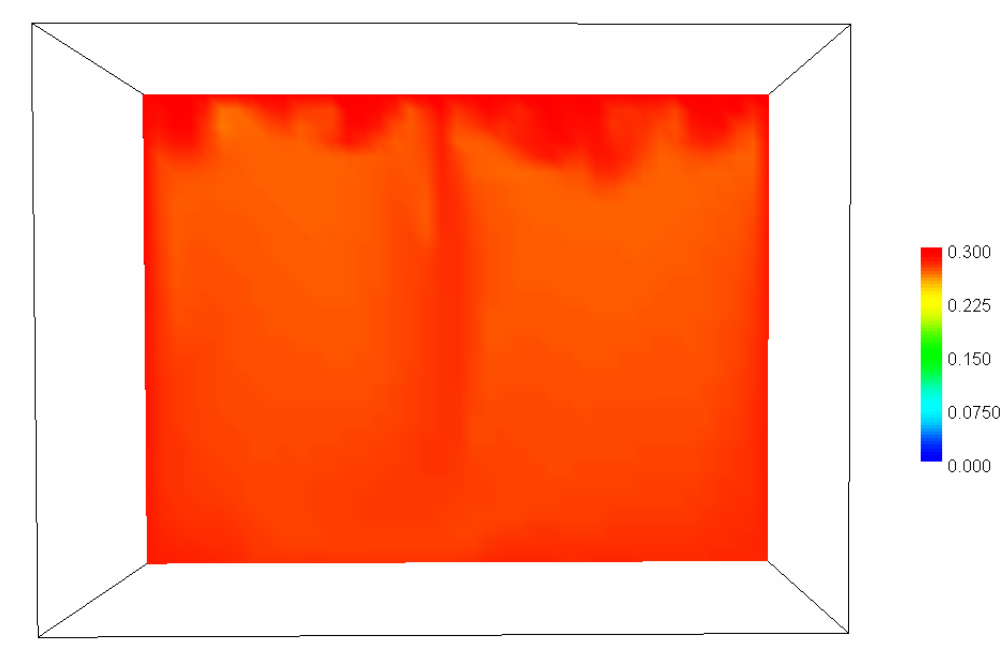

Time = 2.066949E+06 (170)

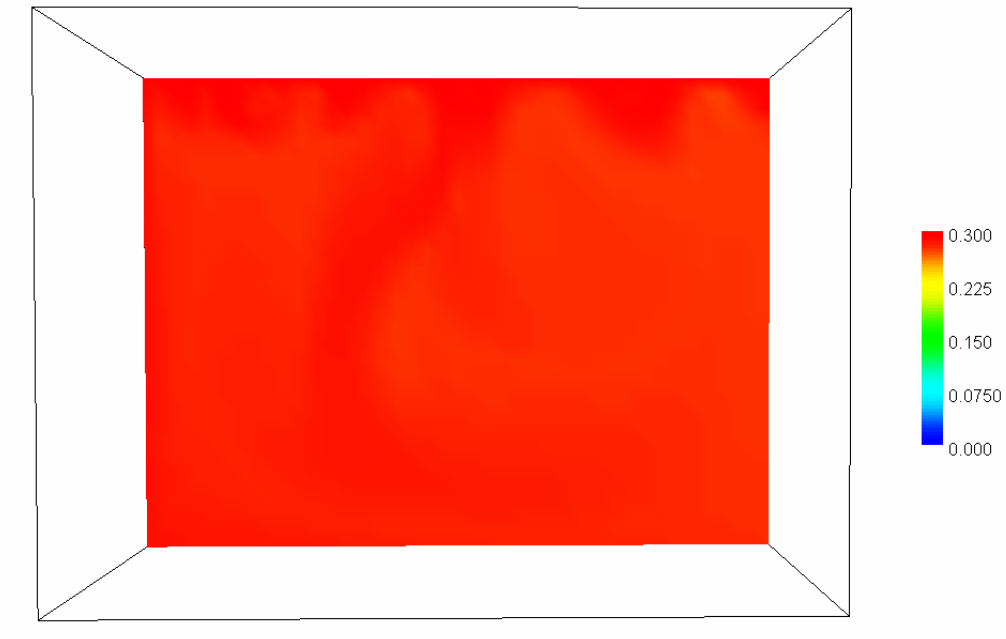

Time = 3.101473E+06 (180)

Figure 4.12 (g) - continued

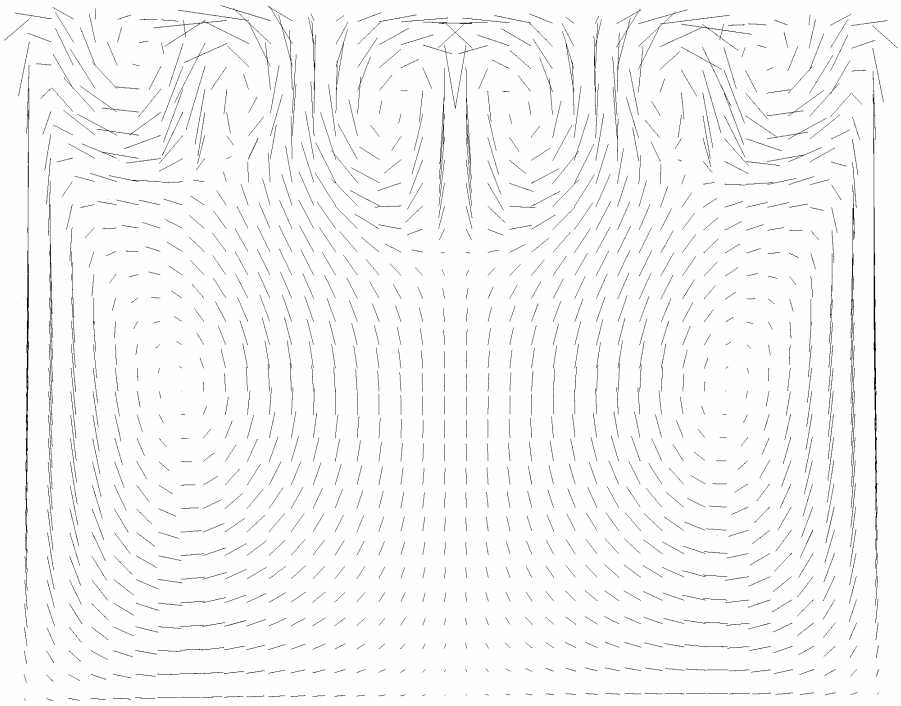

Figure 4.13 Velocity vector field corresponding to Figure 4.11.

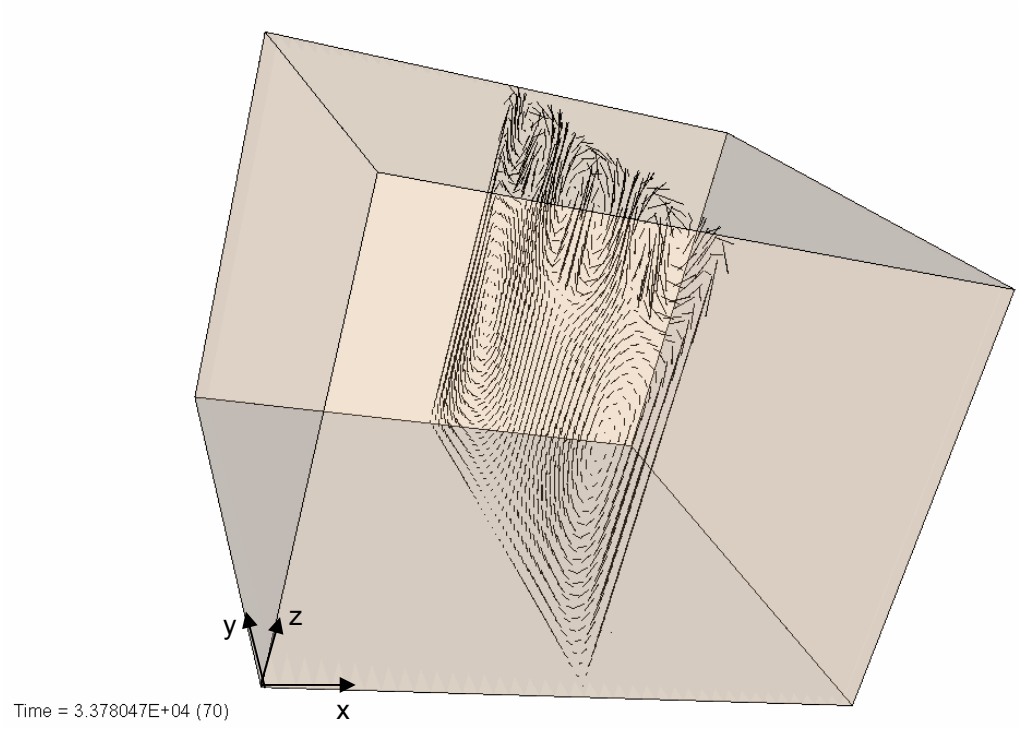

Figure 4.14 Convection cells shown in the velocity field illustrate the axes are parallel to the aperture on the x-z plane.

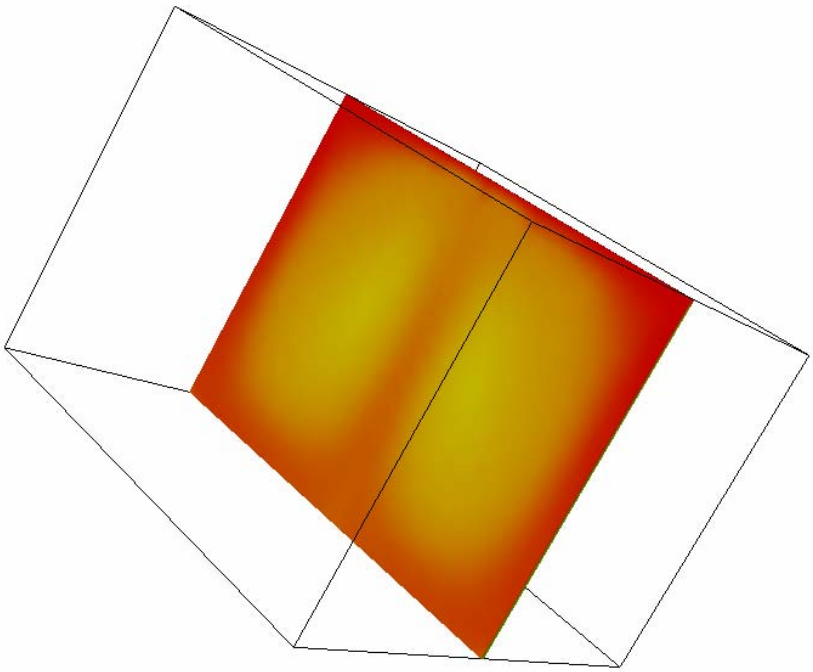

Figure 4.15 Convection cells shown to be symmetric along the fracture plane. Same model as in Figure 4.11.

Chapter 5 SUMMARY AND CONCLUSIONS

Saline formation fluids overlying on top of less dense formation fluids creates a potential for free convection to occur through low-permeability shales. There are many factors controlling the onset of free convection in heterogeneous geologic units. Among these, the permeability is the most fundamental physical parameter affecting the thermalhaline convection of fluids in the aquifers. Most important findings of these numerical modeling experiemnts on free convection through heterogeneous shales and permeability heterogeneity controls on free convection are summarized below.

1. Stochastic modeling of variable-density flow illustrates that free convection can occur within and across the heterogeneous shale zone under certain conditions. Free convection is favored by high concentration difference between the invading dense fluid and the background formation water, well-connected high permeability zones across the layer, high mean permeability, and high vertical correlation length of the permeability field. The dense plumes take preferential pathways which are composed of connected high permeability zones. These high permeability pathways could be facies changes, microfractures, or fracture zones. Even though they may occupy a small portion of the total volume, high permeability zones are very important for free convection and can have a dominant effect on fluid flow and contaminant transport. Using patch analysis to delineate flow pathways for

dense plumes provides a way to characterize permeability heterogeneity effects.

2. Characteristics of heterogeneous permeability fields, such as mean, standard deviation, and correlation length, are important for the onset and further development of the dense finger plumes. An increase in the mean, standard deviation, and vertical correlation length promotes the initiation and propagation of free convection. Among the three characteristics, correlation length is the most important and controlling factor with respect to changing the structure of a permeability field. Correlation length variations bridge the gap between totally random fields to regular or ordered heterogeneous media.
3. Threshold permeability (k_t) is the minimum permeability for free convection to occur in the heterogeneous permeability field. It must be exceeded in order for instabilities to initiate and grow. Threshold permeability decreases with increasing mean, standard deviation, and vertical correlation length. The calculated threshold permeability for the series of permeability realizations for a single shale layer in this study is on the order of 10^{-15} m^2.
4. Critical permeability (k_c) is defined as the permeability that forms the connected pathways for free convection through the heterogeneous shale layer. It must be exceeded in order to have convection reach the bottom of the heterogeneous layer through the connected high permeability zones. It increases with increasing mean, standard deviation, and vertical correlation

length. Convective instable flow will dissipate if the permeability is below the critical permeability and there is not a well-connected high permeability flow pathway.

5. The onset of free convection is especially sensitive to the boundary conditions. Numerical modeling shows that dual heterogeneity of sand-shale layer cake model destabilizes instability and promotes free convection. This is because:
   1) the downward free convection flow initiated in the sand layer can transport a large amount of solute down to the shale layer and continue to generate instabilities because the inertial moment helps to generate perturbation or interfacial disturbances;
   2) the high-permeability sand can connect to high permeability zones near the top boundary of shale to form a continuous preferential pathway for free convection to percolate through, and further development of free convection in the shale layer depends on the internal structure of the shale permeability;
   3) having a permeable sand layer on top of the shale destabilizes the instabilities and promotes free convection because the critical Rayleigh number for the onset of free convection is decreased when the top boundary is permeable.

In addition, this has the implication of free convection happening more often than expected in sediments, such as in the Gulf of Mexico Basin, because sand/sandstones and shales are often interbedded.

6. For heterogeneous unfractured shale, the plume development depends on the permeability distribution. Therefore, the circulation of brines can either penetrate through the shale-sand sequences or be killed inside the sequences, depending on the existence of well-connected high permeability patches. When shales have secondary permeability of fractures, dense groundwater can convect quickly through the fractures and circulate through the sand-shale sequences on geologic time scales.
7. Theoretical analysis and numerical modeling results on the onset of free convection in fractures surrounded by low-permeability shale show that:
    a) The critical Rayleigh number for the initiation of convective flow for a parallel-plate fracture is several orders in magnitude greater than that for horizontal infinite porous layer.
    b) For large fractures with infills, the critical Rayleigh number approximates $4\pi^2$ when the aperture is of the same order of magnitude as the height of the layer (i.e., the aspect ratio is ~1.0);
    c) When the fracture aspect ratio (b/H) is smaller than 0.5, the critical Rayleigh number can be approximated by a function depending only on

this dimensionless ratio. This critical Rayleigh number function closely approximates the theoretical values at aspect ratio as small as 10^{-8};

d) When free convection initiates, the convection cells show themselves on the fracture plane with axes parallel to the fracture aperture.

8. Two-dimensional models are inadequate to capture the initiation and further development of free convection in fractured low-permeability rocks with respect to aspect ratios. Whereas convective flow doesn't show on the cross-section perpendicular to the fracture plane (because of high critical Rayleigh number with small aspect ratio required for free convection), convective flow easily occurs on the fracture plane with a large aspect ratio of thickness to height. Only three-dimensional models can adequately simulate free convection through fractures with non-unit thickness along the strike direction.

Numerical modeling results show that transient convection occurs when the Rayleigh number is too high. These transient convection cells generate and disappear at different locations and the pattern keeps changing through time. Therefore, convective flow can easily occur in fractures and transport dense fluid through fractures under no hydraulic gradient.

In summary, the following conclusions are made based on numerical modeling results of convective flow and solute transport through heterogeneous shales:

1) Free convection can occur through heterogeneous low permeability shales.

2) Increases in the mean, standard deviation, and vertical correlation length of the permeability field promote free convection in models with different system geometries and boundary conditions.

3) The internal structure of the heterogeneous field is critical in controlling the onset and development of the instabilities.

4) Critical permeability from patch analysis of the permeability structure further proves that free convection is enhanced with increasing mean, standardard deviation, and vertical correlation length.

5) The upper and lower layers of sand are important in initiating free convection and promote convective flux across these boundaries.

6) Free convection can easily occur in fractures and transport dense fluid through fractures under no hydraulic gradient.

7) The critical Rayleigh number for the initiation of convective flow for a parallel-plate fracture is several orders in magnitude greater than that for horizontal infinite porous layer.

8) For large fracture with infill materials, the critical Rayleigh number is approximating $4\pi^2$ when the aperture is of the same order of magnitude as thee height of the layer (i.e., the aspect ratio is ~1.0).

9) When the fracture aspect ratio (b/H) is smaller than 0.5, the critical Rayleigh number can be approximated by a function depending only on this

dimensionless ratio. This critical Rayleigh number function shows great closeness to the theoretical values at aspect ratio as small as 10^{-8}.

10) When free convection initiates, the convection cells show themselves on the fracture plane with axes parallel to the fracture aperture. Numerical modeling results show that transient convection occurs when the Rayleigh number is too high. These transient convection cells generate and disappear at different locations and the pattern keeps changing through time

Therefore, density-driven free convection could be a mechanism for high density groundwater to circulate through heterogeneous geologic media. Finding methods to map aquifer heterogeneity and incorporating the basic characteristics of the permeability field in free convection prediction would be beneficial to field studies and testing free convection in low-permeability strata.

Discussions and future research

Groundwater flow in low-permeability environments associated with fine-grained sedimentary deposits (such as shales and clays) has received increasing effort and attention due to its important role in the evolution of groundwater flow systems in sedimentary basins and minimizing exposure to moving groundwater for geologic disposal of radioactive waste materials. In the regional flow system, density-driven convective flow could be important and dominant when there is no hydraulic gradient or relatively small opposing hydraulic gradient. For unfractured low-permeability sedimentary rocks, such as shales and mudstones, density-driven free convection can be an effective transport mechanism because the circulating pattern of upwelling and downwelling flows may increase the residence time for the geochemical evolution of the pore fluids and solids. Therefore, regional groundwater flow models may need to incorporate coupled flow with density variations.

Vertical tiny fractures may be difficult to detect in the field (mostly by vertical boreholes), but they are important for dense fluid flow through low-permeability shales. SUTRA modeling results show free convection occurs on the fracture plane. Unless field observations are made from the place where tiny fractures are abundant, it is not safe to say that free convection can not happen in low-permeability shales. The study by Harrison et al. (1992) suggested that small

hydraulically active fractures in the clayey barrier may cause rapid and large-scale contamination of groundwater beneath the barrier.

Laboratory experiments on free convection through a column of porous material show the irregular pattern of convective cells which is quite different from theoretical solution of free convection for simple model scenarios. The symmetric circulating upwelling and downwelling flow is replaced by non-symmetric elongated fingering plumes in porous media. Factors and physical parameters responsible for the observed pattern are not clearly stated in the literature. Viscosity and local heterogeneity of permeability could be among these factors. More efforts are needed on the numerical modeling part in order to reproduce the patterns observed in the lab.

So far, most of the studies focus on free convection in faults and fractures that is due to thermal heating or thermal gradient. There are no equivalent solute-driven analogs. Large scale study of groundwater flow in low-permeability environments suggests the existence of fracture networks. Study of the interaction between the fracture walls and the matrix can solve the boundary effect on the onset of free convection in discrete vertical fractures. The theoretical critical Rayleigh number needs to be obtained for coupled flow equations with appropriate boundary conditions for a layer or fracture bounded by permeable upper and bottom boundaries. Corresponding laboratory experiments on fractured

media are needed to study free convection through fractures with upper and lower boundary being permeable.

APPENDIX A

Fluid and mass conservation equations used in SUTRA model

The equations solved by SUTRA are the fluid mass balance equation:

$$\frac{\partial(\phi\rho)}{\partial t} = -\nabla \bullet (\phi\rho\mathbf{V}) + Q_p \tag{A-1}$$

and solute mass balance equation:

$$\frac{\partial(\phi\rho C)}{\partial t} = -\nabla \bullet (\phi\rho\mathbf{V}C) + \nabla \bullet [\phi\rho(D_0\mathbf{I} + \mathbf{D}) \bullet \nabla C] + Q_p C \tag{A-2}$$

Flow and solute transport equations are coupled through groundwater density, which is a linear function of concentration (assume isothermal):

$$\rho(C,T) = \rho_0 + \frac{\partial\rho}{\partial C}(C - C_0) \tag{A-3}$$

In addition, the equations are coupled through the fluid velocity in the general form of Darcy's law:

$$\mathbf{v} = \frac{k(x,z)}{\phi\mu}(\nabla P - \rho g) \tag{A-4}$$

where $C(x, z, t)$ is the solute concentration (M_s/M), $\mathbf{v}(x, z, t)$ is fluid velocity (L/T), $\rho(x, z, t)$ is fluid density (M/L^3), $\mathbf{D}(x, z, t)$ is mechanical dispersion tensor (L^2/T), $\mathbf{I}$ is identity tensor, $\phi(x, z)$ is aquifer porosity, D_0 is the molecular diffusion coefficient of solute in pure fluid (L^2/T), $Q_p(x, z, t)$ is fluid mass source ($M/L^3/T$), $k(x, z)$ is permeability tensor (L^2), μ is fluid dynamic viscosity ($M/L/T$),

$P(x, z, t)$ is fluid pressure ($M/L/T^2$), g is gravity vector (L/T^2), ρ_0 is fluid density when $C = C_0$, C_0 is a base solute concentration, and $\partial\rho/\partial C$ is a constant coefficient of density variability.

Appendix B

2D SUTRA pre-processor

```
     PROGRAM    SGSIMK_D5

!***********************************************************
!
!  PROGRAM: SGSIMK_D5     FOR SIGMA1, SIGMA2, SIGMA3 MODELS
!
!  PURPOSE:  TO GENERATE K FIELDS W/ CORRESPONDING X,Y
!            COORDINATES
!
!            AND CREATE INPUT .D5  .D55 FILES FOR SUTRA.
!***********************************************************

       IMPLICIT DOUBLE PRECISION (A-H,O-Z)

         PARAMETER(NSIM=30,NMX=500,NMY=100,E=2.71828182846)

         DIMENSION  SIM(NSIM,NMY,NMX), SK(NSIM,NMY,NMX)
         DIMENSION  CC(NMX*NMY)
         DIMENSION  YY(NSIM,NMY,NMX)
         DIMENSION  X(NMX), Y(NMY)
         DIMENSION  XD(NMX+10),YD(NMY+10)
         CHARACTER*3  FNAME(NSIM)
         CHARACTER*4  F1(NSIM), F2(NSIM)
         CHARACTER*13  FFNAME
         CHARACTER*14  FD
         CHARACTER*15  FT
         CHARACTER*50   FILEPATH1,FILEPATH2
         CHARACTER*40   FNAME3(NSIM)
         CHARACTER*41   FNAME4(NSIM)
         CHARACTER*25    FILEPATHIN

         DATA FNAME/'K01','K02','K03','K04',  &
                    'K05','K06','K07','K08', &
                    'K09','K10','K11','K12', &
                    'K13','K14','K15','K16', &
                    'K17','K18','K19','K20', &
                    'K21','K22','K23','K24', &
                    'K25','K26','K27','K28', &
                    'K29','K30'/

         DATA F1/'KK01','KK02','KK03','KK04',  &
                    'KK05','KK06','KK07','KK08', &
                    'KK09','KK10','KK11','KK12', &
                    'KK13','KK14','KK15','KK16', &
                    'KK17','KK18','KK19','KK20', &
```

```
                    'KK21','KK22','KK23','KK24', &
                    'KK25','KK26','KK27','KK28', &
                    'KK29','KK30'/

!=============================================================
!---START PROGRAMMING ------------------------
!--------------- COPYRIGHT BY MINGJUAN SHI -----------
!

    MPTY= 0
    N_SIM=30
    DELTX=1.0
    DELTY=1.0
      TOTALX=300.0
      TOTALY=20.0
      NX=300
      NDX=NX+1
      NY=20
      NDY=NY+1
      NODES=NDX*NDY
      NELEMENTS=NX*NY
      C0=1.0
      CBACK=0.0
      T0=0.0
      X(1)=DELTX/2.0
      Y(1)=DELTY/2.0
      XD(1)=0.0
      YD(1)=0.0
      CINIT=0.0
      PINIT=0.0
      P0=0.0
      CCK=1000.0*9.81

!-------ASSIGN INITIAL C TO EACH NODE--------
       DO I=1,NDX
         DO J=1,NDY-1
           II= NDY*(I-1)+J
             CC(II)=CBACK
           END DO
           CC(I*NDY)=C0
       END DO
!-----------------------------------------

      DO I=2, NX
         X(I)=X(I-1)+DELTX
         XD(I)=XD(I-1)+DELTX
      END DO
      XD(NX+1)=XD(NX)+DELTX

      DO I=2,NY
         Y(I)=Y(I-1)+DELTY
```

```
         YD(I)=YD(I-1)+DELTY
       END DO
     YD(NY+1)=YD(NY)+DELTY

10   FORMAT (1X,F10.2)

!=================================================
!------START READING IN SIMULATED K-VALUES-----------
!-------------------------------------------------
       WRITE(*,*) 'INPUT THE MODEL PATH HERE, SUCH AS
            K60_100_100.1 (13 CHARACTERS)'
       READ(*,*)   FFNAME
         FILEPATHIN = 'C:\MYMODEL\'//FFNAME //'\'
       OPEN(100,DEFAULTFILE=FILEPATHIN,FILE='SGSIM.OUT',
            STATUS='OLD')
       READ(100,*)
         READ(100,*)
         READ(100,*)             !IGNORE THE FIRST 3 LINES

         I= 1
         DO WHILE ( .NOT. EOF(100) )

               DO IY=1,NY
                  DO IX=1,NX
                       READ(100,*) SIM(I,IY,IX)

                    END DO
               END DO
           I=I+1
          END DO

        CLOSE(100)

       DO I=1,N_SIM
              DO IY=1,NY
                  DO IX=1,NX
         YY(I,IY,IX)=3.0*SIM(I,IY,IX)-17.0
         SK(I,IY,IX)=10**YY(I,IY,IX)
                    END DO
               END DO
            END DO

!=========================================================

      WRITE(*,*)  'PLEASE WAIT ......'

       DO II=1,N_SIM

     FFNAME="KDATA/"//FNAME(II)//".DAT"
```

```
      OPEN(II,
      DEFAULTFILE=FILEPATHIN,FILE=FFNAME,STATUS='REPLACE')

               DO IY=1,NY
                   DO IX=1,NX
                    CCX=(IX-1)*DELTX+DELTX/2.0
                    CCY=(IY-1)*DELTY+DELTY/2.0
                    WRITE(II,*) CCX,CCY,SK(II,IY,IX)

                      END DO
                END DO
           CLOSE(II)

              END DO
!===========OUTPUT ================================

          DO II=1,N_SIM

      FD='KDATA/'//F1(II)//'.DAT'

      OPEN(II, DEFAULTFILE=FILEPATHIN,FILE=FD,STATUS='REPLACE')

               DO IY=1,NY
                   DO IX=1,NX
                     CX=(IX-1)*DELTX+DELTX/2.0
                     CY=(IY-1)*DELTY+DELTY/2.0
                     WRITE(II,*) CX, CY, YY(II,IY,IX)

                      END DO
                END DO
           CLOSE(II)

              END DO
!===========OUTPUT -LN(K) ======================

          DO II=1,N_SIM

      FT='KDATA/'//F1(II)//'0.DAT'

      OPEN(II, DEFAULTFILE=FILEPATHIN,FILE=FT,STATUS='REPLACE')

               DO IY=1,NY
                   DO IX=1,NX
                          CX=(IX-1)*DELTX+DELTX/2.0
                      CY=(IY-1)*DELTY+DELTY/2.0
                        WRITE(II,*) CX, CY, -LOG(SK(II,IY,IX))

                      END DO
                END DO
           CLOSE(II)
```

```
            END DO
!----------OUTPUT ALL K -------------------------
       OPEN(2,DEFAULTFILE=FILEPATHIN,
      FILE='KDATA/ALL_K.DAT',STATUS='REPLACE')
         DO I=1,N_SIM
            DO IY=1,NY
                 DO IX=1,NX
                      WRITE(2,*)  SK(I,IY,IX)
                   END DO
              END DO
         END DO

         CLOSE(2)

!=====================================================
      WRITE(*,*)
      WRITE(*,*) 'FINISHED EXPORTING ALL K VALUES.'
      WRITE(*,*) 'NEXT IS TO EXPORT D5 AND D55 INPUTS TO SUTRA;'
      WRITE(*,*) 'PLEASE WAIT ......'

!------------- CALCULATE SOME PARAMETERS FIRST ---------
      FN=N_SIM
      NBI=1+2*(NDY+1)          ! SEE SUTRA MENU P250 FOR NBI
      NPBC=2
      NUBC=(NDX)
      NPINCH=0
        NSOP=0
        NSOU=0
        NOBS=0
        NTOBS=99

      DO I=1, FN

!================================================
!--CREATE INPUT *.D5 FOR SUTRA ------
!----------------------------------------
      FNAME3(I)=FILEPATHIN//'SUTRAIN/'//F1(I)//'.D5'

    OPEN(I, FILE=FNAME3(I),STATUS='REPLACE' )

  WRITE(I,12) 'SUTRA SOLUTE TRANSPORT : FREE CONVECTION OR NOT '
12   FORMAT(A48)
      WRITE(I,11) '* DENSE SOLUTE ON TOP'
      WRITE(I,13) '** HETEROGENEOUS MODEL TO STUDY FREE
      CONVECTION'
11  FORMAT(A21)
13  FORMAT(A47)
      WRITE(I,17)NODES,NELEMENTS,NBI,NPINCH,NPBC,NUBC,NSOP,NSOU,N
      OBS,NTOBS
17   FORMAT(10I5)
```

```
!     '4961 4800   85    0    2  242    0    0    0    0'
!--DATASET 3 FORMAT IS : 10 * I5
!-----4961: # OF NODES
!-----4800: # OF ELEMENTS
!-----85: FULL BANDWIDTH=2*(MAX.NODE DIFFERENCE)+1
!-----0 : # OF PINCH NODES
!-----2 : # OF NODES AT WHICH PRESSURE IS CONSTANT OR FUNCTION OF
TIME
!-----242 : # OF NODES AT WHICH C OR T('C) IS CONSTANT OR
FUNCTION OF TIME
!-----0   : # OF NODES AT WHICH FLUID SOURCE/SINK IS A CONSTANT
OR F(TIME)
!-----0   : # OF NODES AT WHICH ENERGY/SOLUTE MASS SOURCE/SINK IS
CONSTANT
 !            OR F(TIME)
!-----0   : # OF NODES AT WHICH OBSERVATIONS ARE MADE, 0 FOR NO
OBSERVATION
!-----0   : MAX. # OF TIME STEPS ON WHICH OBSERVATIONS ARE MADE
      WRITE(I,*) '   0    0    0   +1   +0'
!---DATASET 4 FORMAT IS : 5* I5
!-----------0  : 0 FOR SIMULATION OF ONLY SATURATED FLOW, 1 FOR
BOTH UNSATURATED
!               AND SATURATED FLOW
!-----------1  : 1 FOR SIMULATION W/ STEADY-STATE GW FLOW, 0 FOR
TRANSIENT GW FLOW
!               IF FLUID DENSITY CHANGES W/ TIME, IT MUST BE SET
TO 0,
!-----------1  : 0 FOR TRANSIENT SOLUTE/ENERGY TRANSPORT, 1 FOR
STEADY-STATE
!-----------1  : READ D55 FOR COLD START,  -1 FOR READ D55 TO
RESTART
!-----------1  : 1 TO STORE RESULTS TO D66 FOR LATER USE, 0 FOR
CANCEL STORAGE.
      WRITE(I,*) '   0.00D0        5.00D+3        5.00D+3'
!----DATASET 5 FORMAT IS : G10.0   G15.0   G15.0
!-------FIRST:  UPSTREAM WEIGHT FROM 0 TO 1
!-------SECOND: PRESSURE BOUNDARY CONDITION
!-------THIRD : C/T BOUNDARY CONDITION
      WRITE(I,*) ' 305    8.64000D+04    6.31152D+08        10
1.5    2.62980D+06    1    1'
!--- DATASET 6 FORMAT : I5, G15.0, G15.0  I10  G10.0  G15.0  I5
I5
!------1 : MAX. TIME STEPS
!------2 : INITIAL TIME STEP   1DAY
!------3 : TOTAL SIMULATION TIME  20 YRS
!------4 : # OF TIME STEPS IN TIME STEP CHANGE CYCLE, 12
!------5 : MULTIPLIER FOR TIME STEP CHANGE CYCLE, USUALLY 1.0--
1.5
!------6 : MAX.TIME STEP WHEN USING TIME STEP MULTIPLIER   1
MONTH
!------7 : # OF TIME STEPS IN PRESSURE SOLUTION CYCLE = 1
```

```
!------8 : # OF TIME STEP IN T/C SOLUTION CYCLE =1
      WRITE(I,*) '  12   +0   +0    0   +0   +0   +1   +1'
!---DATASET 7 FORMAT : 8 * I5
!-----1 : PRINT OUT ON EVERY N*XX
!-----2 : 1 FOR PRINT OUT NODE COORDINATES, ELEMENT THICKNESS AND
POROSITIES
 !        0 FOR NO OUTPUT
!-----3 :1 FOR PRINT OUT ELEMENT PERMEABILITIES AND
DISPERSIVITIES,0 TO CANCEL
!-----4 :PRINT NODE INCIDENCE AND PINCH NODE INCIDENCE
!-----5 :PRINT PRESSURE AT ALL NODES
!-----6 :PRINT CONCENTRATION OR TEMP. AT ALL NODES
!-----7 :PRINT FLUID VELOCITY AT ELEMENT CENTROIDS
!-----8 :PRINT FLUID MASS BUDGET AND ENERGY/SOLUTE MASS BUDGET
EACH TIME
      WRITE(I,*) '       50  1.00D+05  1.00D-01'
!---DATASET 8 FORMAT :I10  G10.0 G10.0
!-----1 :MAX.# OF ITERATION DURING EACH TIME STEP TO RESOLVE NON-
LINERAITY
  !      SET TO +1 FOR NON-ITERATIVE SOLUTION
!-----2 :PRESSURE CONVERGENCE CRITERION
!-----3 :TRANSPORT SOLUTION CONVERGENCE CRITERION
      WRITE(I,*) ' 4.50D-10         1  1.000D-9   1.0D+03
0.00D+00  7.00D+02  1.00D-03'
!-----DATASET 9 FORMAT: 7* G10.0
!-----1 :FLUID COMPRESSIBLITY
!-----2 :FLUID SPECIFIC HEAT, BLANK FOR SOLUTE TRANSPORT
SIMULATION
!-----3 :FLUID DIFFUSIVITY
!-----4 :FLUID DENSITY AT BASE CONCENTRATION OR TEMP.
!-----5 :BASE VALUE OF C/T OF FLUID AT WHICH BASE FLUID DENSITY
IS SPECIFIED
!-----6 :FLUID COEFFICIENT OF DENSITY CHANGE W/ C/T:
ROU=ROU0+XX*(U-U0)
!-----7 :FLUID VISCOSITY
      WRITE(I,*) '  1.0D-08         0         0   2.6D+03'
!----DATASET 10 FORMAT :4* G10.0
!----1:SOLID MATRIX COMPRESSIBILITY
!----2:SOLID GRAIN SPECIFIC HEAT, BLANK FOR SOLUTE TRANSPORT
!----3:SOLID GRAIN DIFFUSIVITY, BLANK FOR SOLUTE TRANSPORT
!----4:DENSITY OF SOLID GRAIN
      WRITE(I,30) 'NONE'
!----DATASET 11 FOR ADSORPTION PARAMETERS : FORMAT IS A10 G10.0
G10.0
30  FORMAT(A4)
      WRITE(I,*) '   0.00D0    0.00D0    0.00D0    0.00D0'
!------DATASET 12 FOR ENERGY/SOLUTE MASS
      WRITE(I,*) '   0.00D0 -0.981D+1'
!-----DATASET 13 FOR ORIENTATION OF COORDINATES TO GRAVITY,FORMAT
G10.0 G10.0
!----1:COMPONENT OF GRAVITY VECTOR IN +X DIRECTION
```

```
!----2:COMPONENT OF GRAVITY VECTOR IN +Y DIRECTION
    WRITE(I,*) 'NODE      1.00      1.00      1.00      0.15'
!-----DATASET 14A: 5X 4*G10.0
!-----1:SCALORX   2:SCALORY    3:SCALORTHICKNESS
4:SCALORPOROSITY
      TT=1.0
    DO J=1,NX+1
             DO L=1, NY+1
  !---NODE#, X, Y, 1.0, 1.0
          WRITE(I,34)  L+(J-1)*(NY+1),XD(J),YD(L),TT,TT
34    FORMAT(I5, 5X, 4F10.2)
!---DATASET 14B
          END DO
    END DO

      WRITE(I,33) 'ELEMENT      1.0D+00   1.0D+00     0.000
1.00      1.00      1.00      1.00'
!-----DATASET 15A-------------
33  FORMAT(A80)

!---ELEMENT#, MAX.PERMEABILITY,MIN.PERMEABILITY,ANGLE FROM +X
DIRECTION TO MAX.K COUNTERCLOCKIWSELY
!     LONGITUDINAL DISPERSIVITY IN THE DIRECTION OF MAX.K,
LONGITUDINAL DISPERSIVITY IN MIN.K DIRECTION
!     TRANSVERSE DISPERSIVITY IN MAX K AND TRANSVERSE
DISPERSIVITY IN MIN.K DIRECTION
    DO J=1,NX
             DO L=1, NY
       WRITE(I,35)  L+(J-1)*NY, SK(I,L,J),SK(I,L,J),
TT,TT,TT,TT,TT
35   FORMAT(I5, 5X, 2ES10.2, 5F10.2)
!------DATASET 15B------------
          END DO
      END DO

!-INITIAL PRESSURE AND CONCENTRATION----------------

   WRITE(I,91) 1, 1000*9.81*20, CBACK
!--NODE#, P AT THIS NODE, C AT THIS NODE
   WRITE(I,91) NX*(NY+1)+1, 1000*9.81*20, CBACK  !--C0=0.2
91  FORMAT(I5,2F20.2)
   WRITE(I,*)
'0000000000000000000000000000000000000000000000000000000000000000'

!------DATASET 20 FOR SPECIFIED C AT NODES

      DO JJ=1, NX+1
    WRITE(I,21) JJ*(NY+1), C0 !--UNCHANGED C=C0, TOP LINE
21  FORMAT(I5,F20.2)
    END DO
```

```
    WRITE(I,*)
'0000000000000000000000000000000000000000000000000000000000000000 '

!---DATASET 21 IS OMITTED

!--ELEMENT AND ITS 4 SURROUNDING NODES:
!---DATASET 22 FOR ALL ELEMENTS---------
    DO IJ=1, NX
         DO II=1,NY
      WRITE(I,22) II+(IJ-1)*NY,II+(IJ-
1)*(NY+1),II+IJ*(NY+1),II+IJ*(NY+1)+1,II+(IJ-1)*(NY+1)+1

22   FORMAT(5I6)
!---DATASET 22: ELEMENT, NODE1, NODE2, NODE3, NODE4, START FROM
      1 COUNTERCLOCKWISE
         END DO
      END DO

    CLOSE(I)
!-----END OF INPUT DATA FOR D5 ------------
!!=========================================================
!---------- GENERATE D55 FILES ----------------------------

    FNAME4(I)=FILEPATHIN//'SUTRAIN/'//F1(I)//'.D55'

    OPEN(I, FILE=FNAME4(I),STATUS='REPLACE' )
    WRITE(I,29)  T0
29  FORMAT(F20.2)

      DO I4=1,(NODES+3)/4

      NODENUMBER=I4*4-3
!--HOW TO GET NXINDEX,NYINDEX FROM THIS OVERALL NODENUMBER?

        IY=MOD(NODENUMBER,(NY+1))
        IF(IY .EQ. 0) THEN
        IY=NY+1
        END IF

  WRITE(I,36) CCK*(TOTALY-YD(IY)),CCK*(TOTALY-
YD(IY+1)),CCK*(TOTALY-YD(IY+2)),CCK*(TOTALY-YD(IY+3))

36   FORMAT(4ES20.2)
    END DO

     DO I4=1,(NODES+3)/4
        II= I4*4-3

     WRITE(I,36) CINIT,CINIT,CINIT,CINIT
     END DO
```

```
    CLOSE(I)

!----------END DO OF I=1, FN -------------
    END DO
!===================================

!---------------------------------------
        END PROGRAM SGSIMK_D5
```

APPENDIX C

Input file for sgsim

```
                  PARAMETERS FOR SGSIM
                  ********************

START OF PARAMETERS:
NODATA.DAT                        \DATA FILE
1   2   0   3   0                 \COLUMN: X,Y,Z,VR,WT
-1.0    1.0                       \DATA TRIMMING LIMITS
1                                 \0=TRANSFORM THE DATA, 1=DON'T
SGSIM.TRN                         \OUTPUT TRANSFORMATION TABLE
0     30.0                \ZMIN,ZMAX(TAIL EXTRAPOLATION)  N(0,1)
1       0.0                       \LOWER TAIL OPTION, PARAMETER
4       2.0                       \UPPER TAIL OPTION, PARAMETER
SGSIM.OUT                         \OUTPUT FILE FOR SIMULATION
1                                 \DEBUGGING LEVEL: 0,1,2,3
SGSIM.DBG                         \OUTPUT FILE FOR DEBUGGING
189037                            \RANDOM NUMBER SEED
0                                 \KRIGING TYPE (0=SK, 1=OK)
30                                \NUMBER OF SIMULATIONS
300   0.5     1.0                 \NX,XMN,XSIZ
20    0.5     1.0                 \NY,YMN,YSIZ
1     0.5     1.0                 \NZ,ZMN,ZSIZ
0                                 \0=TWO PART SEARCH, 1=DATA-NODES
1                                 \MAX PER OCTANT(0 -> NOT USED)
10.0                              \MAXIMUM SEARCH RADIUS
0.0  0.0  0.0  1.0  1.0           \SANG1,SANG2,SANG3,SANIS1,2
0    8               \MIN, MAX DATA# FOR SIMULATION A GRID NODE
8                 \NUMBER SIMULATED NODES TO USE FOR ANOTHER NODE
1    0.0                           \NST, NUGGET EFFECT
2   5.0   1.0                      \IT,  AA,  CC
0.0  0.0   0.0  500  1.0           \ANG1,ANG2,ANG3,ANIS1,ANIS2
```

APPENDIX D

patch analysis

```
!  PATCH.F90
!
!  FUNCTIONS:
!     PATCH      -
!
!  MINGJUAN SHI  11/04/1999
!                MODIFIED JULY, 2003
!*************************************************************
!
!  PROGRAM: PATCH
!
!  NOTE:     PATCH ANALYSIS OF PERMEABILITY FIELD.
!
!*************************************************************

      PROGRAM PATCH

      IMPLICIT DOUBLE PRECISION (A-H, O-Z)

      PARAMETER(N=100,M=100, NM=5000,FN=60, NP=1000,
                IDN=1000,IN=900)
!-- M : ROW NUMBER,
!-- N : COLUMN NUMBER,
!-- FN: FILE NUMBER,
!-- NP: NUMBER OF GROUPS/PATCHES
!--IDN:TOTAL NUMBER OF GROUPS
!-- IN:

      DIMENSION  X(N), Y(M), TK1(NM),TK(FN,N,M),TMAX(FN),TMIN(FN)
      DIMENSION  WT(FN,N),W(M),XX(NM),YY(NM),SUMM(N)
      DIMENSION  PA(NP),IKVALUE(N,M),PSIZE(FN,NP),PAREA(FN,NP)
!     DIMENSION  PADIS(FN,NP), PORIEN(FN,NP)
      DIMENSION  NPP(FN),WT2(FN,N),SUMM1(N),SUMM2(N),WTNL(FN,N)
      DIMENSION  ADTOP(FN), AHCNT(FN),AVCNT(FN),ACNT(FN)
      DIMENSION  FMAXAREA(FN),FMINAREA(FN),FMAXDTOP(FN),
                 FMINDTOP(FN)
      DIMENSION  FMAXHCNT(FN),FMINHCNT(FN),FMAXVCNT(FN),
                 FMINVCNT(FN)
      DIMENSION  FMAXTCNT(FN),FMINTCNT(FN)
      DIMENSION  NPCOLOR(FN,N,M),IDCT(2),NUMP(FN,N,M),
                 IPHNUM(FN,N,M)
      DIMENSION  ID_GROUP(FN,IDN), NUM_IN_G(FN,IDN),TOP(IDN,IDN),
                 INDX1(IDN)
      DIMENSION  AREA(FN,IDN), DTOP(FN,IDN),AVGAREA(FN)
      DIMENSION  VCNT(FN,IDN),HCNT(FN,IDN),ICNT(FN,IDN),
                 CNT(FN,IDN)
```

```
      DIMENSION  G_X(FN,IN,IDN),G_Y(FN,IN,IDN),NID(IN),
                  DISMIN(FN,NM)
      DIMENSION  IGROUPA(FN,NM),IGROUPB(FN,NM)
      DIMENSION  NX_ROW_P(FN,IDN,N),NROW_G(FN,IDN),
            NROW_G1(FN,IDN)
      DIMENSION  ID_COMP(NP),NXMAX_G(FN,IDN)

!-WT(FILE,X), W-WEIGHT(Z), TK(FILE,X,Z)--REAL PERMEABILITY,
TK1(X*Z)-TOTAL
!-WTNL---NON_LINEAR WEIGHT
!-ID_GROUP(FN,IDN)-ID OF EACH GROUP, IDN-IS THE TOTAL NUMBER OF
GROUPS

      CHARACTER*4   F2,F1,FF, FNAME(FN)
      CHARACTER*3   PCOLOR(FN), PVALUE(FN)
      CHARACTER*12  FNAME1(FN), FNAME2(FN)
      CHARACTER*25  MODELPATH

      DATA FNAME/'RZ01','RZ02','RZ03','RZ04',  &
               'RZ05','RZ06','RZ07','RZ08', &
               'RZ09','RZ10','RZ11','RZ12', &
               'RZ13','RZ14','RZ15','RZ16', &
               'RZ17','RZ18','RZ19','RZ20', &
               'RZ21','RZ22','RZ23','RZ24', &
               'RZ25','RZ26','RZ27','RZ28', &
               'RZ29','RZ30'/
      DATA PCOLOR/'P01','P02','P03','P04','P05','P06','P07', &
            'P08','P09','P10','P11','P12','P13','P14','P15',
            'P16','P17', &
            'P18','P19','P20','P21','P22','P23','P24','P25',
            'P26','P27', &
            'P28','P29','P30'/
      DATA PVALUE/'P01','P02','P03','P04','P05','P06','P07', &
            'P08','P09','P10','P11','P12','P13','P14','P15',
            'P16','P17', &
            'P18','P19','P20','P21','P22','P23','P24','P25',
            'P26','P27', &
            'P28','P29','P30'/

! BODY OF PATCH
      NX=120
      NZ=40
      DELTX=5.0
      DELTY=3.75
      TOTALY=DELTY*NZ
      TOTALX=DELTX*NX
      TKMIN=1.0E-20
      TKMAX=1.0E-10
      MAXK=-LOG10(TKMAX)
      MINK=-LOG10(TKMIN)
      IDCT(1)=1
```

```
      IDCT(2)=0

      DO  J3=1,NZ               !--1,2,3,..
          W(J3)=1.0/(J3-41.0)**2
      END DO

!-------------------------------------------------------------
       DO I=1, FN

       FNAME1(I)='../'//FNAME(I)//'.DTT'
       NOTEND=0

       OPEN(I, FILE=FNAME1(I), STATUS='OLD')
       J=1

       DO WHILE (NOTEND .EQ.0 )

       READ(I, *, IOSTAT=NOTEND)  XX(J), YY(J), TK1(J)
       J=J+1
       END DO

       IF(NOTEND .EQ. -1) THEN
         NUM_K=J-1

       ELSE
         WRITE(*,*) 'PROBLEM READING K DATA FILE', FNAME1(I)
         WRITE(*,*) 'IOSTAT= ', NOTEND
       ENDIF
!--READ FIRST----------------------------

      TMAX(I)=TK1(1)
       TMIN(I)=TK1(1)

      DO IX=1,NX
          DO IZ=1,NZ
           KZ=(IX-1)*NZ+IZ

           TK(I,IX,IZ)=TK1(KZ)
           X(IX)=XX(KZ)
           Y(IZ)=YY(KZ)

             IF(TK1(KZ) .GT. TMAX(I))  TMAX(I)=TK1(KZ)
             IF(TK1(KZ) .LT. TMIN(I))  TMIN(I)=TK1(KZ)
            END DO
       END DO

      WRITE(*,*) ' MAX  AND MIN ', I,  TMAX(I), TMIN(I)

!---FINISH CONVERT K AND FIND MAX, MIN OF K IN EACH
!   REALIZATION
```

```
      DO II=1,NX
       SUMM(1)=W(1)*(LOG10(TK(I,II,1))-LOG10(TMIN(I)))
       SUMM1(1)=W(1)
       SUMM2(1)=W(1)*TK(I,II,1)
    !   SUMM(1)=W(1)*(TK(I,II,1)) !OLD VERSION USE WEIGHT*K(I)
      !SUM :W(I)*(LOGK(I)-LOGKMIN)
      !SUM1:W(I)
      !SUM2:W(I)*K(I)

        DO JJ=2,NZ
        SUMM(JJ)=SUMM(JJ-1)+W(JJ)*(LOG10(TK(I,II,JJ))-
                 LOG10(TKMIN))
        SUMM1(JJ)=SUMM1(JJ-1)+W(JJ)
        SUMM2(JJ)=SUMM2(JJ-1)+W(JJ)*TK(I,II,JJ)
        END DO

      WT(I,II)=SUMM(JJ-1)/NZ
   !---WT=SUM(W(I)*(LOGK(I)-LOGKMIN))/N  ---AS OUTPUT IN
            FORT.1***
        WT2(I,II)=1.0/SUMM1(JJ-1)*SUMM2(JJ-1)
   !--WT2=SUM(W(I)*K(I))/SUM(W(I)) ---------AS OUTPUT IN
            FORT.5***

      END DO

!--PATCH ANALYSIS FOR EACH REALIZATION: ----------
      IPRANGE=2
      IPCENTER=10
      IMIN1=(-LOG10(TMIN(I)))
      IMIN=20
!--ASSIGN 1 OR 0 TO EACH CELL
      DO IPX=1,NX
         DO IPZ=1,NZ
            IKVALUE(IPX, IPZ)=IMIN-(-LOG10(TK(I,IPX,IPZ)))
              IPV=IKVALUE(IPX,IPZ)
              IF(IPV.GE.(IPCENTER-IPRANGE) ) THEN
                  NUMP(I,IPX,IPZ)=1
                    NPCOLOR(I,IPX,IPZ)=IDCT(1)
              ELSE
                  NUMP(I,IPX,IPZ)=0
                    NPCOLOR(I,IPX,IPZ)=IDCT(2)
              ENDIF
!--NUMP(I,X,Z) IS 0 OR 1 FOR EACH CELL
         END DO
      END DO

!--DELINEATE PATCH AND CALCULATE ITS AREA AND CONNECTIVITY
   DO IH=1,NX
     DO IV=1,NZ
         IPHNUM(I,IH,IV)=0
! IPHNUM(I,X,Z) IS PATCH# FOR EACH CELL
```

```
       END DO
   END DO

   INITNUM=1
   INDEXPH=1
   INDEXCUR=1
!--DEFINE PATCH NUMBER TO EACH GRID
   DO IV=1,NZ
      DO IH=1,NX
      IPV=NUMP(I,IH,IV)
!-NUMP(I,X,Y) IS THE LOG(K) OF THIS CELL
     IF(IV.EQ.1) THEN ! FIRST ROW
        IF (IH.EQ.1) THEN   ! FIRST COLUMN
            IF(IPV.EQ.1) THEN      ! THIS FIRST CELL IS 1
          IPHNUM(I,IH,IV)=INDEXPH
              INDEXPH=INDEXPH+1
              END IF
       ELSE ! IH!=1,FIRST ROW,HORIZONTAL MOVE TO IH=2,3 ...NX
            IF(IPV.EQ.1) THEN
                IL=NUMP(I,IH-1,IV) !FIND IT'S LEFT NUMBER
            IF(IL.EQ.1) THEN  !IF LEFT NUMBER IS 1
            IPHNUM(I,IH,IV)=IPHNUM(I,IH-1,IV)
      !CURRENT PATCH NUMBER IS ASSIGNED THE SAME AS LEFT PATCH#
                ELSE
                 IPHNUM(I,IH,IV)=INDEXPH
      !LEFT IS NOT 1,ITSELF IS 1, ASSIGN A NEW PATCH# TO IT
                   INDEXPH=INDEXPH+1
                ENDIF
             ENDIF
          ENDIF
       ELSE ! NOT FIRST ROW, THEN GO DOWN
         IF(IH.EQ.1) THEN ! OTHER ROW, BUT FIRST COLUMN
            IUP=NUMP(I,IH,IV-1)
              IF(IPV.EQ.1) THEN
              IF(IUP.EQ.1) THEN !IF CURRENT IS 1 AND UP IS 1 ,
                  IPHNUM(I,IH,IV)=IPHNUM(I,IH,IV-1)
      ! ASSIGN UP PATCH# TO CURRENT PATCH NUMBER
             ELSE
      ! IF UP IS 0, THEN ASSIGN NEW PATCH# TO THIS CELL
                IPHNUM(I,IH,IV)=INDEXPH
                  INDEXPH=INDEXPH+1
             ENDIF
              ENDIF
       ELSE
      ! NOT THE FIRST ROW, AND NOT FIRST COLUMN, MOVE TO RIGHT

            IF(IPV.EQ.1) THEN
              IL=NUMP(I,IH-1,IV)
              IUP=NUMP(I,IH,IV-1)
                IF((IL.EQ.0) .AND. (IUP.EQ.0)) THEN
                   !IF CURRENT CELL IS 1, UP AND LEFT ARE ALL 0,
```

```
            !THEN ASSIGN NEW PATCH# TO THE CURRENT CELL
          IPHNUM(I,IH,IV)=INDEXPH
            INDEXPH=INDEXPH+1
       ENDIF

           IF((IL.EQ.1) .AND. (IUP.EQ.0)) THEN
       !IF LEFT IS 1 AND UP IS 0, THEN GET LEFT PATCH#
       IPHNUM(I,IH,IV)=IPHNUM(I,IH-1,IV)
       ENDIF
       IF((IL.EQ.0) .AND. (IUP.EQ.1)) THEN
             ! IF LEFT IS 0 AND UP IS 1, THEN GET UP PATCH#
       IPHNUM(I,IH,IV)=IPHNUM(I,IH,IV-1)
       ENDIF

    !IF BOTH LEFT AND UP ARE 1, AND UP PATCH#==LEFT PATCH#
        !THEN GET UP PATCH#
 IF((IL.EQ.1) .AND. (IUP.EQ.1) .AND. (IPHNUM(I,IH-
1,IV).EQ.IPHNUM(I,IH,IV-1))) THEN
          IPHNUM(I,IH,IV) = IPHNUM(I,IH,IV-1)
      ENDIF

      IF((IL.EQ.1) .AND. (IUP.EQ.1)) THEN
       !IF UP AND LEFT ARE 1, BUT LEFT PATCH# < UP PATCH#
       !THEN CURRENT CELL TAKES THE SMALL PATCH#
        IF( IPHNUM(I,IH-1,IV).LT.IPHNUM(I,IH,IV-1)) THEN
         NSMALL=IPHNUM(I,IH-1,IV)
               NLARG=IPHNUM(I,IH,IV-1)
               IPHNUM(I,IH,IV)=NSMALL
         DO IG=1,IV ! Z DIRECTION, WAS NZ
                 DO IGG=1,IH ! X DIRECTION,  WAS NX
                      IF(IPHNUM(I,IGG,IG).EQ.NLARG) THEN
!THEN CHANGE ALL LARGE PATCH# TO THIS SMALL #
                        IPHNUM(I,IGG,IG)=NSMALL
             END IF
           END DO
          END DO
        ELSE
IF(IPHNUM(I,IH-1,IV).GT.IPHNUM(I,IH,IV-1)) THEN
!IF LEFT PATCH# > UP PATCH#, REASSIGN SMALL AND LARGE #
! AND DO THE SAME UPDATE AS ABOVE
          NSMALL=IPHNUM(I,IH,IV-1)
                NLARG=IPHNUM(I,IH-1,IV)
                IPHNUM(I,IH,IV)=NSMALL
          DO IG=1,IV ! Z   WAS NZ
                 DO IGG=1,IH   ! X  WAS NX
                      IF(IPHNUM(I,IGG,IG).EQ.NLARG) THEN
                        IPHNUM(I,IGG,IG)=NSMALL
             END IF
           END DO
          END DO
         ENDIF
```

```
              ENDIF
              ENDIF
          ENDIF
         ENDIF
      END DO
      END DO

!----COUNT EACH PATCH AND CALCULATE AREA, CONNECTIVITY
!IDN IS THE TOTAL # OF GROUPS(PATCHES), IDN=1000
      DO JJ=1, IDN
        ID_GROUP(I, JJ)=0
        NUM_IN_G(I,JJ)=0
!NUMBER OF CELLS IN EACH PATCH
      ENDDO

      IDD=1
! COUNT OF HOW MANY PATCHES IN EACH REALIZATION

!-FIND WHAT GROUP/PATCH NUMBERS ARE ;
      DO J=1,NZ
        DO K=1,NX
! IPHNUM(I,X,Z) IS PATCH# FOR EACH CELL
          I1=IPHNUM(I,K,J)      ! O OR 1 OR 2....
            IF(I1.NE.0) THEN ! PATCH# NOT 0,
                IT=0
! CONTROL DIRECTION OF LOOP, SET FIRST APPEAR
! OF EACH NEW PATCH# TO GO DOWN TO IF(IT.EQ.0)
                  DO III=1, IDD
                    IF (ID_GROUP(I,III).NE.0) THEN
        ! FRIST STEP, ID_GROUP(ALL)= 0, SO END DO
                        IF (ID_GROUP(I,III).EQ.I1) THEN
                          NUM_IN_G(I,III)=NUM_IN_G(I,III)+1
                          IT=1  ! RESET IT, BUT KEEP IDD
                        ENDIF
                      ENDIF
            ENDDO
            IF (IT.EQ.0) THEN ! NEW PATCH APPEARS
! GIVE INITIAL VALUE TO PATCH#, AND CELL #S IN THIS PATCH
                  ID_GROUP(I,IDD)=I1
              NUM_IN_G(I,IDD)=1
                  IDD=IDD+1
! IDD IS COUNT FOR TOTAL PATCH GROUP
                ENDIF
           ENDIF
      ENDDO
    ENDDO
!======= IPH=IDD-1
!-NUMBER OF GROUPS/PATCH IN EACH REALIZATION
```

```
!---FIND DISTANCE TO TOP BOUNDARY
      DO II=1,IDD-1  ! TOTAL # OF PATCH
      INDX1(II)=0  ! TOTAL CELLS COUNT IN EACH PATCH
      IGO=ID_GROUP(I,II)
       DO I1=1,NZ
         DO J1=1,NX
            IGW=IPHNUM(I,J1,I1)
            IF(IGW.EQ.IGO) THEN
      ! THE CELL'S PATCH# IS THE CURRENT PATCH BEING EXAMINED

           INDX1(II)=INDX1(II)+1
      ! USED IN NUM_IN_G(I,INDEX)
              TOP(II,INDX1(II))=Y(I1)
      ! GET EACH Y INSIDE THE GROUP
      ! GET (X, Y) FOR EACH CELL IN EACH PATCH
              G_X(I,II,INDX1(II))=X(J1)
              G_Y(I,II,INDX1(II))=Y(I1)
        ENDIF
             DTOP(I,II)=TOP(II,1)-DELTY/2
       ! FIRST ROW,
             IF(INDX1(II).GT.1) THEN
                 DO IL=1,INDX1(II)-1
       ! COMPARE THE NEXT TOTOP DISTANCE AND GET THE SHORTEST
                 IF( TOP(II,IL+1).LT.TOP(II,IL) ) THEN
                 DTOP(I,II)=TOP(II,IL+1)-DELTY/2
                 ENDIF
             END DO
         ENDIF
        END DO  ! END OF X LOOP
        END DO ! END OF Z LOOP
!-------------------------------------------------------
!CALCULATE WIDTH (#OF DELTX) IN EACH ROW OF EACH PATCH
!        X0=G_X(I,II,1)
!           Y0=G_Y(I,II,1)
!           NROW_G(I,II)=(G_Y(I,II,NUM_IN_G(I,II))-Y0)/DELTY+1
!      WRITE(*,*) ' STOP .....', NUM_IN_G(I,II),NROW_G(I,II)

      DO LID=1,NUM_IN_G(I,II)
           ID_COMP(LID)=0  ! SEE IF THIS CELL HAS BEEN COMPARED
        END DO
        NROW=0  ! NUMBER OF ROWS IN EACH PATCH
        DO I5=1, NUM_IN_G(I,II)
            IF(ID_COMP(I5).EQ.0) THEN
      ! IF CELL HAS NOT BEEN COMPARED
              NROW=NROW+1       ! THEN START NEW ROW
              NX_ROW_P(I,II,NROW)=0
      !SET THIS ROW HAS 0 CELLS FIRST
              DO KK=I5,NUM_IN_G(I,II) ! DO LOOP FROM I5 AFTER
                 IF(G_Y(I,II,I5).EQ.G_Y(I,II,KK)) THEN
      ! IF AFTER CELL'S Y EQUALS
                NX_ROW_P(I,II,NROW)=NX_ROW_P(I,II,NROW)+1
```

```
                        !INCREASE NUMBER OF CELLS IN THIS PATCH
                    ID_COMP(KK)=1
      !REMOVE THIS CELL B/C ITS VALUE=PREVIOUS
                    ENDIF
                ENDDO
               ENDIF
        NROW_G1(I,II)=NROW ! NUM OF ROWS IN THIS PATCH
         ENDDO ! END OF I5

!*******************************************************
! GET MAXIMUM WIDTH OF EACH ROW IN EACH PATCH
     NMX=NX_ROW_P(I,II,1)
     DO KL=2, NROW_G1(I,II)
        NM1=NX_ROW_P(I,II,KL)
            IF( NM1.GT.NMX) THEN
              NMX=NM1
        ENDIF
       ENDDO
        DD=0
     NXMAX_G(I,II)=NMX
     HCNT(I,II)=1.0/NMX ! HORIZONTAL CONNECTIVITY

! CALCULATE VERTICAL AND TOTAL CONNECTIVITIES------
       DO K=1, NROW_G1(I,II)
            DD=DD+NX_ROW_P(I,II,K)
         ENDDO
         VCNT(I,II)=1.0*NROW_G1(I,II)*NXMAX_G(I,II)/DD
! VERTICAL

       CNT(I,II)=VCNT(I,II)/HCNT(I,II)*(1.0-DTOP(I,II)/TOTALY)
! TOTAL CONNECTIVITY

!       WRITE(*,*) ' V C ', VCNT(I,II), CNT(I,II)
!       PAUSE 2222
       END DO ! END OF II(PATCH) LOOP
!-------------------------------------------
!--THEN CALCULATE DISTANCE BETWEEN EACH PAIR OF PATCHES
    INDXG=1
      DO IK=1,IDD-2
         IG1=ID_GROUP(I,IK)
         IK1=IK
           DO IJ=IK+1,IDD-1
              IJ1=IJ
              IGROUPA(I,INDXG)=ID_GROUP(I,IK)
          IGROUPB(I,INDXG)=ID_GROUP(I,IJ)

      DISMIN(I,INDXG)=SQRT((G_X(I,IK,1)-
      G_X(I,IJ,1))**2+(G_Y(I,IK,1)-G_Y(I,IJ,1))**2)
                    DO M2=1,NUM_IN_G(I,IK)
                        DO N2=1,NUM_IN_G(I,IJ)
```

```
    DIST=SQRT((G_X(I,IK,M2)-G_X(I,IJ,N2))**2+(G_Y(I,IK,M2)-
    G_Y(I,IJ,N2))**2)
       IF(DIST.LT.DISMIN(I,INDXG)) THEN
           DISMIN(I,INDXG)=DIST
         END IF
                  END DO
                    END DO
                    INDXG=INDXG+1
            END DO
      END DO
!============================================================
!------AREA , DISTANCE TO THE TOP AND DISTANCE BETWEEN GROUPS
    AREA1=DELTX*DELTY   !-AREA OF EACH GRID CELL
      AREA(I,1)=NUM_IN_G(I,1)*AREA1
      SUM=0
      SUMDTOP=0.0
      SUMHCNT=0.0
      SUMVCNT=0.0
      SUMCNT=0.0
     FMAXDTOP(I)=DTOP(I,1)
     FMINDTOP(I)=DTOP(I,1)
       FMAXHCNT(I)=HCNT(I,1)
       FMINHCNT(I)=HCNT(I,1)
       FMAXVCNT(I)=VCNT(I,1)
       FMINVCNT(I)=VCNT(I,1)
       FMAXTCNT(I)=CNT(I,1)
       FMINTCNT(I)=CNT(I,1)
       FMAXAREA(I)=AREA(I,1)
       FMINAREA(I)=AREA(I,1)
    NPP(I)=IDD-1


     DO IPP=1, IDD-1
       AREA(I,IPP)=NUM_IN_G(I,IPP)*AREA1
       SUM=SUM+AREA(I,IPP)

         SUMDTOP=SUMDTOP+DTOP(I,IPP)
       SUMHCNT=SUMHCNT+HCNT(I,IPP)
         SUMVCNT=SUMVCNT+VCNT(I,IPP)
         SUMCNT=SUMCNT+CNT(I,IPP)
     IF(AREA(I,IPP) .GT. FMAXAREA(I)) FMAXAREA(I)=AREA(I,IPP)
     IF(AREA(I,IPP) .LT. FMINAREA(I)) FMINAREA(I)=AREA(I,IPP)
       IF(DTOP(I,IPP) .GT. FMAXDTOP(I)) FMAXDTOP(I)=DTOP(I,IPP)
       IF(DTOP(I,IPP) .LT. FMINDTOP(I)) FMINDTOP(I)=DTOP(I,IPP)

     IF(HCNT(I,IPP) .GT. FMAXHCNT(I)) FMAXHCNT(I)=HCNT(I,IPP)
     IF(HCNT(I,IPP) .LT. FMINHCNT(I)) FMINHCNT(I)=HCNT(I,IPP)
       IF(VCNT(I,IPP) .GT. FMAXVCNT(I)) FMAXVCNT(I)=VCNT(I,IPP)
       IF(VCNT(I,IPP) .LT. FMINVCNT(I)) FMINVCNT(I)=VCNT(I,IPP)

       IF(CNT(I,IPP) .GT. FMAXTCNT(I)) FMAXTCNT(I)=CNT(I,IPP)
```

```
     IF(CNT(I,IPP) .LT. FMINTCNT(I)) FMINTCNT(I)=CNT(I,IPP)

       END DO
      AVGAREA(I)=SUM/(IDD-1)
        ADTOP(I)=SUMDTOP/(IDD-1)
        AHCNT(I)=SUMHCNT/(IDD-1)
        AVCNT(I)=SUMVCNT/(IDD-1)
        ACNT(I)=SUMCNT/(IDD-1)
!============================================================

!--DETAILED OUTPUT OF PATCH PARAMETER TO P01.PCH

     OPEN(101,FILE=PVALUE(I)//'.PCH', STATUS='REPLACE')
       WRITE(101, *) 'PATCH_ID   #CELLS    AREA(M^2)  DISTANCE TO
      TOP(M)'

       DO IP=1,IDD-1
              WRITE(101, 27)
      ID_GROUP(I,IP),NUM_IN_G(I,IP),AREA(I,IP),  DTOP(I,IP)
          DO IG=1,NUM_IN_G(I,IP)
          WRITE(101,*)  G_X(I,IP,IG),G_Y(I,IP,IG)
          END DO
       ENDDO
       WRITE(101,28)  'AVERAGE_AREA (M^2)             ',
      AVGAREA(I)
       WRITE(101,*) '----------------------'
      DO IS=1,INDXG-1
           WRITE(101,*)  IGROUPA(I,IS), IGROUPB(I,IS),
            DISMIN(I,IS)
      END DO

       WRITE(101, 188) ((IPHNUM(I,IE2,IE1),IE2=1,NX),IE1=1,NZ)
     CLOSE(101)


!--OUTPUT TO P01.PAR ---------

      OPEN(109, FILE=PVALUE(I)//'.PAR', STATUS='REPLACE')
      WRITE(109,*) 'PATCH ANALYSIS RESULTS FOR REALIZATION', I
      WRITE(109,176) 'PATCH DEFINITION: K IN THE RANGE OF 10^-
      ',MAXK+1,'---10^-',MINK-(IPCENTER-IPRANGE), '   M^2'
      176 FORMAT(A41,I2,A7,I2,A6)
      WRITE(109,*)'-----------------------------------------------
      --------------------'
      WRITE(109, *) 'P_ID# CELLS_P AREA(M^2)    START_X
      START_Y    DEPTH(M)  H_CNTY  V_CNTY  CNTY'

       DO IP=1,IDD-1

      IF(NUM_IN_G(I,IP) .GT. 1) THEN
```

```
      WRITE(109, 277)
      ID_GROUP(I,IP),NUM_IN_G(I,IP),AREA(I,IP),G_X(I,IP,1),G_Y(I,
      IP,1),DTOP(I,IP),HCNT(I,IP),VCNT(I,IP),CNT(I,IP)
277   FORMAT(I4,I8,4(F11.3),3(F8.2))
27    FORMAT(2(I4),2(F6.2))
     END IF

       ENDDO


      WRITE(109,28)  'AVERAGE      ', AVGAREA(I),
      ADTOP(I),AHCNT(I),AVCNT(I),ACNT(I)
28    FORMAT(A12, F11.2,25X,4F8.2)
      WRITE(109,*) '-------------------------------------------
      ---'
      WRITE(109,*) '      PATCH_ID    PATCH_ID     PROXIMITY
      DISTANCE(M)'
      DO IS=1,INDXG-1
           WRITE(109,29)  IGROUPA(I,IS), IGROUPB(I,IS),
           DISMIN(I,IS)
29       FORMAT(2I12, F14.2)
        END DO

      CLOSE(109)


!--WRITE 1 OR 0 FOR EACH CELL
      OPEN(77, FILE=PCOLOR(I)//'.DAP', STATUS='REPLACE')
      WRITE(77,*)

      DO L1=1,NX
         DO L2=1,NZ
            WRITE(77, *)  X(L1), Y(L2), NPCOLOR(I, L1, L2)
       END DO
      END DO
      CLOSE(77)


      OPEN(78, FILE=PVALUE(I)//'.TXT', STATUS='REPLACE')
      WRITE(78, 188)  ((NPCOLOR(I,J0,I0),J0=1,NX),I0=1,NZ)
188     FORMAT(40(1X, 120(I1),/))
      CLOSE(78)


      CLOSE(I)  !--FINAL CLOSE EACH REALIZATION---
      END DO
!---END OF I ==========================================


!============================================================
!----OUTPUT FOR SUMMARY OF PATCH ANALYSIS, LIKE PID,
```

```
      AREA:MAX,MIN,AVE.
!----DTOP:MAX,MIN,AVE, HCONNECTIVITY:MAX,MIN,AVE.........

     OPEN(990,FILE='PRESUTLS.OUT', STATUS='REPLACE')
       WRITE(990,*) 'PATCH ANALYSIS SUMMARY----'
       WRITE(990,110)
110   FORMAT(36X,'AREA',26X,'DEPTH TO TOP',18X,'VERTICAL
      CONNECTIVITY',9X,'HORIZONTAL CONNECTIVITY',7X,'TOTAL
      CONNECTIVITY',10X,'CONVECT/NOT CONVECT')
      WRITE(990,112)
112   FORMAT('REALIZATION','   NUMBER OF PATCHES     ',
      5('MAX.',6X,'MIN.',6X,'AVE.',6X))
      DO I=1,FN
      WRITE(990,120)
      I,NPP(I),FMAXAREA(I),FMINAREA(I),AVGAREA(I),FMAXDTOP(I),FMI
      NDTOP(I),ADTOP(I),FMAXVCNT(I),FMINVCNT(I),AVCNT(I),FMAXHCNT
      (I),FMINHCNT(I),AHCNT(I),FMAXTCNT(I),FMINTCNT(I),ACNT(I)
120   FORMAT(I10,I20,15F10.2)


     END DO
     CLOSE(990)


!--WEIGHTED ANALYSIS FOR EACH COLUMN-------
      OPEN(20, FILE='KMAX.TXT')
      DO I=1, FN
        WRITE(20, *)  I, TMAX(I), TMIN(I)
      END DO
      CLOSE(20)

      WRITE(*,*)  ' STOP ....... '

    DO I=1, FN
        OPEN(UNIT=I+10,STATUS='REPLACE')
        WRITE(I+10,*) ' OUTPUT RESULTS FOR REALIZATION ', I
        WRITE(I+10,*) ' HORIZONTAL DISTANCE(M)
            WEIGHTED_ARITHMETIC_MEAN'
        WRITE(I+10,*)
        DO J=1,NX
          WRITE(I+10, *)  X(J), WT(I,J)
      END DO
        CLOSE(I+10)
    END DO

    DO I=1, FN
        OPEN(UNIT=I+50,STATUS='REPLACE')
        WRITE(I+50,*) ' OUTPUT RESULTS FOR REALIZATION ', I
        WRITE(I+50,*) ' HORIZONTAL DISTANCE(M)   NORMALIZED K '
        WRITE(I+50,*)
        DO J=1,NX
```

```
          WRITE(I+50, *)  X(J), WT2(I,J)
      END DO
        CLOSE(I+50)
    END DO
!-------------------------------
      END PROGRAM PATCH
```

APPENDIX E

SURFER SCRIPT

```
=====================================
        Option Base 1

Sub Main
        'Declares SurferApp, Wks, Doc, Plotwindow, Title, Map and
        'MapTitle as objects
        Dim SurferApp As Object
        Dim Wks As Object
        Dim PlotDoc(100), PlotDoc1 As Object
        Dim Pltwindows(100) As Object
        Dim plotwindow As Object
        Dim map, Map2, PostMap As Object
        Dim contourMap, contourMap2 As Object
        Dim MapFrame, MapFrame2,MapFrameOver As Object
        Dim MapTitle As Object
        Dim Shapes(100) As Object
        Dim PageSetup As Object
        Dim Axes, Axis, Axis2 As Object
        'Declares File as a string
        Dim File, Filename As String
        Dim Filepath, kFilepath As String
        Dim GridFile, kGridFile, kInfile As String
        Dim Title As String
        Dim levels, levels2 As Object
        'Declares retValue as a Boolean
        Dim retValue As Boolean
        'Declares MapNumber as an integer
        Dim MapNumber, PageNumber As Integer
        Dim MinX, MaxX, MinY, MaxY , intervalX, intervalY As Integer
        'Creates an instance of the Surfer Application object and assigns it to the
        'variable named "SurferApp"
        Set SurferApp = CreateObject("Surfer.Application")
        'Makes Surfer visible
        SurferApp.Visible = True
'=========================================================
'====change model here and need to change axis setscale method==========
'====change n_files if for multiple plotting========
   modelpath$ = "c:\MyModel\sandshales301\"
   Filename$ = "kk56"
```

```
   modelname$ = Mid$(modelpath$,12,13)
   n_files = 1
         plotsperpage = 8
         intervalX = 100
         LVLFile$ = "c:\MyCodes\surferplots\c01.lvl"
         'cc1.lvl is for c=1.0 to 0.1 every 0.1 interval

'------------ stop inputting parameters -----------------
'=====================================================
   File = modelpath$ + "extracted\" + Filename$
   sutrapath$ = modelpath$ + "sutraplots\"
   gridpath$ = modelpath$ + "sutragrids\"
   kgridpath$ = modelpath$ + "kgrids\"
   klvlfile$ = "c:\mycodes\surferplots\k10_54.lvl"
   Kfilename$ = Filename$ + "0.dat"
   kInfile = modelpath$ + "kdata\"+ Kfilename$
      kGridFile = kgridpath$ + Filename$ +".grd"
      kreturnfile$ = Dir(kGridFile)

'===start extracted data processing=========
         'Opens I.dat in a new worksheet document and assigns it to
         'the variable named "Wks"
         Set Wks = SurferApp.Documents.Open(File+"I.dat")
' Read in the Stat data from the eXtract OutFile:
Nplots = Val(Wks.Cells(3,3))-1

SVal$=Wks.Cells(1,3)
MinX= Val(Wks.Cells(1,3))
MaxX= Val(Wks.Cells(1,6))

MinY= Val(Wks.Cells(2,3))
MaxY= Val(Wks.Cells(2,6))
intervalY = MaxY
SurferApp.ActiveDocument.Close

'--k grid:
 SurferApp.GridData( DataFile:=kInfile,xcol:=1,ycol:=2,zcol:=3,
DupMethod:=srfDupNone, _
                  xMin:=MinX, xmax:=MaxX, ymin:=MinY, ymax:=MaxY,
Algorithm:=srfKriging, _
                  ShowReport:=False, OutGrid:=kGridFile)
```

```
'=========================================
' Load the N.data file into a worksheet window
Set Wks = SurferApp.Documents.Open(File +"N.dat")

im = 1  'Plot Number
PageNumber = 0        'PageNumber
Top1 = 0.0
Left1= 0.0

For MapNumber = 1 To Nplots Step 1
                I=MapNumber
 'Forms the map title by concatentating the column titles in the first row of the
worksheet
                Title = Wks.Cells (1, MapNumber + 3)

          If (MapNumber Mod plotsperpage = 1) Then
             im = im + 1
            'add one NEW page and set it as a new plot document
             Set PlotDoc(im)= SurferApp.Documents.Add(srfDocPlot)
             Set Shapes(im) = PlotDoc(im).Shapes
                Set PageSetup = PlotDoc(im).PageSetup
                PageSetup.Orientation = srfLandscape
           End If
  ' Set plotwindow = PlotDoc(im).Windows(1)
  ' plotwindow.AutoRedraw = False

      GridFile = gridpath$ + Filename$ + "_"+ CStr(MapNumber)+".grd"
      GridFilename$ = Filename$ + "_"+CStr(MapNumber)+ ".grd"
      returnfile$ = Dir(GridFile)

      'if no grid file found, then go ahead gridding
                'Grids the specified data file using the Kriging algorithm and
                'assigns the return value to the variable named "retValue"
'--C grid:

                SurferApp.GridData(DataFile:=File + "N.dat", xCol:=1, _
                        yCol:=2, zCol:=MapNumber+3, Algorithm:=srfKriging, _
                        ShowReport:=False, OutGrid:=GridFile)

'============add k field as Background ==================
   Set MapFrame2=Shapes(im).AddContourMap(kGridFile)
   Set Map2 = MapFrame2.Overlays(1)
```

```
Map2.Levels.LoadFile(klvlfile$)
Map2.FillContours = True
Map2.SmoothContours = srfConSmoothMed
MapFrame2.Selected = True

'=======add C contour maps to MapFrame ===============
        Set MapFrame =Shapes(im).AddContourMap(GridFile)
        Set map= MapFrame.Overlays(1)

map.Levels.LoadFile(lvlfile$)
map.FillContours= True
map.SmoothContours = srfConSmoothMed
MapFrame.Selected = True

'=============
' Turn off screen redrawing to speed up this procedure
 old_update_setting = MapFrame.Application.ScreenUpdating
 MapFrame.Application.ScreenUpdating = False
 old_update_setting2 = MapFrame2.Application.ScreenUpdating
 MapFrame2.Application.ScreenUpdating = False

 For Each Axis In MapFrame.Axes

   With Axis
    .ShowLabels = False
    .AutoScale = False
    .MajorTickType  = srfTickNone
    .MinorTickType  = srfTickNone
   End With
 Next Axis
'============================

' Adjust the left and bottom axes
 For Each Axis In MapFrame2.Axes

  If Axis.AxisType = srfATRight Or Axis.AxisType = srfATTop Then
   With Axis
    .ShowLabels = False
    .AutoScale = False
    .MajorTickType  = srfTickNone
    .MinorTickType  = srfTickNone
   End With
```

```
  End If

If Axis.AxisType = srfATLeft   Then

   With Axis
    .SetScale(MinY,MaxY,MaxY,MinY,MaxY,0,0)  'min, max, majorinterval,
firststick, last stick,cross1,cross2
    .LabelFont.Size =8
    .LabelOffset = 0.1
    .MajorTickType  = srfTickOut
    .MajorTickLength = 0.03
    .MinorTickType  = srfTickNone
    .AutoScale= False
   End With

End If

If Axis.AxisType = srfATBottom   Then

   With Axis
    .SetScale(MinX,MaxX,intervalX,MinX,MaxX,0,0)
    'min, max, majorinterval, firststick, last stick,cross1,cross2

    .MajorTickType  = srfTickOut
    .MajorTickLength = 0.01

    .MinorTickType  = srfTickNone
    .LabelFont.Size =8
    .LabelOffset = 0.03
    .AutoScale= False
   End With

End If

Next Axis
'==============================
' Restore the previous screen setting
 MapFrame.Application.ScreenUpdating = old_update_setting
 MapFrame2.Application.ScreenUpdating = old_update_setting2
'====================
    'Shapes(im).SelectAll
    PlotDoc(im).Selection.OverlayMaps    'overlay 2 maps
```

```
   PlotDoc(im).Selection.Align(HorzAlign:=srfHACenter,
   VertAlign:=srfVACenter)

'=====================
'Arrange each plot on the same page
PlotDoc(im).Selection.Width = 4.95      '2 columns' of graphs
PlotDoc(im).Selection.Height = (8.0-0.5)/(plotsperpage/2.0)
 '2 columns' of graphs
 'plotsperpage=8
If (MapNumber Mod plotsperpage) <> 0 Then
Top1 =  8.0-(Int( ((MapNumber Mod plotsperpage)+1) /2) -1 ) * _
   ((8.0-0.15)/(plotsperpage/2.0))  'multiply by height
PlotDoc(im).Selection.Top = Top1
Else
Top1 =  8.0-(Int( ((MapNumber Mod plotsperpage)+plotsperpage) /2 )-1) _
* ((8.0-0.15)/(plotsperpage/2.0))  'multiply by height
PlotDoc(im).Selection.Top = Top1
End If

left1 = (((MapNumber Mod plotsperpage) Mod 2 +3) Mod 2 )*5.0 + 0.5
PlotDoc(im).Selection.Left = left1

PlotDoc(im).Selection.DeselectAll

PlotDoc(im).Shapes.AddText(left1+4.0, Top1+0.08, Right$(Title, 8))

                  If (MapNumber Mod plotsperpage = 0) Then
                  PageNumber = PageNumber +1
                  'Positions the map title used below the map and assigns it to
                  'the variable named "MapTitle"
                  PlotDoc(im).Shapes.AddText(8.25, 0.25, modelname$+"      "+
                  Filename$ + "-over"+ CStr(PageNumber))

      PlotDoc(im).SaveAs( sutrapath$ + Filename$
         +"_CK"+CStr(PageNumber)+".srf")
      End If

'Returns to the beginning of the For loop

Next MapNumber
'================
'last page :
```

```
        PageNumber = PageNumber +1
                    'Positions the map title used below the map and assigns it to
                    'the variable named "MapTitle"
                    PlotDoc(im).Shapes.AddText(8.25, 0.25, modelname$ +"      "+
                    Filename$ + "-"+ CStr(PageNumber))

          '         plotwindow.AutoRedraw = True

        PlotDoc(im).SaveAs( sutrapath$ + Filename$
          +"_CK"+CStr(PageNumber)+".srf")

          SurferApp.Documents.CloseAll
      SurferApp.Quit

'end of plotting concentration
'=====================================

End Sub
```

APPENDIX F

SURFER SCRIPT

```
        Option Base 1

Sub Main
        'Declares SurferApp, Wks, Doc, Plotwindow, Title, Map and
        'MapTitle as objects
        Dim SurferApp As Object
        Dim Wks As Object
        Dim PlotDoc(100), PlotDoc1 As Object
        Dim Pltwindows(100) As Object
        Dim plotwindow As Object
        Dim map, Map2, PostMap As Object
        Dim contourMap, contourMap2 As Object
        Dim MapFrame, MapFrame2,MapFrame1 As Object
        Dim MapTitle As Object
        Dim Shapes(100) As Object
        Dim PageSetup As Object
        Dim Axes, Axis, Axis2 As Object
        'Declares File as a string
        Dim File, Filename As String
        Dim Filepath, kFilepath As String
        Dim GridFile, kGridFile, kInfile As String
        Dim Title As String
        Dim levels, levels2 As Object
        'Declares retValue as a Boolean
        Dim retValue As Boolean
        'Declares MapNumber as an integer
        Dim MapNumber, PageNumber As Integer
        Dim MinX, MaxX, MinY, MaxY , intervalX, intervalY As Integer
        'Creates an instance of the Surfer Application object and assigns it to the
        'variable named "SurferApp"
        Set SurferApp = CreateObject("Surfer.Application")
        'Makes Surfer visible
        SurferApp.Visible = True
'=========================================================
'====change model here and need to change axis setscale method========
'====change n_files if for multiple plotting========
   modelpath$ = "c:\MyModel\sigma1model00\"
   Filename$ = "kk22"
   modelname$ = Mid$(modelpath$,12,13)
```

```
   n_files = 1
         plotsperpage = 8
         intervalX = 100
   LVLFile$ = "c:\MyCode\surferplots\c01.lvl"
'cc1.lvl is for c=1.0 to 0.1 every 0.1 interval

'------------ stop inputting parameters -----------------
'=================================================
   File = modelpath$ + "extracted\" + Filename$
   sutrapath$ = modelpath$ + "sutraplots\"
   gridpath$ = modelpath$ + "sutragrids\"
   kgridpath$ = modelpath$ + "kgrids\"
   klvlfile$ = "c:\mycode\surferplots\k10_54.lvl"
   Kfilename$ = Filename$ + "0.dat"
   kInfile = modelpath$ + "kdata\"+ Kfilename$
      kGridFile = kgridpath$ + Filename$ +".grd"
      kreturnfile$ = Dir(kGridFile)

'===start extracted data processing=========
         'Opens I.dat in a new worksheet document and assigns it to
         'the variable named "Wks"
         Set Wks = SurferApp.Documents.Open(File+"I.dat")
' Read in the Stat data from the eXtract OutFile:
Nplots = Val(Wks.Cells(3,3))-1

SVal$=Wks.Cells(1,3)
MinX= Val(Wks.Cells(1,3))
MaxX= Val(Wks.Cells(1,6))

MinY= Val(Wks.Cells(2,3))
MaxY= Val(Wks.Cells(2,6))
intervalY = MaxY
SurferApp.ActiveDocument.Close

'--k grid:
 SurferApp.GridData( DataFile:=kInfile,xcol:=1,ycol:=2,zcol:=3,
DupMethod:=srfDupNone, _
                  xMin:=MinX, xmax:=MaxX, ymin:=MinY, ymax:=MaxY,
Algorithm:=srfKriging, _
                  ShowReport:=False, OutGrid:=kGridFile)

'=============================================
```

```
' Load the N.data file into a worksheet window
Set Wks = SurferApp.Documents.Open(File +"N.dat")

im = 1  'Plot Number
PageNumber = 0        'PageNumber
Top1 = 0.0
Left1= 0.0

For MapNumber = 1 To Nplots Step 1
                    I=MapNumber
 'Forms the map title by concatentating the column titles in the first row of the
worksheet
                    Title = Wks.Cells (1, MapNumber + 3)

           If (MapNumber Mod plotsperpage = 1) Then
              im = im + 1
            'add one NEW page and set it as a new plot document
             Set PlotDoc(im)= SurferApp.Documents.Add(srfDocPlot)
             Set Shapes(im) = PlotDoc(im).Shapes
                    Set PageSetup = PlotDoc(im).PageSetup
                    PageSetup.Orientation = srfLandscape
            End If
  ' Set plotwindow = PlotDoc(im).Windows(1)
  ' plotwindow.AutoRedraw = False

       GridFile = gridpath$ + Filename$ + "_"+ CStr(MapNumber)+".grd"
       GridFilename$ = Filename$ + "_"+CStr(MapNumber)+ ".grd"
       returnfile$ = Dir(GridFile)

       'if no grid file found, then go ahead gridding
                    'Grids the specified data file using the Kriging algorithm and
                    'assigns the return value to the variable named "retValue"
'--C grid:
       If (returnfile$ ="") Then
                    SurferApp.GridData(DataFile:=File + "N.dat", xCol:=1, _
                              yCol:=2, zCol:=MapNumber+3, Algorithm:=srfKriging, _
                              ShowReport:=False, OutGrid:=GridFile)
       End If
'============add k field as Background ==================
    Set MapFrame2=Shapes(im).AddContourMap(kGridFile)
    Set Map2 = MapFrame2.Overlays(1)
Map2.Levels.LoadFile(klvlfile$)
```

```
Map2.FillContours = True
Map2.SmoothContours = srfConSmoothMed
MapFrame2.Selected = True

'=======add C contour maps to MapFrame ===============
                Set MapFrame =Shapes(im).AddContourMap(GridFile)
      Set map= MapFrame.Overlays(1)

map.Levels.LoadFile(lvlfile$)
map.FillContours= True
map.SmoothContours = srfConSmoothMed
MapFrame.Selected = True

'======add velocity postmap to MapFrame1 ===========

                Set MapFrame1 =
PlotDoc(im).Shapes.AddPostMap(DataFileName:=File + "E.dat", xCol:=1, _
        yCol:=2, AngleCol:=(MapNumber*2+4) )
      Set PostMap = MapFrame1.Overlays(1)

      PostMap.Symbol.Set = "GSI Default Symbols"
      PostMap.Symbol.Index= 60
      PostMap.SymFrequency = 23
PostMap.SetSymbolScaling(Method:=srfPostSqRoot,SymbolHeight1:=0.01,
SymbolHeight2:=0.03, _
   ScaleValue1:=-20, ScaleValue2:=-5, heightcol:= MapNumber*2 + 3)

      MapFrame1.Selected = True
'=============
' Turn off screen redrawing to speed up this procedure
 old_update_setting = MapFrame.Application.ScreenUpdating
 MapFrame.Application.ScreenUpdating = False
 old_update_setting1 = MapFrame1.Application.ScreenUpdating
 MapFrame1.Application.ScreenUpdating = False
 old_update_setting2 = MapFrame2.Application.ScreenUpdating
 MapFrame2.Application.ScreenUpdating = False
'========================
 For Each Axis In MapFrame.Axes

  With Axis
   .ShowLabels = False
   .AutoScale = False
```

```
    .MajorTickType  = srfTickNone
    .MinorTickType  = srfTickNone
   End With
  Next Axis
'==========================
'MapFrame2 is k field
' Adjust the left and bottom axes
  For Each Axis In MapFrame2.Axes

   If Axis.AxisType = srfATRight Or Axis.AxisType = srfATTop Then
    With Axis
     .ShowLabels = False
     .AutoScale = False
     .MajorTickType  = srfTickNone
     .MinorTickType  = srfTickNone
    End With
   End If

If Axis.AxisType = srfATLeft   Then

    With Axis
     .SetScale(MinY,MaxY,MaxY,MinY,MaxY,0,0)  'min, max, majorinterval,
firststick, last stick,cross1,cross2
     .LabelFont.Size =8
     .LabelOffset = 0.1
     .MajorTickType  = srfTickOut
     .MajorTickLength = 0.03
     .MinorTickType  = srfTickNone
     .AutoScale= False
    End With

End If

If Axis.AxisType = srfATBottom   Then

    With Axis
     .SetScale(MinX,MaxX,intervalX,MinX,MaxX,0,0)  'min, max, majorinterval,
firststick, last stick,cross1,cross2

     .MajorTickType  = srfTickOut
     .MajorTickLength = 0.01
```

```
    .MinorTickType  = srfTickNone
    .LabelFont.Size =8
    .LabelOffset = 0.03
    .AutoScale= False
   End With

End If

Next Axis
'================================

 ' Restore the previous screen setting
 MapFrame.Application.ScreenUpdating = old_update_setting
 MapFrame1.Application.ScreenUpdating = old_update_setting1
 MapFrame2.Application.ScreenUpdating = old_update_setting2
'====================
    'Shapes(im).SelectAll
    PlotDoc(im).Selection.OverlayMaps    'overlay 2 maps
    PlotDoc(im).Selection.Align(HorzAlign:=srfHACenter,
VertAlign:=srfVACenter)

'====================
'Arrange each plot on the same page
PlotDoc(im).Selection.Width = 4.95      '2 columns' of graphs
PlotDoc(im).Selection.Height = (8.0-0.5)/(plotsperpage/2.0)
'2 columns' of graphs
                                    'plotsperpage=8
If (MapNumber Mod plotsperpage) <> 0 Then
Top1 =  8.0-(Int( ((MapNumber Mod plotsperpage)+1) /2) -1 ) * _
   ((8.0-0.15)/(plotsperpage/2.0))  'multiply by height
PlotDoc(im).Selection.Top = Top1
Else
Top1 =  8.0-(Int( ((MapNumber Mod plotsperpage)+plotsperpage) /2 )-1) _
* ((8.0-0.15)/(plotsperpage/2.0))  'multiply by height
PlotDoc(im).Selection.Top = Top1
End If


left1 = (((MapNumber Mod plotsperpage) Mod 2 +3) Mod 2 )*5.0 + 0.5
PlotDoc(im).Selection.Left = left1

PlotDoc(im).Selection.DeselectAll
```

```
PlotDoc(im).Shapes.AddText(left1+4.0, Top1+0.08, Right$(Title, 8))

                    If (MapNumber Mod plotsperpage = 0) Then
                    PageNumber = PageNumber +1
                    'Positions the map title used below the map and assigns it to
                    'the variable named "MapTitle"
                    PlotDoc(im).Shapes.AddText(8.25, 0.25, modelname$+"      "+
                    Filename$ + "-KCV"+ CStr(PageNumber))

        PlotDoc(im).SaveAs( sutrapath$ + Filename$
           +"_KCV"+CStr(PageNumber)+".srf")
        End If

'Returns to the beginning of the For loop

Next MapNumber
'================
'last page :

        PageNumber = PageNumber +1
                    'Positions the map title used below the map and assigns it to
                    'the variable named "MapTitle"
                    PlotDoc(im).Shapes.AddText(8.25, 0.25, modelname$ +"      "+
                    Filename$ + "-KCV"+ CStr(PageNumber))

           '        plotwindow.AutoRedraw = True

        PlotDoc(im).SaveAs( sutrapath$ + Filename$
           +"_KCV"+CStr(PageNumber)+".srf")

           SurferApp.Documents.CloseAll
     SurferApp.Quit

'end of plotting concentration
'==================================

End Sub
```

APPENDIX G

FORTRAN PROGRAM

```
      PROGRAM FLUXCAL
!------------------------------
!    MAIN PURPOSE IS TO CALCULATE FLUX:
!     CALCULATE SOLUTE MASS FLUX ACROSS SOURCE BOUNDARY AND
!     NUSSELT NUMBER
!     FLUX IS FOR VELOCITY AND CONCENTRATION
!     NUSSELT NUMBER IS ACTUAL MASS FLUX TO DIFFUSIVE MASS FLUX
!
!     BASED ON FENSTEMAKER'S SUTRAEXTRACT
!------------------------------
      IMPLICIT DOUBLE PRECISION (A-H,O-Z)
      IMPLICIT INTEGER (I-N)

      EXTERNAL  LOOKFOR
      INTEGER   FOUNDIT, CCTEMP

      PARAMETER  MAXELE=10000, MAXTSTEPS=50,MAXXX=350,MAXXY=50

      CHARACTER *1  CH1,CH2
      CHARACTER *120  LINEIN
      CHARACTER *6  TTYPE, DNAME
      CHARACTER *4  DATIME

      CHARACTER *12  CTITLE,TTILE,PTITLE,FVMTITLE,FVATITLE
      CHARACTER *4   DSNAME(30)
      CHARACTER *12  D5FILE,D6FILE
      CHARACTER *14  NDATFILE,EDATFILE,IDATFILE
      CHARACTER *25  FILEPATHIN
      CHARACTER *33  FILEPATH1
      CHARACTER *34  FILEPATH2
      CHARACTER *30  FILEPATH3
      CHARACTER *13  FFNAME
      CHARACTER *15  FLFILE
      CHARACTER *10  FLFILE1

      REAL X, Y
      REAL XE,XEMIN,XEMAX,YE,YEMIN,YEMAX,MAXPERM,MINPERM
      REAL MINX,MAXX,MINY,MAXY,MINDELTX,MAXDELTX,MINDELTY
      REAL  DUMMY,ETIME,POR,THICK,MAXDELTY

      DIMENSION ETIME(0:MAXTSTEPS,1:7),NTIME(0:MAXTSTEPS)
      DIMENSION CONC(0:MAXTSTEPS,0:MAXELE)
      DIMENSION PRES(0:MAXTSTEPS,0:MAXELE)
      DIMENSION TEMP(0:MAXTSTEPS,0:MAXELE)
      DIMENSION FVMAG(0:MAXTSTEPS,0:MAXELE)
      DIMENSION FVANG(0:MAXTSTEPS,0:MAXELE)
```

```
      DIMENSION X(MAXELE),Y(MAXELE),XE(MAXELE),YE(MAXELE)
      DIMENSION XEMIN(MAXELE),YEMIN(MAXELE)
      DIMENSION XEMAX(MAXELE),YEMAX(MAXELE)
      DIMENSION POR(MAXELE),THICK(MAXELE),MAXPERM(MAXELE)
      DIMENSION MINPERM(MAXELE)
      DIMENSION CC(MAXXX,MAXXY,MAXTSTEPS)
      DIMENSION VV(MAXXX,MAXXY,MAXTSTEPS)
      DIMENSION VVA(MAXXX,MAXXY,MAXTSTEPS)
      DIMENSION ANU(MAXXX,MAXXY,MAXTSTEPS)
      DIMENSION SMFLUX(MAXXX,MAXXY,MAXTSTEPS)

       DATA DSNAME/'KK01','KK02','KK03','KK04',  &
                   'KK05','KK06','KK07','KK08', &
                   'KK09','KK10','KK11','KK12', &
                   'KK13','KK14','KK15','KK16', &
                   'KK17','KK18','KK19','KK20', &
                   'KK21','KK22','KK23','KK24', &
                   'KK25','KK26','KK27','KK28', &
                   'KK29','KK30'/

01  CONTINUE

        PRINT *, 'TYPE IN THE MODEL NAME (13 CHARACTERS)--- '
        READ(*,*)   FFNAME
        FILEPATHIN = 'C:\MYMODEL\'//FFNAME //'\'

    NROW_BNDY= 20       !
    N_FILES = 1

!=======================================================
    DO IJ= 1, N_FILES

      PRINT*, 'NAMING FILES....'
      IF((DSNAME(IJ) .EQ.'NONE') .OR. (DSNAME(IJ) .EQ. 'NONE'))
GOTO 1000
      DSNAME(IJ)= ADJUSTR(DSNAME(IJ))
      D5FILE=DSNAME(IJ)//'.D5'
      D6FILE= DSNAME(IJ)//'.D6'
      NDATFILE=DSNAME(IJ)//'N.DAT'
      EDATFILE=DSNAME(IJ)//'E.DAT'
      IDATFILE=DSNAME(IJ)//'I.DAT'

      PRINT *, 'INITIALIZING VARIABLES AND ARRAYS ...'
      MINX=MAXELE
      MAXX=-MAXELE
      MINY=MAXELE
      MAXY=-MAXELE
      MINDELTX=99999.999
      MAXDELTX=-99999.999
      MINDELTY=99999.999
      MAXDELTY=-99999.999
```

```
      CMIN=99999.999
      CMAX=-99999.999
      MINV=99999.999
      MAXV=-99999.999
      PMIN=1D9
      PMAX=1D9
      NPLOTS=0

 09   FORMAT(A120)
 10   FORMAT(A1)

  !-----------------------------------------
  ! INITIALIZING ARRAYS AND OTHER DATA

      CONC=0.0D0
      PRES=0.0D0
      X=0.0E0
      Y=0.0E0
      THICK=0.0E0
      POR=0.0E0
      ETIME(1,1)=0.0E0
      NSTEP=0
      NX=0
      NY=0
      OFFSET=0

      FILEPATH1= FILEPATHIN//'SUTRAIN/'
!------OPEN D5 FILES AS UNIT=15 ------------
!-----------------------------------------------
      OPEN(UNIT=15,DEFAULTFILE=FILEPATH1,FILE=D5FILE,
           STATUS='OLD')
      PRINT*, 'OPENED D5 FILE'

!-----NUMBER OF NODES: NN
!-----NUMBER OF ELEMENTS:  NE
!-----VALUES OF X,Y, THICKNESS AND POROSITY
!-----GET DIFFUSION COEFFICIENT D

      READ(15,32) TTYPE
  32  FORMAT(6X,A6)

      READ(15,10) CH1
      READ(15,10) CH1
      READ(15,33) NN,NE,NBI,NPINCH,NPBC,NUBC,NSOP,
           NSOU,NOBS,NTOBS
  33  FORMAT(10I5)
      PRINT*, 'NN= ',NN, ' NE = ', NE

      DO I =1,5
         READ(15,32) (DNAME)
      END DO
```

```
      READ(15,59) FCOMP,FSHEAT,FDIFF,FDENS,VBASE,XBETA,FVISCO
59    FORMAT(7(F10.0))

      DO I=1,4
         READ(15,32)  (DNAME)
      END DO

      READ(15,35) DNAME,XSCALE,YSCALE,THSCALE,PORFAC
35  FORMAT(A4,4(6X,F4.2))

36  FORMAT (I5,5X,2F10.4,F10.3,F10.4)

      DO I =1,NN
         READ(15,36) N,X(I),Y(I),THICK(I),POR(I)
         X(I)=X(I)*XSCALE
         MINX=MIN(X(I),MINX)
         MAXX=MAX(X(I),MAXX)
         Y(I)=Y(I)*YSCALE
         MINY=MIN(Y(I),MINY)
         MAXY=MAX(Y(I),MAXY)
         THICK(I)=THICK(I)*THSCALE
         POR(I)=POR(I)*PORFAC
      END DO

      IE=1
      READ(15,10) CH1
      DO I=1,NN
         IF((Y(I).NE.0) .AND. (X(I).NE.0)) THEN
            READ(15,39)  N,MAXPERM(IE),MINPERM(IE)
              YE(IE)=Y(I)
              XE(IE)=X(I)
              IE=IE+1
            END IF
      END DO
 39 FORMAT (I5,5X,2(2X,D8.2))

      NSKIP=(NSOP+NSOU+NPBC+NUBC)
      IF(NSOP.GT.0) NSKIP=NSKIP+1
      IF(NSOU.GT.0) NSKIP=NSKIP+1
      IF(NPBC.GT.0) NSKIP=NSKIP+1
      IF(NUBC.GT.0) NSKIP=NSKIP+1
      PRINT*, 'NSOP = ',NSOP,'NSOU= ', NSOU
      PRINT*, 'NPBC = ',NPBC,'NUBC= ',NUBC
      PRINT*, 'NSKIP = ',NSKIP

      DO I=1,NSKIP
        READ(15,10) CH1
      END DO

      DO I=1,NE
```

```
         READ(15,42)  LL,IN1,IN2,IN3,IN4
         IF(I.NE.LL) THEN
            PRINT*, '*****ERROR READING IN
            NODES!!',I,LL,IN1,IN2,IN3,IN4
             READ *, N99
          END IF

            XE(I)=((X(IN1)+X(IN2)+X(IN3)+X(IN4))/4)
            YE(I)=((Y(IN1)+Y(IN2)+Y(IN3)+Y(IN4))/4)
      END DO
 42   FORMAT(5I6)

      CLOSE(UNIT=15)
      PRINT*, 'CLOSED D5 FILE.'

!-------------------------------------------
!------BEGIN D6 DATA EXTRACTION--------------------
!-------------------------------------------
    FILEPATH2 = FILEPATHIN //'SUTRAOUT/'
      OPEN(UNIT=16,DEFAULTFILE=
      FILEPATH2,FILE=D6FILE,STATUS='OLD')
      PRINT*, 'OPENED D6 FILE.'

      DO I=1,((NN+NE)+3950)
        READ(16,10) CH1    ! SKIP THE FIRST NN+NE + 500 LINES
                           ! THESE ARE INITIAL INPUT IN D5 FILE
      END DO

44    READ(16,09,END=900)  LINEIN

!-----------------------------------------
      CALL LOOKFOR(LINEIN,FOUNDIT)
!-----------------------------------------

LOOKUP :  SELECT CASE (FOUNDIT)

      CASE (1)
!-----------DO NOTHING, CASE 1 IS INITIAL CONDITION-----

      CASE (2)
! FIND RESULTS FOR TIME STEP, AND READ TIME STEP: NSTEP

      NSTEP=NSTEP+1

      IF(NTIME(NSTEP-1) .LT. 9000) THEN
          BACKSPACE(16)
          READ(16,104)  NTIME(NSTEP)
      ELSE
          NTIME(NSTEP)=9999
      END IF
```

```
104 FORMAT(32X,I5)

!-------------------------------------
        CASE (3)        ! FIND ELAPSED TIME

        BACKSPACE(16)
        READ(16,105)  ETIME(NSTEP,1)
        READ(16,106) (ETIME(NSTEP,I),I=2,7)
105   FORMAT(31X,E11.4)
106   FORMAT(31X,E11.4)

!-------------------------------------
        CASE (4)            !FIND CONCENTRATION

        READ(16,10) CH1
        READ(16,10) CH1

        DO I=1,NN,6
        READ(16,107) N1,CONC(NSTEP,I),N2,CONC(NSTEP,I+1), &
           N3,CONC(NSTEP,I+2),N4,CONC(NSTEP,I+3), &
            N5,CONC(NSTEP,I+4),N6,CONC(NSTEP,I+5)

        CMAX=MAX(CMAX,CONC(NSTEP,I),CONC(NSTEP,I+1), &

CONC(NSTEP,I+2),CONC(NSTEP,I+3),CONC(NSTEP,I+4),CONC(NSTEP,I+5))


CMIN=MIN(CMIN,CONC(NSTEP,I),CONC(NSTEP,I+1),CONC(NSTEP,I+2), &
          CONC(NSTEP,I+3),CONC(NSTEP,I+4),CONC(NSTEP,I+5))

        END DO

        CCTEMP=0
!-------------------------------------------
       CASE (5)          !FIND PRESSURE

       READ(16,10) CH1
       READ(16,10) CH1

       DO I=1,NN,6

          READ(16,107) N1,PRES(NSTEP,I),N2,PRES(NSTEP,I+1), &
       N3,PRES(NSTEP,I+2),N4,PRES(NSTEP,I+3),N5,PRES(NSTEP,I+4),&
         N6,PRES(NSTEP,I+5)


PMAX=MAX(PMAX,PRES(NSTEP,I),PRES(NSTEP,I+1),PRES(NSTEP,I+2), &
         PRES(NSTEP,I+3),PRES(NSTEP,I+4),PRES(NSTEP,I+5))


PMIN=MIN(PMIN,PRES(NSTEP,I),PRES(NSTEP,I+1),PRES(NSTEP,I+2), &
```

```
        PRES(NSTEP,I+3),PRES(NSTEP,I+4),PRES(NSTEP,I+5))

       END DO

107  FORMAT(7X,6(1X,I5,1X,1PD15.8))

!-------------------------------------------------
        CASE (6)        !FIND FLUID VELOCITY TITLE

!-----------------------------------------
        CASE (7)  !FIND FLUID VELOCITY MAGNITUDE AND READ THEM

          READ(16,10) CH1
            READ(16,10) CH1

            DO I=1,NE,6
              READ(16,107) N1,FVMAG(NSTEP,I),N2,FVMAG(NSTEP,I+1),
&N3,FVMAG(NSTEP,I+2),N4,FVMAG(NSTEP,I+3),N5,FVMAG(NSTEP,I+4), &
             N6,FVMAG(NSTEP,I+5)

FVMAX=MAX(FVMAX,FVMAG(NSTEP,I),FVMAG(NSTEP,I+1),FVMAG(NSTEP,I+2),
&             FVMAG(NSTEP,I+3),FVMAG(NSTEP,I+4),FVMAG(NSTEP,I+5))


FVMIN=MIN(FVMIN,FVMAG(NSTEP,I),FVMAG(NSTEP,I+1),FVMAG(NSTEP,I+2),
&             FVMAG(NSTEP,I+3),FVMAG(NSTEP,I+4),FVMAG(NSTEP,I+5))

          END DO

!-------------------------------------------------
       CASE (8)   !FIND FLUID VELOCITY ANGLE AND READ THEM

          READ(16,10) CH1
            READ(16,10) CH1

        DO I=1,NE,6
        READ(16,107) N1,FVANG(NSTEP,I),N2,FVANG(NSTEP,I+1), &

N3,FVANG(NSTEP,I+2),N4,FVANG(NSTEP,I+3),N5,FVANG(NSTEP,I+4), &
          N6,FVANG(NSTEP,I+5)

          END DO

!-----------------------------------------------------

       CASE (9)         !FIND TEMPERATURE

          READ(16,10) CH1
            READ(16,10) CH1

            DO I=1,NN,6
```

```
              READ(16,107) N1,TEMP(NSTEP,I),N2,TEMP(NSTEP,I+1), &
       N3,TEMP(NSTEP,I+2),N4,TEMP(NSTEP,I+3),N5,TEMP(NSTEP,I+4),
&
               N6,TEMP(NSTEP,I+5)


TMAX=MAX(TMAX,TEMP(NSTEP,I),TEMP(NSTEP,I+1),TEMP(NSTEP,I+2), &
              TEMP(NSTEP,I+3),TEMP(NSTEP,I+4),TEMP(NSTEP,I+5))

TMIN=MIN(TMIN,TEMP(NSTEP,I),TEMP(NSTEP,I+1),TEMP(NSTEP,I+2), &
            TEMP(NSTEP,I+3),TEMP(NSTEP,I+4),TEMP(NSTEP,I+5))

          END DO

            CCTEMP=1
!-------------------------------------------------------------
        CASE DEFAULT

!-------------------------------------------------------------

      END SELECT LOOKUP

!=============================================================

       IF(NSTEP.LT.MAXTSTEPS) THEN

          GOTO 44
            ELSE
              PRINT*, 'MAX NUMBER OF STEPS HAS BEEN READ, CHECK
                  INPUT DATA..'
              READ(*,*)  N99
       END IF

900  CONTINUE

        NPLOTS=NSTEP+1
        CLOSE(UNIT=16)

!=============================================================
!--------END OF D6 EXTRACTION ----------------------------
!-------------------------------

        PRINT *, ''
        PRINT *, ' END OF D6 FILE.'
        PRINT *, 'CALCULATE SOLUTE FLUX AND NU ....'

!+++++++++++++++++++++++++++++++++++++++++++++++++++++++++++++
!----FROM NN AND NE TO CALCULATE NX, NY---------

      NY= ((NN-NE-1)-INT(SQRT((NN-NE-1)**2-4.0*NE)))/2.0
      NX=NN-NE-NY-1
```

```
    NXD=NX+1
    NYD=NY+1

!---------ASSIGN CONC(NTSTEPS, INODE) TO CC(IX,IY,IT)------

    DO IT=1,NSTEP

       DO II=1,NN
           IYY=INT(II/NYD)
         IXX=MOD(II,NYD)

         IF((IYY.EQ.0)) THEN
           I=1
               J=IXX
         ELSE
                IF(IXX.EQ.0) THEN
                      I=IYY
                        J= NYD
                  ELSE
                     I=IYY+1
                     J=IXX
                  END IF
         ENDIF

         CC(I,J,IT) = CONC(IT,II)
         VV(I,J,IT) = FVMAG(IT,II)
         VVA(I,J,IT)= FVANG(IT,II)
       END DO

!------THEN CALCULATE FLUX FOR EACH ELEMENT AND NU ACROSS SOURCE
BOUNDARY-----------

      DO IX= 1,NX

          DO IY=1,NY

             IELE=IX*IY
             ILBNODE= (IX-1)*NDY+IY
             ILUNODE= ILBNODE+1
             IRBNODE= IX*NDY+IY
             IRUNODE= IRBNODE+1


CCENTER=1.0/4.0*(CONC(IT,ILUNODE)+CONC(IT,ILBNODE)+CONC(IT,IRUNOD
E)+CONC(IT,IRBNODE))

!----SOLUTE MASS FLUX--------
             SMFLUX(IX,IY,IT) = CCENTER * VV(IX,IY,IT)

!----------NUSSLT NUMBER --------
```

```
      DELTC= 1.0/2.0*(CONC(IT,ILUNODE)-
CONC(IT,ILBNODE)+CONC(IT,IRUNODE)-CONC(IT,IRBNODE))
         DELTY= Y(ILUNODE)-Y(ILBNODE)

          ANU(IX,IY,IT)= SMFLUX(IX,IY,IT)*DELTY/FDIFF/DELTC

          END DO

         END DO

      END DO   ! END OF IT FOR TIME LOOP

!++++++++++++++++++++++++++++++++++++++++++++++++++++++++
!----OPEN FILE FOR OUTPUT OF SOLUTE FLUX AND NU FOR EACH IT OR
NTSTEP TIME

      PRINT*, ' FINISH  HERE....'
        PAUSE 11111

        FILEPATH3 = FILEPATHIN // 'FLUX/'
         FLFILE= DSNAME(IJ)//'TOPFLUX'//'.DAT'
         OPEN(UNIT=20,DEFAULTFILE = FILEPATH3, FILE=FLFILE)
         PRINT *, 'OUTPUT SOLUTE FLUX AND NU .... '

          WRITE(20, 220) (XE(I*NROW_BNDY), I=1,NX)
220    FORMAT(15X,300F6.1)

        DO IT=1,NSTEP

             WRITE(20, 290)  ETIME(IT,1),
(SMFLUX(I,NROW_BNDY,IT), I=1,NX)
         END DO
290     FORMAT(F15.0,300F12.8)
        CLOSE(20)
!-------------------------------------------------
        ITT=2
        FLFILE1= DSNAME(IJ)//'_T.DAT'
        OPEN(UNIT=25, DEFAULTFILE= FILEPATH3, FILE=FLFILE1)

        WRITE(25,220)  (XE(I*NROW_BNDY), I=1,NX)

          DO IY=1,NY

            WRITE(25,290) YE(IY*1), (SMFLUX(IX,IY,ITT), IX=1,NX)

          END DO

         CLOSE(25)

1000   CONTINUE
        PRINT*, 'NORMAL EXIT !'
```

```
!-------------------------------------------------------
        END DO     ! END OF DSNAME LOOP
        STOP

        END PROGRAM FLUXCAL
!!!====================

!-----------------------------------------------------
! ---FIND HEADERS IN THE D6 FILE
! ---INPUT: A 120_CHARACTER LINE
! ---OUTPUT: AN INTEGER FOUNDONE , RETURN 0 IF NO HEADER IS FOUND
!-----------------------------------

        SUBROUTINE  LOOKFOR(LINEIN, FOUNDONE)

      PARAMETER INITCOND= 'I N I T I A L   C O N D I T I O N S'
      PARAMETER ICLEN=35
      PARAMETER RESFORTSTEP= 'RESULTS FOR TIME STEP'
      PARAMETER RSLEN=21
      PARAMETER ELAPTIME= 'ELAPSED TIME'
      PARAMETER ETLEN=12

      PARAMETER CONCTITLE= 'C  O  N  C  E  N  T  R  A  T  I  O
N'
      PARAMETER CTLEN=37
      PARAMETER TEMPTITLE= 'T  E  M  P  E  R  A  T  U  R  E'
      PARAMETER TTLEN=31

      PARAMETER PRESSTITLE= 'P  R  E  S  S  U  R  E'
      PARAMETER PTLEN=22
      PARAMETER FVTITLE= 'F  L  U  I  D    V  E  L  O  C  I  T
Y'
      PARAMETER FVTLEN=40

      PARAMETER FVMAGTITLE= 'M A G N I T U D E'
      PARAMETER FVMTLEN=17
      PARAMETER FVANGTITLE= 'A N G L E'
      PARAMETER FVATLEN=9


      IMPLICIT INTEGER(I-N)
      INTEGER FOUNDONE

      CHARACTER*120  LINEIN

      FOUNDONE= 0

      DO I=1,(120-41)

      IF(LINEIN(I:I+ICLEN).EQ.INITCOND)  FOUNDONE=1
               IF(LINEIN(I:I+RSLEN).EQ.RESFORTSTEP)  FOUNDONE=2
```

```
                IF(LINEIN(I:I+ETLEN).EQ.ELAPTIME)  FOUNDONE=3
                IF(LINEIN(I:I+CTLEN).EQ.CONCTITLE)  FOUNDONE=4
                IF(LINEIN(I:I+PTLEN).EQ.PRESSTITLE)  FOUNDONE=5
                IF(LINEIN(I:I+FVTLEN).EQ.FVTITLE)  FOUNDONE=6
                IF(LINEIN(I:I+FVMTLEN).EQ.FVMAGTITLE)  FOUNDONE=7
                IF(LINEIN(I:I+FVATLEN).EQ.FVANGTITLE)  FOUNDONE=8
                IF(LINEIN(I:I+TTLEN).EQ.TEMPTITLE)  FOUNDONE=9

            END DO

        END SUBROUTINE

!================================================================
```

REFERENCES

Anderson, R.N., Cathless, L.M., III, Nelson, H. R., Jr., 1991a. "Data cube" depicting fluid flow history in Gulf Coast sediments, Oil and Gas Journal, 89 (44), p. 60-65.

Anderson, R.N., He, W., Hobart, M.A., Wilkinson, C.R., Nelson, H. R., 1991b. Active fluid flow in the Eugene Island area, offshore Louisiana. Geophysics: The Leading Edge, Vol.10, No.4, p.12-17.

Anderson, R.N., Flemings, P., Losh, S., Austin, J., Woodhams, R., 1994. Gulf of Mexico growth fault drilled, seen as oil, gas migration pathway, Oil and Gas Journal, 94 (23), p. 97-104.

Anderson, R.N., 1995. Migration pathway for hydrocarbons within a fault zone conduit in the Eugene Island 330 Field of offshore Louisiana, Geological Society of America, 1995 annual meeting, Abstracts with Programs, 27 (6), p. 328.

Aplin, A. C., Fleet, A. J., and Macquaker, J. H. S. (eds.), 1999, Muds and Mudstones: Physical and Fluid-Flow Properties: Geological Society Special Publication No, 158, London, 190p.

Aplin, A.C., Yang, Y. & Hansen, S.,1995. Assessment of the compression coefficient of mudstones and its relationship to detailed lithology. Marine and Petroleum Geology 12, 955-963.

Bear, J., Tsang, C.-F., and de Marsily, G., 1993, Flow and Contaminant Transport in Fractured Rocks: Academic Press, San Diego, 560p

Beck, J.L., 1972. Convection in a box of porous material saturated with fluid. The Physics of Fluids, vol.15, no.8, p.1377-1383.

Belitz, K. and Bredehoeft, J.D., 1988. Hydrodynamics of Denver Basin: Explanation of subnormal fluid pressure. Am. Assoc. Petl. Geol. Bull., v.72, no.11, p.1334-1356.

Berkowitz, B., Balberg, I., 1992, Percolation approach to the problem of hydraulic conductivity in porous media. Transport in porous media, V.9, No.3, p.275-286.

Berkowitz, B., Balberg, I., 1993, Percolation theory and its application to groundwater hydrology, Water Resources Research, V.29, No.4, p775-794.

Berkowitz, B.,1994. Modelling flow and contaminant transport in fractured media, Advances in Porous Media, 2, p. 397-451.

Berkowitz, B., 1995, Analysis of fracture network connectivity using percolation theory. Mathematical Geology, Vol.27, No.4, p467-483.

Best, M.E. and Katsube, T.J., 1993. Possible effect of overpressure on shale permeabilities, Society of Exploration Geophysicists Expanded Abstracts with Biographies, 1993 Technical Program, 63rd Annual Meeting and International Exhibition, p.1237-1240.

Best, M.E., Katsube, T.J., 1995. Shale permeability and its significance in hydrocarbon exploration. The leading Edge, March, p165-170.

Bethke, C.M., 1986a. Inverse hydrologic analysis of the distribution and origin of Gulf Coast-type geopressured zones, J. Geophys. Res., v.91, no.B6, p.6535-6545.

Bjorlykke, K., Mo, A., and Palm, E., 1988. Modeling of thermal convection in sedimentary basins and its relevance to diagenetic reactions, Marine and Petroleum Geology, v.5, no.4, p.338-351.

Blanchard, P.E., and Sharp, J.M. Jr., 1985, Free convection in Gulf coast reservoirs, Transactions, Southwest Section, AAPG, v.1, no.69, p.141.

Blanchard, P.E., 1987. Fluid flow in compacting sedimentary basins. Ph.D. dissertation, University of Texas at Austin, 190p.

Blatt, H., Middleton, G., Murray, R., 1980. Origin of sedimentary rocks, 2 edn., 766p, ISBN: 0136427103.

Bodner, D.P., 1985. Heat variations caused by groundwater flow in growth faults of the South Texas Gulf Coast basin. M.S. thesis, University of Texas at Austin, 189p.

Bodner, D.P., Blanchard, P.E., and Sharp, J.M.Jr., 1988. Temperature variations in the Sourth Texas subsurface. AAPG Bulletin, v.72, no.1, p.21-32.

Borst, R. L., 1982. Some effects of compaction and geological time on the pore parameters of argillaceous rocks, Sedimentology, 29 (2), p. 291-298.

Brace, W. F., Walsh, J. B., Frangos, W. T., 1968. Permeability of granite under high pressure, Journal of Geophysical Research, 73 (6), p. 2225-2236.

Brace, W.F., 1980. Permeability of crystalline and argillaceous rocks. Int. J. Rock Mech. Min. Sci. & Geomech. Abstracts 17, p.241-251.

Bredehoeft, J.D. and Hanshaw, B., 1968. On the maintenance of anomalous fluid pressures, I, Thick sedimentary sequences, Geol. Soc. Am. Bull., n.79, no.9, p.1097-1106.

Bredehoeft, J. D, 1980. Permeability of clay and shale, AAPG Bulletin, 64 (5), p. 680, 1980. Meeting: APG-SEPM-EMD annual meeting, Denver, Colo., United States, June 8-11, 1980.

Bredehoeft, J.D. and Norton, D.L., 1990. The role of fluids in crustal processes. Natl. Acad. Press: Washington, DC, United States.

Broadbent, S.R., and Hammersley, J.M., 1957. Percolation processes: 1. Crystals and mazes. Proc. Camb. Phil. Soc., 53, p.629.

Bryant, W.R., Hottman, W., and Trabant, P., 1975. Permeability of unconsolidated and consolidated marine sediments, Gulf of Mexico. Marine Geotechnology. v.1, no.1, p.1-14.

Caltagirone, J.P., Thermalconvective instabilities in a horizontal porous layer, J. Fluid Mech., 1975, vol.72, p.269-287.

Capuano, R.M., 1993. Evidence of fluid flow in microfractures in geopressured shales. AAPG Bulletin, V.77, No.8, p.1303-1314.

Cartwright, Joseph A, 1994. Episodic basin-wide hydrofracturing of overpressured early Cenozoic mudrock sequences in the North Sea Basin, Marine and Petroleum Geology, 11 (5), p. 587-607, illus. incl. geol. sketch map, sects., block diag., 11 refs, 1994.

Cartwright, J. A, Dewhurst, D. N., 1998. Layer-bound compaction faults in fine-grained sediments, Geological Society of America Bulletin, 110 (10), p. 1242-1257, illus. incl. sects., 3 tables, sketch maps, 71 refs, 1998.

Casting, C., Genter, A., Bourgine, B., Chiles, J.P., Wendling,J., and Siegel,P. 2002. Taking into account the complexity of natural fracture systems in reservoir single-phase flow modeling. Journal of Hydrology, vol.266, p.83-98.

Cathles, L.M., 1990. Scales and effects of fluid flow in the upper crust, Science, vol.248, p.323-329.

Clennell, M.B., Dewhurst, D.N., Brown, K.M. & Westbrook, G.K., 1999. Permeability anisotropy of consolidated clays: in (Aplin, A. C., Fleet, A. J., and Macquaker, J. H. S., eds.), 1999, Muds and Mudstones: Physical and Fluid-Flow Properties: Geological Society Special Publication No, 158, London, p. 79-96.

Chiles, Jean-Paul, Geostatistics : modeling spatial uncertainty. / New York / 1999.

Corbet, T.F. and Bethke, C.M., 1992. Disequilibrium fluid pressures and groundwater flowin the western Canada sedimentary basin. J. Geophys. Res., v.97, no.B5, p.7203-7217.

Davis, S.H., 1967. Convection in a box: Linear theory, J. Fluid Mech., vol.30, p.465-478.

Davis, J. M., Wilson, J.L., Phillips, F. M., and Gotkowitz, M. B., 1997, Relationship between fluvial bounding surfaces and the permeability correlation structure: Water Resources research, v. 33, p. 1843-1854.

Deutsch, C. V., Journel, A.G., 1997. GSLIB geostatistical software library and user's guide. 2nd ed., Oxford University Press, New York . 344p.

Dewhurst, D.N., Aplin, A.C. and Sarda, J.P., 1995. Controls on the permeability of compacting mudstones. Report de Institute Fraccais du Petrole, 42555.

Dewhurst, D. N, Aplin, Andrew C., Sarda, Jean-Paul, Yang, Yunlai, 1998. Compaction driven evolution of porosity and permeability in natural mudstones; an experimental study, Journal of Geophysical Research, B, Solid Earth and Planets, 103 (1), p. 651-661.

Dewhurst, D. N., Yang, Y., and Aplin, A. C., 1999. Permeability and fluid flow in natural mudstones: in (Aplin, A. C., Fleet, A. J., and Macquaker, J. H. S., eds.), 1999, Muds and Mudstones: Physical and Fluid-Flow Properties: Geological Society Special Publication No, 158, London, p. 23-44.

Dewhurst, D.N., Cartwright, J.A., and Lonergan, L., 1999a. The development of polygonal fault systems by syneresis of colloidal sediments. Marine and Petroleum Geology, 16, p.793-810.

Diersch, H.-J.G., Kolditz, O., 2002. Variable-density flow and transport in porous media: approaches and challenges. Advances in Water Resources, v.25, p.899-944.

Djordjevic, Zorica V., Stanley, H. E. and Margonila, A., 1982. Site percolation threshold for honeycomb and square lattices. J. Phys. A: Math.. Gen. 15, L405-L412.

Elder, J.W., 1967. Transient convection in a porous medium, Journal of Fluid Mechanics, v.27, no.3, p.609-623.

Evans, D.G., Nunn, J.M., 1989. Free thermohaline convection in sediments surrounding a salt column. Journal of Geophysical Research, V.94, No.B9, p.12,413-12,422.

Evans, D.G., Nunn,J.A., and Hanor, J.S., 1991. Mechanisms driving groundwater flow near salt domes, Geophysical Research Letters, v.18, p.927-930.

Fenstemaker, T.R., 2000. Density-driven free convection across low permeability strata, south Texas Example. Unpublished MS thesis. UT Austin. 131p.

Fetter, C.W., 2001. Applied hydrogeology, 4th Edition. Prentice Hall, 598p.

Freeze, R.A. and Cherry, J.A., 1979. Groundwater: Prentice-Hall, Englewood Cliffs, N.J., 604p.

Freeze, R. A., 1975. A stochastic-conceptual analysis of one-dimensional groundwater flow in nonuniform homogeneous media, Water Resources Research, 11 (5), p. 725-741.

Frisch, H.L. and Hammersley, J.M., 1963. J. Soc. Indust. Math., 11, p.894.

Fyfe, W., Price, N., and Thompson, A., 1978. Fluids in the earth's crust, Amsterdam: Elsevier.

Galloway, W.E., Hobday, D.K., and Magara, K., 1982. Frio Formation of the Texas coastal plain – depositional systems, structural framework, and hydrocarbon distribution. AAPG Bulletin, v.66, no. 6, p.649-688.

Galloway, W.E., and Hobday, D.K., 1996. Terrigenous Clastic Depositional Systems, 2nd ed.: Berlin, Springer Verlag, 489p.

Galloway, W. E., and Sharp, J. M., Jr., 1998a. Characterizing aquifer heterogeneity within terrigenous clastic depositional systems: in Sedimentology and Stratigraphy in Aquifer Heterogeneity (Fraser, G. S., and Davis, M. W., eds.), Concepts in Hydrogeology and Environmental Geology, Society for Sedimentary Geology, Tulsa, OK., v.1, p.85-90.

Galloway, W. E., and Sharp, J. M., Jr., 1998b. Hydrogeology and characterization of fluvial aquifer systems: in Sedimentology and Stratigraphy in Aquifer Heterogeneity (Fraser, G. S., and Davis, M. W., eds.), Concepts in Hydrogeology and Environmental Geology, Society for Sedimentary Geology, Tulsa, OK., v.1, p. 91-106.

Goovaerts, Pierre, 1997. Geostatistics for natural resources evaluation. New York.

Graf, T., and Therrien, R., 2004. On the use of the Elder convection experiment as a benchmark problem for variable-density transport models. GSA Abstracts with Programs, v.36, p.174.

Griffiths, F. J., Joshi, R. C., 1989. Change in pore size distribution due to consolidation of clays, Geotechnique, 39 (1), p.159-167

Griffiths, F. J., Joshi, Ramesh C., 1990. Clay fabric response to consolidation, Applied Clay Science, 5 (1), p. 37-66.

Gueguen, Y. David, C. and Gavrilenko, P., 1991. Percolation networks and fluid transport in the crust. Geophysical Research Letters, Vol.18, No.5, p.931-934.

Harrison, B., Sudicky, E.A., and Cherry, J.A., 1992. Numerical analysis of solute migration through fractured clayey deposits into underlying aquifers. Water Resources Research, v.28, no.2, p.515-526.

Hassanizadeh, S. M., and Leijnse, T., 1988. On the modeling of brine transport in porous media: Water Resources Research, v. 24, p. 1781-1795.

Heling, Dietrich, 1970. Micro-fabrics of shales and their rearrangement by compaction, lithification of clastic sediments, 2, Sedimentology, 15 (3-4), p.247-260.

Henry, H.R., 1964. Interfaces between salt water and fresh water in coastal aquifers, U.S. Geol. Surv. Water Supply Pap., 1613-C, p.C35-C84.

Hohn, M.E., 1988. Geostatistics and Petroleum Geology: New York, Van Nostrand Reinhold, 264p.

Horseman, S. T., Harrington, J. F., 1996. Evidence for thresholds, pathways and intermittent flow in argillaceous rocks, Fluid flow through faults and fractures in argillaceous formations; proceedings of a joint NEA/EC workshop. Bern, Switzerland, June 10-12, 1996, p. 85-103, illus. incl. block diag., 1998. ISBN: 92-64-16021-3.

Hsieh, P.A. and Winston, R.B., 2002. User's guide to model viewer, a program for three-dimensional visualization of groundwater model results. USGS Open-File Report 02-106.

Katsube, T. J, Mudford, Brett S., Best, M. E., 1991. Petrophysical characteristics of shales from the Scotian Shelf, Geophysics, 56 (10), p. 1681-1689.

Katsube, T.J. and Williamson, M., 1994a. Shale petrophysics and basin charge modeling. Current Research 1994-D, Geological Survey of Canada, p.179-188.

Katsube, T. J., Williamson, M. A., 1994b. Effects of diagenesis on shale nano-pore structure and implications for sealing capacity. Bain, D. C. (editor), Hall, P. L. (editor), Shaw, H. F. (editor), Spears, D. A. (editor), Issue devoted to papers read at a conference on Diagenesis, overpressure and reservoir quality, Clay Minerals, 29 (4), p. 451-461, Meeting: Diagenesis, overpessure and reservoir quality, Cambridge, United Kingdom, March 26, 1993.

Katsube, T.J. and Coyner, K., 1994c. Determination of permeability-compaction relationship from interpretation of permeability-stress data for shales from eastern and northern Canada. Current Research 1994-D, Geological Survey of Canada, p.169-177.

Katsube, T. J, Williamson, M., 1995. Permeabilities and pore structure of subsiding shales with implications of fluid expulsion, Abstracts with Programs - Geological Society of America, 27 (6), p. 461, 1995. Meeting: Geological Society of America, 1995 annual meeting, New Orleans, LA, United States, Nov. 6-9, 1995.

Keller, C.K., G. van der Kamp, and Cherry, J.A., 1989. A multiscale study of the permeability of a thick clayey till. Water Resources Research. V.25, no.11, p.2299-2317.

Kitanidis, P.K., 1997. Introduction to geostatistics: applications to hydrogeology. Cambridge university press, 249p.

Kolditz, O., Ratke, R., Diersch, H.G., and Zielke, W. 1998. Coupled groundwater flow and transport: 1. Verification of variable density flow and transport models. Advances in Water Resources, Vol.21, no.1, p.27-46.

Koltermann, C. E., and Gorelick S. M., 1996. Heterogeneity in sedimentary deposits: A review of structure-imitating, process-imitating, and descriptive approaches: Water Resources Research, v. 32, p. 2617-2658.

Lamb, H., 1932. Hydrodynamics. Cambridge University Press.

Land, L. S., 1991. Evidence for vertical movement of fluids, Gulf Coast sedimentary basin: Geophysical Research Letters, v. 18, p. 919-922.

Land, L. S., Mack, L. E., Milliken, K. L., and Lynch, F. L., 1997. Burial diagenesis of argillaceous sediment, south Texas Gulf of Mexico sedimentary basin: A reexamination: Bull., Geol. Soc. America, v. 109, p. 2-15.

Lapwood, E.R., 1948. Convection of a fluid in a porous medium. Proc. Camb. Phil. Soc., vol.44, p.508-520.

Larson, R.G., Scriven, L.E., and Davis, H.T., 1981. Percolation of two phase flow in porous media. Chem. Eng. Sci. 36, 57-73.

Leroueil, S., Bouclin, G., Tavenas, F., Bergeron, I. & LA Rochelle, P., 1990. Permeability anisotropy of natural clays as a function of strain. Canadian Geotechnical Journal, 27, p.568-579.

Lonergan, L., and Cartwright, J. A., 1999. Polygonal faults and their influence on deep water sandstone reservoir geometries, Alba Field, United Kingdom Central North Sea: Am. Assoc. Petrol. Geologists Bull., v. 83, p. 410-432.

Losh, S., Eglinton, L.B., Schoell, M., and Wood, J.R., 1999. Vertical and lateral fluid flow related to a large growth fault, South Eugene Island Block 330 Field, Offshore Louisiana. AAPG Bulletin, v.83, no.4, p.468-504.

Lowell, R.P., 1991. Modeling continental and submarine hydrothermal systems, Rev. Geophys., vol.29,p.457-476.

Lowell, R.P. and Shyu, C.T., 1978. On the onset of convection in a water-saturated porous box: effect of conducting walls, Letters in Heat and Mass Transfer, vol.5, p.371-378.

Lynch, F.L., 1994. The effects of depositional environment and formation water chemistry on the diagenesis of Frio formation (Oligocene) sandstones and shales, Aransas, Nueces, And San Patricio Counties, Texas. Unpublished PhD dissertation. UT Austin.

Lynch, F. L., 1997, Frio Shale mineralogy and the stoichiometry of the smectite-to-illite reaction: the most important reaction in clastic sedimentary diagenesis: Clays and Clay Minerals, v. 45, p. 618-631.

Magara, K., 1978. Compaction and fluid migration, 319 pp., Elsevier, New York.

Malkovsky, V.I. and Pek, A.A, 1997. Conditions for the onset of thermal convection of a homogeneous fluid in a vertical fault. Petrology, vol.5, no.4, p.381-387.

Malkovsky, V.I. and Pek, A.A, 1999. Onset conditions of free thermal convection of a single-phase fluid in a horizontal porous layer with depth-dependent permeability, Izvestiya, Physics of the Solid Earth, vol.35, no.12, p.990-994.

Malkovsky, V.I. and Pek, A.A, 2004. Onset of thermal convection of a single-phase fluid in an open vertical fault. Physics of the Solid Earth, vol.40, no.8, p.672-679.

McKenna, T.E., Sharp, J.M., Jr., and Lynch, F.L., 1996, Thermal conductivity of Wilcox and Frio sandstones in South Texas (Gulf of Mexico Basin): Am. Assoc. Petrol. Geologists Bull, v.80, p.1203-1215.

McKenna, T.E., Sharpm J.M., Jr., 1997. Subsurface temperature, fluid pressures, and salinities in the Rio Grande Embayment, Gulf of Mexico Basin, USA: in L. Wenhan (ed.) Proceedings of the 30th International Geological Congress, v.8, p. 263-274.

McKenna, T.E., 1997. Geologic and hydrologic constraints on fluid and heat flow in overpressured rocks of the Rio Grande Embayment, Gulf of Mexico Basin. Ph.D. dessertation, University of Texas at Austin, 241p.

McKibbin, R. and O'Sullivan, M.J., 1980. Onset of convection in a layered porous medium heated from below. J. Fluid Mech., vol.96, part 2, p.375-393.

Mello, U.T., Karner, G.D., 1992. The history of sediment overpressuring in the Gulf of Mexico Basin and its effect on thermal maturation. American Association of Petroleum Geologists, 1992 annual convention abstracts, p.88.

Mello, U.T., Karner, G.D., Anderson, R.N., 1994. A physical explanation for the positioning of the depth to the top of overpressure in shale-dominated sequences in the Gulf Coast basin, United States, Journal of Geophysical Research, B, Solid Earth and Planets, 99 (2), p. 2775-2789.

Mello, U.T., Karner, G. D., Anderson, R. N., 1995. Role of salt in restraining the maturation of subsalt source rocks, Marine and Petroleum Geology, 12 (7), p. 697-716

Mello, U.T., Karner, G. D., 1996. Development of sediment overpressure and its effect on thermal maturation; application to the Gulf of Mexico basin, AAPG Bulletin, 80 (9), p. 1367-1396.

Mendoza, C.A., Frind, E.O., 1990a. Advective-dispersive transport of dense organic vapours in the unsaturated zone: I. Model development. Water Resources Research, vol.26, no.3, p.379-387.

Mendoza, C.A., Frind, E.O., 1990b. Advective-dispersive transport of dense organic vapours in the unsaturated zone: II. Sensitivity analysis. Water Resources Research, vol.26, no.3, p.388-398.

Mitchelle, J.K., Hooper, D.R. & Campanella, R.G., 1965. Permeability of compacted clay. Journal of the soil mechanics and foundation division, ASCE, 91, p.41-65.

Morin, R., and Silva, A.J., 1984. The effects of high pressure and high temperature on some physical properties of ocean sediments, J. Geophys. Res., v.89, no.B1, p.511-526.

Morton, R.A., and Land, L.S., 1987. Regional variations in formation water chemistry, Frio Formation (Oligocene), Texas Gulf Coast, AAPG Bulletin, v.71, no.2, p.191-206.

Murphy, H.D., Convective instabilities in vertical fractures and faults, J. Geophys. Res.B, 1979, vol. 84, p.6121-6130.

Neglia, S., 1979. Migration of fluids in sedimentary basins. Am. Assoc. Pet. Geol. Bull., v.63, no.4, p.573-597.

Neuzil, C.E., 1986. Groundwater flow in low-permeability environments, Water Resources Research, 22(8), 1163-1195.

Neuzil, C.E., 1993. Low fluid pressure within the Pierre Shale: A transient response to erosion, Water resources research, 29(7), 2007-2020.

Neuzil, C.E., 1994. How permeable are clays and shales? Water Resources Research vol.30, no.2, p.145-150.

Nield, D.A., 1968. Onset of thermohaline convection in a porous medium. Water Resources Research, vol.4, p.553-560.

Nield, D.A., and Bejan, A., 1999. Convection in porous media, Springer-Verlag, New York. 546p.

Oldenburg, C.M., and Pruess, K. 1995. Dispersive transport dynamics in a strongly coupled groundwater-brine flow system. Water Resources Research, vol.31, no.2, p.289-302.

Olsen, Harold W., 1962. Hydraulic flow through saturated clays, Clays and clay minerals, V. 9--Natl. Conf. Clays and Clay Minerals, 9th, 1960, Proc., p.131-161.

Prasad, A., and Simmons, C.T., 2003, Unstable density-driven flow in heterogeneous porous media: A stochastic study of the Elder (1967b) "short heater" problem. Water Resources Research, v.39, no.1, 1007, SBH 4-1.

Ranganathan, V., Hanor, J.S., 1988. Density-driven groundwater flow near salt domes, Chemical Geology, v.74, no. 1-2, p.173-188.

Ranganathan, V., Hanor, J.S., 1989. Perched brine plumes above salt domes and dewatering of geopressured sediments, Journal of Hydrology, v.110, no. 1-2, p.63-86.

Revil, A. and Cathles, L.M., III, 1999. Permeability of shaly sands. Water Resources Research, 35 (3), p. 651-662.

Rayleigh, Lord (J.W. Strutt), 1916. On convection currents in a horizontal layer of fluid when the higher temperature is on the under side, Philos. Mag., Ser.6, 32, p.529-546.

Schincariol, R. A., and Schwartz, F. W., 1990, An experimental investigation of variable density flow and mixing in homogeneous and heterogeneous media: Water Resources Research, v. 26, p. 2317-2329.

Schincariol, R.A., F.W. Schwartz and C.A. Mendoza 1994. On the generation of instabilities in variable density flow. Water Resources Research, 30(4), 913-927.

Schincariol, R.A., F.W. Schwartz and C.A. Mendoza 1997. Instabilities in variable density flows: Stability analyses for homogeneous and heterogeneous media, Water Resource Research, 33(1), 31-41.

Schincariol, R.A. 1998. Dispersive mixing dynamics of dense miscible plumes: natural perturbation initiation by local-scale heterogeneities. Journal of Contaminant Hydrology. Vol.34, p.247-271.

Schlomer, S. and Kross, B.M., 1997. Experimental characterization of the hydrocarbon sealing efficiency of caprocks. Marine and Petroleum Geology. V.14, p.565-580.

Screaton, E.J., Wuthrich, D.R., and Dreiss, S.J., 1990. Permeabilities, fluid pressures, and flow rates in the Barbados ridge complex. J. Geophys. Res., v.95, no.B6, p.8997-9007.

Sharp, J.M.Jr., Galloway, W.E., Land, L.S., McBride, E.F.,Blanchard, P.E.,Bodner, D.P.,Dutton,S.P., Farr, M.R.,Gold, P.B., Jackson,T.J., Lundegard, P.D., Macpherson, G.L. and Milliken, K.L., 1988. Diagenesis, , edited by G.V. Chilingarian and K.H. Wolf. Elsevier Science Publishers, Amsterdam.

Sharp, J.M. Jr., Fenstemaker, T.R., Simmons, C.T., McKenna, T.E. and Dickson, J., 2001. Potential salinity-driven free convection in a shale-rich sedimentary basin: Example from the Gulf of Mexico basin in south Texas, the American Association of Petroleum Geologists Bulletin, V.85, No.12, pp.2089-2110.

Sharp, J.M.Jr., Shi, M., and Galloway, W.E., 2003. Heterogeneity of fluvial systems – control on desity-driven flow and transport, special issue of Environmental and Engineering Geoscience, v.9, p.5-17.

Shevenell, L., Moore, G.K., and Dreier, R.B., 1994, Contaminant spread and flushing in fractured rocks at the S-3 Ponds site, Oak Ridge, TN, Ground Water Monitoring and Remediation, XIV(2), 120-129.

Shi, M.J. and Sharp, J.M.,Jr., 2001. Characterizing and modeling heterogeneity of low-permeability stratified units. GSA Abstracts with programs.

Shi, M., and Sharp, J.M. Jr., 2003. Delineation of free convection pathways in a heterogeneous low-permeability unit. Eos. Trans. AGU, v.84, no.46, p.591.

Shikaze, S.G. and Sudicky, E.A., 1994. Simulation of dense vapor migration in discretely fractured geologic media. Water Resour. Res., vol.30, no.7, p.1993-2009.

Shikaze, S.G., Sudicky, E.A. and Schwartz, F.W., 1998. Density-dependent solute transport in discretely-fractured geologic media: is prediction possible? J. of Contam. Hydro., vol.34, p.273-291.

Silva, A.J., Hetherman, J.R., and Calnan, D.I., 1981. Low-gradient permeability testing of fine-grained marine sediments, ASTM Special Technical Publication 746, edited by T.F. Zimmie and C.O. Riggs, p.121-136, American Society for Testing and Materials, Philadelphia, Penn.

Simmons, C. T., and Narayan, K. A., 1997, Mixed convection processes below a saline disposal basin: Jour. Hydrology, v. 194, p. 263-285.

Simmons, C. T., Narayan, K. A., and Wooding, R. A., 1999a, On a test case for density dependent flow and solute transport models: The salt lake problem: Water resources research, v. 35, p. 3607-3620..

Simmons, C. T., Sharp, J. M., Jr., and Robinson, N. I., 1999b, Density-driven free convection in zones of inverted salinity through fractured low-permeability units in the Gulf of Mexico Basin, Texas, USA: Water 99 Joint Congress, Inst. of Engineers, Australia, Brisbane, v. 2, p.739-744.

Simmons, C. T., and Sharp, J. M., Jr., 2000, On variable-density groundwater flow in heterogeneous porous media: in Groundwater: Past Achievements and Future Challenges (eds., Sililo, O., et al.), Proceedings of the 30th Congress, International Association of Hydrogeologists, Cape Town, South Africa, p. 425-430.

Simmons, C. T., Fenstemaker, T. R., and Sharp. J. M., Jr., 2001, Variable -density groundwater flow and solute transport in heterogeneous porous media: approaches, resolutions, and future challenges: Jour. Contaminant Hydrology, 52 (2001) 245-275.

Simmons, C.T., Sharp, J.M.Jr., 2002. Density-driven flow and transport in fractured low permeability geologic layers: Case study from the Gulf of

Mexico Basin, Texas, USA. In preparation to submit to Water Resources Research.

Simpson, M.J., and Clement, T.P., 2003. Theoretical analysis of the worthiness of Henry and Elder problems as benchmarks of density-dependent groundwater flow models. Advances in Water Resources, v.26, p.17-31.

Smith, A. 2004. Mixed convection and density-dependent seawater circulation in coastal aquifers. Water Resources Research, vol.40, W08309, doi:10.1029/2003WR002977.

Snow, D.A., 1965. Parallel plate model of fractured permeable media. PhD Dissertation, University of California, Berkeley-CA.

Stauffer, D., 1985, Introduction to percolation theory: Taylor and Francis Ltd., London, 124p.

Sudicky, E.A., and Frind, E.O., 1982. Contaminant transport in fractured porous media: analytical solutions for a system of parallel fractures. Water Resources Research, vol.18, p.1634-1642.

Sudicky, E.A., McLaren, R.G., 1992. The Laplace transform Galerkin technique for large-scale simulation of mass transport in discretely fractured porous formations. Water Resources Research, v.28, no.2, p.499-514.

Tang, D.H., Frind, E.O., and Sudicky, E.A. 1981. Contaminant transport in fractured porous media: analytical solution for a single fracture. Water Resources Research, vol.17, p.555-564.

Tavenas, F.,Jean, P., Leblond, P., Leroueil, S., 1983a. The permeability of natural soft clays; Part II, Permeability characteristics, Canadian Geotechnical Journal, 20 (4), p. 645-660.

Tavenas, F., Leblond, P., Jean, P., & Leroueil, S., 1983b. The permeability of natural soft clays. Part 1: Methods of laboratory measurement. Canadian Geotechnical Journal, 20, 629-643.

Tournier, C., Genthor P., and Rabinowicz, M., 2000. The onset of natural convection in vertical fault planes: consequences for the thermal regime in crystalline basements and for heat recovery experiments. Geophys. J. Int., vol.140, p.500-508.

Trimmer, D., 1980. Effect of pressure and stress on water transport in intact and fractured gabbro and granite. Journal of Geophysical Research. B, December 10, 1980. vol.85, issue 12, p.7059-7071.

Turcotte, D. and Schubert, J., 1985. Geodynamics, New York: Wiley, 1982.

Voss, C. I., 1984, SUTRA: A finite-element simulation model for saturated-unsaturated fluid density-dependent groundwater flow with energy transport or chemically reactive single-species solute transport: U. S. Geological Survey Water-Resources Investigation Report 84-4369, 409p.

Voss, C. I., and Souza, W. R., 1987, Variable density flow and solute transport simulation of regional aquifers containing a narrow freshwater-saltwater transition zone: Water Resources Research, v. 23, p. 1851-1866.

Voss, C.I. and Provost, A.M., 2003. SUTRA: A model for saturated-unsaturated variable-density groundwater flow with solute or energy transport. USGS Water-Resource Investigations Report 02-4231.

Walls, Joel D., Nur, Amos M., Bourbie, T., 1982. Effects of pressure and partial water saturation on gas permeability in tight sands; experimental results, JPT. Journal of Petroleum Technology, 34 (4), p. 930-936.

Wang, C. and Xie, X. 1998. Hydrofracturing and episodic fluid flow in shale-rich basins-A numerical study. AAPG Bulletin, V.82, No.10, p.1857-1869.

Walraevens, K. and Cardenal, J., 1999. Prefential pathways in an Eocene Clay: hydrogeological and hydrogeochemical evidence: in (Aplin, A. C., Fleet, A. J., and Macquaker, J. H. S., eds.), 1999, Muds and Mudstones: Physical and Fluid-Flow Properties: Geological Society Special Publication No, 158, London, p.175-186.

Wang, C.Y., 1994. Thermal convective instability of a horizontal saturated porous layer with a segment of inhomogeneity, Appl. Sci. Res., vol.52, p.147-160.

Weatherill, D., Simmons, C.T., Voss, C.I., and Robinson, N.I., 2004. Testing density-dependent groundwater models: two-dimensional steady state unstable convection in infinite, finite and inclined porous layers, Adv Water Resour., v.27, p.547-562.

Weaver, R.R., Frape, S.K. and Cherry, J.A. 1991. Multi-level monitoring of groundwater flow and chemistry in a low-permeability shale formation near Sarnia, Ontario.

Webb, E. K., and Davis, J. M., 1998, Simulation of the spatial heterogeneity of geologic properties: An overview: : in Sedimentology and Stratigraphy in Aquifer Heterogeneity (Fraser, G. S., and Davis, M. W., eds.), Concepts in Hydrogeology and Environmental Geology, Society for Sedimentary Geology, Tulsa, OK., v.1, p.1-24.

Wilkinson, D., Willemsen, J. F., 1983, Invasion percolation: a new form of percolation theory. J. Phys. A: Math. Gen. 16, 3365-3376.

Wilkinson, D., Barsony, M., 1984. Monte Carlo study of invasion percolation clusters in two and three dimensions. J. Phys. A: Math. Gen. 17, L129-L135.

Winston, R.B. and Voss, C.I., 2004. SutraGUI: A graphical user interface for SUTRA, A model for groundwater flow with solute or energy transport. USGS Open-File Report 03-285.

Wooding, R.A., Tyler, S.W., and White, I., 1997. Convection in groundwater beneath an evaporating playa lake: 1. Onset of Instability. Water Resources Research, v.33, no.6, p.1199-1217.

Woods, J. A., Teubner, M.D., Simmons, C.T., and Narayan K.A., 2003. Numerical error in groundwater flow and solute transport simulation. Water Resources Research, vol.39,no.6, 1158, doi: 10.1029/2001WR000586.

Yang, J. and Edwards, R.N., 2000. Predicted groundwater circulation in fractured and unfractured anisotropic porous media driven by nuclear fuel waste heat generation. Can. J. Earth Sci., Vol.37, p.1301-1308.

Yin, C. S., He, W., Anderson, R. N., 1993. Mapping lateral porosity variation in a geopressured zone using seismic dataAnonymous, Society of

Exploration Geophysicists; expanded abstracts with biographies; 1993 technical program; 63rd annual meeting and international exhibition, SEG Annual Meeting Expanded Technical Program Abstracts with Biographies, 63, p. 1330-1333.

Young, A., Low, P.F., and McLatchie, A.S., 1964. Permeability studies of argillaceous rocks, J. Geophys. Res., v.69, no.20, p.4237-4245.

Zebib, A. and Kassoy, D.R., Onset of natural convection in a box of water-saturated porous media with large temperature distribution, Phys. Fluids, 1977, vol.20, p.4-9.

Zhou, D., Stenby, E.H., 1993, Interpretation of Capillary pressure curves using invasion percolation theory. Transport in porous media 11:17-31.

VITA

Mingjuan Shi was born in Yingkou city of Liao Ning Province, Northeast of China on January 19, 1970, the daughter of Xianglan Wang and Chunpu Shi. She was raised on the Liao He Coastal Plain with a sister, Mingyuan Shi, and a brother, Mingquan Shi. She graduated from the No.1 high school in the city and attended Qingdao Ocean University majoring in geophysics. She received her Bachelor of Engineering degree in 1991 and later earned a MS degree in geophysics in 1994. On June 10, 1996, she married Haixiang Ni and before long she went to the Graduate School of North Carolina State University. She got a MS degree in geology in 1999 while he was working at IBM. In June, 1999, they moved to Austin, TX to start pursuing her PhD study. On June 11, 2001, they became the happy parents of Christina Yuge Ni. Upon finishing her PhD, they are going to move to Houston where she will work in the petroleum industry.

Temporary address: 201 Wilcrest Dr. #6904, Houston, TX 77042

This dissertation was typed by the author.